

RAMAN SPECTROSCOPY OF TRANSFUSABLE RED BLOOD CELLS

by

Chad Garry Atkins

B.Sc. (Hons), University of Waterloo, 2007

M.Sc., Memorial University of Newfoundland, 2009

A THESIS SUBMITTED IN PARTIAL FULFILLMENT OF
THE REQUIREMENTS FOR THE DEGREE OF

DOCTOR OF PHILOSOPHY

in

THE FACULTY OF GRADUATE AND POSTDOCTORAL STUDIES
(Chemistry)

THE UNIVERSITY OF BRITISH COLUMBIA
(Vancouver)

November 2016

© Chad Garry Atkins, 2016

Abstract

Blood banking is an essential aspect of modern healthcare. When red blood cells (RBCs) are stored, they degrade over time as a result of various chemical and biological processes leading to an accumulation of waste products and oxidative damage, among others. Significant growth in the application of Raman spectroscopy (RS) to biomedical problems has made it a feasible tool for investigating biochemical changes associated with storage of RBCs. It was hypothesized that RS could be used to monitor *in situ*, non-destructively and non-invasively, certain structural and compositional changes associated with these ageing effects as they occur in storage bags. The presence of a relationship between these changes and the viability of RBCs would have substantial implications for the health care industry.

Preliminary results demonstrated the oxygenation state of hemoglobin in stored RBCs changed in a manner that was donor-dependent and that closely tracked the morphological index, a qualitative metric for evaluating cell quality. Investigations of the storage-solution supernatant revealed that lactate, a metabolic waste product, accumulated at different rates in stored bags and displayed more rapid accumulation in units from male donors than units from female donors.

It was shown that spatially offset Raman spectroscopy (SORS) could measure stored RBC biochemistry through the plastic bag. Spectra collected with SORS compared well with previously-obtained conventional Raman spectra. Thus, information about the contents of a stored unit could be obtained without breaching its sterility. These outcomes provided proof-of-concept for the development of a SORS-based instrument to measure storage bag contents in a rapid and non-invasive manner.

The results reported in this thesis fall into two distinct categories. Regarding the observed data, the substantial inter-donor variability and gender and age effects have significant implications for the design of clinical trials, the collection and administration of donated blood, and clinical use. Regarding instrumentation, obtaining chemical information from stored RBCs using RS will enable new research directions for the field of transfusion medicine and obtaining this information *in situ* from storage bags will have utility for quality control in a blood bank or hospital setting.

Preface

“I have noticed that even people who claim everything is pre-destined, and that we can do nothing to change it, look before they cross the road”

Stephen Hawking

This thesis contains completed research that has been the result of numerous collaborations with multi-disciplinary scientists.

The latter portion of Chapter 2 was the result of an investigative review done by myself and Kevin Buckley (School of Chemistry, National University of Ireland - Galway). We both contributed to compiling the relevant scientific literature pertaining to the application of Raman spectroscopy for the analysis of blood components. I completed the bulk of the writing. Editorial suggestions were made by Georg Schulze (Michael Smith Laboratories, The University of British Columbia) and my supervisors, Michael Blades and Robin Turner. This portion of Chapter 2 has been accepted to the journal *Applied Spectroscopy* for publication as a focal point review article.

Chapter 3 was a collaborative research effort between myself, Deborah Chen (Department of Pathology, The University of British Columbia), and Georg Schulze. I formulated the research plan, experimental Raman data was acquired solely by myself, and data processing occurred with guidance from Georg Schulze. Morphology measurements were performed solely by Deborah Chen. The chapter was written by myself with input from Georg Schulze. Revisions and edits were done by myself, Georg Schulze, Michael Blades, and Robin Turner. Chapter 3 will be submitted to a spectroscopy journal for publication.

Chapter 4 represents an alternative sampling approach to the work presented in Chapter 3. The research plan was formulated solely by myself and the experimental data was acquired solely by myself, with samples provided by Deborah Chen. Data analysis was done by myself, Kevin Buckley, and Georg Schulze. The chapter was written by myself, with input from Kevin Buckley and Georg Schulze. Revisions and edits were done by all parties involved, including Dana Devine (Department of Pathology, The University of British Columbia) and my supervisors, Michael Blades and Robin Turner. Chapter 4 is the combination of a conference proceeding and a published manuscript:

Atkins, C. G.; Buckley, K.; Chen, D.; Schulze, H. G.; Devine, D. V.; Blades, M. W.; Turner, R. F. B. Raman Spectroscopy of Stored Red Blood Cells: Evaluating Clinically Relevant Biochemical Markers in Donated Blood. *Proc. of SPIE – Clinical and Biomedical Spectroscopy and Imaging IV* **2015**, 9537, 95370X-95370X-7.

Atkins, C. G.; Buckley, K.; Chen, D.; Schulze, H. G.; Devine, D.V.; Blades, M. W.; Turner, R. F. B. Raman Spectroscopy as a Novel Tool for Monitoring Biochemical Changes and Inter-Donor Variability in Stored Red Blood Cell Units. *Analyst* **2016**, 141, 3319-3327.

Chapter 5 is a continuation of previous chapters. The research plan was jointly formulated by Kevin Buckley and myself, and we both contributed to the collection of Raman data. The chapter was written by Kevin Buckley and myself, with input from Georg Schulze. As before, revisions and edits were done by all authors, including Dana Devine and my supervisors, Michael Blades and Robin Turner. The work from Chapter 5 has been previously published:

Buckley, K.; Atkins, C.G.; Chen, D.; Schulze, H. G.; Devine, D. V.; Blades, M. W.; Turner, R. F. B. Non-Invasive Spectroscopy of Transfusable Red Blood Cells Stored Inside Sealed Plastic Blood-Bags. *Analyst* **2016**, *141*, 1678-1685.

Ethics approvals were necessary before research with human blood could begin. The procedures were initially approved by the Clinical Research Ethics Board (CREB) at The University of British Columbia, Office of Research Services on July 14th, 2011 (UBC CREB Number H11-00992), and by the Biosafety Ethics Board at The University of British Columbia, Biosafety Committee (B15-0114). The project also received the approval of the Research Ethics Board of Canadian Blood Services.

Table of Contents

Abstract.....	ii
Preface.....	iv
Table of Contents	vii
List of Tables	xiii
List of Figures.....	xiv
List of Abbreviations	xxiv
Acknowledgements	xxviii
Dedication	xxx
Chapter 1: Introduction	1
1.1 Preamble	1
1.2 Basics of Blood Chemistry	2
1.2.1 Red Blood Cells	3
1.2.1.1 RBC Membrane	4
1.2.1.2 RBC Metabolism	6
1.2.1.2.1 Influence of RBC Oxygenation State.....	8
1.2.1.3 Hemoglobin.....	9
1.2.1.4 <i>In Vivo</i> RBC Life Cycle and Breakdown.....	13
1.2.1.5 Abnormalities, Pathologies, and Vulnerabilities	14
1.3 Blood Banking and RBC Transfusion Medicine	17
1.3.1 Properties of Blood Storage	18
1.3.2 RBC Storage Lesion	21

vii

1.3.2.1	Metabolic Storage Lesion	22
1.3.2.2	Enzymatic Storage Lesion	22
1.3.2.3	Oxidative Storage Lesion.....	23
1.3.2.4	Physiological Storage Lesion.....	23
1.3.3	Health Risks Associated with Stored RBCs	24
1.3.3.1	Clinical Trials.....	25
1.3.3.2	Controversy	25
1.3.4	Administration of Blood Transfusion	27
1.4	Storage-Related Problems in Current Blood Banking Practice	28
1.5	Assessing RBC Blood Quality.....	29
Chapter 2: Raman Spectroscopy and its Application to the Analysis of Blood		30
2.1	Optical Spectroscopy	30
2.2	Molecular Energetics	30
2.3	Molecular Vibrations	33
2.4	The Raman Effect	34
2.4.1	Classical Derivation of the Raman Effect.....	38
2.5	General Raman Instrumentation	42
2.6	Advantages and Disadvantages of Raman Spectroscopy	46
2.7	Application of Raman to Blood	48
2.7.1	Blood Research and Raman Instrumentation.....	49
2.7.1.1	Enhanced Raman Spectroscopy	50
2.7.2	Literature Review of Published Applications	51
2.7.2.1	Hemoglobin and RBCs	51

2.7.2.1.1	Isolated Hemoglobin	51
2.7.2.2	Raman Studies of Intact RBCs	57
2.7.2.2.1	Intracellular Hemoglobin	57
2.7.2.2.2	Laser Tweezers Raman Spectroscopy of Hemoglobin and RBCs	60
2.7.2.2.3	RBC Membrane.....	62
2.7.2.2.4	RBC Cellular Biology	63
2.7.2.2.5	RBC Transfusion.....	64
2.7.2.3	Hemoglobin, RBCs, and Disease.....	64
2.7.2.3.1	Malaria	65
2.7.2.3.2	Genetic Blood Disorders	68
2.7.2.3.3	Other Diseases and Disorders	69
2.7.2.4	White Blood Cells.....	71
2.7.2.4.1	Introduction and General Appearance of Raman Spectrum.....	71
2.7.2.4.2	Cancer and Disease	76
2.7.2.5	Platelets	78
2.7.2.6	Plasma and Serum.....	80
2.7.2.6.1	Screening for Metabolites and Other Chemical Species	81
2.7.2.6.2	Cancer.....	86
2.7.2.6.3	Other Diseases.....	90
2.7.2.7	Whole Blood	92
2.7.2.7.1	Introduction and General Appearance of Raman Spectrum.....	92
2.7.2.7.2	Forensic Science.....	95
2.7.2.7.3	Disease Detection.....	97

2.7.2.7.4	<i>In Vivo</i> Raman Analysis of Blood.....	98
2.7.2.8	Conclusions and Future Directions	102
2.7.2.8.1	Limitations in Blood Raman Research	104
2.7.2.8.2	Statistical Power Derived from Experiments	104
2.7.2.8.3	Direction of the Field	105
Chapter 3: Interrogating Ageing Effects and Quality in Banked Red Blood Cells		107
3.1	Introduction.....	107
3.2	Experimental	110
3.2.1	Blood Collection and Sampling	110
3.2.1.1	Dry-Fixed Smear Analysis.....	111
3.2.1.2	Bulk RBC Analysis.....	111
3.2.1.3	Morphological Index.....	113
3.2.2	Data Collection	114
3.2.3	Data Processing.....	116
3.3	Results and Discussion	117
3.3.1	Raman Spectrum of Dry-Fixed Smears	117
3.3.2	Raman Spectrum of Liquid Samples	123
3.3.3	Stored RBC Quality	126
3.3.4	Raman Spectra and Stored RBC Quality	128
3.4	Conclusions.....	137
Chapter 4: Raman Spectroscopy as a Novel Tool for Monitoring Biochemical Changes and Inter-Donor Variability in Stored Red Blood Cell Units		139
4.1	Introduction.....	139

4.2	Experimental	141
4.2.1	Blood Collection	141
4.2.2	Supernatant Preparation	141
4.2.3	Data Collection	142
4.2.4	Data Processing and Analysis	143
4.3	Results and Discussion	143
4.3.1	Raman Spectrum of Stored RBC Supernatant	143
4.3.2	Variation with Storage Time.....	148
4.3.3	Quantification of Lactate	154
4.3.4	Interpretations of Donor Characteristics and Variability.....	156
4.3.5	Future Directions	159
4.4	Conclusions	161
 Chapter 5: Non-Invasive Spectroscopy of Transfusable Red Blood Cells Stored Inside		
Sealed Plastic Blood-Bags.....		162
5.1	Introduction.....	162
5.2	Experimental	164
5.2.1	Blood Collection	164
5.2.2	Data Collection and Processing	166
5.2.2.1	Collection of SORS Data	166
5.2.2.2	Collection of Supporting Data	167
5.3	Results.....	168
5.4	Discussion	177
5.4.1.1	Oxygenation State of Hemoglobin.....	177

5.4.1.2	Relationship Between Storage Lesion and Patient Outcome.....	178
5.5	Conclusions.....	180
Chapter 6: Conclusions and Future Work		181
6.1	Raman Spectroscopy as a Tool for Interrogating Ageing Effects and Quality in Banked Red Blood Cells	181
6.2	Raman Spectroscopy as a Novel Tool for Monitoring Biochemical Changes and Inter-Donor Variability in Stored Red Blood Cell Units	182
6.3	Non-Invasive Spectroscopy of Transfusable Red Blood Cells Stored Inside Sealed Plastic Blood-Bags.....	184
6.4	Outcomes and Future Work	185
6.4.1	Improvement to Clinical Trials	185
6.4.2	Improvement to Transfusion.....	186
6.4.3	Future Work	186
6.4.3.1	Smears of Stored RBCs	186
6.4.3.2	Characterization of Supernatant.....	187
6.4.3.3	Instrument Development.....	187
6.4.3.4	Assessment of Other Blood Products	188
6.5	Summary of Findings and Overall Impact.....	188
References		190

List of Tables

Table 3-1: Gold-standard morphology scoring system. Images and scoring protocol were adopted from Reference 349 and reprinted with permission from John Wiley & Sons, Inc.....	114
Table 3-2: Best fits and corresponding fit parameters for each donor. Power fit curves were of the form $f(x) = a \cdot x^b$, while linear fits were of the form $f(x) = p_1 \cdot x + p_2$	134
Table 4-1: Prominent bands and their respective vibrational modes	146
Table 5-1: A list of the more prominent Raman bands in the SORS spectra	171

List of Figures

Figure 1-1: A tube of fractionated non-coagulated whole blood. The distinct layers of blood shown represent plasma, a buffy coat (WBCs and platelets), and RBCs	3
Figure 1-2: Schematic representation of a healthy RBC membrane. The figure shows a cross-sectional view of the membrane with interactions between peripheral and integral proteins. Adapted and reprinted from Reference 8 with permission from John Wiley & Sons, Inc.	5
Figure 1-3: Image of RBCs taken with a scanning electron microscope at a magnification of $\times 20,000$. Reprinted from Reference 10 with permission from Nature Publishing Group	6
Figure 1-4: Anaerobic glycolysis via the Embden-Meyerhof pathway. The process requires the input of ATP, but produces a net gain of both ATP and lactate. Adapted and reprinted from Reference 12 with permission from SIMTI Servizi srl unipersonale	7
Figure 1-5: Simplified scheme representing the effect of oxygenation state on the RBC metabolism. Note: 2,3-BPG is the same molecule as 2,3-DPG. Reprinted from Reference 13 with permission from SIMTI Servizi srl unipersonale.....	9
Figure 1-6: Hemoglobin structure. On the left, the four subunits (two α chains and two β chains) are shown in their quaternary structure, each with a heme group in a hydrophobic pocket. [©Richard Wheeler, title:1GZX Haemoglobin.png, CC BY-SA 3.0] The chemical structure of the heme group is shown on the right	11
Figure 1-7: Hemoglobin oxygen dissociation curve in the absence of allosteric effectors (dash-dot-dotted line), in the presence of CO_2 (dashed line) and 2,3-DPG (dash-dotted line), and in whole blood (solid line). Note: 1 torr is approximately 1 mmHg. Reprinted from Reference 21 with permission from John Wiley & Sons, Inc.....	12

Figure 1-8: Current production method for separating donated whole blood as implemented nationwide by Canadian Blood Services (CBS) in 2006. In this process, known as the buffy coat production method, multiple “buffy coats” - a mixture of platelets and WBCs - are pooled together to enhance platelet recovery. RBCs are isolated from the primary spinning stage. Adapted and reprinted from Reference 35 with permission from John Wiley & Sons, Inc.	18
Figure 1-9: Cell morphologies of stored RBCs. Reprinted from Reference 64 with permission from Springer International.....	24
Figure 2-1: Jablonski diagram depicting various quantized energy levels for electronic and vibrational states	32
Figure 2-2: Schematic representation of the scattering pathways: (a) Stokes, (b) Rayleigh, and (c) anti-Stokes.....	35
Figure 2-3: A Raman spectrum of the mineral realgar (As_4S_4) is shown in the anti-Stokes and Stokes regions. Even though the Stokes photons represent a loss of energy from the incident light, common convention is to display the transitions on the positive side of the horizontal axis. The intensity of the Rayleigh line (0 cm^{-1}) is suppressed by a holographic filter in the spectrometer. Reprinted from Reference 93 with permission from John Wiley & Sons, Inc.	37
Figure 2-4: Simplified block diagram of the main components in a Raman instrument.....	42
Figure 2-5: Typical schematic of a Raman microspectrometer. The main components are present in the system: laser source, notch filter, diffraction grating, CCD detector	45
Figure 2-6: Resonance Raman spectra of oxyHb as reported in 1972. The scattering geometry is shown schematically at the top of the diagram. Both the direction and the polarization vector of the incident laser radiation are perpendicular to the scattering direction. The scattered radiation is analyzed into components perpendicular (I_{\perp}) and parallel (I_{\parallel}) to the incident polarization vector.	

The exciting wavelength was 568.2 nm and concentrations ~0.5 mM. Reprinted from Reference 110 with permission from the author	53
Figure 2-7: Resonance Raman spectra of hemoglobin, Hb- ¹⁶ O ₂ and Hb- ¹⁸ O ₂ at 15°C, pH 7.4, 488 nm excitation. The band at 567 cm ⁻¹ appeared when hemoglobin was oxygenated, and shifted when oxygenated with an isotope. This mode was assigned to Fe-O ₂ stretching. Reprinted from Reference 112 with permission from Springer-Verlag	55
Figure 2-8: Raman spectra of oxygenated single erythrocytes recorded using different excitation wavelengths. The spectra presented are averaged from four spectra of different erythrocytes under the same conditions. Reproduced from Reference 144 with permission from John Wiley & Sons, Inc.....	59
Figure 2-9: Photomicrograph of <i>P. falciparum</i> -infected erythrocytes (late trophozoite stage) showing the food vacuoles containing hemozoin. The arrows indicate the laser targets, namely the food vacuole and the surrounding hemoglobin. The corresponding spectra are compared with synthesized β-hematin. Reproduced with permission from Fig. 2 in Reference 189. Permission provided by Elsevier	66
Figure 2-10: The spectra of a single intact granulocytes as obtained by Puppels et al. The data confirmed the difference between the cytoplasm (spectrum A) and the nucleus (spectrum B) in the same cell. Spectrum C is from a chromatid of a Chinese hamster lung cell and functions to confirm the similarity of the chromatid to the nucleus spectrum in B whose contributions are subsequently confirmed to be mainly DNA and protein. Reprinted from Reference 212 with permission from Macmillan Publishers Ltd: Nature, Copyright (1990).....	72
Figure 2-11: Morphological characteristics of the different WBCs (neutrophil: A and E, eosinophil: B and F, monocyte: C and G, lymphocyte: D and H) are displayed visually in the	

images presented on the left and averaged Raman spectra of the cytoplasm, nucleus, and background region are plotted on the right. Reprinted with permission from Reference 223.

Copyright (2012) American Chemical Society..... 74

Figure 2-12: Plot for the Raman difference spectroscopy results (647 nm excitation) for cell spectra of first image minus other images showing variations in the carotenoid molecules (a) image 1 to image 2, (b) image 1 to image 3, (c) image 1 to image 4, (d) image 1 to image 5, (e) image 1 to image 6, (f) image 1 to image 7, (g) image 1 to image 8, (h) image 1 to image 9 and (i) image 1 to image 10. As the carotenoid cellular content decreases, the carotenoid bands increase in the difference spectra. Adapted from Reference 224 with permission from John Wiley & Sons, Inc..... 75

Figure 2-13: Mean Raman spectra of WBCs compared to various leukemia (OCI-AML3) and tumor (BT-20, MCF-7) cell lines measured with a dedicated microfluidic glass chip. Spectra were background corrected and normalized and the grey region were used in the statistical analysis by the authors. Reproduced from Reference 228 with permission from The Royal Society of Chemistry..... 77

Figure 2-14: Mean Raman spectra of single platelets and tentative peak assignments (abbreviations: Phe, phenylalanine; Tyr, tyrosine; Trp, tryptophan; Pro, proline). Reprinted from Reference 237 with permission..... 80

Figure 2-15: Early Resonance Raman (514.5 nm excitation) work showing enhanced vibrational spectra of a) blood plasma (heparin, subjects fasted 12 h), b) petroleum ether extract of alcohol-denatured blood plasma in chloroform, and c) β -carotene in chloroform. Reproduced with permission from Fig. 1 in Reference 243. Permission provided by Elsevier 82

Figure 2-16: (a) Normalized mean SERS spectra of blood plasma from 60 normal, 25 early stage nasopharyngeal cancer (T1) and 75 later stage nasopharyngeal cancer (T2-T4) patients. (b) Difference spectra calculated from the mean SERS spectra among the three groups. Reproduced from Reference 271 with permission from Macmillan Publishers Ltd: Scientific Reports, Copyright (2014).....	89
Figure 2-17: Raman spectra (1064 nm excitation) from blood constituents. Reproduced with permission from Fig. 8 in Reference 293. Permission provided by Elsevier	94
Figure 2-18: Sample resonance Raman spectra of one animal showing the dynamic changes in the deoxy and oxyhemoglobin spectral peaks in response to hemorrhage. Note the progressive changes in the deoxy- and oxyhemoglobin spectral peaks in relationship to each other indicating a greater percentage of deoxyhemoglobin as hemorrhage progresses. Reprinted from Reference 326 with permission from Wolters Kluwer Health, Inc.....	100
Figure 3-1: Experimental method of dry-fixed smear. A drop of stored RBCs was deposited onto a gold-coated slide and smeared across that slide using a spreader slide. The cells were then dry-fixed under a stream of air.	111
Figure 3-2: Experimental method for the bulk RBC analysis. A glass microscope double-welled-slide is shown on the left and a cross-section of a single-welled-slide is shown on the right. ~200 μL of a stored RBC sample is added into the well which is then isolated from atmosphere using a coverslip slide.	112
Figure 3-3: Shown are three averaged spectra collected from the liquid RBCs of Donor 34 over an extended period of accumulation time. The same sample region is analyzed for all 45 accumulations. The inset is a magnified view of the $1200\text{-}1230\text{ cm}^{-1}$ region.	116

Figure 3-4: (A) A bright-field microscope image showing clusters of RBCs that have aggregated together during the fixation process. The inset depicts the edge of the smear at a single-cell level.	
(B) The average (10 accumulations, 100 second accumulation each) Raman spectrum of (powdered) hemoglobin is shown vertically offset while the average Raman spectra of dry-fixed smears for 5 different donors are also shown. The inset depicts the variation for the bands found in the 1520-1680 cm^{-1} region for the donors	119
Figure 3-5: The progression of storage for RBC samples from two donors, Donor 1 (top) and Donor 6 (bottom), using the smear technique.....	121
Figure 3-6: (A) Spectra obtained from stored liquid RBCs (2 days of storage) for three different donors are presented. The inset is a magnification of the 1500-1660 cm^{-1} region. The excitation beam was focused through the coverslip and into the turbid media. (B) The effect of storage length is shown for these three donors by inspection of the oxygenation marker band region of 1200-1230 cm^{-1}	123
Figure 3-7: The ratio of marker bands (1208 cm^{-1} /1222 cm^{-1}) associated with hemoglobin oxygenation states as determined from the stored liquid RBC analysis. The inset highlights the trends for Donors 40 and 42.....	126
Figure 3-8: The absolute morphology index results for seven donors. Counts were done in duplicate and these scores were within $<\pm 5\%$. The regression lines were obtained using power-curve fits.....	128
Figure 3-9: A cross-correlation plot of the morphological index (MI) and the oxygenation state (OS). Data was included only if time-points were comparable (± 1 day).	129
Figure 3-10: Complete data set obtained for Donor 39. The top row depicts plots related to MI scores while the bottom row presents the OS ratios. Column A represents plots of the raw data,	

Column B represents the fitting process used to match the storage range, and Column C is the final data. Power fit and linear fit curves are shown in each case.	131
Figure 3-11: Morphology scores and spectral ratios are normalized and compared. Circle data points are the morphology scores and triangles represent the normalized spectral ratios for all donors.....	132
Figure 4-1: (A) A bright-field image showing the uneven topography of a typical drop of supernatant. (B) The average (10 spectra, 100 second accumulation each) Raman spectrum of RBC supernatant after two days of storage (in black), a Raman spectrum of pure SAG-M solution (in blue), and a Raman spectrum of (powdered) hemoglobin (in red); both supernatant and hemoglobin spectra show contributions from the internal porphyrin ring and from the amide modes (753 cm^{-1} , $1500\text{-}1600\text{ cm}^{-1}$).....	144
Figure 4-2: Distribution of two distinct spectral features across the width of a dried-drop supernatant sample after two days of storage. The x-axis approximately corresponds to Figure 4-1A; the drop looks inhomogeneous but the <i>chemical composition</i> across the drop is uniform for the chemicals of interest.....	148
Figure 4-3: (A) The development of the supernatant spectrum over the course of a 42 day storage-period. The dominant spectral change is the increase in band-intensity at 853 cm^{-1} . (B) and (C) show PCA and BTEM analyses of the whole data set (all donors, all time-points) that isolate other spectral changes that are associated with the 853 cm^{-1} band. (D) is a Raman spectrum of pure sodium lactate.	149
Figure 4-4: (A) The change in relative intensity of the 853 cm^{-1} (lactate) band with storage age for two (randomly chosen) donors (donor 9 and donor 18) is shown for all supernatant sample	

points. (B) The average value of the lactate band at each time-point is shown for all 30 donors (bars are \pm std. dev.).....	151
Figure 4-5: Every supernatant spectrum has a contribution (or ‘loading’) from the first PCA eigenvector shown in Figure 4-3B, the average contribution increases with storage age, and the variability between donors (the std. dev.) increases from (approximately) day 21	153
Figure 4-6: The current practice is to use 'fresh' blood (≤ 8 days) for very ill infants. The Raman supernatant data shows that lactate content can vary by a factor of approximately two after 8 days (each data point is measurement of a single individual at a single time-point).....	154
Figure 4-7: The comparison of Raman spectral intensity for the 853 cm^{-1} lactate band with traditional quantification of lactate concentration as determined by a YSI analyzer.	156
Figure 4-8: Intensity changes of the 853 cm^{-1} lactate band for females (reds) and males (blue) reveal gender-related differences in lactate dynamics during storage. Separate gender-based linear fits show that lactate levels in blood from female donors increase more slowly than in blood from male donors	157
Figure 4-9: Intensity changes of the 853 cm^{-1} lactate band for younger females (light red), older females (red), younger males (light blue), and older males (blue). Linear fits suggest both age- and gender-related differences. The slowest lactate increases in stored RBCs occur for younger females	158
Figure 5-1: A standard bag of transfusable RBCs in a PVC blood-bag (the white panel obscures barcodes and identification-labels).	165
Figure 5-2: Position A is the set-up for collecting a conventional Raman spectrum with the laser line centered on the microscope’s focal point (the cross-hairs). In order to collect a SORS	

spectrum, the laser illumination line was moved 200 μm away from the focal point using the beam-steer alignment mirrors (Position B)..... 167

Figure 5-3: The schematic diagram of a blood-bag on the left shows two different experimental geometries: conventional Raman spectroscopy, in which the backscattered light is from the laser illumination point (geometry A) and SORS, in which the collection point is laterally offset from the laser illumination point by 200 μm (geometry B). The plots on the right show the corresponding spectral data..... 169

Figure 5-4: The SORS spectrum of the blood-bag contents (from Figure 5-3; top trace) plotted with a conventional Raman spectrum of RCC (i.e., the contents of a blood-bag; bottom trace). Both spectra exhibit many of the same Raman bands, in particular those associated with hemoglobin 170

Figure 5-5: A) A comparison between a SORS spectrum of 27 day old RBCs and a SORS spectrum of 1 day old RBCs (from a different donor). B) Emphasis on spectral features related to oxygenation in the 1200-1650 cm^{-1} region, the increase in intensity of the bands at $\sim 1212 \text{ cm}^{-1}$ and $\sim 1547 \text{ cm}^{-1}$ (dotted lines) reveal that the 1 day old RBCs are oxygenated and the 27 day old RBCs are partially deoxygenated. The Raman features associated with molecular bonds that do not change confirmation or position with oxygenation, are unchanged 173

Figure 5-6: The data from each bag were decomposed with multivariate (Principal Component) analysis. The primary difference between the spectra (the first eigenvector) was associated with oxygenation/deoxygenation, as shown in the bottom panel in Figure 5-7. The degree to which each spectrum is dominated by this eigenvector is plotted here. The large scatter and absence of any simple relationship is discussed below 175

Figure 5-7: Certain regions of the RBC spectrum are seen to vary with oxygenation (see Figure 5-5). The eigenvector which correlates with oxygenation-changes is plotted in the bottom panel. The top panel shows Donor 1, an example of an RBC unit where oxygenation decreases with storage age (spectra are on the left and the trend from Figure 5-6 is on the right). The middle panel shows Donor 14, an example of an RBC unit where oxygenation increases with storage age (again, spectra are on the left and the trend from Figure 5-6 is on the right). 176

List of Abbreviations

1,3-DPG	1,3-diphosphoglycerate
2,3-DPG	2,3-diphosphoglycerate
2PG	2-phosphoglycerate
3PG	3-phosphoglycerate
AFM	Atomic force microscopy
ANOVA	Analysis of variance
AS	Additive solution
ATP	Adenosine 5'-triphosphate
ADP	Adenosine diphosphate
BTEM	Band target entropy minimization
CARS	Coherent anti-stokes Raman spectroscopy
CBS	Canadian Blood Services
CCD	Charge-coupled device
CDB3	Cytoplasmic domain of Band 3
CI	Confidence interval
CRP	C-Reactive protein
deoxyHb	Deoxygenated hemoglobin
DNA	Deoxyribonucleic acid
DHAP	Dihydroxyacetone phosphate
F-1,6-BP	Fructose-1,6-bisphosphate
FDA	Food and Drug Administration

GAP	Glyceraldehyde 3-phosphate
G6PD	Glucose-6-phosphate dehydrogenase
GSH	Glutathione
GSSG	Glutathione disulfide
Hb	Hemoglobin
HbA	Normal adult hemoglobin
HbA _{1c}	Glycated normal adult hemoglobin
HIV	Human immunodeficiency virus
HOS	High oxygenation state
Ig	Immunoglobulin
IR	Infrared
LOS	Low oxygenation state
LTRS	Laser tweezers Raman spectroscopy
metHb	Methemoglobin
MI	Morphological index
MPO	Myeloperoxidase
NAD	Nicotinamide adenine dinucleotide
NADPH	Nicotinamide adenine dinucleotide phosphate
NMR	Nuclear magnetic resonance
NPC	Nasopharyngeal cancer
OS	Oxygenation state
oxyHb	Oxygenated hemoglobin
PCA	Principal component analysis

PEP	Phosphoenolpyruvic acid
PFK	Phosphofructokinase
Phe	Phenylalanine
PO ₂	Partial pressure of oxygen
PPP	Pentose phosphate pathway
Pro	Proline
PVC	Polyvinyl chloride
RBC	Red blood cell
RCC	Red cell concentrate
RNA	Ribonucleic acid
ROS	Reactive oxygen species
RRS	Resonance Raman spectroscopy
RS	Raman spectroscopy
SAG-M	Saline-adenine-glucose-mannitol
SCD	Sickle cell disease
SEM	Scanning electron microscopy
SERS	Surface-enhance Raman spectroscopy
SESORS	Surface-enhanced spatially offset Raman spectroscopy
SIRS	Systematic inflammatory response system
SOD	Superoxide dismutase
SORS	Spatially offset Raman spectroscopy
SVR	Support vector regression
TCRS	Turbidity-corrected Raman spectroscopy

TERS	Tip-enhanced Raman spectroscopy
Trp	Tryptophan
Tyr	Tyrosine
UV	Ultra-violet
UVRRS	Ultra-violet resonance Raman spectroscopy
WBC	White blood cells
WNV	West Nile virus

Acknowledgements

Within the walls of graduate school, there can often be internal stress to publish meaningful research and advance through the traditional academic career ladder. I am thankful to my supervisors, Robin Turner and Michael Blades, for providing me with the flexibility to avoid this stress and explore my own interests, both inside and outside of the laboratory. From the moment I sat down with these two gentlemen, I knew I had discovered the people who would mentor me through the course of my degree.

There are several other research colleagues deserving of special thanks: Chris Sherwood, for support with any biological or cell-based problem I had; Stanislav Konorov, for demonstrating what it means to be a dedicated scientist; Georg Schulze, for never simply giving me the answer to a question without pushing the boundaries of my knowledge, both as a scientist, but also as a person (Georg, I think the next lunch is on me); Deborah Chen, for constantly taking time out of her own schedule to lend me a hand; and Kevin Buckley, for introducing Irish slang into my vocabulary (often in the presence of hoodie girl and a lunch-time sambo).

I am indebted to the organizations that were kind enough to provide financial assistance over the course of my degree: NSERC, the Walter C. Sumner Foundation, The Killam Trusts, Metrohm USA, and the Society for Applied Spectroscopy.

I believe that comprehension of a topic is best demonstrated when you have the ability to explain it well to others. I have had the privilege of working with many fantastic educators over the course of my degree, and their influence has helped shaped my impressions of what it means to be a good instructor. Jane Maxwell, Dan Bizzotto, and Robin Stoodley, the dedication you demonstrate in creating a successful learning atmosphere for your students is admirable; working

with you was a pleasure. Robin, observing your behavior and mannerisms in the labs helped mold my own philosophies towards teaching and student interaction.

Those who are close to me know that loyalty is a trait I significantly value in my friends. Over the course of this degree, there are several people who have always been supportive. Benjamin Loosely and Spencer Serin, “All for one, and one for all” (no, I am not made up of D-amino acids). Jared Stang and Thomas Depew, it was a pleasure to converse with you on the way to hockey games. To the rest of the Black Aces, it was a heck of a ride. Chris Joblin, thank you for providing me with a couch to sleep under and a kitchen floor to sleep on. JFo, thanks for letting me behave like your older brother. Margaret Wu, thanks for being you. Brad Hutton, thanks for the drinks. Shawn O’Neill, Joel VanderMarel, and Ali “Tugboat” Hussain (the roommates and Team Sub Four), I felt privileged to wear team socks and was always proud to bring up the rear. Ali and Jen, I’m grateful to have been a part of your adventure with Ila.

I would be remiss if I neglected to thank those who have been fixtures for me despite considerable distance between us. Jon Creelman, you’ve had my back since we rolled together on Smith Avenue. Patrick McIssac, Adam Woodland, Prince Smith, Justin Warren, you always remind me why I’m proud to be a Newfoundlander.

To all these friends, I quote the great Dominic Toretto: “I don’t have Friends. I got Family. Ride or Die.”

Finally, Uncle Paul, Aunt Joanne, Mitchel, Justin, and Frosty, thanks for supporting me every step of the way. To my parents: I don’t know if you’ve ever truly understood what it is I do, or why I chose to spend the entirety of my twenties as a student of science, but you’ve never made me feel guilty for walking my own path. For that, I cannot say Thank You enough. Garry, Audrey, and my sister Krista, this would not have happened without you. <3

“The purpose of literature is to turn blood into ink”

T.S. Eliot

To all the blood that has made this possible

Chapter 1: Introduction

1.1 Preamble

The safe and effective transfusion of stored red blood cells (RBCs) is the cornerstone of modern health care, and has been the core of transfusion therapy for nearly a century.¹ The utility of RBC transfusion as a crucial component to medical care brought about the advent of the blood bank and its ability to stock an inventory of blood products. Decades of research has resulted in the improvement of storage conditions that extend the lifespan of stored RBCs, and current regulatory conditions in Canada permit storage of a particular unit for up to 42 days. Despite the significant progress that has been made in the field of RBC storage, blood banks lack efficient methods to determine the quality of stored RBCs. The research objective of this thesis was to demonstrate that Raman spectroscopy can be used to measure changing biochemical features associated with stored RBCs and that such measurements can be done rapidly, non-destructively, and non-invasively, without breaching the sterility of the storage bag.

Raman spectroscopy is an analytical method useful for the analysis of biological systems, including that of intact cells, tissues, and biological fluids.² All active vibrational modes of each constituent present in the sample are simultaneously observed through vibrational frequencies dependent upon molecular bonds and their local environment. In turn, the corresponding vibrational spectra are complex and provide insight into distinct features of molecular structure. Such insight for blood and its individual components, as determined by Raman spectroscopy, is reviewed in section 2.7 of Chapter 2.

The particular strength of Raman spectroscopy in the context of blood is its potential to provide structural information in a non-invasive manner, by measuring vibrational features of an

analyte through the side of an enclosure or through a physical barrier. This thesis represents the first demonstration of the Raman technique to assess stored RBCs, and describes progress towards a non-invasive Raman analysis capable of measuring stored RBCs through the side of their plastic barrier. The following sections of this introductory chapter will provide background information on the biology of RBCs as it pertains to details that are emphasized in the research chapters.

Specifically, in Chapter 3, oxidative damage and its effects on the RBC membrane, hemoglobin, and morphology are explored as efforts are made to measure the loss of overall cell quality using Raman. The metabolic pathways associated with RBCs are introduced below in section 1.2.1.2, and the progression of these pathways during storage conditions is assessed in Chapter 4. The preliminary results of Chapter 5 demonstrate potential to discern the oxygenation state of hemoglobin from non-destructive, through-plastic measurements of stored RBC units. The final chapter contains concluding remarks and describes the future direction of the methodology as it applies to RBCs and related blood components.

1.2 Basics of Blood Chemistry

Blood is a bodily-fluid that constantly circulates through the heart and blood vessels. Transportation is one of its main responsibilities, as it delivers necessary substances such as oxygen and nutrients to tissues and carries waste products to the lungs, liver, and kidneys for removal from the body.³ It is composed of three different cellular components (outlined below) which each have distinct roles in maintaining the body's health.

When extracted from the body, the natural response of blood is formation of a clot. If the removed blood is instead mixed with an anticoagulant, the cellular components will gradually fractionate into three discrete layers based on their relative density (Figure 1-1): the top phase

(comprising ~55% of total blood volume) is called plasma and is a pale yellow aqueous matrix comprising all non-corpuscular components of whole blood; the middle layer (<1% of total blood volume) is referred to as a buffy coat (due to its yellowish-white, or ‘buff’, color) and is composed of white blood cells (WBCs) and small cell-like fragments, called platelets; and the bottom layer (~45% of total blood volume) is red in color and is composed of RBCs. The research chapters presented in this thesis all relate specifically to this RBC fraction.

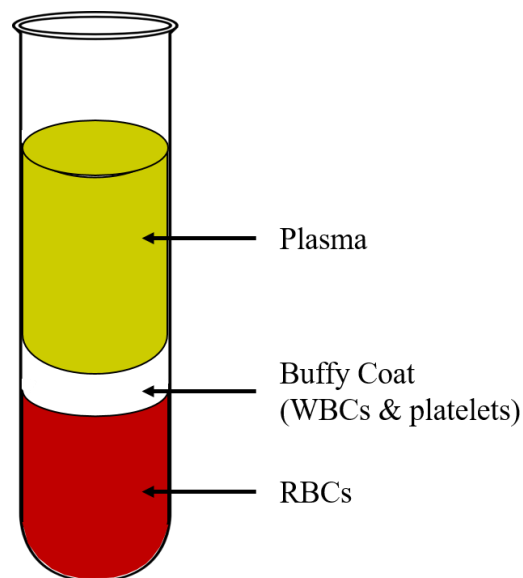


Figure 1-1: A tube of fractionated non-coagulated whole blood. The distinct layers of blood shown represent plasma, a buffy coat (WBCs and platelets), and RBCs.

1.2.1 Red Blood Cells

RBCs are the most abundant type of blood cells, and the typical human red cell has a mean diameter of 8 μm , a thickness of 2 μm , a surface area of 140 μm^2 , and a volume of 90 fL.⁴ Their specific function is transportation of oxygen between the lungs and the tissues. RBCs lack the ability to synthesize proteins due to the absence of traditional cell organelles (e.g., a nucleus,

mitochondria, ribosomes, etc.)⁵ but possess components specialized for gas exchange and gas transport, such as metabolic regulators, hemoglobin, and a cell membrane (see below).

1.2.1.1 RBC Membrane

The RBC membrane separates the internal components of the cell from the surrounding aqueous environment, and its fundamental structure is that of a phospholipid bilayer. More specifically, the membrane is a sheath broadly consisting of lipids (~40%), proteins (~50%), and to a lesser degree, carbohydrates (~10%). Phospholipids are asymmetrically distributed between the two leaflets of the membrane, and lipids on the inner leaflet can be exposed on the outer cell surface during cell distress. As red cells continually pass through the body's numerous capillaries (on the order of 2 to 3 μm), deformability, a characteristic that depends on interactions between the membrane components, is particularly important.⁶

About half of the membrane mass is made up of over 100 different proteins that can all be divided into one of two classes: integral proteins, which span the phospholipid bilayer and are in contact with both sides of the membrane (e.g., Band 3), or peripheral proteins, which form an underlying structural lattice on the inner surface of the membrane (e.g., spectrin and actin).⁷ A schematic of the red cell membrane (Figure 1-2) shows that peripheral proteins attach to the internal ends of the integral proteins; it is the integrated properties of this skeletal structure that generate the disc-shaped, inward-curving morphology of healthy RBCs.

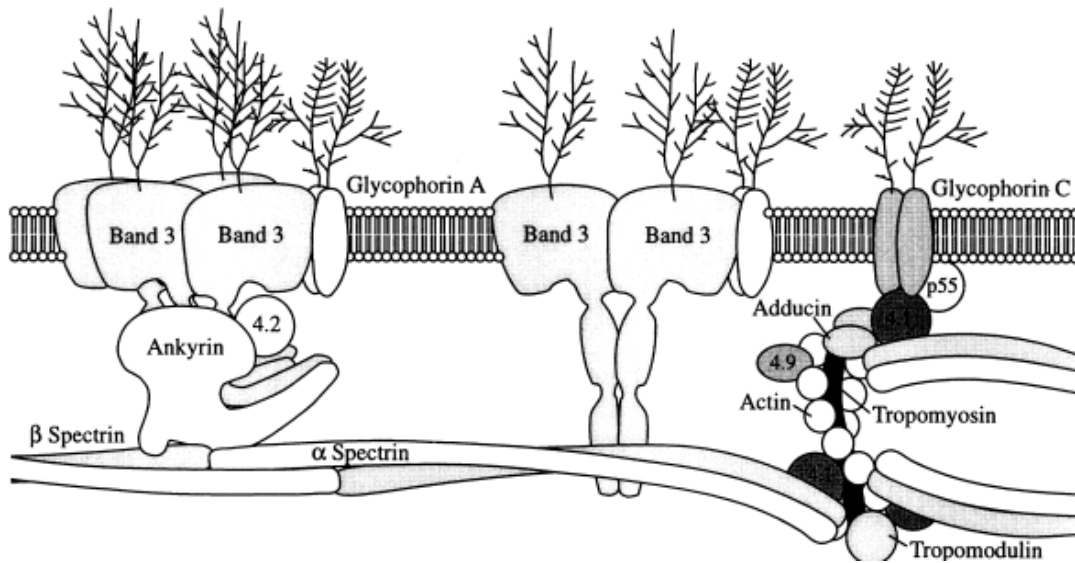


Figure 1-2: Schematic representation of a healthy RBC membrane. The figure shows a cross-sectional view of the membrane with interactions between peripheral and integral proteins. Adapted and reprinted from Reference 8 with permission from John Wiley & Sons, Inc.

This biconcave disc (Figure 1-3) shape of healthy red cells maximizes the cell surface-area-to-volume ratio. Moreover, the RBC membrane is highly elastic, rapidly responds to applied fluid pressures, and has a structural resistance stronger than steel.⁹ Compared to a sphere with the same volume, the surface-area-to-volume ratio of the red cell is 30% higher and this, along with its special membrane properties, permits reversible deformation of the cell and facilitates its gas exchange processes. Any alteration of membrane properties could therefore interfere with optimal RBC function. A variety of means, both normal and pathological, can disrupt the structural and functional integrity of the membrane.

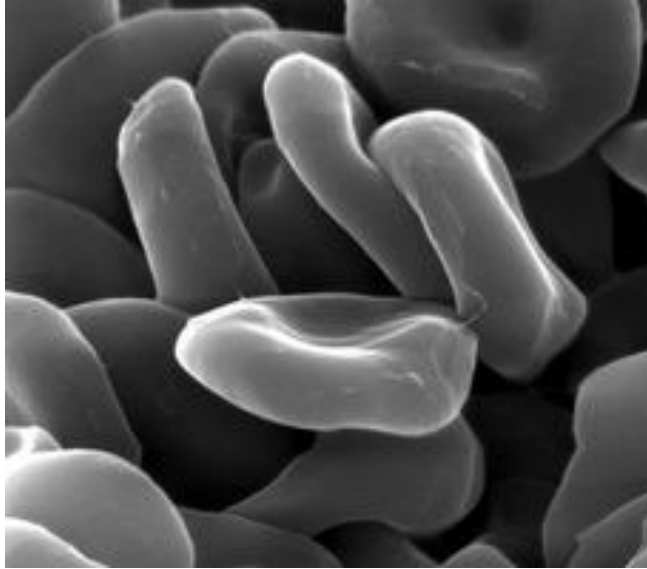


Figure 1-3: Image of RBCs taken with a scanning electron microscope at a magnification of $\times 20,000$. Reprinted from Reference 10 with permission from Nature Publishing Group.

1.2.1.2 RBC Metabolism

RBCs need energy for the maintenance of membrane ion-pumps, for protecting the membrane from oxidative stress, and for preserving the oxidation state of iron atoms integral to oxygen transport (section 1.2.1.3). Without mitochondria, RBCs are unable to generate energy from the citric acid cycle. They instead are reliant on less efficient glycolytic pathways: the Embden-Meyerhof pathway (anaerobic glycolysis, Figure 1-4), the Rapoport-Luebering shunt, the met-hemoglobin (metHb) reductase pathway, and the pentose phosphate pathway (PPP). The activation of these metabolic pathways is dictated by (*in vivo*) changing tissue conditions.

The Embden-Meyerhof pathway is the main metabolic pathway and metabolizes ~90% of the glucose entering the red cell. For every glucose molecule introduced, the net output is 2 molecules of adenosine 5'-triphosphate (ATP), 2 molecules of lactate, 2 molecules of the reduced form of nicotinamide adenine dinucleotide (NADH), and 2 protons. The ATP supplied by this

pathway is responsible for restoring proper morphology and the intracellular ion balances¹¹ that are disturbed when RBCs pass through small capillaries.

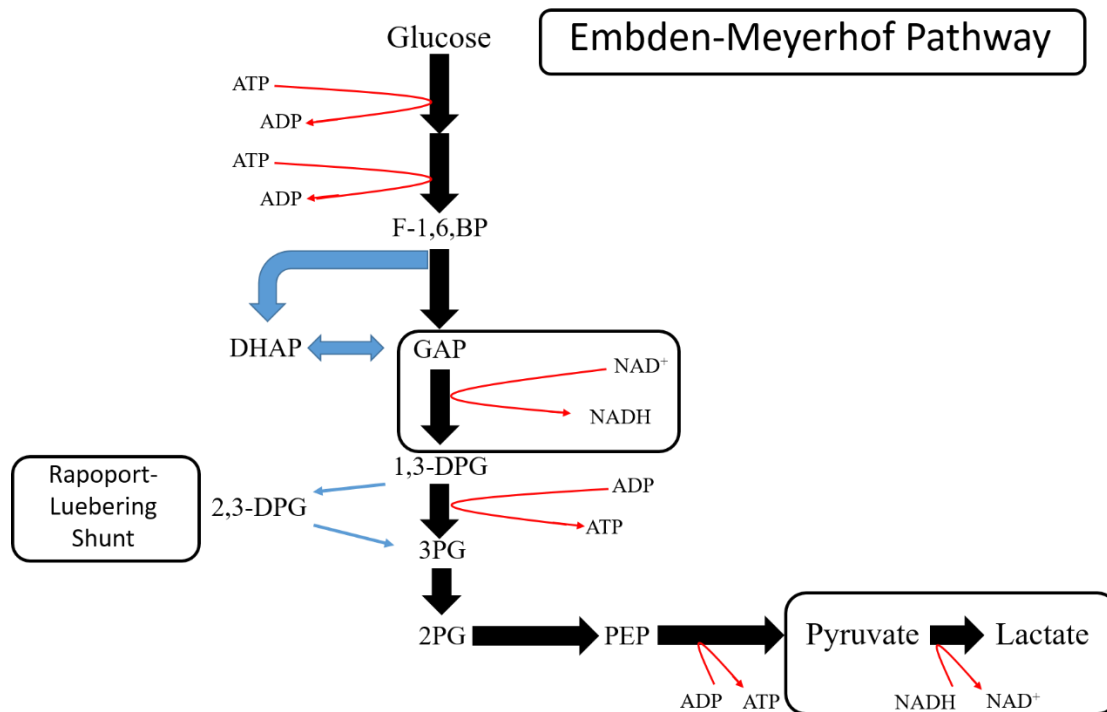


Figure 1-4: Anaerobic glycolysis via the Embden-Meyerhof pathway. The process requires the input of ATP, but produces a net gain of both ATP and lactate. Adapted and reprinted from Reference 12 with permission from SIMTI Servizi srl unipersonale.

The Rapoport-Luebering shunt produces 2,3-diphosphoglycerate (2,3-DPG), an effector molecule that modulates the release of oxygen from the RBC. When venous blood reaches a threshold proportion of deoxygenated RBCs, the glycolysis pathway is shunted to produce more 2,3-DPG, thereby decreasing the RBC affinity for oxygen and allowing more of the gas to be released at any tissue-oxygen tension.⁵ The amount of 2,3-DPG produced depends on an enzyme which is pH-sensitive and causes the rate of glycolysis to increase or decrease as the pH rises or

falls, respectively. The methHb reductase pathway depends on NADH to keep the iron atoms of hemoglobin in their reduced (Fe^{2+}) and active form.

The PPP is activated when glutathione (GSH), a peptide that protects against reactive oxygen species (ROS) and membrane damage, is oxidized. The PPP supplies 2 molecules of the reduced form of nicotinamide adenine dinucleotide phosphate (NADPH). These molecules continuously reconvert oxidized glutathione, as glutathione disulfide (GSSG), back to its reduced form (GSH).

1.2.1.2.1 Influence of RBC Oxygenation State

Activation of the Embden-Meyerhof pathway by enzymes is heavily reliant on the integral membrane protein, Band 3, and intracellular cycling of the cells' oxygenation-deoxygenation states drives the modulation.¹³ When the cell is deoxygenated, its oxygen-carrying component, hemoglobin, binds to Band 3 in preparation for oxygen uptake¹⁴; this creates competition between key metabolic enzymes that bind to Band 3 for activation and ultimately leads to enzyme release from the membrane.¹⁵ Therefore, when glucose enters the cell, its metabolism will follow that of the anaerobic glycolysis pathway, which produces ATP for membrane stability, or the PPP shunt, which produces a sufficient level of NADPH necessary for cell protection from ROS.

In the high oxygenation state (HOS), RBCs are fully oxygenated, the oxygen load is high, and glucose is preferentially metabolized by the PPP to ensure adequate protection from oxidative stress. In the low oxygenation state (LOS), glycolytic enzymes are displaced from the membrane and there is increased glucose consumption via glycolysis, increasing ATP and 2,3-DPG production (Figure 1-5). Overall, the PPP shunt is about two times more active (at any pH) in fully

oxygenated samples.^{16–18} This fact demonstrates the utility in knowing the oxygenation status of RBCs, and hemoglobin oxygenation will be further explored in Chapters 3 and 5.

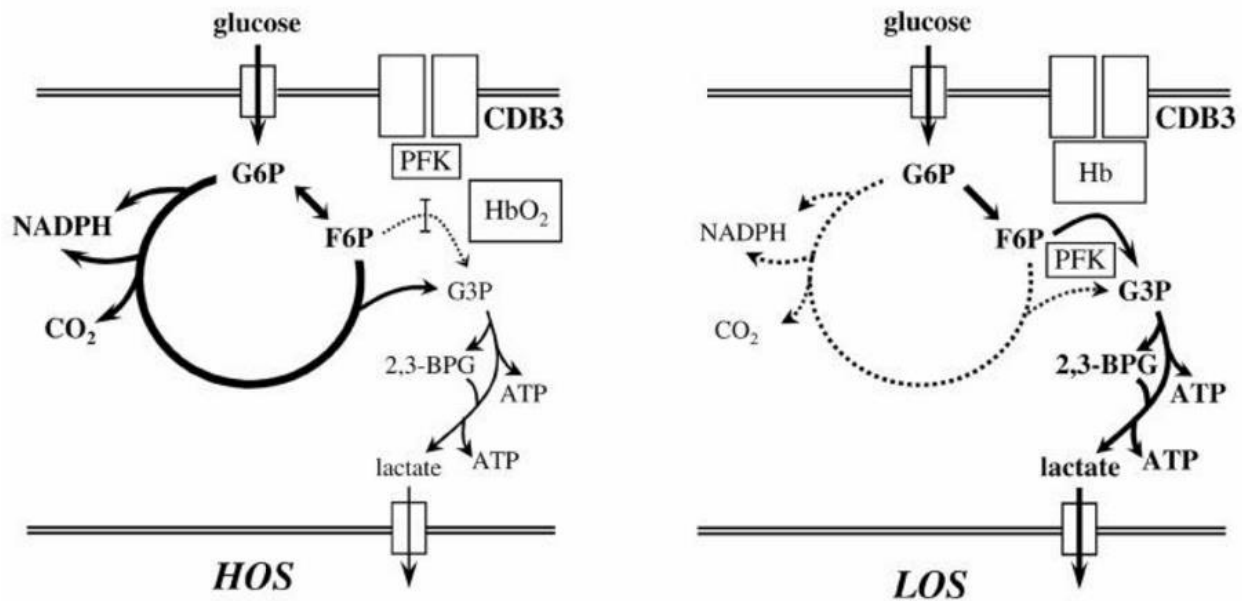


Figure 1-5: Simplified scheme representing the effect of oxygenation state on the RBC metabolism. Note: 2,3-BPG is the same molecule as 2,3-DPG. Reprinted from Reference 13 with permission from SIMTI Servizi srl unipersonale.

1.2.1.3 Hemoglobin

Hemoglobin is the main intracellular component of the red cell, constituting approximately 30% to 34% of its contents by weight,¹⁹ and is solely responsible for the delivery of oxygen. At a hemoglobin concentration of 15 g/dL, 100 mL of whole blood contains ~20 mL of oxygen (at pH = 7.4, T = 37°C, and PO₂ = 100 mmHg). Under basal conditions, approximately 20% to 25% of oxygen transported by red cells is released and the corresponding open binding sites are then occupied by carbon dioxide for transport to the lungs.⁵

Normal type A adult hemoglobin (HbA) comprises >97% of total hemoglobin. HbA is composed of four subunits: two α and two β polypeptide chains with 141 amino acids and 146 amino acids, respectively. Each subunit contains a heme group non-covalently bound in a hydrophobic pocket created by the polypeptide chain (Figure 1-6). Each heme group contains an iron atom coordinated by four nitrogens of a porphyrin ring and a histidine amino acid from one of the subunits (referred to as “proximal histidine”). The sixth coordination iron bond is the site responsible for oxygen binding and is stabilized by another histidine amino acid (referred to as “distal histidine”). The oxidation state of the iron atom is crucial to the functionality of hemoglobin as a carrier of oxygen, and three different models have emerged over the last several decades to describe the behavior of iron through oxygenation cycles. The most recent model, and one that has been supported by experimental results, was proposed by Joseph J. Weiss and describes how an oxygen molecule binds to a low-spin deoxygenated ferrous iron (Fe^{2+}), withdraws an electron to temporarily form a superoxide anion ($\text{O}_2^{\bullet-}$), and forces iron to adopt a low-spin ferric (Fe^{3+}) state. When oxygen is released, the electron is returned to iron, re-forming its low-spin ferrous state. It is this form of iron (low-spin Fe^{2+}) that is capable of reversibly-binding oxygen while an oxidized form of iron (high-spin Fe^{3+}) is not capable of oxygen uptake. As implied in section 1.2.1.2, when hemoglobin contains an iron atom in this Fe^{3+} state, it is referred to as metHb.

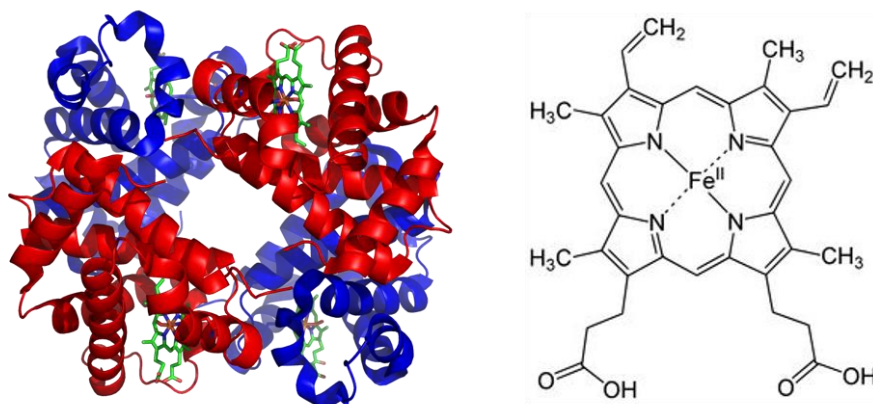


Figure 1-6: Hemoglobin structure. On the left, the four subunits (two α chains and two β chains) are shown in their quaternary structure, each with a heme group in a hydrophobic pocket. [©Richard Wheeler, title:1GZX Haemoglobin.png, CC BY-SA 3.0] The chemical structure of the heme group is shown on the right.

There are two quaternary arrangements of the hemoglobin tetramer that are more stable than all others: one dominates when the iron atoms are saturated with oxygen (oxyHb), and the other prevails when the binding sites are vacant (deoxyHb). The deoxyHb structure is characterized by the presence of salt bridges between subunits, producing a constrained or taut (T) configuration, and the oxyHb conformation breaks these salt bridges, thereby giving the subunits a relaxed (R) form. Furthermore, the tetrameric structure of hemoglobin is believed to be an evolutionary improvement from more basic oxygen-binding proteins, as the uptake of oxygen by one monomer eases uptake by other monomers, and similarly, release of one oxygen facilitates release of the others (i.e., hemoglobin monomers are cooperative).²⁰ This cooperativity explains why the relationship between PO_2 and bound oxygen content is sigmoidal in the hemoglobin

oxygen dissociation curve (Figure 1-7). Without cooperativity, as is the case in some primitive oxygen-binding proteins, the oxygen dissociation curve would exhibit a hyperbolic relationship.

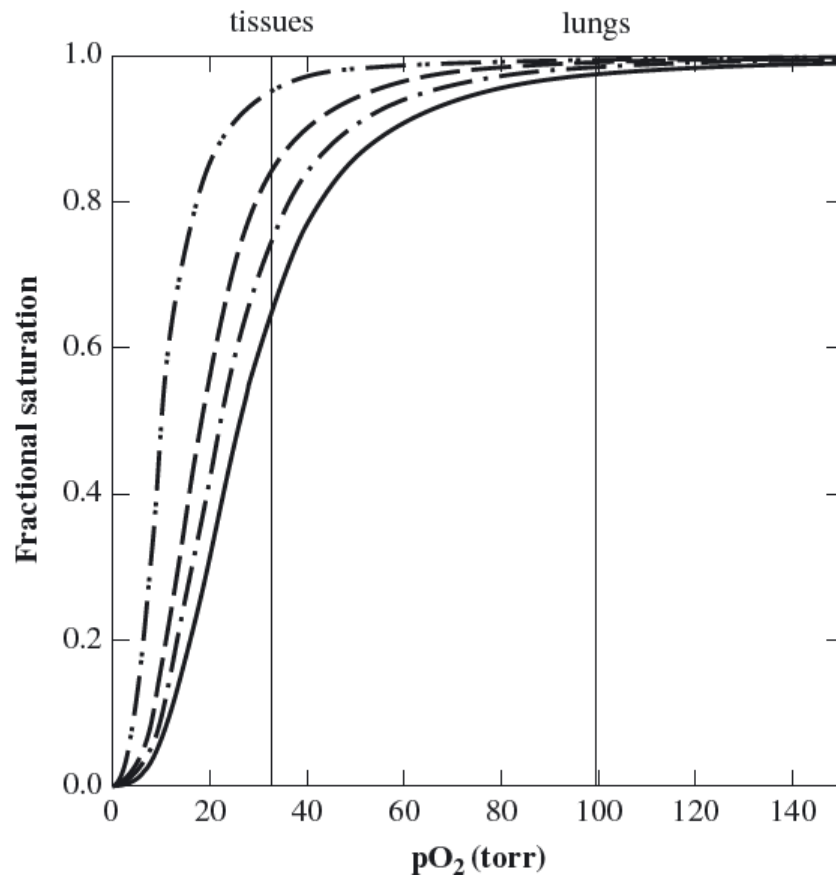


Figure 1-7: Hemoglobin oxygen dissociation curve in the absence of allosteric effectors (dash-dot-dotted line), in the presence of CO₂ (dashed line) and 2,3-DPG (dash-dotted line), and in whole blood (solid line). Note: 1 torr is approximately 1 mmHg. Reprinted from Reference 21 with permission from John Wiley & Sons, Inc.

Fully oxygenated hemoglobin (oxyHb) is ligated with four oxygen molecules. As demonstrated from the oxygen dissociation curve, ~97% of hemoglobin is saturated with oxygen

in the lungs (where PO_2 is about 100 torr). The oxygen pressure at which 50% of the hemes are saturated with oxygen is called the p_{50} and is the measure for hemoglobin oxygen affinity. At standard conditions, ($pH = 7.4$, $T = 37\text{ }^{\circ}C$, $PCO_2 = 40\text{ mmHg}$) the p_{50} as extracted from the oxygen dissociation curve in Figure 1-7 is 26 torr. The exact value of p_{50} depends on several factors that can influence the binding of oxygen to hemoglobin: one is temperature, and the others involve ligands that affect the function of hemoglobin by manipulating its conformation (allosteric effectors, which include protons, 2,3-DPG, and carbon dioxide).²² Each of these ligands affects the oxygen dissociation curve (i.e., the oxygen affinity) differently, and, as expected, ligands such as protons and carbon dioxide will have different concentrations throughout the body. For example, there are less protons in the lungs (i.e., high pH) and more protons in active tissues such as muscles (i.e., low pH), leading to a lower and higher p_{50} , respectively. This p_{50} shift is called the Bohr effect and is physiologically-relevant because it favors oxygen uptake in the lungs and release into tissues.

1.2.1.4 *In Vivo* RBC Life Cycle and Breakdown

The life cycle for normal human RBCs in circulation is approximately 110 to 120 days, a time-frame that can significantly vary depending on an individual's physical fitness.^{23,24} The metabolic and mechanical stress of repeated deformations as the cells traverse the circulatory system eventually causes a decrease in cell flexibility. Circulation becomes more difficult, and these aged cells undergo lysis (rupturing of the cell membrane) or phagocytosis (removal by macrophages).

The spleen filters unfit RBCs from the circulation. RBCs enter the organ through arterioles and pass through a small 2 to 5 μm orifice (the approximate size of some capillaries) before re-

entry into general circulation. Abnormally rigid cells are trapped and removed via phagocytosis. The RBC itself is also capable of communicating to the body its senescent status by externalizing specific membrane lipids that serve as markers for recognition by macrophages. Once removed by a macrophage, RBCs are broken down by enzymes and essential components such as amino acids and iron are recovered and reused. The heme porphyrin ring is broken and the opened tetrapyrrole, a compound known as bilirubin, is carried to the liver where it is excreted into the bile.

Though less frequent, red cells can also lyse in circulation releasing hemoglobin directly into the bloodstream. The tetramer quickly undergoes dissociation into α - β dimers because it is unstable in plasma; these dimers bind to a plasma protein and the complex is processed in a similar fashion to the phagocytosis described above.

1.2.1.5 Abnormalities, Pathologies, and Vulnerabilities

RBC abnormalities and pathologies can potentially shed light on the types of damage that are incurred during prolonged storage while vulnerabilities might indicate the specific processes or pathways that predispose RBCs to damage during storage. They can involve the membrane, metabolic pathways, and hemoglobin.

Pathological disorders affecting the RBC membrane and shape are hereditary conditions such as elliptocytosis, spherocytosis, and stomatocytosis. In these conditions, the interactions between integral and peripheral membrane proteins are disrupted or the density of the peripheral protein network is changed, thereby diminishing the biconcave disc cell shape.

Hemolytic anemia is the most common metabolic disorder and is caused by a genetic glycolytic enzyme defect (such as pyruvate kinase deficiency), creating a dramatic reduction in ATP formation. Unable to maintain flexibility and other properties of its shape, the RBC is

removed from circulation. Another common enzyme defect causing hemolytic anemia is glucose-6-phosphate dehydrogenase (G6PD) deficiency,²⁵ resulting in reduced NADPH production. Because the intracellular oxidants cannot then be neutralized, the polypeptide chains of hemoglobin denature and precipitate, forming a structure known as a Heinz body.

Genetically abnormal metHb reductase results in a complete inability to convert metHb (Fe^{3+}) to active hemoglobin (Fe^{2+}). Patients who are homozygous for this condition can accumulate between 20% to 40% metHb in RBCs. For heterozygous patients, the partial enzyme complement is generally sufficient to maintain reduced hemoglobin under normal conditions.⁵

Abnormalities of the hemoglobin molecule can disrupt functionality, and most deviations are caused by mutations affecting particular amino acids in the polypeptide chains. Some substitutions alter hemoglobin's affinity for oxygen by interfering with the transition from a T state to an R state, while other substitutions affect the oxidation state of the heme iron. One of the more common pathological defects is the substitution of valine for glutamic acid in the sixth position of the β chain, producing a variant of hemoglobin referred to as hemoglobin S. When deoxygenated, this hemoglobin S variant polymerizes into inflexible aggregates, a state that deforms the cell into "sickle-like" shapes, the morphology responsible for sickle cell anemia.

Given that oxygen is constantly exchanged within the cell, the potential for the production of ROS, in a variety of ways, is especially high. ROS can damage all parts of the cell including the membrane, metabolic pathway components, and hemoglobin. The superoxide anion ($\text{O}_2^{\bullet-}$) is created from the normal cycling of oxygen that occurs in hemoglobin when a molecule leaves an iron atom (Fe^{2+}), goes into solution, and binds to another iron atom; oxygen keeps an electron from the iron and forms $\text{O}_2^{\bullet-}$ and metHb. The superoxide dismutase (SOD) enzyme converts this anion to hydrogen peroxide which in turn can produce other kinds of oxygen radicals, such as hydroxyl,

perhydroxyl, and peroxy ($\cdot\text{OH}$, $\cdot\text{OOH}$ and $\text{ROO}\cdot$, respectively). If enzymatic protection against such auto-oxidation is inadequate, ROS species can multiply and become destructive.

The RBC membrane is rich in unsaturated organic molecules with weak C-H bonds that are particularly prone to undergo auto-oxidation.²⁶ Oxidative damage can also disrupt the linking sites of peripheral proteins with integral proteins. Indeed, the membrane seems especially vulnerable to both chemical damage from ROS and repair mechanisms that are not readily accessible.²⁷ For example, $\cdot\text{OH}$ is the major radical responsible for lipid peroxidation, which in turn produces an unstable lipid radical that further reacts with oxygen and produces a peroxy-fatty acid radical. A repetitive cycle then propagates through the lipid membrane, where new radicals assist in forming radicals of neighboring molecules.

Operation of the Embden-Meyerhof pathway causes increased acidosis from accumulating protons that inhibit critical enzymes in the pathway; this slows glycolysis and ATP formation.²⁸ Because ATP is necessary for maintaining cell shape and flexibility, repairing membrane lipids, and energizing metabolic pumps that control electrolyte flux across the membrane lipids⁵, this pathway must function normally and lactate must continually be eliminated. Thus, RBCs are metabolically vulnerable from normal operation of the Embden-Meyerhof pathway when waste products cannot be eliminated.

Oxidative damage is a key vulnerability of hemoglobin and the metHb reductase enzyme plays an important role in keeping the iron atoms of hemoglobin in their reduced (Fe^{2+}) form. However, as described above, the iron can “rust” from repeated oxygenation cycles²⁹ and produce inactive metHb (Fe^{3+}).²⁶ The oxidation disrupts the position of the reduced iron atom, causing it to sit within the plane of the porphyrin ring of the heme group, and the hydrophobic pocket that is suitable for the binding of oxygen is compromised.

Alluded to above in the context of ROS, the oxidation mechanism is given in Equation (1.1).³⁰



Damaging oxidative processes can propagate quickly because a single oxidized heme (Fe^{3+}) can effect the other three polypeptide chains within the same tetramer. For example, a random distribution of 20% Fe^{3+} would imply 58% of hemoglobin with at least one oxidized subunit.²⁹ Such a molecule is dysfunctional because it is incapable of transitioning to the deoxy state, causing a loss of active hemes and eventually decreased oxygen transport. MetHb also disrupts other features of the red cell, as the oxidized hemoglobin binds irreversibly to some integral proteins, creating alterations to the cytoskeleton.

1.3 Blood Banking and RBC Transfusion Medicine

The era of modern transfusion dates back to the early 1900s and coincided with the identification of the ABO blood groups.³¹ It was at this point in time when health care professionals realized that the oxygen transport functionality of blood was not limited to exist *within* an individual, but could be transferred to benefit *other* individuals who had experienced an injury involving excessive blood loss. Subsequent development of anticoagulant and preservative solutions led to the establishment of the modern blood bank³² (detailed historical accounts have been described elsewhere^{33,34}). Today, blood banking refers to the process of extracting blood from a donor, separating it into its various components, and storing the final products to be transfused at a later date according to the needs of a given patient. Such therapeutic transfusion of banked RBCs is now a frontline treatment for restoring tissue oxygenation after blood loss.

1.3.1 Properties of Blood Storage

When whole blood is donated, it is collected into an anticoagulant solution, composed of citrate, phosphate, and dextrose, designed to preserve cellular function and to prevent blood from clotting during storage. The last few decades have seen substantial development in the processing of blood products and more importantly, in the techniques for preserving these products outside of the body. Through these advances, it has been realized that the separation of whole blood into its individual component parts (plasma, RBCs, WBCs, and platelets) is best achieved through multiple centrifugation steps, as presented in Figure 1-8.

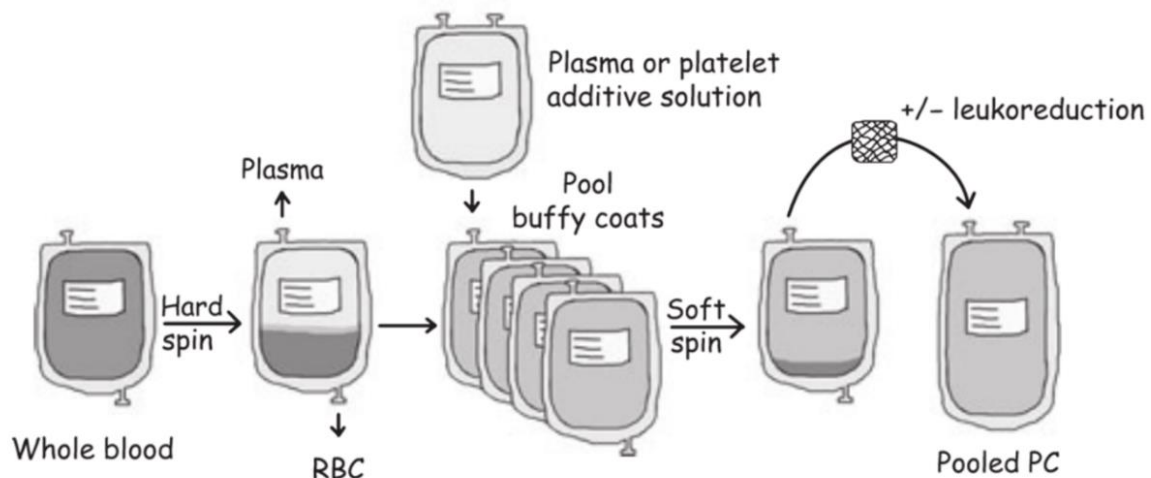


Figure 1-8: Current production method for separating donated whole blood as implemented nationwide by Canadian Blood Services (CBS) in 2006. In this process, known as the buffy coat production method, multiple “buffy coats” - a mixture of platelets and WBCs - are pooled together to enhance platelet recovery. RBCs are isolated from the primary spinning stage. Adapted and reprinted from Reference 35 with permission from John Wiley & Sons, Inc.

Such processing technology has led to the development of large-scale blood banking facilities and resulted in countless lives being saved. However, demand for blood products is continually rising and managing the supplies is a global challenge faced by all blood service agencies. The main difficulty arises from storage limitations inherent to even the most sophisticated approaches for safe blood product storage. Despite adhering to these storage conditions, blood products degrade much quicker *ex vivo* than *in vivo* and stored products from different donors will degrade at different rates.^{28,36} Yet it is the responsibility of these blood banking facilities to manage supplies and demands of various hospitals and distribute product of the highest quality to those most in need. Accurately determining quality, however, is a challenge that *cannot* be addressed by merely ranking the products according to their collection date. Instead, a technology is desired that can rapidly and accurately assess the extent of degradation in a non-destructive way without invasive sampling of the storage unit contents.

To provide a biocompatible *ex vivo* environment, donated RBCs are mixed with a buffered additive solution (AS) intended to prevent coagulation, provide nutrients, and extend storage life.³⁷ Furthermore, RBC-AS mixtures are stored at 4°C in specialized plastic blood-bags where they remain until transfusion. In the absence of technology for *in situ* monitoring, current regulatory requirements tacitly assume that all RBCs stored under such optimal parameters will maintain their viability for 42 days.^{38,39} This much shorter *ex vivo* survival period is to be expected as the prescribed environment for stored RBCs is not physiologically optimal and degradation products accumulate instead of being automatically recycled. However, donor-to-donor variations are not accounted for and a static outdate age misrepresents the multitude of negative effects that can shorten the shelf-life of stored RBCs to significantly less than 42 days.

In Canada (with the exception of Quebec), the entire process from collection to processing for storage and eventual distribution to hospital sites is overseen by Canadian Blood Services (CBS). The median storage time between collection and transfer to hospital sites varies, but is typically about 6 to 8 days.⁴⁰ The median age of blood at the time of transfusion is also variable, but is typically 15 to 20 days.⁴⁰ Hospitals attempt to employ a 'first-in-first-out' strategy for managing their on-site collections, and over the course of a standard fiscal year, the total rate of discard due to outdate (by hospitals and the CBS combined) is approximately 3%. Therefore, a large portion of transfused blood may be close to the 42 day limit, and concerns have been raised that older RBCs may be responsible for a variety of post-transfusion illnesses and deficiencies (see section 1.3.3 for more).⁴¹⁻⁴⁴

This assigned outdate age originates from empirical studies which established 42 days as the maximum storage time compatible with the following two FDA guidelines concerning the usability of RBC product: 1) stored RBCs must maintain cellular integrity (free hemoglobin is <1% of total hemoglobin as measured by spectrophotometry), and 2) there must be a post-transfusion RBC survival rate of >75%.⁴⁵ These guidelines permit a considerable amount of degradation products and symptoms, collectively known as storage lesion (section 1.3.2), to be present in RBCs near the 42 day storage limit. If blood from different donors ages differently, and different patients exhibit different sensitivities to storage lesion present in transfused blood, then for some units and/or some patients, the 42 day window may actually be too long. Yet significantly reducing the storage age limit raises the risk of RBC shortages as the percentage of collections that would be discarded due to outdate would rise considerably.

1.3.2 RBC Storage Lesion

Because the prescribed environment for stored RBCs is not physiologically optimal, RBCs are more susceptible to the various vulnerabilities outlined above. Starting from the moment RBCs are collected and prepared for storage, the cells experience progressive damage that may affect their viability, decrease their ability to carry oxygen, and increase the generation of potentially harmful waste products. As this progression is complex and poorly understood, it is not clear in what order the resulting defects occur. However, it is clear that many of the symptoms are interconnected, and while the majority of these alterations can be readily measured in a laboratory, they are extremely challenging to assess *in situ* within a storage bag. Furthermore, because the extent of such defects and alterations cannot be readily measured immediately prior to transfusion, their clinical impact is not easy to evaluate. This decline in red cell quality is known as the storage lesion and encompasses many degradation symptoms,^{34,46–51} principally those listed below:

- morphological changes (e.g., microvesicle formation, decreased cell volume, shape loss)
- decrease in ATP (breakdown of glycolysis, leads to decrease in the phosphorylation of structural proteins and, in turn, loss of deformability)
- formation of hemoglobin variants (metHb, denatured and dimerized forms)
- decrease in regulating molecules (e.g., 2,3-DPG)
- important antioxidant factors (e.g., NADP, NADPH, GSH, etc.) are no longer recycled (leading to ROS, oxidative damage to membrane lipids, etc.)
- increased expression of phosphatidyl serine, a membrane phospholipid component
- decreased pH due to buildup of lactic acid and accumulation of protons

The aberrations associated with RBC storage lesion can be divided into four different categories: metabolic, enzymatic, oxidative, and physiological.²⁸

1.3.2.1 Metabolic Storage Lesion

Increased acidosis from operation of the Embden-Meyerhof pathway inhibits the activity of key enzymes leading to a decreased production of ATP and other molecules capable of protecting against oxidative damage. At an acidic pH, 2,3-DPG will break down. Because the 2,3-DPG shunt bypasses one of the two ATP making steps in glycolysis, 2,3-DPG is made at the expense of ATP. During the initial stages of storage, the pH of donated blood begins to decrease from ~7.4 and the breakdown of 2,3-DPG leads to an initial burst of ATP production. However, the pH continues to drop and by the second or third week of storage, concentrations of important glycolytic products (ATP, NADP, NADPH) are all decreasing. The subsequent decrease in flux through the PPP pathway causes a significant decrease in the concentration of GSH and the ability of stored cells to avoid oxidative damage is diminished.⁵² The transfusion community is aware of the difficulties presented by pH and, even within the initial manufactured storage solution provided, the pH value can vary over a modest but clinically significant range.²⁸

1.3.2.2 Enzymatic Storage Lesion

Enzymatic storage lesion is said to contribute to damage of the carbohydrates and protein segments of the membrane. The risk of such a mechanism occurring is related to residual WBCs that could be present within a unit post-processing and reducing their presence ameliorates the effects of enzymatic storage lesion.⁵³ Leucoreduction increases red cell recovery by ~2% and reduces hemolysis (cell rupture) by half over the course of storage. However, there are still trace

numbers of WBCs within a leucoreduced RBC unit, and WBC breakdown releases enzymes such as proteases, lipases, and glycosidases⁵¹ that can target the red cell surface.⁵⁴

1.3.2.3 Oxidative Storage Lesion

A stored RBC is continually exposed to oxygen during its storage life via a semi-permeable plastic storage bag and initial levels of oxyHb present in the collected whole blood. Though the rates at which they occur are lower because cells are stored at a low temperature, the main oxidative reactions that can occur *in vivo* (dealkylation of lipids in the membrane, damage to integral proteins essential for cytoskeleton, etc.) can also occur in storage. In the absence of ATP, it is more difficult for the cell to counter or repair such breakdown⁵⁵ resulting in a morphological transformation that occurs from the normal disc shape to an abnormal cell with thorny-like protrusions, called an echinocyte.⁵⁶ Eventually the protrusions bleb off the cell leading to the formation of microvesicles.⁵⁷⁻⁶⁰ With the loss of membrane area, the favorable surface-area-to-volume ratio is decreased and the cell becomes more spherical, making it more difficult to traverse circulation. Over time, both the observed stiffness⁶¹ and the density of the cytoskeleton network⁶² increases for aged cells. Attempts to reduce oxidative damage have been made by storing cells under anaerobic conditions.⁶³

1.3.2.4 Physiological Storage Lesion

During the storage period, RBCs evolve from a biconcave disc to echinocytes (Figure 1-9) and it is the spiny protrusions which eventually bleb from the membrane surface, resulting in microvesicle release. These shape changes are related to an increasingly acidic environment and decreased ATP concentration. When the shape changes are not accompanied by oxidative damage,

which is rarely the case, they can be reversed when placed in an environment with normal ATP concentration and cell electrolytes. However, when microvesicles are released, a substantial loss of membrane material occurs and regeneration of the smooth biconcave disc shape is not possible as RBCs have no mechanism in place to synthesize the lost material. Such cells are rigid spheres that will either undergo hemolysis in storage or will be removed from circulation after transfusion. Having knowledge of the morphology of cells would therefore be important prior to a transfusion, as a unit with a large presence of sphere echinocytes would create extra stress on the clearance mechanism of a patient.

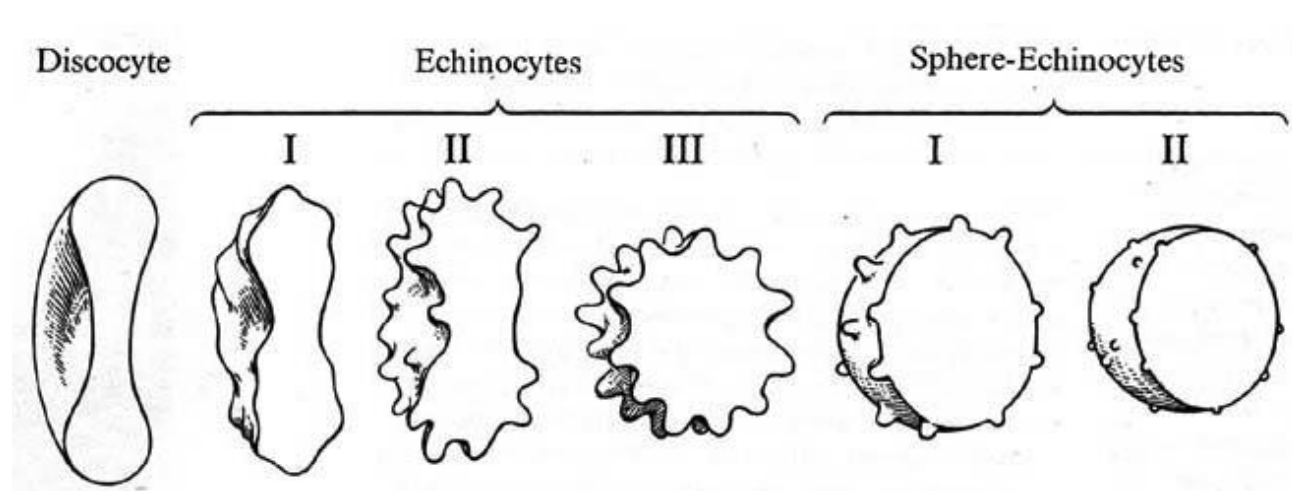


Figure 1-9: Cell morphologies of stored RBCs. Reprinted from Reference 64 with permission from Springer International.

1.3.3 Health Risks Associated with Stored RBCs

It is intuitive that the longer donated RBCs are stored, the higher the risk of significant storage lesion development. Therefore, there is concern that the longer RBCs are stored, the higher the potential that transfusion could result in deleterious effects. One of the more controversial and

heavily debated issues is whether RBC transfusion affects the morbidity and mortality of the recipient.⁶⁵

Historically, investigations of adverse patient outcomes from transfusions of stored RBCs, using observational analyses, animal models, and studies involving volunteers, have proved provocative, controversial and contradictory.⁶⁶ To resolve conflicting results, studies have been undertaken to investigate the effects of transfusing aged blood on specific groups of patients thought to be particularly vulnerable to storage lesion: cardiac, trauma, critical care, etc.⁶⁷ While some of these reports have demonstrated positive correlations between adverse effects and age of transfused blood,^{68–71} others have not.^{72–74} Interpreting the results is complicated by the fact that RBCs with mild storage lesion can recover functionality hours after transfusion, while RBCs with severe storage lesion may not recover and might impose a burden on the recipient.⁷⁵

1.3.3.1 Clinical Trials

Much effort has been expended on randomized and controlled studies to obtain definitive evidence of the deleterious effects of storage lesion on morbidity and mortality.^{76–78} The results of these multiple-year studies have started to appear and some have suggested that storage age may have no relationship to negative outcomes,^{66,79–81} though more data are needed. In any case, the presence of storage lesion clearly creates a product that is not optimal for transfusion and complicates the management of inventories of RBC concentrate.

1.3.3.2 Controversy

Problems arise when the progression of storage lesion is not completely reliant on the proxy measure of storage age, the metric used in studies that are both observational in nature and those

that are properly controlled, but instead is based on the characteristics of individual donors. This discrepancy could have serious implications concerning the results that have been presented and the efforts that have attempted to characterize the effect of storage age on patient outcomes.

If initial blood quality and subsequent storage lesion progression significantly differ between donors, there is a likelihood that a bias has been created against a definitive correlation with “age” and outcomes. For example, it is known that the likelihood of hemolysis increases with storage duration.⁸² Technologists working in blood banks are tasked with identifying badly storing RBC units by sight (i.e., units that undergo hemolysis will have a distinct reddish supernatant) and removing them from active inventory.⁸³ If, as anecdotal evidence suggests, older RBCs from male donors are more prone to lysis than those from female donors, an effective prejudice against using older RBCs from male donors could arise. This would tend to deplete “standard-issue” inventory of more harmful units and enrich it with blood from female donors that have more favorable biochemical conditions within the stored unit. Hence, a differential harmful outcome upon transfusion of older RBCs compared to fresh RBCs would be less likely to be observed. It could also be postulated that RBCs from a younger person would be likely to be more metabolically active, and their donated “fresh” RBCs could actually be more susceptible to develop a severe storage lesion. Such “fresh” RBCs could represent a more detrimental load to transfusion recipients compared to older RBCs. This scenario could contribute to the observed and counterintuitive tendencies of older RBCs being safer than fresh RBCs.⁶⁶ Therefore, to obtain valid data about the effects of RBC storage lesion on recipients, randomized clinical trials must use the determined extent of storage lesion, and not storage age, as the independent variable. Such trials, however, must wait until appropriate technology for determining the extent of storage lesion pre-transfusion is developed.

1.3.4 Administration of Blood Transfusion

The management of a blood banking system is an enormously challenging task from an administrative standpoint. This is because blood banking organizations are responsible for screening donated blood to ensure its safety, managing their banked libraries to provide adequate availability, and minimizing costs.

- Over the last several decades, screening has been in place for a variety of harmful transfusion hazards, such as hepatitis, human immunodeficiency virus (HIV), and West Nile virus (WNV).⁸⁴
- Blood banks have to maintain a complex inventory of rapidly outdated products, which is complicated by blood types. Even though the AB blood group can accept blood from donors of the other types, and everyone can receive group O negative (“universal donor”) blood, to avoid waste of inventory, it is believed to be better if everyone gets their own type (except in emergencies).
- Transfusion is laden with costs. Money is needed to staff a transfusion facility and to buy reagents, refrigerators, freezers, centrifuges, systems for blood testing, etc. The blood is provided for free by volunteer donors, but there is still an associated administrative cost. Recent estimates suggest the per-RBC-unit costs between \$522 and \$1183.⁸⁵

Donors are unique in their combinations of health, lifestyles, diet, gender, age, travel histories, etc., and some individuals are desirable as donors for their genetic or phenotypic traits (e.g., those with O negative blood group). It is required that different components isolated from individual blood donors stay linked because risks related to mislabeling or contamination affect

all products of a donation.⁸⁶ Recipients can also have highly specific transfusion requirements, (e.g., phenotypically-matched platelets or red cells). Considering these factors together, blood banks are responsible for creating orderly records and maintaining these records indefinitely.

The administration of blood becomes even more challenging when the ownership of liability is taken into consideration. If governments are responsible for the welfare of their citizens, are they also responsible for any failures associated with blood safety? Due to awareness of transfusion complications such as HIV and hepatitis C during the 1980s, blood banking agencies often operate independent of governmental agencies. Furthermore, as the populations of citizens in developed countries age, proper management of blood inventories will become more critical as the cost, in terms of both dollars and patient health, increases.

1.4 Storage-Related Problems in Current Blood Banking Practice

When discussing whether particular units of stored RBCs contribute to adverse effects in transfusion recipients, the decision-making process should be less about whether the unit is “fresh” or “old”, but instead about the degree of storage lesion. Unfortunately, there are no methods by which blood bank technicians could determine the extent of storage lesion without sampling the cells from a particular unit, an action which renders a unit no longer sterile for transfusion.

Furthermore, it is not well known how specific donor characteristics (i.e., health, lifestyles, diet, gender, age, to name a few)⁸⁷ would affect the ageing of a particular unit in storage. The ability to predict storage lesion progression from observable donor characteristics might lead to enhanced administrative decision making. Currently, inventories are managed with storage age as the proxy measure of quality and as mentioned above, most institutions abide by the principle of “first-in, first-out.” If donated units age independently from one another, RBCs that don’t store

well would need to be used sooner, regardless of their exact donation date. A blood bank therefore requires an ability to predict the storability of a unit to reduce costs and improve clinical safety.

1.5 Assessing RBC Blood Quality

RBC transfusions act to improve tissue oxygenation for those patients who are anemic, or those who have undergone serious blood loss. They have been implemented for over a century, and during this time, countless lives have been saved. RBC collection, storage, and usage vary between countries, but well-over millions of transfusions happen globally each year. Although the introduction of blood banking and its corresponding administration has made blood safer than ever, safety and administrative efficiencies can still be improved.

The work presented in this thesis is the first demonstration of Raman spectroscopy for assessing stored RBC quality. This analytical technique will show potential for analyzing individual units of stored blood and providing specific donor-dependent trends, based on the presence of biochemical molecules within the unit. Progress has been made towards obtaining through-plastic measurements of stored RBC units. This method will permit a more refined approach to blood system management based on a new strategy that takes into account the variations of RBC quality from individual donors.

Chapter 2: Raman Spectroscopy and its Application to the Analysis of Blood

2.1 Optical Spectroscopy

Spectroscopy is a measurement of the interaction of light (electromagnetic radiation) with various materials. Modern techniques use radiation from the ultra-violet (UV) to the infrared (IR) regions of the spectrum and samples range from inorganic to living tissue in nature. In general, when such light is incident upon a sample, the incident photons may be absorbed, modified, scattered, or may not interact with the material at all and pass directly through it. The degree to which each of these processes occurs is dictated by the chemical nature of the material and the specific wavelength of light. The amount of light absorbed, emitted, or scattered by a sample is a measure of the molecular energy levels in the system, and by analyzing this information, it is possible to determine aspects related to the sample's composition.

2.2 Molecular Energetics

Every molecule has a total energy which can be split into four components: electronic energy, vibrational energy, rotational energy, and translational energy.

$$\mathbf{E_{Total} = E_{Electronic} + E_{Vibration} + E_{Rotation} + E_{Translation}} \quad (2.1)$$

The last component, the translational energy, describes the kinetic energy of the bulk system as it travels through space. The first three components (electronic, vibrational, rotational), however, are directly related to specific states of the molecule and are therefore called “internal”

components: the electronic component is related to the orbitals of the molecule inhabited by electrons, the vibrational component describes the movement of bonded atoms, and the rotational component is a measure of the movement of atoms on their internal axes. These three factors have discrete non-zero energy levels (i.e., they are quantized) that depend on the atomic composition of the system; the most probable state of a molecule at room temperature is its lowest-energy state and is referred to as a ground-state.⁸⁸

The energetics of each internal component are vastly different and the technique of optical spectroscopy can therefore be used to reveal specific chemical detail about any system. For example, the energy associated with electron population is roughly three orders of magnitude greater than the vibrational energy, which is roughly three orders of magnitude greater than the rotational energy. Multiple vibrational levels populate a given electronic state, and multiple rotational levels are said to populate individual vibrational states. When a system undergoes a perturbation, the total energy of the system is subject to change as these internal states undergo transitions between their quantized levels. Figure 2-1 shows a basic representation of the electronic levels (denoted by S_0 to S_2) and the vibrational levels in the S_0 electronic state (denoted by ν_0 to ν_4) of a molecule (rotational levels are not included).

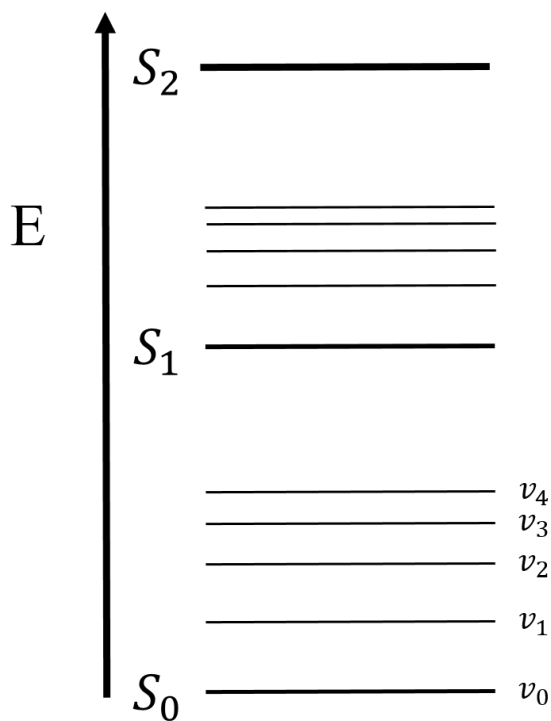


Figure 2-1: Jablonski diagram depicting various quantized energy levels for electronic and vibrational states.

The energetic difference between electronic transitions and vibrational transitions defines the type of information that can be extracted from each using techniques of spectroscopy. While there are specific transitions that are possible for valence electrons in a system, the spacing between vibrational energy levels is directly related to the local chemical environment of a particular bond, and this allows vibrational spectroscopy to have the specificity to distinguish molecules from one another.

In this chapter, a summary of current scientific literature on the analysis of blood and blood components using the variant of vibrational spectroscopy known as normal Raman spectroscopy will be presented.

2.3 Molecular Vibrations

To understand the nature of vibrational states, it is first important to describe how they are modeled. Chemical molecules are composed of atoms which have a defined mass and are connected by “elastic” bonds. As a result, these atoms are able to perform periodic motions relative to one another. The simplest model of a vibrating molecule describes an atom bound to a very large mass by a weightless spring. The classical bond has a length, characterized by the vibrationally averaged position of the atom at the end of the bond. The force required to move the atom by a certain distance (x) from its equilibrium position is proportional to a force constant (f , a measure of the bond strength) and is described by Equation (2.2).

$$F = f \cdot x \quad (2.2)$$

Combining Newton’s Second Law and solving the resulting differential equation, the motion of the displaced atom is that of a simple harmonic oscillator whose frequency (ν) is described by Equation (2.3), a form of Hooke’s law:

$$\nu = \frac{1}{2\pi} \sqrt{\frac{f}{\mu}} \quad (2.3)$$

where μ is the reduced mass of the atoms involved in the system:

$$\mu = \frac{m_1 m_2}{m_1 + m_2} \quad (2.4)$$

The frequency of the vibration defines the condition of a particular bond: it will increase as the strength of the bond increases, and will decrease as the reduced mass increases, as governed by Equation (2.3). If it was possible to measure the frequencies originating from vibrations of atoms within complex systems, then it would be possible to identify various chemical functional groups based on their different bond strengths (i.e., as force constants are proportional to bond order, C-C and C=C will have different frequencies) or based on their different reduced masses (i.e., O-H alcohol bond vs C-H alkane bond).

2.4 The Raman Effect

First reported in 1928 by Chandrasekhara Venkata Raman,⁸⁹ the Raman effect, which he initially called “feeble fluorescence” and then termed “a new radiation”,⁹⁰ is a molecular process whereby scattered photons have different frequencies (i.e., energies) due to their interaction with vibrational modes. The mechanism of the Raman effect is based on the interaction of the sample with a monochromatic light (having an energy $h\nu_0$) and is essentially a two-step process. In the first step, the incident photon forces the electron cloud of the molecule to be distorted at the frequency ν_0 , thereby creating an oscillating dipole moment. This perturbation forces the molecule to exist in a ‘virtual state’ (labelled in Figure 2-2), a short-lived intermediate state that has no quantum-mechanical solution. In the second step, a scattered photon emerges from the system which returns the system to a particular vibrational state in the S_0 electronic state.

There are three scattering pathways that are associated with the Raman effect, and the only difference between them are the initial and final vibrational states. The most probable pathway (called Rayleigh scattering) accounts for the vast majority of scattered photons and is a case where the released photons are elastically scattered (i.e., the final vibrational state is the same as the initial

state). The other two pathways exist when photons are inelastically scattered (i.e., the final vibrational state is different from the initial state). In one case, a small portion of energy from the incident light ($h\nu_0$) is lost to the vibrational energy levels and appears as photons with energies $h(\nu_0 - \nu_1)$, $h(\nu_0 - \nu_2)$, etc. In the second case, if the vibrational levels ν_1 , ν_2 , etc., are close to the ground state, they will have a noticeable population at room temperature as determined by the Boltzmann distribution. In this case, molecules in these vibrationally excited states interact with the incident radiation and return to the ground state. This results in scattered photons with energies of $h(\nu_0 + \nu_1)$, $h(\nu_0 + \nu_2)$, etc. These shifts to lower and higher energy are respectively known as Stokes and anti-Stokes Raman scattering,⁹¹ and all scattering pathways are labelled in the Jablonski diagram of Figure 2-2.

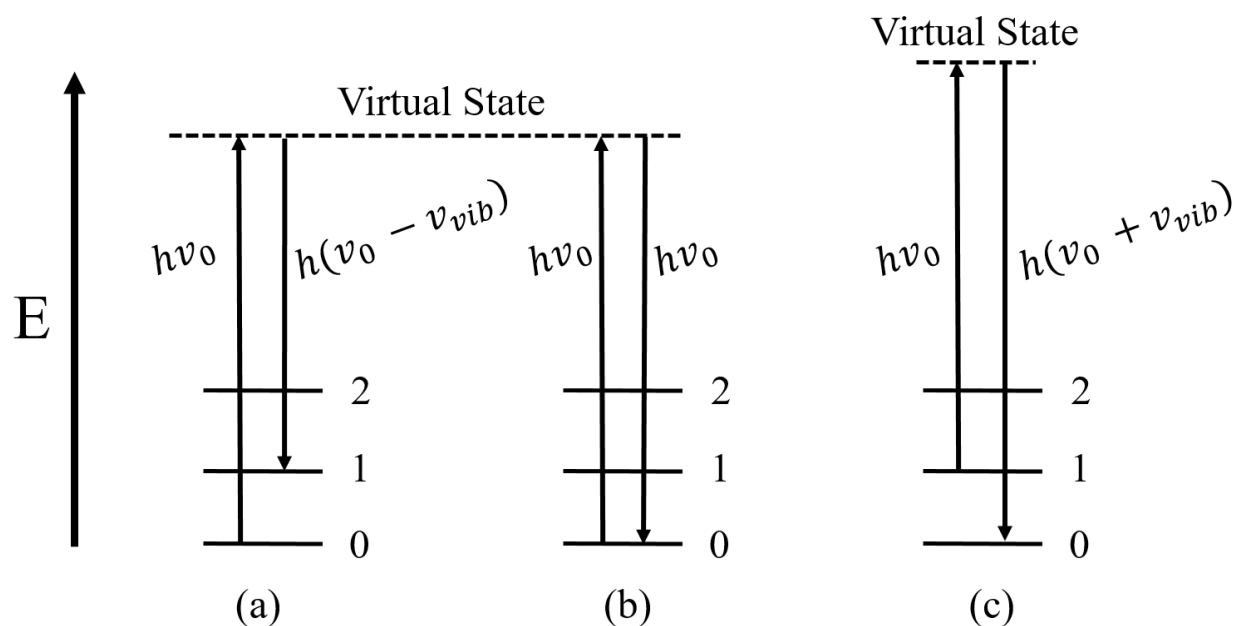


Figure 2-2: Schematic representation of the scattering pathways: (a) Stokes, (b) Rayleigh, and (c) anti-Stokes.

As the contributing modes to the scattering pathways are different, the measured intensities of the pathways are also quite different. The elastic scattering is $>10^6$ times more likely to occur than the inelastic alternatives, meaning the actual Raman photons are extremely rare in comparison. Furthermore, the intensity of photons generated via the anti-Stokes pathway is much less than the Stokes pathway; as described, the creation of anti-Stokes photons requires that the molecule must exist in a vibrationally excited state when the incident photon is impinging. Even if this excited state is populated, the vibrational ground state will be the most highly populated state at room temperature, and the Stokes intensity will therefore be far greater than the anti-Stokes pathway.

The information from scattered photons produces a Raman spectrum that is a characteristic fingerprint for a given sample. A Raman spectrum is a plot of scattered light intensity vs. energy (in units of wavenumbers, expressed as cm^{-1}) and the peaks that appear on the spectrum represent molecular vibrations; their position is a direct reflection of the bond strength between particular groups of atoms. In fact, these positions are often reported as Raman shifts which describes the magnitude of the shift from the Rayleigh scattered line ($h\nu_0$) which is positioned at 0 cm^{-1} . Because both the Stokes and anti-Stokes transitions involve the same vibrational level, the absolute difference between the incident light-frequency and their scattered frequencies is identical. Therefore, the peaks represented by the Stokes and anti-Stokes Raman photons are symmetrically distributed about the Rayleigh line.⁹²

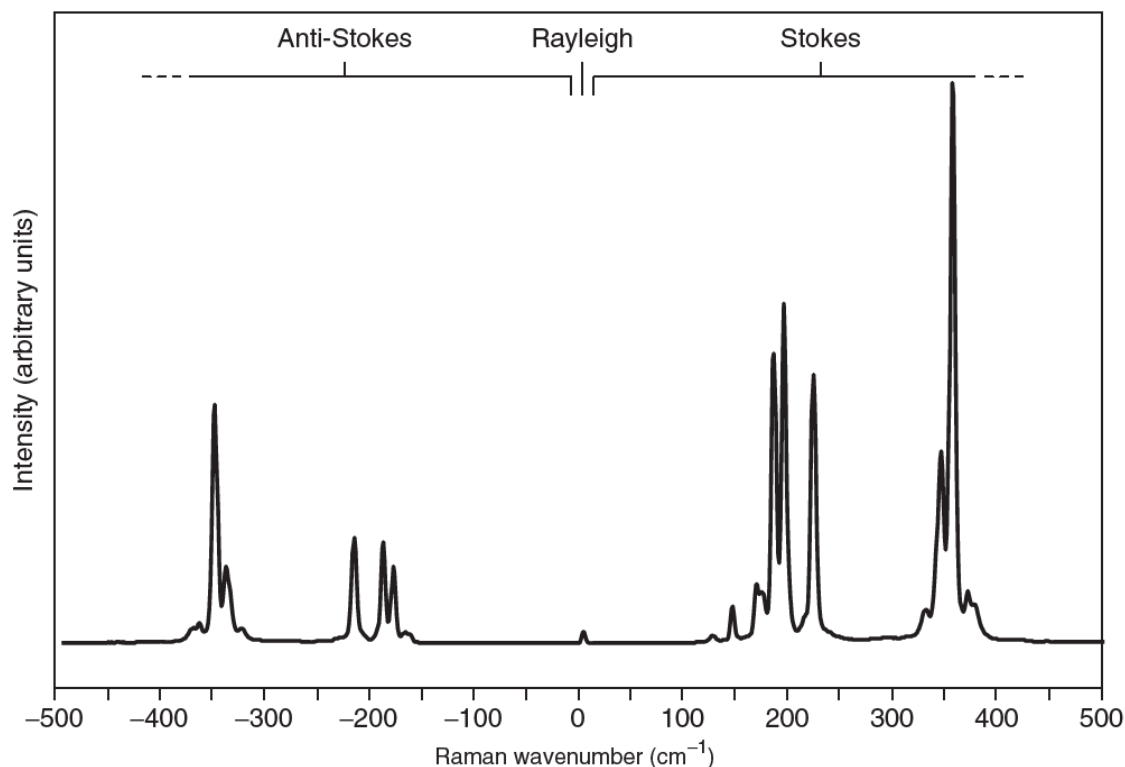


Figure 2-3: A Raman spectrum of the mineral realgar (As_4S_4) is shown in the anti-Stokes and Stokes regions. Even though the Stokes photons represent a loss of energy from the incident light, common convention is to display the transitions on the positive side of the horizontal axis. The intensity of the Rayleigh line (0 cm^{-1}) is suppressed by a holographic filter in the spectrometer. Reprinted from Reference 93 with permission from John Wiley & Sons, Inc.

Finally, as the magnitude of the Raman shift depends on specific molecular vibrations, Raman spectra are independent of the excitation wavelength used, allowing for comparison of Raman spectra collected with different excitation light sources. However, this should not be confused with the fact that the intensity of the Raman scattering depends on the excitation source (inversely proportional to λ^4) and that intensities from different sources cannot be compared as different wavelengths may stimulate electronic transitions.

2.4.1 Classical Derivation of the Raman Effect

In all forms of spectroscopy, there is a mechanism by which the incident radiation interacts with the molecular energy levels. For Raman spectroscopy, the mechanism has its origins in the phenomenon of light scattering, in which the electromagnetic radiation interacts with a deformable (polarizable) electron cloud. The previous descriptions have used Jablonski diagrams to depict the energetic requirements for quantized transitions between various internal molecular states. However, these discussions do not model the properties of the incident light and how they influence the Raman effect. The classical approach for achieving this involves treating the scattering molecule as a collection of atoms undergoing simple harmonic vibrations, while neglecting the quantization of the vibrational energy. A more appropriate treatment of light scattering using quantum theory would treat both the incident radiation and the molecule as quantum particles, and would involve relativistic effects⁹⁴; such efforts are beyond the scope of this thesis and the classical approach is outlined.

The incident light is associated with an electric field, and the electric field strength (E) is expressed by:

$$E = E_0 \cos 2\pi\nu_0 t \quad (2.5)$$

where E is the time-dependent intensity, E_0 the maximum amplitude, and ν_0 is the frequency. When a molecule is placed in such a fluctuating electric field, its electrons are displaced relative to its nuclei and an oscillating induced dipole (μ) is created that will re-emit (scatter) light at the frequency of the dipole oscillation (ν_0). The induced dipole moment is proportional to the field strength:

$$\mu = \alpha E \quad (2.6)$$

In this equation, the proportionality constant α is known as the polarizability. In actuality, the induced dipole is not represented by just one term, but instead by a series of terms. A more general expression defines the induced dipole as:

$$\mu = \alpha E + \beta EE + \gamma EEE + \dots \quad (2.7)$$

where μ is the polarizability, and β , γ , etc. are known as hyper-polarizability constants. The magnitude of these components typically drops by 10 orders for each higher-order term, and these terms are the foundation for other utilities of the Raman effect, collectively referred to as non-linear Raman spectroscopy. This is beyond the scope of the research presented in this thesis.

Upon substitution of Equation (2.6) with Equation (2.5):

$$\mu = \alpha E = \alpha E_0 \cos 2\pi\nu_0 t \quad (2.8)$$

the induced dipole will scatter radiation of frequency ν_0 .

Now consider that the scattering body has vibrational modes of its own – a normal mode Q_k , for example, with a vibrational frequency of ν_k . The nuclear displacement created by this mode is described by:

$$Q_k = Q_k^0 \cos 2\pi\nu_k t \quad (2.9)$$

If the oscillation of this vibration changes the polarizability, the effect can be written as:

$$\alpha = \alpha_0 + \left(\frac{\partial \alpha}{\partial Q_k^0} \right) Q_k + \text{higher order terms} \quad (2.10)$$

Multiplying by E gives:

$$\mu = \alpha_0 E + \left(\frac{\partial \alpha}{\partial Q_k^0} \right) Q_k E \quad (2.11)$$

And substituting Equations (2.5) and (2.9) for E and Q_k , the expression for μ now becomes:

$$\mu = \alpha_0 E_0 \cos 2\pi\nu_0 t + E_0 Q_k^0 \left(\frac{\partial \alpha}{\partial Q_k} \right) \cos 2\pi\nu_0 t \cos 2\pi\nu_k t \quad (2.12)$$

Using a trigonometric identity for the product of two cosines, this can be rewritten as:

$$\mu = \alpha_0 E_0 \cos 2\pi\nu_0 t + \frac{1}{2} E_0 Q_k^0 \left(\frac{\partial \alpha}{\partial Q_k} \right) [\cos 2\pi(\nu_0 + \nu_k)t + \cos 2\pi(\nu_0 - \nu_k)t] \quad (2.13)$$

The three terms of this equation represent the three major scattering pathways observed in a Raman spectroscopy experiment: the first term is the elastic scattering (Rayleigh scattering), the second

term (frequency $\nu_0 + \nu_k$) is anti-Stokes Raman scattering, and the third term (frequency $\nu_0 - \nu_k$) is Stokes Raman scattering.⁹¹ From an experimental standpoint, Rayleigh scattered light has no information pertaining to vibrational modes within the system, and so it has no spectroscopic value.

Within a polyatomic molecule, numerous vibrational modes exist. In order for any of these vibrational modes to be measurable via the Raman effect (i.e., Raman active), Equation (2.14) shows that scattering can only occur when:

$$\left(\frac{\partial \alpha}{\partial Q_k}\right) \neq 0 \quad (2.14)$$

It is therefore evident that the molecule's polarizability must change during a particular vibration for it to be considered Raman active.⁹³ Thus, the scattering intensity, all else being equal, is dependent on the ease with which a molecule's electron cloud can be distorted. Generally, as the volume of molecular orbitals increases, polarizability of the molecule also increases.

Once such active modes have been identified, however, it cannot be assumed that each will have the same intensity of scattered light. The mathematical expression describing the total intensity of a Raman band with shift frequency ν_{vib} is:

$$I = k \cdot I_0(\nu_0 - \nu_{vib})^4 \alpha^2 \quad (2.15)$$

For molecules of high symmetry, symmetric vibrations that do not distort the molecule are intense in the Raman spectrum.⁹¹ If there are vibrations which do significantly distort the molecule, the

Raman intensity of the mode is high if the atoms involved in the vibration are polarizable (e.g., sulfur or iodine). The intensity of scattered light is also influenced by many external factors, such as the size of the particle under illumination, the frequency of the incident light, the orientation of the incident light with regard to a given bond, and the intensity of the wavelength light.⁹⁵

2.5 General Raman Instrumentation

Having discussed theoretical aspects of the Raman effect, it becomes relevant to understand the basic components a Raman instrument needs to measure scattered light associated with the Raman effect. The main requirements are a light source, a dispersion system, and a detector, which are oriented as shown in Figure 2-4.

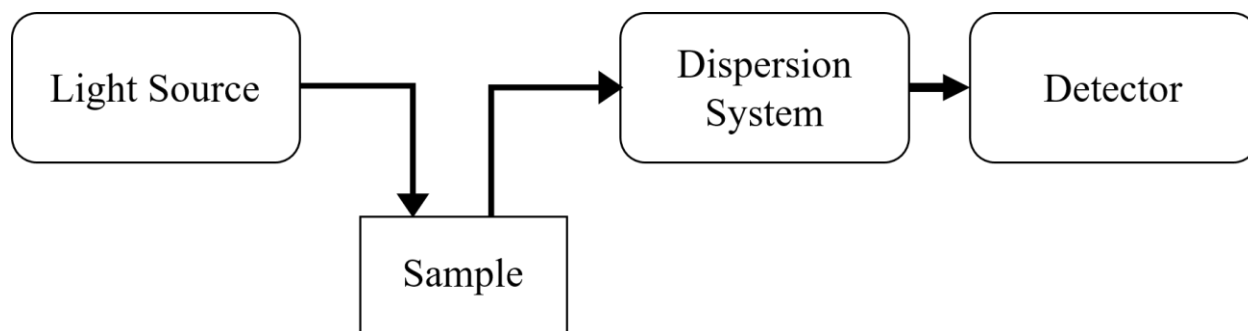


Figure 2-4: Simplified block diagram of the main components in a Raman instrument.

The general principles behind each of these main components will be discussed below, with more technical explanations being beyond the scope of this thesis.

- Light source. Over the last several decades, the driving force behind most improvements in Raman spectroscopy instrumentation has been addressing the inherent weakness of the

Raman effect. Not only does the information-rich inelastic scattering occur much less readily than the Rayleigh scattering, but scattering efficiencies are highly dependent on molecular cross-sections. To combat these issues, an intense light source is required. In addition, the stability and power output of the source needs to be taken into consideration. If the output of the laser is not stable, noise caused by source fluctuation would be introduced, and if the sample of interest is biological in nature, it would have sensitive components whose functions are dependent on structural integrity. Important advances in diode laser research and fabrication have led to instruments that can provide a stable, high intensity output at wavelengths below the damage threshold for most samples.

- **Dispersion System.** A Raman instrument requires that the source radiation is directed onto the sample of interest, and that the resulting scattered light is collected into a dispersion system capable of separating individual wavelengths of light. Such functionality would allow the less-intense inelastic photons to be distinguished from the Rayleigh photons, but would also separate the inelastic photons from each other, creating a spectrum that represents the various vibrational modes of the system. Lenses and filters are crucial at each step in the process. The laser is usually focused onto the sample using a lens and a filter with sharp cut-off characteristics, such as a holographic notch filter, is used to reject the Rayleigh line. For separation of the inelastically scattered photons, a monochromator equipped with a diffraction grating is used to disperse collected light across a slit for sequential processing by a detector. This component is also integral in discriminating against sources of noise such as stray light.

- Detector: Since very few incident photons cause an inelastic scattering event, the detection system must be extremely sensitive and able to detect small numbers of photons over the dark noise background. These are not easy demands and the development of the technique was hampered because early detectors, such as photographic plates, were unable to meet these challenges. The most common detector in current instruments is the charge-coupled device (CCD), which is a semi-conductor capable of measuring impinging photons by creating a proportional electrical current which can be read (“clocked-out”)⁹⁶ by electrodes and recorded by a computer interface. The overall sensitivity and quantum efficiency of a CCD are its major advantages, while its major weakness is a limited spectral window (several intermediate spectra must be obtained and attached if a full spectral scan is desired). CCD’s are also often cooled to reduce the dark current formed by spontaneous (thermal) production of current in the semi-conductor.⁹⁷

One development in the field of Raman instrumentation that has seen significant growth in the last decade is the concept of coupling the spectrometer with an optical microscope (Figure 2-5).

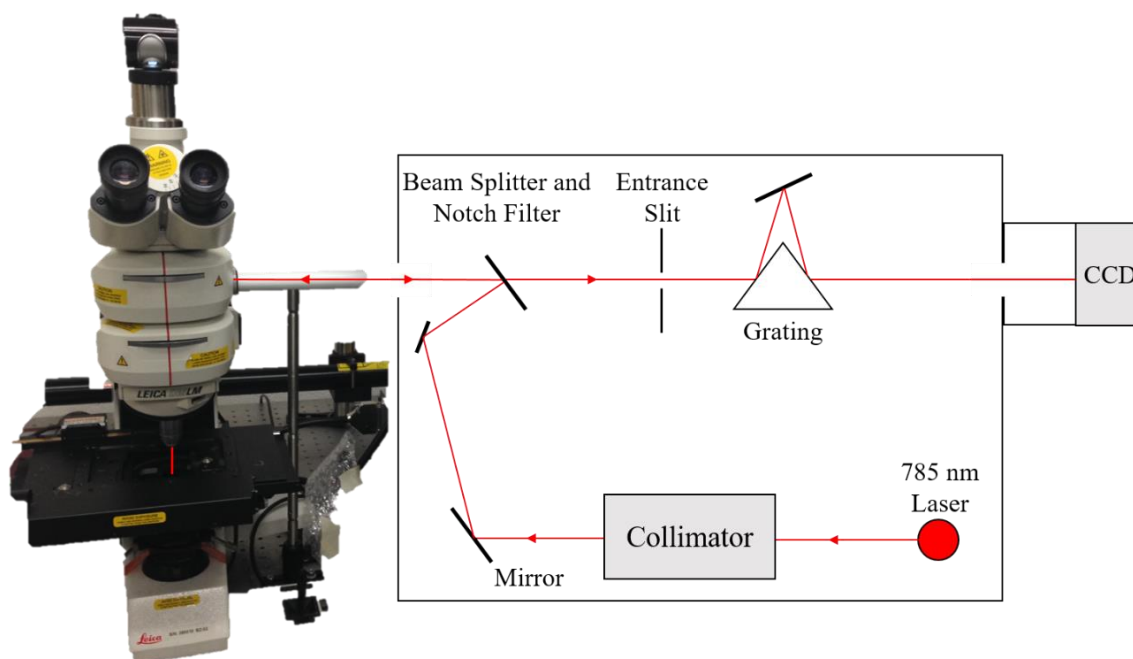


Figure 2-5: Typical schematic of a Raman microspectrometer. The main components are present in the system: laser source, notch filter, diffraction grating, CCD detector.

In such a setup, the objective lens of the microscope focuses the laser to a small point on the sample and then also acts to collect the resulting scattered light. In a confocal microscope setup, the most common configuration is a backscattered geometry, where scattered light is collected back into the objective lens. When a high-numerical aperture objective is used, the microscope experimental setup is able to provide high spatial resolution approaching the diffraction limit.⁹⁶

All experimental results contained in this thesis were collected with a Raman microspectrometer represented by the schematic in Figure 2-5.

2.6 Advantages and Disadvantages of Raman Spectroscopy

Raman spectroscopy offers benefits over more traditional forms of vibrational spectroscopy.

- The ease of adjusting the experimental setup of a Raman apparatus means that spectra can be obtained from very small samples, whether solid, liquid, or gas, and with little sample preparation or need for chemical labels.
- Water is a weak scatterer, a crucial advantage making biological systems accessible to investigations.
- The excitation source of a Raman instrument is monochromatic and can operate at a variety of wavelengths in the UV to IR regions.
- Specialized variants of Raman spectroscopy exist which are suited for particular applications (e.g., signal enhancements can be achieved with careful selection of instrumentation and setup).
- The technique can be applied non-destructively through appropriate selection of the incident wavelength and power.
- A Raman spectrum is information rich because it is a superposition of all Raman-active molecular vibrations within a sample and can be used to investigate the sample composition or as a fingerprint of the sample identity.
- Because it is an optical technique requiring little or no sample preparation, it can readily be applied remotely, for example, via fiber-optic probes.

The disadvantages of Raman spectroscopy are well-known and their impact has been reduced extensively over the past few decades through instrument development.

- As previously stated, Raman signals are inherently weak. For every 10^6 photons generated through scattering, only one is a Raman photon.⁸⁸
- Fluorescence is the emission of light after an electronic absorption process. Commonly present in conjugated systems, the light produced from a fluorescence event is approximately 10^6 times stronger than Raman scattering. This magnifies the disadvantage above, though the use of near-IR incident light can help alleviate the problem as fluorescence is less common at this energy. Unfortunately, as previously mentioned, Raman intensity is inversely proportional to λ^4 and moving towards the near-IR reduces the intensity. Another common approach for addressing fluorescence is to “photobleach” the sample, irradiating it for an extended period to quench the fluorophore.⁹⁸ This works well when the fluorescence originates from the matrix, but when the sample itself is fluorescent, as is often the case in biological samples, photobleaching only functions to damage the sample.
- The intense focused beam from the incident light source can create photochemistry. It is often important to consider the effects of laser power on a sample (e.g., degradation or temperature effects) to understand its effect on Raman spectra.
- Ambient light or background radiation can easily overwhelm the scattered light produced by the Raman effect, and for this reason, measurements are regularly performed in a dark room.

2.7 Application of Raman to Blood¹

On December 10th 1930, C.V. Raman collected the Nobel Prize in Physics for his work “... on the scattering of light and for the discovery of the effect named after him”. That same day, and at the same Stockholm ceremony (unusually), Hans Fischer collected the Nobel Prize in Chemistry for “... researches into the constitution of haemin and chlorophyll and especially for his synthesis of haemin” and another scientist, Karl Landsteiner, received the Nobel Prize in Physiology/Medicine for the “... discovery of human blood groups”. In the decades since Raman, Fischer, and Landsteiner were awarded their Nobel prizes, Raman spectroscopy has become an established analytical technique and blood collection, blood transfusion, and blood research have become global enterprises involving many thousands of scientists and clinicians.

Blood is a vital bodily fluid responsible for numerous physiological functions. It is comprised of a yellow liquid medium called plasma in which a large number of cells, namely red blood cells (RBCs, also called erythrocytes), white blood cells (WBCs, also called leucocytes) and platelets (also called thrombocytes), are suspended. Briefly, RBCs transport oxygen and carbon dioxide between cells and the lungs, WBCs fight disease and infection as part of the immune system, and platelets are vital for blood clotting and wound healing. The extracellular plasma also transports various proteins, electrolytes, and clotting factors, and changes in blood chemistry can be used to help assess the health status of patients.

¹ The remainder of this chapter has been accepted as a focal point review article:

Atkins, C.G.; Buckley, K.; Blades, M.W.; Turner, R.F.B. Raman Spectroscopy of Blood and Blood Components. *Applied Spectroscopy* **2016** (accepted).

Numerous diseases, such as diabetes, malaria, sickle-cell disease, and even particular types of cancers, can be characterized by distinct biochemical changes to the composition of blood. For example, an increase in the concentration of a protein called troponin is a very specific and sensitive indicator of heart muscle damage such as that which takes place during a myocardial infarction (heart attack).⁹⁹ Proper diagnosis of these health problems most often requires the application of analytical techniques that can be time-consuming and invasive to a patient. As a result, researchers have used Raman spectroscopy to help characterize blood and its cellular components. Having the means to measure the status of whole blood, as well as its individual components, in a rapid and non-invasive manner would provide clinicians with a diagnostic tool for disease detection and treatment.

The remainder of this chapter is a literature review that will describe the utility of Raman spectroscopy for the evaluation of whole blood and its various components. The sections listed below, which include each individual blood constituent as well as a section on whole blood, will provide a chronological overview of the published applications of Raman in that particular area. For the most part, research that did not directly utilize blood from a human or an animal (i.e., an analyte mixed with a single component of plasma, such as the globular protein albumin) was excluded. The future direction of the field, as well as its limitations, will also be briefly discussed.

2.7.1 Blood Research and Raman Instrumentation

Different variants of Raman spectroscopy have been applied to the study of blood and each has its own advantages and disadvantages. The variant introduced at the start of this chapter is conventional Raman spectroscopy (also referred to as spontaneous Raman spectroscopy¹⁰⁰), and when applied to the field of blood research, the preferred instrumental set-up couples a Raman

spectrometer to an optical microscope (Figure 2-5) . This set-up is capable of creating high-spatial resolution and enabling the interrogation of individual cells, through experimental methods known as optical tweezing and laser trapping. With regard to the exceptional resolution, the technique can create a contrast from differing molecular compositions allowing the collection of images on the micron scale based on Raman spectra. To achieve single-cell tweezing, the focused laser beam creates a gradient force strong enough to trap dielectric objects using only a few mW of excitation power.

Components that are of interest when it comes to blood (proteins, nucleic acids, lipids, and carbohydrates, among others) exist in low concentrations, and because the conversion efficiency of generating Raman photons from the excitation laser is inherently small, the intensity of scattered photons will be low. Furthermore, these molecular components can exhibit substantial fluorescence capable of masking the existence of Raman signals. Raman studies involving blood often involve variants capable of providing Raman-intensity enhancements.

2.7.1.1 Enhanced Raman Spectroscopy

One of the most common enhancements methods for Raman spectroscopy is to use an excitation wavelength whose energy coincides with an electronic transition. This “resonance Raman” spectroscopy (RRS) approach improves the scattering cross-section and selectively enhances (by orders of magnitude) certain features primarily related to the bonds of the molecule affected most by the electronic transition closest to the frequency of the excitation light. The choice of wavelength depends on the analyte of interest; for example, resonant enhancement for hemoglobin occurs with excitation of the Soret band (the S_0 to S_2 electronic transition, refer to Figure 2-1) at approximately 400 nm. RRS has been previously reviewed elsewhere.¹⁰¹

Another common practice for enhancing Raman signal is with surface-enhanced Raman spectroscopy (SERS). First reported in the 1970s^{102,103}, SERS functions to enhance Raman scattering using metallic surfaces or nanoparticles with plasmonic resonance characteristics, with reports of effective Raman cross-sections being increased by up to 14 or 15 orders of magnitude. It can be performed either directly (“label-free”, where observed bands are associated with analytes themselves) or indirectly (characteristic spectrum of the SERS label changes in the presence of analyte). The field of SERS has grown rapidly since the late 1990s and has recently been reviewed.¹⁰⁴

Variants of SERS also exist, such as tip-enhanced Raman spectroscopy (TERS)¹⁰⁵, which combines the sensitivity of SERS with the spatial resolution of scanning probe microscopy. The Raman enhancement occurs at the tip of a near-atomically sharp stylus, typically coated with gold, which enables surface characterization and the study of individual molecules with sub-nanometre spatial resolution. A more recently adapted variant, Surface-enhanced spatially offset Raman Spectroscopy (SESORS)¹⁰⁶, combines SERS with spatially offset Raman spectroscopy (SORS - a technique described in Chapter 5). The advantage of SESORS is the ability to implant a metallic substrate into a subject and obtain the subsequent chemical information by performing a measurement through the covering layer (e.g., skin).

2.7.2 Literature Review of Published Applications

2.7.2.1 Hemoglobin and RBCs

2.7.2.1.1 Isolated Hemoglobin

Hemoglobin, the main constituent of the RBC described in section 1.2.1.3 of the introduction, is a very strong resonance Raman scatterer due to its highly conjugated heme sub-

units. Thus, Raman spectra of both RBCs and whole blood are dominated by hemoglobin bands and hemoglobin spectra were the subject of much of the early work in the field.

From mid-1972, groups from Princeton, NJ, USA (Spiro et al.) and Munich, Germany (Brunner et al.) began publishing RRS studies of hemoglobin.¹⁰⁷ Spiro et al. reported the first measurements (568.2 nm excitation)¹⁰⁸ from dilute aqueous solutions of hemoglobin derivatives, and the following month Brunner et al. presented similar Raman results (488 nm excitation) from dilute hemoglobin solutions. In the latter work it was shown that the spectra of oxygenated hemoglobin (oxyHb) and deoxygenated hemoglobin (deoxyHb) differed markedly and that bands at 1220 cm^{-1} and 1360 cm^{-1} shifted upon transition from oxyHb to deoxyHb. It was deduced from this information that these modes were dependent on the displacement between the iron atom and the porphyrin group within the heme structure.¹⁰⁹ Follow-up work from the Princeton researchers demonstrated that the hemoglobin spectrum was polarization dependent (Figure 2-6) and confirmed Albrecht's Vibronic Theory² of on-resonance Raman spectroscopy.¹¹⁰

² Albrecht had theorized that on-resonance Raman had different selection and polarization rules to off-resonance Raman spectroscopy

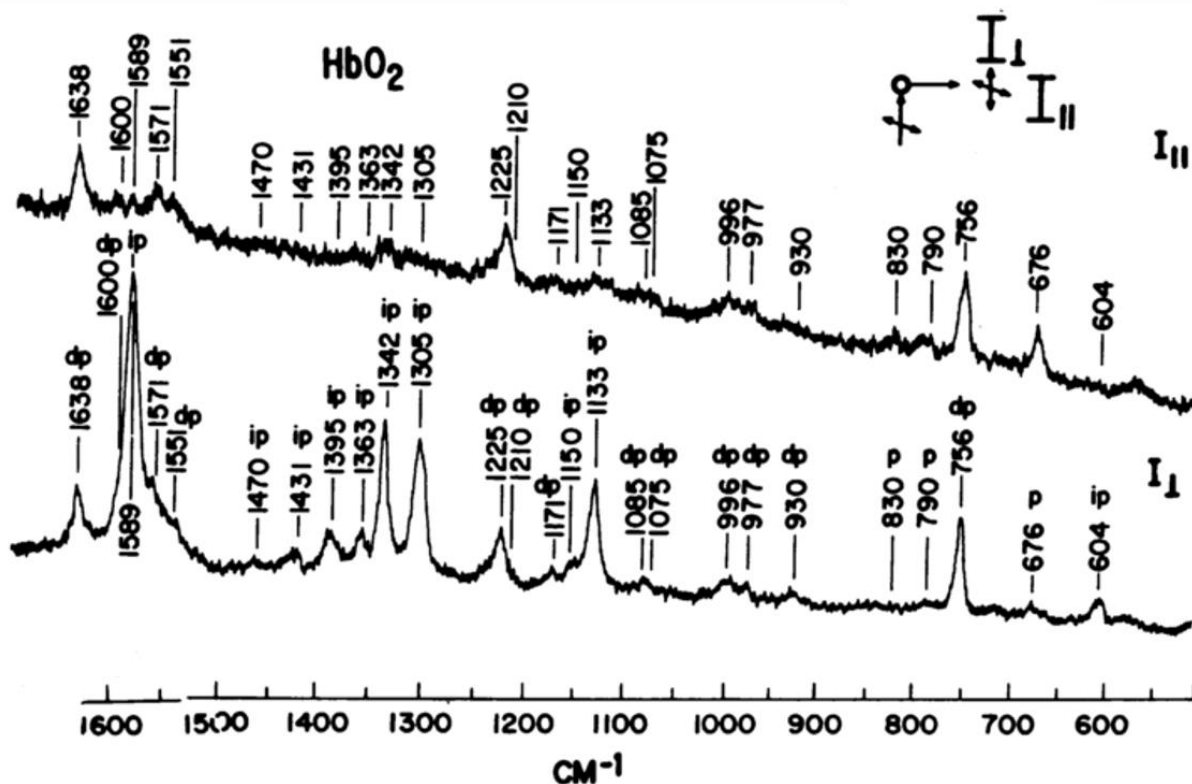


Figure 2-6: Resonance Raman spectra of oxyHb as reported in 1972. The scattering geometry is shown schematically at the top of the diagram. Both the direction and the polarization vector of the incident laser radiation are perpendicular to the scattering direction. The scattered radiation is analyzed into components perpendicular (I_{\perp}) and parallel (I_{\parallel}) to the incident polarization vector. The exciting wavelength was 568.2 nm and concentrations ~ 0.5 mM. Reprinted from Reference 110 with permission from the author.

Brunner and Sussner published a deeper investigation of the oxygenation states of hemoglobin and in it they made the following observations:

- (1) Nearly all Raman lines of deoxyHb were approximately twice as strong as those of oxyHb.
- (2) Three lines at 670, 1376 and 1468 cm^{-1} showed an absolute increase upon deoxygenation.
- (3) Three Raman lines of oxyHb (at 572, 1504, and 1636 cm^{-1}) were completely missing in the spectrum of deoxyHb.
- (4) The line at 1223 cm^{-1} in oxyHb shifted to 1210 cm^{-1} upon deoxygenation.
- (5) The most conspicuous change was the frequency shift of the strongest line at 1376 cm^{-1} in oxyHb to 1355 cm^{-1} in deoxyHb.

They deduced that the majority of Raman lines arise from vibrational modes involving the C-C, C=C and C-N bonds of porphyrin conjugated ring structure.¹¹¹ In follow-up work, Brunner used an oxygen isotope to identify a mode assignable to stretching of the iron-oxygen (Fe-O₂) bond at 567 cm^{-1} (Figure 2-7).¹¹²

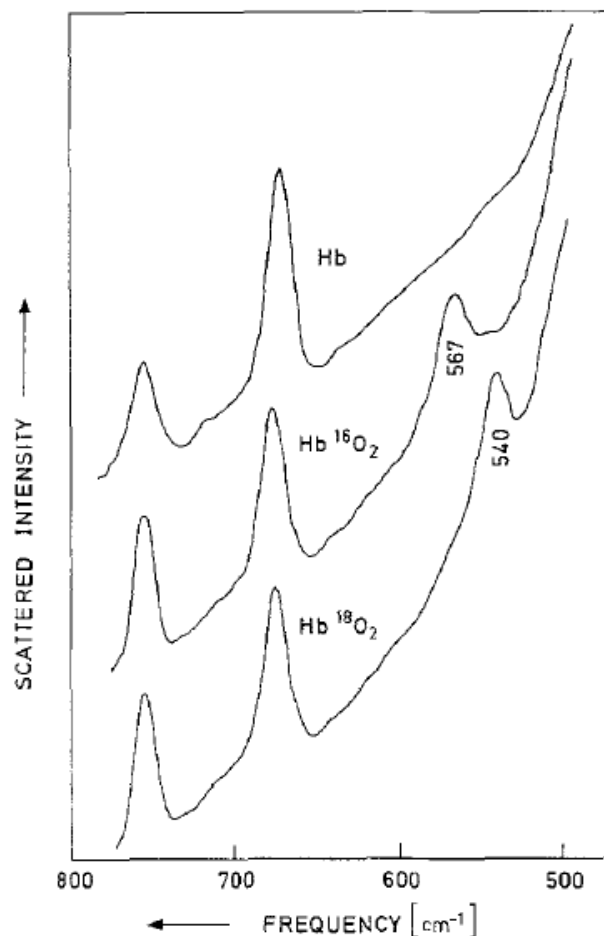


Figure 2-7: Resonance Raman spectra of hemoglobin, Hb- $^{16}\text{O}_2$ and Hb- $^{18}\text{O}_2$ at 15°C, pH 7.4, 488 nm excitation. The band at 567 cm^{-1} appeared when hemoglobin was oxygenated, and shifted when oxygenated with an isotope. This mode was assigned to Fe-O $_2$ stretching. Reprinted from Reference 112 with permission from Springer-Verlag.

Understanding the nature of the Fe-O $_2$ bond was thought to be vital to the elucidation of oxygen binding in hemoglobin and it became the subject of much work. In 1973, Yamamoto et al. studied different forms of hemoglobin protein with RRS (441.6 nm excitation) to deduce the nature of the Fe-O $_2$ bond in oxyHb. Their results showed that iron in oxygenated hemoglobin exists in

the low-spin ferric (Fe^{3+}) state rather than the low-spin ferrous (Fe^{2+}) state.¹¹³ The following year, Spiro et al. published important work on the spin state of the central iron atom¹¹⁴ and they later published a report which described a sample-cell that allowed different forms of hemoglobin to circulate whilst spectra were being collected (thereby reducing absorption and photo-damage).¹¹⁵

Similar work continued into the early 1980s, as the Spiro group^{116,117} and others^{118–122} explored the strength of Fe-O₂ bonds in ligated hemoglobin-like molecules. Throughout the rest of the decade, RRS¹²³ and SERS^{124–126} were deployed to study these different forms of hemoglobin and both the spectral and denaturation properties of these systems were thoroughly characterized. At the end of the 1980s, the Spiro group investigated the dynamics of ligand-binding to hemoglobin, using time-resolved UV resonance Raman (229 nm excitation). The study, which looked at carbonmonoxy-hemoglobin, found the transition time from the relaxed state (oxygenated, R) to the tense state (deoxygenated, T) to be $\sim 20 \mu\text{s}$.¹²⁷

Raman studies of isolated hemoglobin continued into the 1990s. Ozaki et al. deployed near-infrared (NIR) Fourier transform (FT) Raman Spectroscopy (1064 nm excitation) to study met-hemoglobin (metHb), a form of hemoglobin which contains iron in the Fe^{3+} state but cannot bind oxygen.¹²⁸ Later, the Spiro group subjected hemoglobin to chemical alterations in sub-unit regions they suspected to be important to the protein's quaternary structure (they removed C-terminus residues from particular amino acids) and used two different RRS excitations (229 nm and 441.6 nm) to show the alterations increased hemoglobin's oxygen affinity and affected its functionality (the alterations reduced the protein's Bohr Effect and its cooperativity).¹²⁹

Raman analyses of isolated hemoglobin and its many variants¹³⁰ have led to deeper understanding of the metalloprotein's form and function. The oxygenation of hemoglobin has

continued to be of interest and enhancement Raman techniques other than RRS have been applied. Coherent anti-Stokes Raman scattering (CARS) acquired quantitative measurements of oxygen saturation that agreed well with optical absorption analyses,¹³¹ and one of the most highly cited hemoglobin studies was a SERS experiment which obtained spectra from single hemoglobin molecules attached to 100-nm-sized immobilized silver particles.¹³²

2.7.2.2 Raman Studies of Intact RBCs

2.7.2.2.1 Intracellular Hemoglobin

In one of the early studies mentioned above, the investigators compared the spectrum of hemoglobin to the spectrum of intact RBCs and stated that:

“the recorded Raman spectra of erythrocytes were identical to that of oxy- and deoxyHb, respectively, when we used the original suspension or added a small amount of deoxygenating dithionite”.¹¹¹

In 2001, almost thirty years after the original report, workers at Monash University in Victoria, Australia used conventional Raman spectroscopy (633 nm excitation) to record the same oxyHb (R state) and deoxyHb (T state) spectral features inside single *living* erythrocytes.¹³³ The group expanded their efforts in 2002 to include various excitation sources (488 nm, 514 nm, 568 nm, in addition to 633 nm), revealing differences in the spectra (Figure 2-8) that could only be attributed to enhancement mechanisms associated with pre-resonance of the Soret band (~400 nm) and resonance around the Q bands (525-575 nm).¹⁶ Excitation wavelengths between 400-500 nm were shown to enhance the totally symmetric A_{1g} modes while excitation between 500-600 nm

enhanced the anomalously polarized A_{2g} modes and depolarized non-totally symmetric B_{1g} and B_{2g} modes.¹³⁴ In the years that followed, the Monash workers^{135,136} and others^{137,138} went on to characterize the cellular oxygenation/deoxygenation cycle; they would publish evidence of heme ordering within functional RBCs,¹³⁹ report insights related to intracellular heme-aggregation and denaturation,¹⁴⁰ investigate the effects of fixation and dehydration on heme environment of hemoglobin,^{141,142} and use TERS to probe nanoscale oxidation changes on the surfaces of hemoglobin crystals.¹⁴³ This body of work significantly shifted the boundaries of hemoglobin research with conventional Raman spectroscopy from the isolated protein (i.e., model systems using commercial lyophilized protein) to the intra-cellular protein (i.e., examination of hemoglobin in real and living systems).

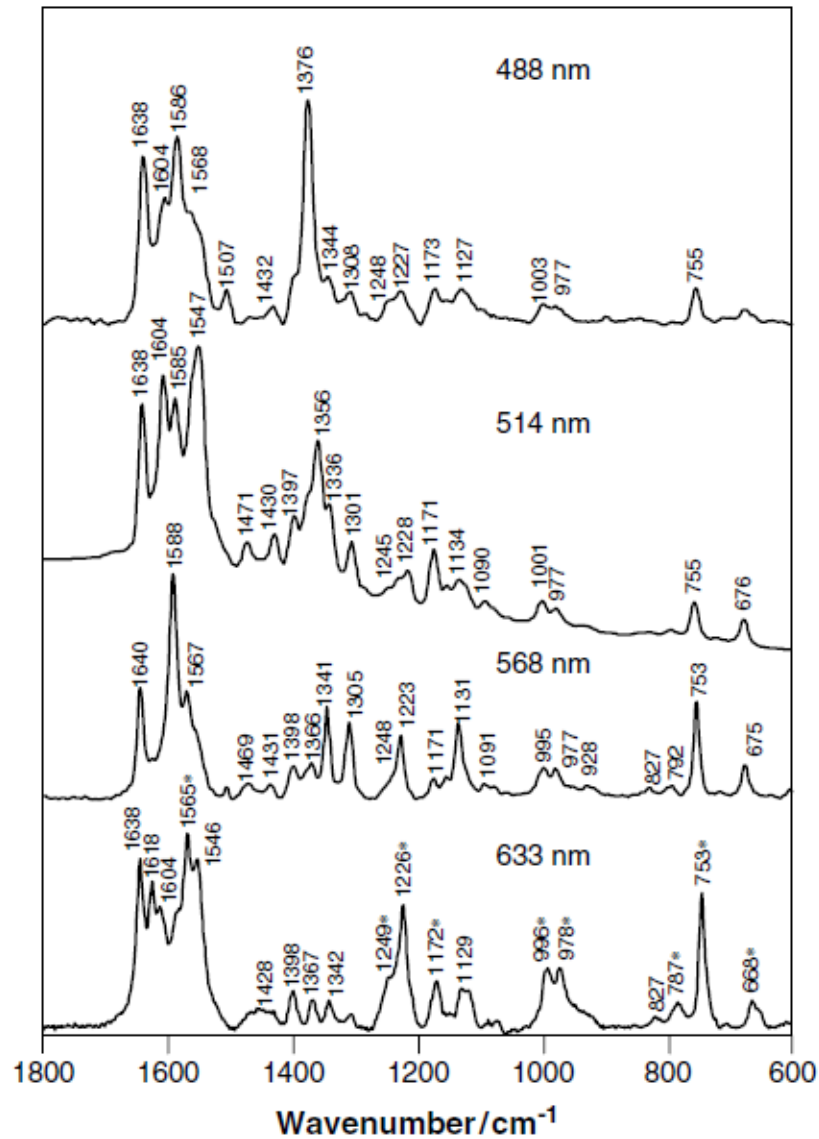


Figure 2-8: Raman spectra of oxygenated single erythrocytes recorded using different excitation wavelengths. The spectra presented are averaged from four spectra of different erythrocytes under the same conditions. Reproduced from Reference 144 with permission from John Wiley & Sons, Inc.

Other recent measurements have shown that two different types of hemoglobin molecule can be resolved inside an intact living erythrocyte (submembrane-hemoglobin and cytosolic

hemoglobin)¹⁴⁵ and that SERS can be used to investigate oxy- and met-RBCs (the SERS spectra show characteristic heme bands, but also exhibit other prominent bands that may have been associated with cell membrane components and/or protein denaturation).¹⁴⁶ One of the co-authors (McNaughton) of the latter study was a member of the Monash group who were responsible for much of earlier work on the oxygenation/deoxygenation cycle. The following year he was involved in another SERS study which characterized the interaction between nanoparticles and hemoglobin/RBCs¹⁴⁷, and the year after that, he co-authored work on hemoglobin's non-fundamental Raman modes¹⁴⁸; enhanced overtones were observed in spectra of RBCs which, interestingly, were not found in hemoglobin solutions. McNaughton and another member of the Monash group (Wood) would go on to publish many Raman studies of pathology in erythrocytes which are discussed in section 2.7.2.3 below.

In 2015, Raman spectroscopy (488 nm excitation) was combined with atomic force microscopy (AFM) to image single RBCs from smears of dried whole blood and internal distributions of Fe²⁺/Fe³⁺ hemes were shown for the first time.¹⁴⁹ The oxidation state of iron is crucial to proper hemoglobin functionality, and Raman imaging of the smears showed the existence of hemichrome (a non-functional form of Fe³⁺ hemoglobin) on the periphery of RBCs, while the internal part of the cell existed in an oxyHb state after dying.

2.7.2.2.2 Laser Tweezers Raman Spectroscopy of Hemoglobin and RBCs

In the early 2000s optical tweezers (instruments that capture, hold, and perform very fine mechanical manipulations on small particles) were combined with Raman spectroscopy to create a new class of scientific instrument. The new 'laser tweezers Raman spectroscopy' (LTRS) instruments could be used to collect chemically-specific information from cells, bacteria, and

viruses. The technique allowed much more detailed investigations of hemoglobin and many of the early demonstrations of LTRS were performed using RBCs as samples.^{150–153}

As LTRS technology has matured, it has been used to refine previous studies that had experienced limitations due to sampling protocols. Dasgupta et al. used LTRS to examine the laser-induced degradation of hemoglobin inside trapped erythrocytes, where the results demonstrated increased intensities of the 975 cm^{-1} , 1244 cm^{-1} , and 1366 cm^{-1} Raman bands “after exposure to 7 mW of NIR light for a few tens of seconds”.¹⁵⁴ These bands were consistent with hemoglobin existing in an aggregated form, confirming earlier work by researchers from the Monash group. Ahlawat et al. then used LTRS to examine the ordering of hemoglobin inside the cell. They observed that particular intensities were dependent on orientation, with the most prominent intensity change occurring in the band at 754 cm^{-1} (pyrrole breathing vibration). The results suggested that hemoglobin “must be present in an ordered arrangement, such that the heme-porphyrin planes are preferentially orientated parallel to the RBCs’ equatorial plane”.¹⁵⁵ LTRS has become an increasingly important technique in the study of living RBCs, for investigations of oxygenation within single cells,^{156–158} and for investigation of the effects of laser-light on RBC biology.^{159–161} LTRS has also been integral for characterizing red cell response to stimulus/stress (e.g., alcohol-induced denaturation,¹⁶² electrical current,¹⁶³ oxidative stress,¹⁶⁴ and pH-changes¹⁶⁵) and has been deployed to compare oxygen uptake of different globin-containing cells.¹⁶⁶ Workers at the Center for Biophotonics, Science and Technology, UC Davis, who contributed to developing the LTRS capability, have studied a number of these phenomena.^{167–169}

2.7.2.2.3 RBC Membrane

As some investigators were elucidating the form and function of RBC hemoglobin, other groups were characterizing RBC membranes. In 1972, Bulkin reported a Raman spectroscopic study (632.8 nm excitation) of human erythrocyte membranes. The spectra of the isolated membranes (called ‘ghost cells’ due to the removal of all internal components) showed bands at 1110 cm^{-1} , 1340 cm^{-1} , 1420 cm^{-1} , and 1445 cm^{-1} that were attributed to:

“the hydrocarbon chains of the fatty acids, with a possible small contribution from the CH_2 groups of cholesterol”.¹⁷⁰

In the mid-70s, Raman was used to study the protein components of RBC ghosts; the results suggested that the protein fraction contained 40-55% α -helix with little β -configuration and that 55-65% of the hydrophobic side chain content of the phospholipid were in the ‘all-trans rigid’ configuration. All Raman modes were “assigned to either protein or phospholipid” at 488 nm excitation, with no suspected contribution from cholesterol.¹⁷¹ Verma and Wallach shed more light on the ‘ghost cell’ system over the following years. They identified two strong bands attributable to conjugated double bond systems¹⁷² (later shown to be carotenoids¹⁷³), studied the effects of transmembrane ion gradients¹⁷⁴, and investigated the sensitivity of temperature/pH to membrane-state transitions in the CH-stretching region.^{175,176} During the same period, other workers discovered specific vibrations related to membrane fluidity, peptide-backbone conformation, and disulfide bonding.¹⁷⁷

The 1970's also saw Raman studies (514.5 nm excitation) of intact erythrocyte membranes and of membranes from which the peripheral proteins had been extracted. The results indicated that the extraction caused considerable changes in the peptide bonds but had little effect on lipids, and that secondary structure of remaining intrinsic membrane proteins was modified.¹⁷⁸ Decades later, the same group published work on the relative lipid and protein contributions to the amide I band (using 488 nm excitation).^{179,180}

More recently, Li et al. used Raman (785 nm excitation) and chemometric analyses to show that 30 minutes of exposure to mid-ultraviolet (UVB) radiation could damage RBC membranes. The data showed a decrease in the amount of α -helix and side-chains (CH_2/CH_3) while the random coil conformation content increased.¹⁸¹

2.7.2.2.4 RBC Cellular Biology

While Raman research into particular RBC components has continued, investigations of whole-cell erythrocyte biology have also been reported. Raman spectroscopy has been used, for example, to study the mechanisms associated with RBC ageing.^{182,183} In these studies, cells were separated by Percoll fractionation (where the lightest 25% were said to be youngest and the heaviest/densest RBCs were said to be oldest) and subjected to line mapping analysis (514.2 nm excitation). The intensity of the 1358 cm^{-1} band (assigned in a previous work to the symmetric half-ring stretch of pyrrole) across the samples suggested that hemoglobin was less uniformly distributed in older RBCs. The authors stated that, in the older cells, hemoglobin molecules “are aggregated and attached to the inside cell membrane” which reduced membrane flexibility and possibly influenced hemoglobin's oxygenation. The authors also suggested that when hemoglobin

is bound to the inside of the membrane, “the reactive oxygen species generated in autoxidation are not efficiently neutralized by the cellular antioxidant enzymes”.¹⁸³

A more recent (2014) study used another variant of Raman spectroscopy (2D Raman correlation spectroscopy) to investigate age-related disintegration of RBCs. The asynchronous spectra in the data set (which represent the overall differences in the time behavior) led the authors to suggest that the heme groups separate themselves from the globin proteins, and the synchronous spectra (which represent the similarities in the time behavior) suggested that the globin proteins break-down into individual amino acids. The data also pointed towards metal ion centers being involved in the disintegration process.¹⁸⁴

2.7.2.2.5 RBC Transfusion

Described in section 1.3.1 of the Introduction, blood banking agencies obtain whole blood from volunteer donors, separate the RBCs by differential centrifugation, suspend them in specially formulated additive solutions such as saline-adenine-glucose-mannitol (SAG-M), and store them in polyvinyl chloride (PVC) blood-bags at 4 °C until needed for transfusion. Chapters 3, 4, and 5 of this thesis describe research efforts where Raman spectroscopy was deployed to elucidate changes related to degradation of stored RBCs.

2.7.2.3 Hemoglobin, RBCs, and Disease

Raman spectroscopy and LTRS studies of pathological hemoglobin and RBCs have become increasingly numerous in recent years.

2.7.2.3.1 Malaria

Malaria is caused by a genus of parasites called *Plasmodium* and is transmitted via the bites of infected mosquitoes. The parasites multiply in the liver of the human body and then infect RBCs where they catabolize hemoglobin and produce a waste-product called hemozoin. Each year, more than 1 million of the (300 to 500 million) people infected with malaria die. The current gold-standard for malaria diagnosis is the microscopic examination of Giemsa-stained blood smears, a process that is time consuming and requires trained operators. Raman researchers have targeted accurate detection of hemozoin as the metric for malaria diagnosis. If hemozoin can be measured, then it is believed changes to the relative intensity of bands in its Raman signature could open avenues for Raman spectroscopy to monitor interactions between hemozoin and drug candidates.

Since the 1990s, researchers have been investigating the possibility of using Raman spectroscopy as an alternative diagnostic tool for malaria. Brémard et al. used RRS to characterize hemozoin¹⁸⁵ and Ong et al. used RRS to characterize infected RBCs.^{186,187} It was mentioned above (section 2.7.2.2.1) that workers at Monash University carried out some of the earliest studies of intracellular hemoglobin^{133,136,188} and that in the years since, two members of the team, Wood & McNaughton, have gone on to do much Raman analysis of pathological erythrocytes. In 2003, Wood, McNaughton and co-workers reported an enhancement of a particular hemozoin Raman band (at 1374 cm⁻¹) that allowed the food vacuole of a *Plasmodium*-infected cell to be imaged (Figure 2-9).¹⁸⁹ The following year, they reported a more detailed Raman study of hematin (the synthetic analog of hemozoin).¹⁹⁰

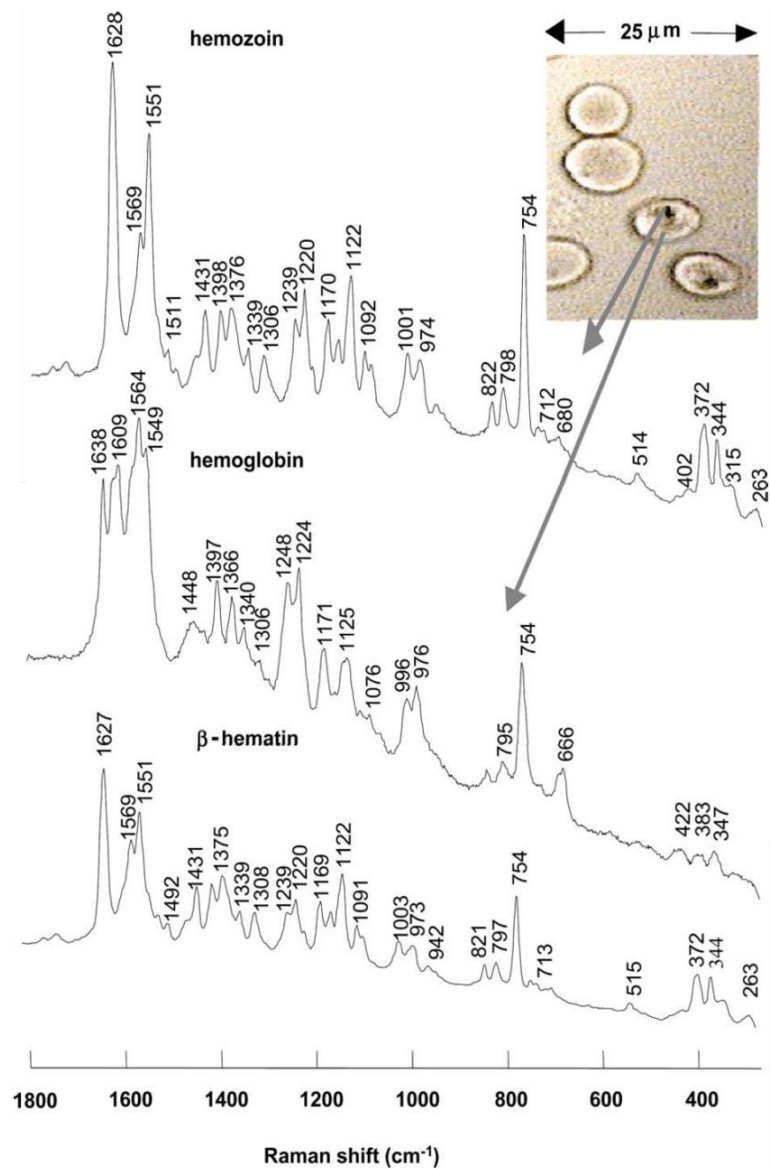


Figure 2-9: Photomicrograph of *P. falciparum*-infected erythrocytes (late trophozoite stage) showing the food vacuoles containing hemozoin. The arrows indicate the laser targets, namely the food vacuole and the surrounding hemoglobin. The corresponding spectra are compared with synthesized β -hematin. Reproduced with permission from Fig. 2 in Reference 189. Permission provided by Elsevier.

In 2007 the Monash workers co-authored a study in which acoustic levitation was used to suspend RBCs and *Plasmodium* cells in place allowing the measurement of the spectral signature of hemozoin in infected cells.¹⁹¹ One of the co-authors of that study, J. Popp, had previously been one of the early workers on LTRS.¹⁹² Popp and his colleagues would go on to investigate hemozoin morphology with visible light (633 nm & 647 nm)¹⁹³ and later introduced a fiber-array based instrument capable of selectively analyzing hemozoin in early stages of malaria infection.¹⁹⁴ Popp would co-author many Raman studies on other types of blood-cells, and these are described in the appropriate sections below.

In 2009 the Monash group combined RRS with partial dark-field microscopy to detect and diagnose malaria signatures in thick blood films.¹⁹⁵ Other groups would go on to use Raman to elucidate hemozoin formation inside malaria-infected erythrocytes; for example, RRS would be coupled with chemometric analysis to map the spatial distribution of heme species inside the cells¹⁹⁶ and LTRS would be used to compare healthy RBCs with cells that were infected with *Plasmodium vivax*.¹⁹⁷ In the latter study, spectral changes occurred in bands associated with heme oxygenation, suggesting a significant fraction of intracellular hemoglobin in the infected cells had a reduced oxygen-affinity.¹⁹⁷

Having developed a solid foundation for the Raman features of hemozoin, research began to investigate practical applications. Wood, McNaughton et al. were the first to study the effect of anti-malarial drugs on the hemozoin spectral signatures. In one study, infected cells were incubated with the most commonly used drug, chloroquine, and structural changes in hemozoin were detected with Raman as several bands became less intense in comparison to control cells.¹⁹⁸ In another study, they demonstrated TERS could potentially be used to analyze drugs binding to the

hemozoin surface inside the digestive vacuole of *Plasmodium* cells.¹⁹⁹ The TERS spectrum showed a similar hemozoin spectral profile to RRS in terms of band position, although the relative enhancement of bands was somewhat different and band shifts were observed.

Raman spectroscopy has most recently been explored in malarial research for achieving real-time diagnosis. In 2013, conventional Raman (532 nm excitation) was used to monitor the progression of malaria in mice. The spectral changes in erythrocytes and plasma were followed over the course of 7 days of infection. Heme-related changes were detected in the very early stages of infection (as little as one day after *Plasmodium* infection) and this was meaningful because existing techniques can struggle in these stages where the parasitemia levels are low (on the order of 0.2%). Further principal component analysis (PCA) indicated erythrocyte membrane changes at day 4, when parasitemia levels reached 3%.²⁰⁰ Detection of hemozoin has also been attempted with SERS in two ways: mixing silver nanoparticles with lysed blood for a SERS analysis, and synthesizing the silver nanoparticles directly inside the parasites. Using the first method the lowest detectable parasitemia level was reported as 0.01% and with the second method, the detection limit was said to be as low as 0.00005% (approximately 2.5 parasites/ μ L of blood).²⁰¹

2.7.2.3.2 Genetic Blood Disorders

While there are numerous blood disorders affecting the human hematologic system, two that have been investigated with Raman spectroscopy are thalassemia and sickle cell disease (SCD). Thalassemia is characterized by abnormal formation of hemoglobin and improper oxygen transport. LTRS has been used to probe thalassemic RBCs and it has been found that both the spectroscopic and mechanical properties of the cells are different in comparison to normal controls.²⁰² SCD results from a point mutation in a codon of the globin gene (a glutamic acid is

replaced by valine). It causes RBCs to assume an abnormal, rigid, sickle-like shape and is associated with a number of acute and chronic health problems, such as severe infections, attacks of severe pain or stroke. The researchers from Monash University (mentioned above) investigated sickle cells and determined that their Raman spectra resembled a normal deoxyHb red cell, but with exaggerated features attributed to hemoglobin aggregation. They were able to image the 1248 cm^{-1} band, a prominent feature of aggregation, and visualize the aggregated hemes within the sickled-cell.¹³⁴ In 2012, the UC Davis group (also mentioned above) used sickle-cells as demonstration samples in one of the early reports of LTRS,¹⁶⁸ and they later used the technique to show that sickle-cells deoxygenated more readily under (optical or mechanical) stress than healthy control cells.¹⁶⁹ Recently, Raman spectroscopy has been proposed as a tool for quick and accurate diagnosis of SCD and a clinical investigation has been performed by researchers from Brazil. The results showed that subtle changes in the polypeptide chain of abnormal hemoglobin could be discerned from the normal hemoglobin variant, and that the chemometric model designed by the group correctly discriminated 100% of the samples in each cell class.²⁰³

2.7.2.3.3 Other Diseases and Disorders

The application of Raman spectroscopy as a tool to probe RBCs has also seen utility for diseases and disorders that have a more convoluted connection to blood chemistry. A 1988 study compared RBCs collected from seven people suffering from rheumatoid arthritis with seven controls and used Raman spectroscopy to measure the rapidity of the hemoglobin oxygenation. The cells from veins of those with rheumatoid arthritis were said to be more oxygenated initially, but remarkably showed a (statistically significant) tendency to take-up atmospheric oxygen more slowly.²⁰⁴ A 2005 study compared RBCs from twelve male patients who had suffered from heart

failure with RBCs from (younger) control donors. The results revealed patients with heart failure exhibited:

- (i) decreased total content of Hb–ligand complexes, such as O₂, CO, and NO
- (ii) an attenuated number of Hb–NO complexes with preserved Fe–Hb bonds
- (iii) sharp decreases in the amount of Hb–NO complexes with cleaved Fe–Hb bonds

The authors stated that (i) and (ii) strongly suggest oxyhemoglobin content was diminished in heart failure. They believed that (iii) contributed to the reduced O₂ tissue supply seen in patients with heart failure.²⁰⁵

Raman spectroscopy of RBC components has also been proposed as a new method of diabetes diagnosis. The envisaged test would be based on the correlation of *in vivo* hemoglobin glycosylation with the average concentration of glucose in blood-plasma. In 2010, it was shown that SERS could be used to detect glycated hemoglobin (HbA_{1c}) at very low concentrations,²⁰⁶ and in 2014, drop-coating deposition Raman spectroscopy was deployed for the same task.²⁰⁷ That same year, Lin et al. demonstrated that damaged membrane lipids (e.g., decreased liquidity and altered phospholipid organization) could be detected using Raman in RBCs collected from diabetic patients. With the aid of multivariate statistical methods (and analysis of the high-wavenumber region of the spectrum), they achieved a diagnostic accuracy of 98.8% for differentiating diabetic from normal RBC membranes.²⁰⁸

Finally, recent Raman studies have investigated heme-proteins from the blood of children with epilepsy,²⁰⁹ and metHb has been measured as a clinical biomarker of pathophysiology, such as nitrite poisoning.^{210,211}

2.7.2.4 White Blood Cells

2.7.2.4.1 Introduction and General Appearance of Raman Spectrum

WBCs are part of the body's immune system and are responsible for fighting bacterial, viral and fungal infections. There are three types of WBCs - monocytes, lymphocytes, and granulocytes - and together they account for approximately 1 percent of blood cells.

Raman analyses of WBCs began in the early 1990s and many of the early studies were published by Puppels et al. at the University of Twente. They showed that Raman could be used to distinguish the WBC nucleus from the cytoplasm (Figure 2-10),²¹² that cytoplasm spectra could be used to distinguish different subtypes of WBCs,²¹³ and that carotenoids (an important class of anti-oxidants) were present in high concentrations at distinct sites in the cytoplasm of specific cell populations.²¹⁴ Another early Raman study of WBCs used RRS to detect cytochrome b558, an enzyme thought to aid the generation of reactive-oxygen species for phagocytosis, in frozen pellets of neutrophilic granulocytes.²¹⁵

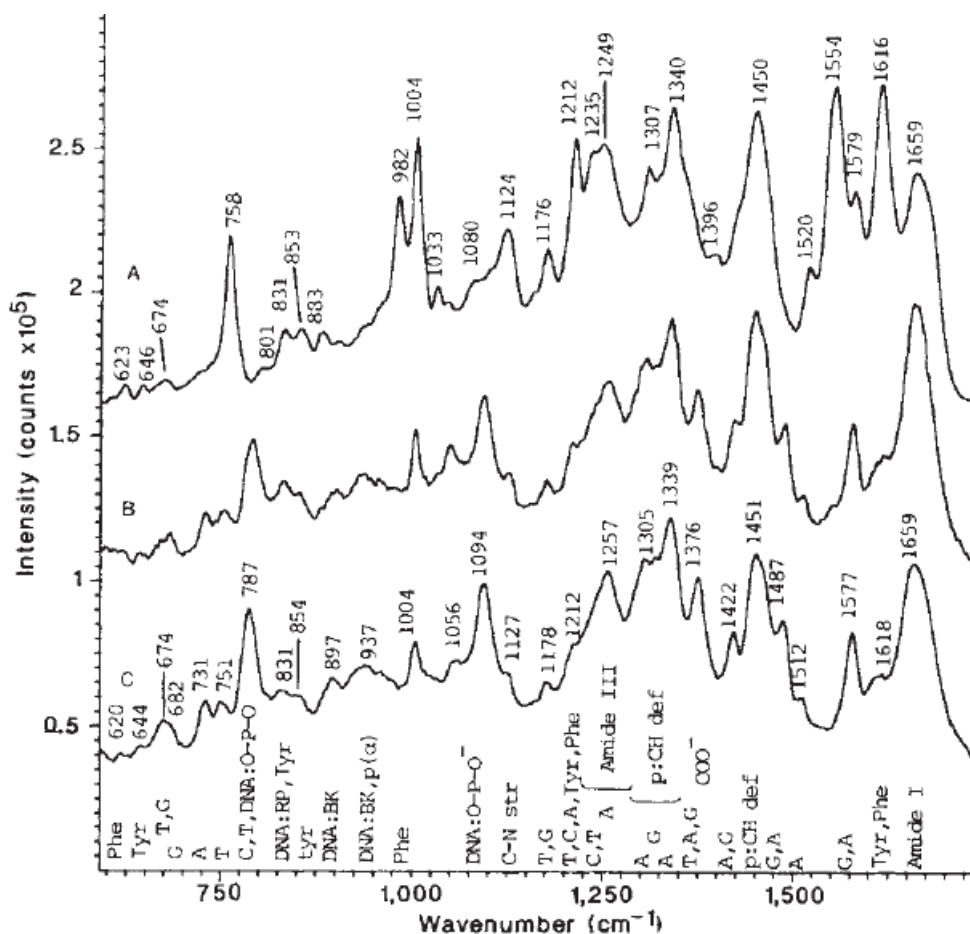


Figure 2-10: The spectra of a single intact granulocytes as obtained by Puppels et al. The data confirmed the difference between the cytoplasm (spectrum A) and the nucleus (spectrum B) in the same cell. Spectrum C is from a chromatid of a Chinese hamster lung cell and functions to confirm the similarity of the chromatid to the nucleus spectrum in B whose contributions are subsequently confirmed to be mainly DNA and protein. Reprinted from Reference 212 with permission from Macmillan Publishers Ltd: Nature, Copyright (1990).

In the 1990's, WBCs were the subject of further Raman analysis by other groups. It was reported that the level of carotenoids in one type of lymphocyte decreased with donor-age,²¹⁶ that

both reduced and oxidized forms of important enzymes cytochrome b558 and myeloperoxidase (MPO) could be distinguished,²¹⁷ and that these important enzymes could be elucidated using Raman (the redox state of both cytochrome b558 and MPO were changed upon cell-activation which demonstrated that processes inside living neutrophils could be monitored using Raman).^{218,219}

Raman studies of WBCs continued through the first decade of the 2000s and new technologies such as Raman mapping²²⁰ and LTRS²²¹ were utilized. One of the more prominent groups in the period were J. Popp and his colleagues at Jena University who combined Raman techniques with statistical analyses (hierarchical cluster analysis, PCA, support vector machines, etc.) to rapidly identify various cells in various body fluids (as mentioned in section 2.7.2.3.1, this group published Raman studies of various types of blood cells, including WBCs). In 2003, they used fluorescence-labelling combined with Raman microspectroscopy to distinguish subtypes of WBCs found in cerebrospinal fluid (interference was avoided by “using an appropriate fluorescence dye and a Raman excitation wavelength [532 nm excitation] far away from the absorption region of the dye”).²²² The group then developed a Raman cell-classifier to create a protocol that would be capable of identifying the two most abundant WBCs (the neutrophilic granulocyte and the mononuclear lymphocyte) from one another. This process, which is illustrated in Figure 2-11, used Raman imaging to visualize morphological features and achieved an accuracy of 94% in the validation step. It was able to predict the identity of unknown cells from a completely different donor with an accuracy of 81% using a single spectrum.²²³

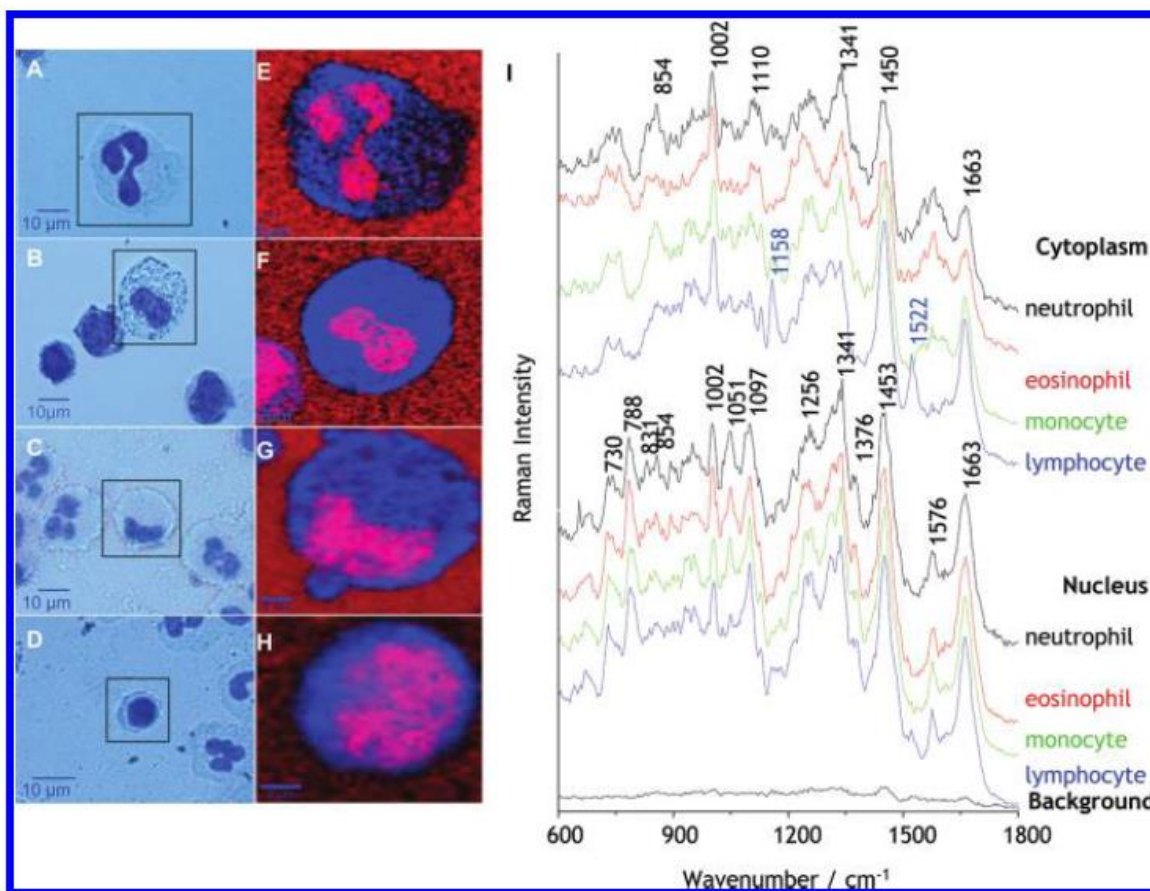


Figure 2-11: Morphological characteristics of the different WBCs (neutrophil: A and E, eosinophil: B and F, monocyte: C and G, lymphocyte: D and H) are displayed visually in the images presented on the left and averaged Raman spectra of the cytoplasm, nucleus, and background region are plotted on the right. Reprinted with permission from Reference 223. Copyright (2012) American Chemical Society.

The group at Jena are not the only ones continuing Raman studies on WBCs. In 2011, Pully et al. used time-lapse Raman imaging to demonstrate that carotenoids, lipids, and RNA could be

tracked in the cytoplasm of live lymphocytes. Using difference spectra (Figure 2-12) they also revealed photo-induced changes to carotenoid molecules.²²⁴

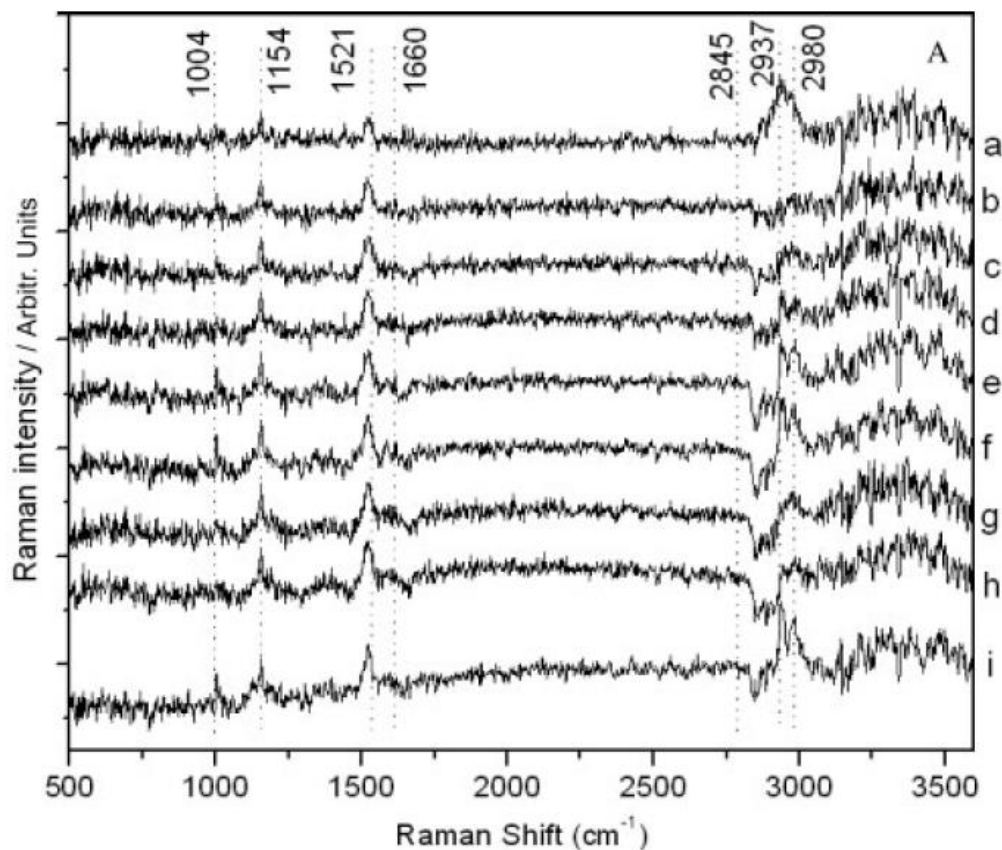


Figure 2-12: Plot for the Raman difference spectroscopy results (647 nm excitation) for cell spectra of first image minus other images showing variations in the carotenoid molecules (a) image 1 to image 2, (b) image 1 to image 3, (c) image 1 to image 4, (d) image 1 to image 5, (e) image 1 to image 6, (f) image 1 to image 7, (g) image 1 to image 8, (h) image 1 to image 9 and (i) image 1 to image 10. As the carotenoid cellular content decreases, the carotenoid bands increase in the difference spectra. Adapted from Reference 224 with permission from John Wiley & Sons, Inc.

2.7.2.4.2 Cancer and Disease

Most Raman studies of diseased WBCs have focused on the discrimination of diseased and healthy cells rather than on the underlying pathology. The earliest work by Schmidt-Ullrich et al. in 1975 used isoelectric focusing and Raman spectroscopy (488 nm excitation) to compare cell membranes that had been isolated from normal hamster lymphocytes and cell membranes that had been isolated from lymphoid cells (cells lacking granules that had been transformed by the DNA virus, SV40). The study showed that membranes of transformed lymphocytes differed from those of normal cells: several defined bands appeared, and two shoulders were replaced by defined bands, with the general explanation that a greater proportion of aspartate-glutamate residues were amidated in the membranes of the transformed cells.²²⁵

More recently, Popp et al. demonstrated that Raman microspectroscopy (785 nm excitation) could be used to characterize WBCs, leukemic cells, and solid tumor cells that were found in peripheral blood and dried on a slide.²²⁶ Aspects of this research were repeated using aqueous suspensions of the cells and produced comparable results.²²⁷ The same group have gone on to combine optical traps (in microfluidic environments) and Raman microspectroscopy to improve their classification of peripheral blood cells.²²⁸ Figure 9 shows Raman results (514 nm excitation) from a dedicated microfluidic glass chip which incorporated functionalities “to separate cells from a reservoir, trap single cells, and sort them according to the Raman-based classification”. The results showed that 77 out of 80 OCI-AML3 cells (96.3%), 83 out of 87 MCF-7 cells (95.4%), 25 out of 29 leucocytes (86.2%) and 75 out of 78 BT-20 cells were correctly classified. Similar discrimination was also achieved in 2011, when a group from Emory University used SERS nanoparticles to probe cells obtained from the blood of 19 patients diagnosed with cancer of the head and neck. The spectral analysis was able to differentiate between circulating tumor cells and

WBCs with high sensitivity, even though the host blood cells outnumbered cancer cells “by 5 to 6 orders of magnitude”.²²⁹

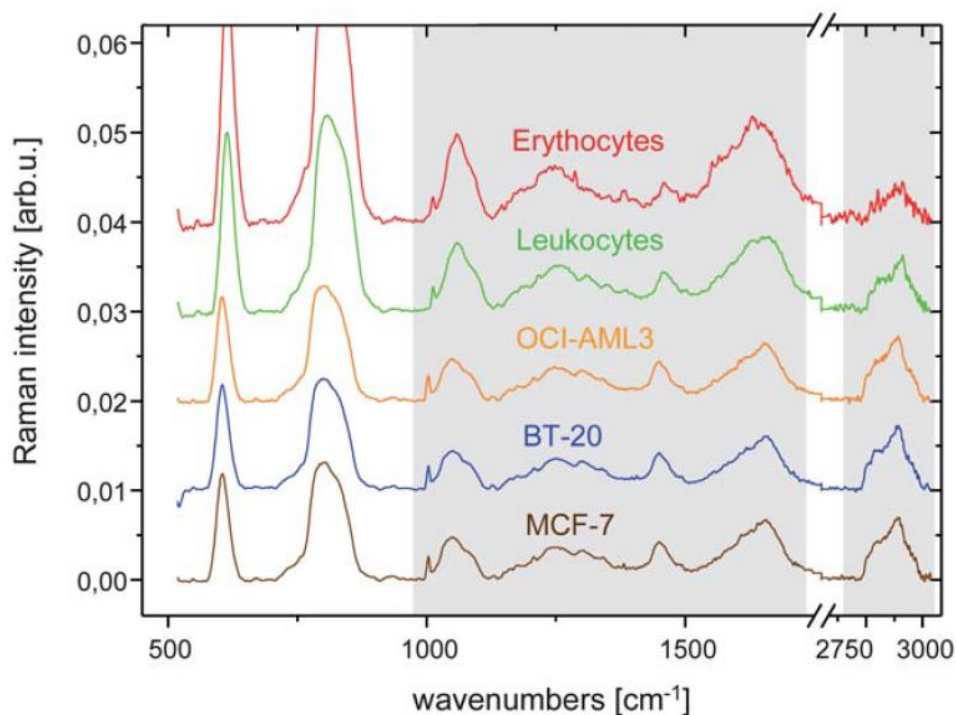


Figure 2-13: Mean Raman spectra of WBCs compared to various leukemia (OCI-AML3) and tumor (BT-20, MCF-7) cell lines measured with a dedicated microfluidic glass chip. Spectra were background corrected and normalized and the grey region were used in the statistical analysis by the authors. Reproduced from Reference 228 with permission from The Royal Society of Chemistry.

In RBC sections above (specifically in sub-sections 2.7.2.2.2 and 2.7.2.3.2) workers at UC Davis were mentioned in relation to LTRS studies of RBCs. This group (Chan et al.) has also reported LTRS studies which compared normal and diseased WBCs. In 2006, they were able to discriminate between unfixed normal human lymphocytes and lymphocytes from cultured cell-

lines (Jurkat and Raji) that were transformed to model leukemia cells. The spectral differences were highly reproducible for each neoplastic cell type with characteristic changes in the peaks associated with DNA and proteins.²³⁰ A couple of years later, the study was reproduced using actual cells from clinical patients, and “the results indicated that, on average, 95% of the normal cells and 90% of the patient cells were accurately classified into their respective cell types.”²³¹

Chan et al. have also used LTRS to measure the effect that doxorubicin, a common chemotherapy drug, had on leukemic lymphocytes at different time points over 72 hours of exposure.²³² The observed changes in the Raman spectra were dependent on drug exposure time (sampling time-points at 24, 48, and 72 hours) and concentration (0.1 μM and 0.5 μM of continuous doxorubicin exposure). The spectral changes included intensity changes in lipid Raman peaks, in DNA Raman peaks, and in phenylalanine peaks. They concluded these features were consistent with various biochemical responses that were expected to occur during the different stages of drug-induced apoptosis. This study was later expanded and hyper-spectral Raman images (785 nm) of lymphocytes were obtained after exposure to doxorubicin with an extra time-point at 96 hours. These results showed significant differences between the biochemical trends in local and global changes of the cells, which suggested that valuable information about the entire cell can be missed if only Raman spectra of localized cell regions are used.²³³

2.7.2.5 Platelets

Platelets are small anucleated cells that are central to blood coagulation, inflammation, wound-healing, angiogenesis (the development of new blood vessels), and other pathophysiological processes. The first Raman investigations of platelets and platelet-structure were reported in the late 1970s when workers in France isolated platelets from whole blood,

washed them, and put them in a continuous-flow system for Raman analysis (488 nm and 514.5 nm excitations). The spectra exhibited three prominent peaks that the authors assigned to vibrations of carotenoids, but they were unable to exclude the possibility that the pigments had not been internalized from plasma.²³⁴ A few years later the same research group analyzed the variations to platelet membrane spectra at eight different temperatures. They claimed that heated platelet-membrane lipids underwent a double thermotropic-state transition, and that there may have been a link between the lipid transitions and the carotenoids.²³⁵

For the following three decades the field stagnated and it wasn't until the mid-2000s that Okpalugo et al., motivated by an interest in films and biomaterials, used Raman and platelets to investigate “the effect of changes in microstructure, surface energy, surface charge condition and electronic conduction on the interaction of human platelets with silicon modified hydrogenated amorphous carbon films”.²³⁶ A few years later a group from the Guangxi Academy of Sciences in China used LTRS to collect Raman spectra (785 nm excitation) from platelets derived from different species (human, pig, rat, and rabbit).²³⁷ Their published spectra are shown in Figure 2-14.

Recently, Raman spectroscopy of platelets has become of interest to workers researching Alzheimer's Disease. In 2011, Chen et al. isolated and analyzed (633 nm excitation) platelets from a mouse-model of Alzheimer's and compared them to healthy controls; notable spectral differences were revealed in the 740 cm^{-1} band (protein side chain vibration) and the 1654 cm^{-1} band (amide I band of the protein α -helix structure).²³⁸ This research has since been expanded, as multi-layer perception²³⁹ and an adaptive Gaussian process algorithm^{240,241} were used as strategies for classifying suspect platelets.

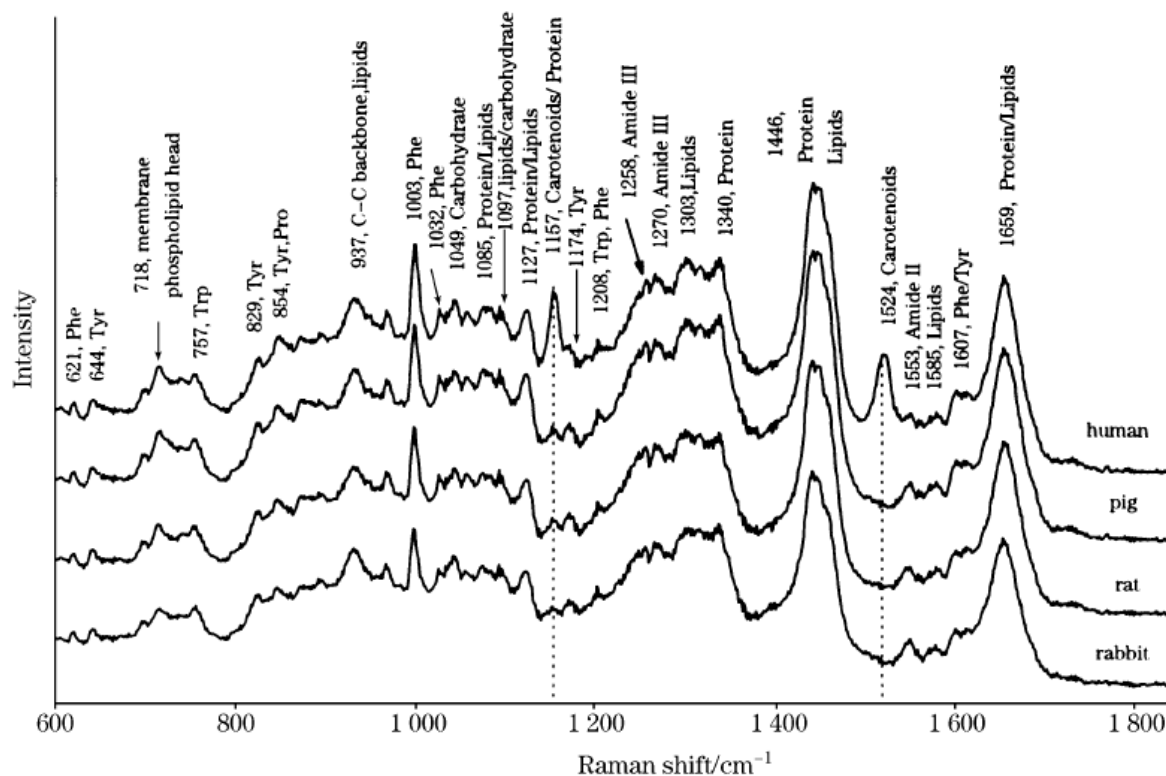


Figure 2-14: Mean Raman spectra of single platelets and tentative peak assignments (abbreviations: Phe, phenylalanine; Tyr, tyrosine; Trp, tryptophan; Pro, proline). Reprinted from Reference 237 with permission.

2.7.2.6 Plasma and Serum

As mentioned above, over 50% of the total volume of blood is plasma, a mildly alkaline aqueous fluid in which the cells are suspended. Plasma is mainly water but it also contains dissolved proteins (e.g., albumins, globulins, fibrinogen), clotting factors, and other metabolically-relevant compounds (e.g., electrolytes, hormones, antibodies, etc.). When the fibrinogen and clotting factors are removed from plasma, the simplified liquid is called serum. Molecular analysis of blood plasma/serum can potentially offer insight into metabolic processes occurring in the body

and there is growing interest in using Raman spectroscopy to develop molecularly-specific, accurate, and reusable plasma/serum sensors for diagnostic and monitoring purposes.

2.7.2.6.1 Screening for Metabolites and Other Chemical Species

The earliest interrogation of blood plasma using Raman spectroscopy was performed by researchers from the University of Göteborg in 1974. They discovered strong Raman scattering bands (514.5 nm excitation) in plasma from healthy patients at 1160 and 1520 cm^{-1} , and assigned the bands to resonance-enhanced conjugated systems of C-C single and double bond stretching vibrations. They also probed plasma from patients that had been suffering from various medical conditions (various forms of bacterial, viral and fungal infections, and various forms of cancer) and found many of those spectra to have more intense fluorescence backgrounds than the healthy samples.²⁴² In 1976, researchers located in New Jersey, USA suggested that the Raman bands in plasma were associated with carotenoids (Figure 2-15),²⁴³ and a decade later (488 nm excitation), the assignment was confirmed with a larger cohort of patients who had been diagnosed with a range of cancers (e.g., malignant tumours and also patients in remission).²⁴⁴

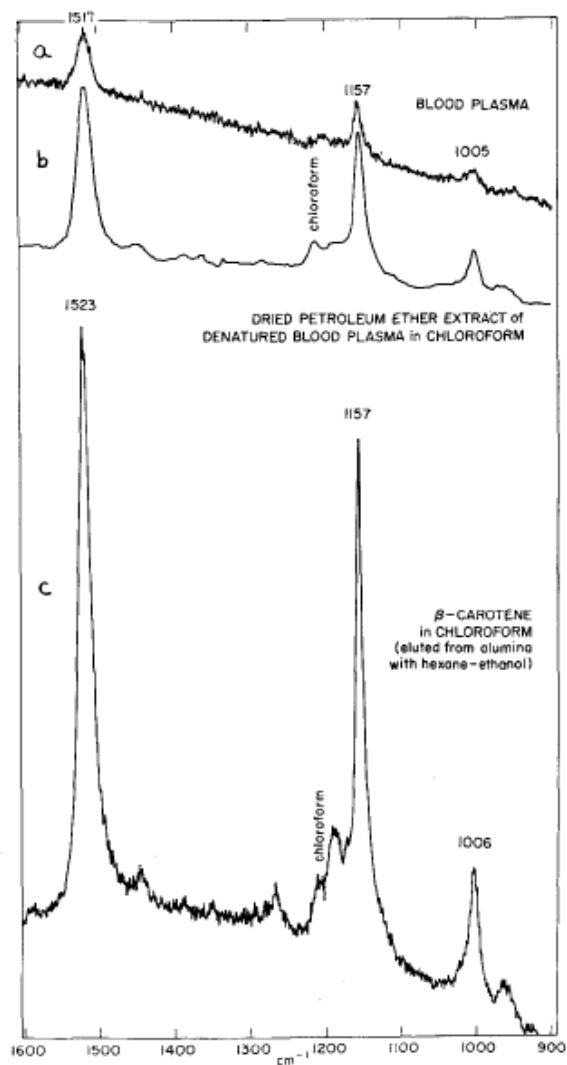


Figure 2-15: Early Resonance Raman (514.5 nm excitation) work showing enhanced vibrational spectra of a) blood plasma (heparin, subjects fasted 12 h), b) petroleum ether extract of alcohol-denatured blood plasma in chloroform, and c) β -carotene in chloroform. Reproduced with permission from Fig. 1 in Reference 243. Permission provided by Elsevier.

The use of Raman spectroscopy to screen for metabolites was dormant for much of the next decade until technological developments brought the field back into focus. In the mid-1990s, Ozaki

et al. attempted to address the fluorescence background problem from plasma by utilizing the chromatic aberration of a lens (514.5 nm excitation) to collect anti-Stokes Raman spectra.²⁴⁵ This approach produced the same strong carotenoid bands as previously described, and, after adding glucose artificially to both plasma and serum, the researchers used the intensity of a band at 1135 cm^{-1} (due to the C-O stretching mode) to estimate glucose concentration. From this time onward, there has been a concerted effort by many groups to measure plasma metabolites at physiological concentrations.

In 1999, two groups investigated human sera from >60 individual donors to predict concentrations of relevant metabolites with the aid of a multivariate model. Qu et al. collected Raman spectra (785 nm excitation) to predict the analyte concentrations of total protein, albumin, triglyceride, and glucose,²⁴⁶ and Berger et al. generated Raman spectra (830 nm excitation) to analyze concentrations for glucose, cholesterol, triglyceride, urea, total protein, and albumin (in both of these studies, experimenters removed macro proteins that masked subtle features in their analytes).²⁴⁷ Researchers in Germany made the next advance when they measured the concentrations of eight analytes in serum from a pool of 247 donors.^{248,249} Berger et al. later implemented a liquid-core optical fiber geometry (830 nm excitation) to enhance the Raman signal from serum and urine samples by 1 to 2 orders of magnitude.²⁵⁰ Another study attempted to avoid the protein-removal step by concentrating spots of the plasma as dried drops; they attempted to quantify fibrinogen and obtained results that were comparable to the traditional gold-standard fibrinogen assay.²⁵¹

The strong fluorescence interference and the inherently weak Raman signals from the lower-concentration components of plasma would always place limits on what could be achieved

with conventional Raman spectroscopy, and in the 2000s research began a shift towards enhancement techniques. At the forefront of this work was the group of R. van Duyne at Northwestern University who developed a glucose sensing platform that consisted of a functionalized SERS-active substrate (785 nm excitation).²⁵² Their preliminary experimental approach demonstrated the potential for quantitative glucose measurements in the presence of bovine serum using the 1462 cm^{-1} line.²⁵³ The next step involved implanting their substrate inside a living animal and verifying if the platform could provide quantitative accuracy *in vivo*.²⁵⁴ Using Sprague-Dawley rats and a new Raman technique known as SESORS, which combined the enhancement of SERS with the depth profiling of SORS, the researchers demonstrated that their platform provided consistent and stable Raman measurements of glucose when implanted and surrounded by interstitial fluid. The SESORS approach eliminated the need to remove the platform from the rat and allowed direct detection of glucose with high accuracy.²⁵⁵

The potential for Raman-sensing of glucose makes it an attractive target for scientific enquiry but other metabolites have also been investigated:

- 1) In 2005, Stosch et al. applied SERS (514.5 nm excitation) with silver colloids to quantitatively determine creatinine, an endogenous degradation product of muscle metabolism and a marker for proper kidney function, in human serum. The addition of pure unfiltered serum to the pre-aggregated silver colloid did not produce characteristic creatinine bands in the SERS spectrum due to interference from proteins.²⁵⁶
- 2) In 2008, Stokes et al. reported a SERS study of blood serum spiked with folic acid. This vitamin is involved in many biosynthetic processes and related to disease processes, such

as certain birth defects, and the experiments showed the potential quantitative Raman (514.5 nm excitation shown to be optimal) detection.²⁵⁷

- 3) Widely used as an indicator of muscular tolerance during exercise, lactic acid is difficult to detect at physiological concentrations with traditional Raman spectroscopy.²⁵⁸ In 2009, Hsu et al. used silver nanoparticles for a SERS measurement to identify and quantify this metabolite, which was demonstrated with sensitivity below physiological concentrations. Once again, interference from non-specific adsorption dominated unless pure human serum was used.²⁵⁹
- 4) A protein native to blood plasma, called C-Reactive protein (CRP), is used as a clinical biomarker of bacterial infection and tissue damage. When inflammation occurs, the concentration of CRP circulating in the blood rises; in 2009, researchers from the University of Southern Denmark acquired Raman spectra of CRP (785 nm excitation) and measured the concentration of CRP in blood plasma from 40 donors.²⁶⁰ As is common in the complex plasma mixture, other proteins interfered with the ability of Raman to provide specificity for a particular component. In this study, however, the authors concluded that CRP could be differentiated from the varying plasma background with the assistance of a multivariate model.
- 5) Researchers in Boston, USA sought to characterize the Raman activity of human blood and its components. One key variable investigated in their experiment was the time dependence of their SERS spectra, and how this data compared with non-SERS spectra. Without the need to isolate or quantify a particular analyte, the researchers did not subject the plasma to filtration prior to analysis, but did allow time on the solid-SERS support for the plasma drop's volume to be reduced from evaporation. The results demonstrated that over a period

of 24 hours after sampling, the SERS spectrum of plasma became dominated by the signature of hypoxanthine, a well-known purine degradation product.¹⁴⁶

Despite the promising results obtained from SERS experiments on analytes in blood plasma, most were proof-of-principle and only demonstrated the possibility of detecting an analyte that was artificially-spiked with the analyte. In 2014, a study on the shortcomings of SERS discussed the lack of published information on: (1) the effect of sample processing (e.g., filtration) and experimental parameters (e.g., excitation wavelength, metal colloid, etc.), (2) the comparison of serum with plasma, and (3) the spectral variability between individuals. They concluded that SERS spectra of both filtered serum and plasma were dominated by two highly-variable metabolites, uric acid and hypoxanthine, and that the inherent problems with reproducibility had profound consequences for the field.²⁶¹

2.7.2.6.2 Cancer

A number of Raman studies have sought to identify, classify, and even quantify biomarkers that may provide information about various forms of cancer. In 2007, researchers based in Mexico investigated serum samples from 23 patients (11 diagnosed with breast cancer and 12 healthy controls) using Raman microspectroscopy (830 nm excitation) and multivariate statistical methods.²⁶² The Raman spectra of the diseased samples and healthy controls were similar but had slight peak shifts and differences in peak intensities; the researchers were able to identify seven ratios of band intensities that appeared significant, and they assigned these ratios to represent proteins, phospholipids, and polysaccharides. Scatter plots from their multivariate analysis, however, did not show a clear discrimination between diseased and healthy patients as the number

of samples was too small. The same methodology was used later for other types of cancers, such as leukemia²⁶³, head & neck cancer,²⁶⁴ and cervical cancer²⁶⁵, and the preliminary results were similar with a reported improvement in class discrimination as presented by a multivariate analysis.

In recent years, C. Murali Krishna et al. from the Chilakapati Laboratory in Mumbai, India have carried out a series of Raman studies using plasma for the investigation of cancer. In 2013, they obtained serum from 40 patients with tongue cancers and compared it with 16 healthy control samples. They observed differences in the bands associated with nucleic acids (the differences suggested an increased cell-free DNA presence) and a decrease in the amount of β -carotene for patients in the cancer group.²⁶⁶ In 2015, they repeated the study using a larger subject cohort (328 donors, 785 nm excitation) and an added dimension of evaluating the serum for the detection of premalignant chemical conditions.²⁶⁷ Another 2015 study from the group investigated the feasibility of discriminating between serum from patients suffering from malignant tumors who had endured a recurrence of their cancer post-surgery and serum from patients suffering from malignant tumors who had not. While the spectra reported negligible pre-surgery differences between serum from recurrence and non-recurrence patients, the post-surgery spectra revealed measurable differences. These changes were attributed to DNA and variable protein content in the groups.²⁶⁸

Researchers from Guangdong, China have carried out similar Raman work regarding cancer detection in plasma. They used the drop-coated deposition technique on plasma from patients with colorectal cancer (15 patients) and from normal healthy controls (21 volunteers). The Raman data (785 nm excitation) suggested an increased level of cell-free DNA and a decreased level of β -

carotene in the cancer group, similar to that reported above. Two mechanisms have been proposed to explain these increased nucleic acid levels in cancer patients' blood (apoptosis/necrosis, or release of intact cells in the bloodstream and their subsequent lysis), while a diminished β -carotene was in agreement with previous reports which suggested a deficiency of anti-oxidant species is an important risk factor for the progression of pre-cancer to cancer.²⁶⁹

The studies of plasma and serum described above were completed using conventional Raman techniques; SERS has also been used in a number of laboratories to tackle similar problems. In 2010, researchers from Fujian Normal University of Fuzhou, China published the first SERS analyses (785 nm excitation) of blood plasma for cancer detection.²⁷⁰ Silver nanoparticles were directly mixed with blood plasma from 76 samples (43 samples came from patients with pathologically confirmed nasopharyngeal carcinomas and 33 from healthy volunteers) and the SERS spectra showed distinct variation between the two patient groups for a variety of bands, while PCA scores were compared to demonstrate the potential for discrimination. In the years that followed, the same group published more studies of nasopharyngeal cancer (NPC)²⁷¹ and numerous other SERS studies which took the same exploratory approach towards the detection of different types of cancers, including gastric cancer^{272–274}, colorectal cancer^{275,276}, and cervical cancer.²⁷⁷ SERS spectra obtained from the 2014 NPC study (Figure 2-16) demonstrated that different tumor (T) stages in NPC have distinct spectral differences. A repeated observation in all of their studies, regardless of the type of cancer, was that the SERS band at 725 cm^{-1} (assigned to the C-H bending mode of adenine) was higher in cancer serum than in normal serum, suggesting abnormal metabolism of DNA bases in the serum of cancer patients.

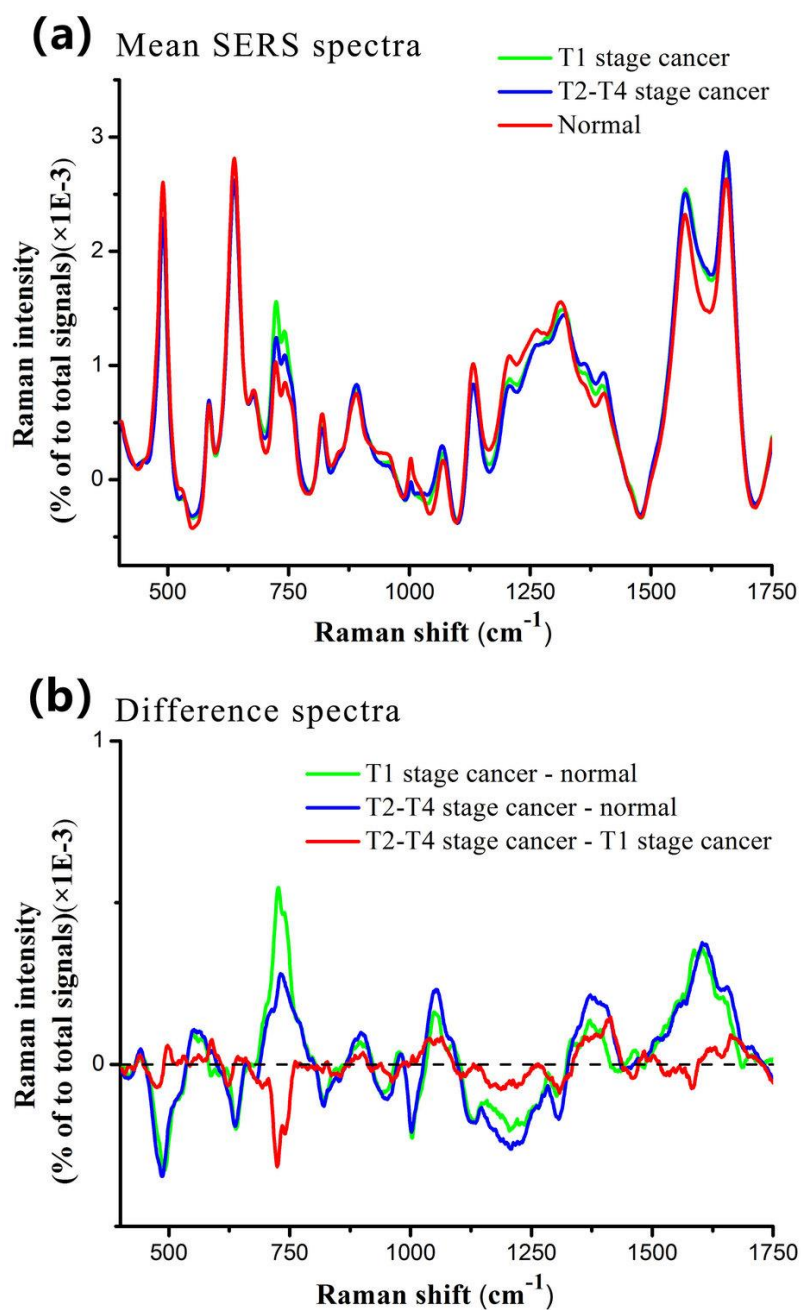


Figure 2-16: (a) Normalized mean SERS spectra of blood plasma from 60 normal, 25 early stage nasopharyngeal cancer (T1) and 75 later stage nasopharyngeal cancer (T2-T4) patients. (b) Difference spectra calculated from the mean SERS spectra among the three groups. Reproduced from Reference 271 with permission from Macmillan Publishers Ltd: Scientific Reports, Copyright (2014).

Another group of researchers from China, at Sichuan University in China, similarly used SERS (633 nm excitation) to discover that the intensities of peaks assigned to nucleic acids and proteins increased in the serum spectra of patients with parotid gland tumors compared to serum spectra from normal healthy controls.²⁷⁸

2.7.2.6.3 Other Diseases

Raman spectroscopy has been used to probe plasma/serum samples from patients with various other types of disease. In 2006, Popp et al. used UV-RRS (244 nm excitation) to study the cryoprecipitated human plasma of patients with thrombotic microangiopathy, a pathology that results in thrombosis (formation of a clot inside a blood vessel).²⁷⁹ At the selected wavelength, Raman signals of aromatic amino acids and proteins were selectively enhanced and the study demonstrated variations in the intensities of bands at 1551 cm^{-1} , 1615 cm^{-1} , and 1650 cm^{-1} (associated with the amide II vibration, in-plane stretching vibrations of aromatic amino acids, and the amide I vibration, respectively). While classifying the two groups using hierarchical cluster analysis was possible, the contribution of lipoproteins to two of these bands raised questions about the effect of sample processing on the plasma as lipids should not have been present in the cryoprecipitated mixture. Almost a decade later, the same group tested Raman spectroscopy of dried plasma (785 nm excitation) as a method for discriminating between bacterial (sepsis) and non-bacterial inflammatory responses (samples from 70 individuals, 31 in former group, 39 in the latter).²⁸⁰ The average spectra from both populations appeared very similar, but when multivariate statistical methods were applied the patient data could be separated, and the authors concluded that there was high potential to distinguish these populations.

Raman spectroscopy of plasma has also been developed to detect dengue fever and malaria:

- Dengue fever is caused by a virus that enters the body through the bite of an infected mosquito. It binds itself to WBCs and replicates within the cells. In 2012, researchers from Pakistan published a preliminary Raman study (442 nm and 532 nm excitations) that compared normal dried serum with dried serum from a dengue patient.²⁸¹ Dengue serum showed two peaks at 1614 and 1750 cm^{-1} , assigned to the presence of immunoglobulin (Ig) G and IgM antibodies. The same group extended their Raman work in 2013 (532 nm excitation) and again in 2016 by including more serum samples and including a multivariate analysis for spectral discrimination. Carotenoid bands in the dengue-infected blood sera disappeared, implying that anti-oxidant protection for cell membranes is diminished. Their discrimination model was tested for six unknown human blood serum samples and produced 100% accuracy in accordance with clinical results.^{282,283}
- Malaria is caused by *Plasmodium* parasites and transmitted via mosquitoes. As described above (section 2.7.2.3.1), most Raman studies of malaria seek to describe the infected erythrocytes, an approach that requires time to scan or image an entire blood smear. The alternative to this traditional approach is to use Raman spectroscopy to measure plasma or serum which has the advantage of measuring malaria-specific changes against a background that is hampered by less background from cellular hemoglobin. One study, which was previously mentioned above, produced results from malaria-infected plasma that did not show a clear trend with respect to time after infection.²⁰⁰ A more recent study compared spectra from plasma of patients infected with malaria to those infected with

dengue fever. The results showed a Raman line associated with β -carotenoids to be present in healthy patients, but that its intensity decreased substantially in the case of malaria and completely disappeared in dengue-infected samples.²⁸⁴

Other diseases or conditions that have been studied using plasma include brain ischemia (insufficient blood flow to the brain)^{285,286}, hepatitis C (disease of the liver)²⁸⁷, pemphigus vulgaris (skin disease)²⁸⁸ and preeclampsia (a condition that can occur during pregnancy).²⁸⁹ Early investigations of plasma in asthma (lung inflammation)²⁹⁰ and Alzheimer's disease (form of dementia)^{291,292} have also been performed.

2.7.2.7 Whole Blood

2.7.2.7.1 Introduction and General Appearance of Raman Spectrum

To the first approximation, a unit volume of human blood comprises ~50% plasma (which is mostly water and thus has a very weak Raman spectrum), 40-45% RBCs (which are, in turn, mainly composed of highly scattering hemoglobin) and the remainder is WBCs/platelets. Thus, with ~150 g of hemoglobin in each litre of whole blood, it is no surprise that the metalloprotein dominates the Raman spectrum and makes analysis of other chemical species difficult.¹²⁸

This fact has not deterred workers from undertaking Raman analysis of whole blood; in 1992 Ozaki et al. used FT-Raman (1064 nm excitation) to obtain a spectrum of whole blood and compared the result to that of coagulated (via laser irradiation) whole blood. The spectra showed that the amide I band had shifted, an indication that hemoglobin was denatured (α -helix structures becoming random coil structures).¹²⁸ In 1997, related work by Schrader et al. would demonstrate

the obvious similarities between Raman features of whole blood and those of erythrocytes (Figure 2-17).²⁹³

Ozaki and colleagues would later use three separate excitation wavelengths (514.5 nm, 720 nm, and 1064 nm) on samples of whole blood and isolated hemoglobin to determine that the 720 nm excitation yielded strong Raman scattering of carotenoids and protein. The wavelength was also shown to give a Raman spectrum of the heme-chromophore, free from fluorescence interference.²⁹⁴ Later work (785 nm excitation) by another group would conclude that dried whole human blood produced spectra with features exclusive to oxyHb, and that hemoglobin aggregation/denaturation would occur if stimulated with an excitation power over 2 mW. The bands associated with these laser-induced effects in whole blood agreed with similar aggregation/denaturation bands assigned by previous research groups in samples of isolated RBCs.²⁹⁵

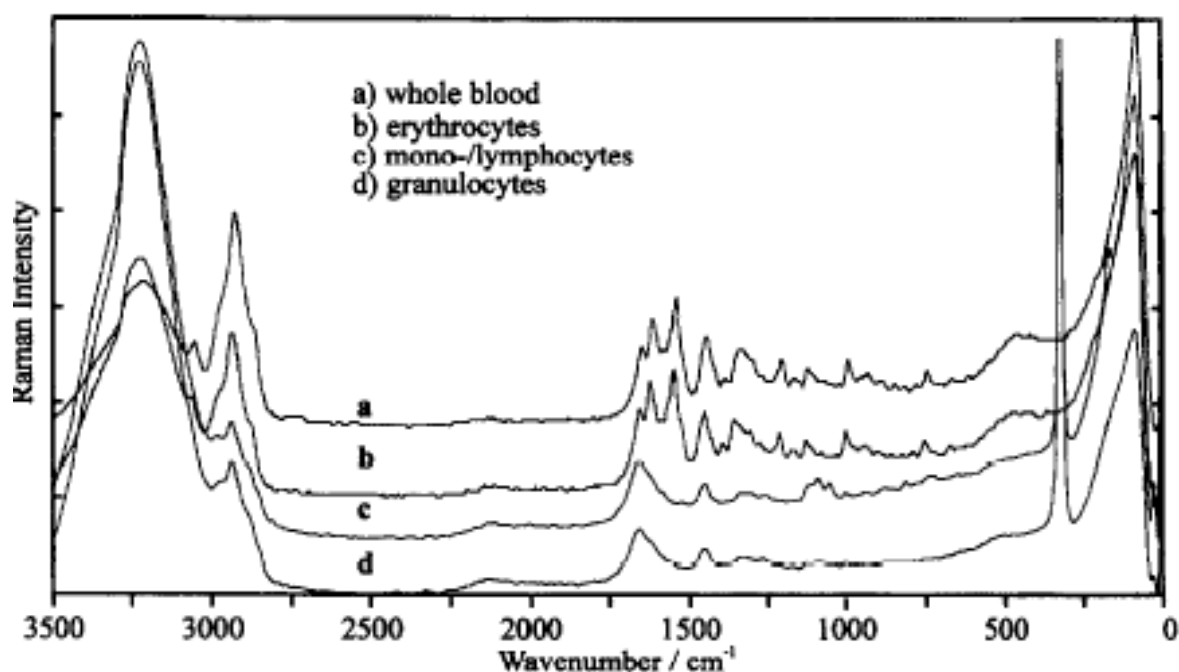


Figure 2-17: Raman spectra (1064 nm excitation) from blood constituents. Reproduced with permission from Fig. 8 in Reference 293. Permission provided by Elsevier.

As mentioned above (section 2.7.2.6.1) the detection and monitoring of glucose in blood has been a prime target for many scientists because of its importance to diabetes medicine. One of the pioneers in the Raman-detection of glucose in whole blood was MIT's Michael Feld. In 1997, his team reported on the feasibility of using Raman (830 nm excitation) to determine spiked concentrations for above-physiological glucose levels in whole blood.²⁹⁶ This work was developed so that the superimposed bands of the analyte could be resolved (preliminary processing of the spectra, with no correction for turbidity, produced significant prediction accuracy for four of six analytes but not for glucose, and these spectra had a lower signal-to-noise ratio than the same analysis performed in serum).²⁴⁷ A 2002 report described an optimized Raman measurement for

turbid samples and showed the first quantitative observation of multiple analytes (including glucose) in whole blood.²⁹⁷

The whole-blood studies described to this point mainly utilized conventional Raman but recently some of the more specialized techniques have also been used in the field. In 2008, researchers from Princeton, New Jersey utilized CARS to record Raman lines associated with RBCs from oxygenated blood and the identified vibrational modes were in very good agreement with previously published data. As is the case for CARS work, the actual shifts for the Raman lines were preserved, while the relative intensities in the CARS spectra differed from the spontaneous analog. The use of CARS, however, meant that spectra could be recorded very quickly and there was no need for microscopy setups, isolation of RBCs, chemical preparation, or long integration times.²⁹⁸ In 2011, a SERS analysis of whole blood was reported by researchers in Italy. Their work showed that conventional Raman and SERS favored different bands at different excitation wavelengths (β -carotene at 514 nm excitation and hemoglobin at 785 nm excitation), so one could selectively probe either β -carotene or hemoglobin bands at 514 nm depending on whether SERS conditions were created (i.e., hemoglobin markers showed up in SERS case at 514 nm excitation).²⁹⁹ Similar phenomena were reported in 2012, when Premarisi et al. showed that the SERS spectrum of whole blood had a storage time-dependence that was not evident in the conventional Raman spectroscopy of whole blood.¹⁴⁶

2.7.2.7.2 Forensic Science

Raman spectroscopy of blood has not been solely concerned with the biochemical, biological and medical domains, as it has also been developed as a forensic tool. In 2008, researchers from Belgium used Raman to analyze miniscule particles of coagulated blood that had

been collected with a standard crime-scene tape-lifting technique. They compared four different excitation wavelengths (488 nm, 514.5 nm, 632.8 nm, and 752.6 nm); each had had different enhancements but none could provide a spectral differentiation between blood particles of human, feline, or canine origin.³⁰⁰

That same year, Igor Lednev and his coworkers published a spectrum of dried whole blood at 785 nm excitation,³⁰¹ followed by a demonstration that multivariate analysis could be used to differentiate human, feline, and canine blood within a confidence interval of 99%.³⁰² The study was later repeated on a larger scale with blood from 12 animal species.³⁰³ In 2010, the same group showed that spectra obtained from multiple spots on the same dried sample were chemically heterogeneous and that the relative contribution of the dominant hemoglobin and fibrin bands varied with each donor.³⁰⁴ The assignment of certain bands to fibrin was later revised³⁰⁵ as more was learned about the effect of intense laser exposure.²⁹⁵ After understanding of the chemical heterogeneity of blood spatters increased, Lednev et al. proposed that multi-dimensional Raman measurements be attempted³⁰⁶ and in 2012 they used the technique to discriminate between dry samples that contained mixtures of human blood and semen. With their multivariate algorithm, mixtures with blood content higher than 80% could not be distinguished from pure blood, while 5% blood in a mixture resulted in a Raman spectrum distinguishable from the spectrum of pure semen³⁰⁷ (later studies would report on the successful discrimination between dry samples of peripheral blood and menstrual blood,³⁰⁸ and also between races³⁰⁹).

Raman analysis of blood is affected when the spatter dries on a non-ideal substrate such as fabric. Bodily fluids are weak to moderate Raman scatterers and often the substrates can contribute can contribute a dominant Raman or fluorescence signal.³¹⁰ Lednev et al. proposed solutions to

this problem (such as varying the excitation laser source and selecting the wavelength that produced the least luminescent for that particular substrate)³¹¹ and they reported statistical methods for reducing the interference.³¹²

In 2012 Boyd et al. reported a study that showed SERS substrates can be used as swabs to collect blood at a crime scene and they demonstrated a sensitivity comparable to traditional chemical-based identification techniques.³¹³ While the researchers state this approach qualifies as non-destructive, Lednev and colleagues have avoided resisted the addition of metal nanoparticles to their samples.³⁰⁴ In 2012, a case of Raman spectroscopy being used in a murder investigation was reported by Janko et al.; they identified hemoglobin in a tissue sample excised from Ötzi, the 5,300 year old ‘Iceman’ whose preserved remains were found near the border of modern-day Austria and Italy in 1991.³¹⁴

2.7.2.7.3 Disease Detection

Detection of disease using Raman analysis of whole blood is the obvious goal for many of the studies outlined above (e.g., 2.7.2.3, 2.7.2.6.2, etc.). Some researchers have gone directly to whole blood and used non-standard techniques to isolate compounds of interest. In 1999, researchers at the University of Wyoming implemented a SERS assay that used an analyte-specific reactive coating to trap the molecule of interest and then perform SERS (632 nm excitation) to selectively enhance its spectrum. Their approach required less time and effort than standard processing of whole blood and enabled bilirubin and salicylate to be probed within the blood (compounds associated with jaundice and poisoning).³¹⁵

In 2004, whole blood from scrapie-infected sheep (a fatal, degenerative disease that affects the nervous systems of sheep and goats, related to BSE or ‘mad cow disease’) was collected and processed (subjected to centrifugation and osmotic shock) to produce pellets rich in pathogenic prion proteins. These pellets were analyzed with Raman spectroscopy (1064 nm excitation) and the data from 31 infected sheep were shown to be statistically different than those from 150 healthy controls (no features attributable to β sheet content were present in the controls).³¹⁶

In 2011, researchers in Taiwan created SERS-based (632 nm excitation) multi-functional biochips (silver nanoparticle substrates coated with vancomycin) for rapid detection of micro-organisms in blood samples spiked with clinically-relevant bacteria. However, this method was hampered by the necessity for chemical-immobilization on the SERS-active substrate, long incubation time, and repeated wash steps to remove non-specifically bound cells.³¹⁷ A later study coupled a compact hybrid electrokinetic mechanism (to exclude blood cells from the matrix) with a SERS-chip substrate to address these disadvantages.³¹⁸

2.7.2.7.4 *In Vivo* Raman Analysis of Blood

If the Raman analysis of whole blood is the end-goal of many of the studies described above, then the ultimate end-point for many of them must be the Raman analysis of whole blood *in vivo*. For example, the development of a non-invasive, transcutaneous glucose monitor would eliminate the need for diabetics to have blood sampled multiple times a day.

Thus far, hemoglobin and various blood metabolites, such as glucose, have been the two areas in literature that have been featured for *in vivo* measurements:

Hemoglobin: Some of the earliest work on *in vivo* whole blood Raman analysis was reported by Chaiken et al. in conference proceedings of the SPIE. The work involved the application of physical pressure to the fingertip (to produce an “un-squeezed” state, blood flow – normal, and a “squeezed” state, blood-flow – altered), and Raman probing of the skin (785 nm and 830 nm excitation). The spectral differences found from the tissue modulation weren’t assigned to chemical species, but the analysis was performed on diabetic patients and said to be capable of measuring physiological variations in glucose.^{319,320} It was later shown that this approach was highly sensitive to an individual’s peripheral microcirculation^{321,322} and the test subject’s hemoglobin concentration.³²³

Much of the early work on the *in vivo* analysis of hemoglobin-oxygenation for surgical applications was carried out by Torres Filho et al. They reported the utility of UVRRS for the simultaneous identifications of oxyhemoglobin and deoxyhemoglobin in the microvessels of a living rat using a single excitation wavelength (406.5 nm in one study,³²⁴ and 532 nm in another³²⁵). When the rat’s hemoglobin saturation (as measured by a commercial oximeter) was <1% (deoxygenated) or >98% (oxygenated), a single Raman peak was observed. For intermediate levels of saturation, the spectra showed two clearly defined hemoglobin peaks in the 1,350–1,400 cm^{-1} . These observations were consistent with the very first Raman studies of hemoglobin carried out by Spiro, Brunner, etc. and outlined above (section 2.7.2.2.1). Torres Filho and colleagues continued this work (using the sublingual mucosa of rats) and published the first pilot study of RRS (406.5 nm excitation) to track microvascular hemoglobin oxygenation in tissue during hemorrhage (Figure 14) and resuscitation.^{326,327} The technique compared well with other important indicators of tissue oxygenation, such as central venous oxygen saturation and lactate concentration, among others. It was concluded that the ability to determine hemoglobin saturation

depended on the amount of tissue present in the light path, and that the optical signal would be too weak to be detected if the layer was too thick. Other investigators have also tackled the challenge of attempting *in vivo* measurements of blood.

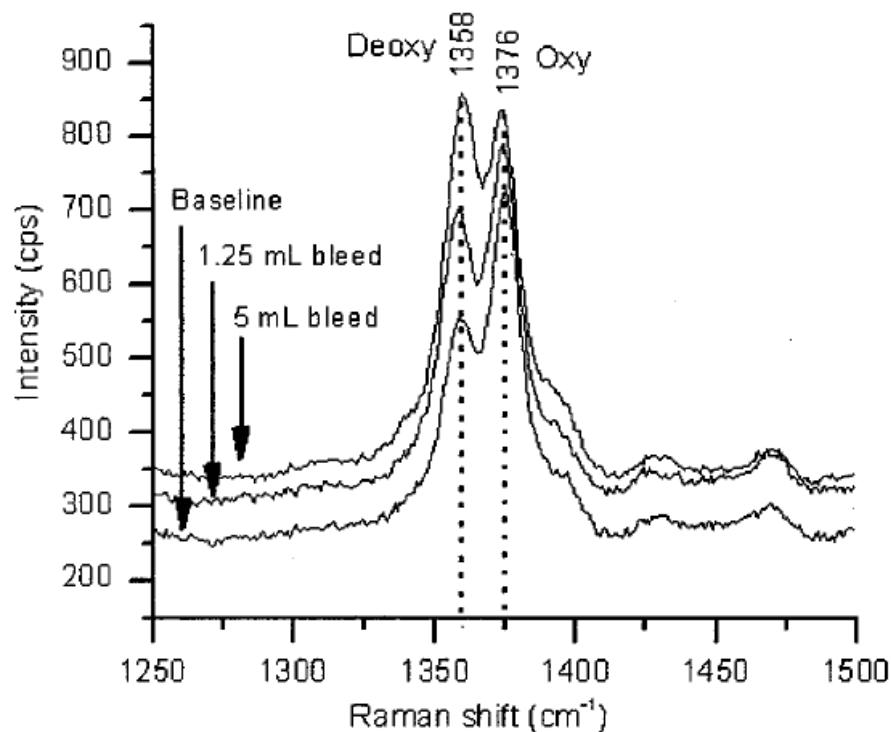


Figure 2-18: Sample resonance Raman spectra of one animal showing the dynamic changes in the deoxy and oxyhemoglobin spectral peaks in response to hemorrhage. Note the progressive changes in the deoxy- and oxyhemoglobin spectral peaks in relationship to each other indicating a greater percentage of deoxyhemoglobin as hemorrhage progresses. Reprinted from Reference 326 with permission from Wolters Kluwer Health, Inc.

More recently, Shao et al. used optical tweezers (785 nm) to capture single RBCs in the microvessel of a mouse ear; their data relied on well-characterized hemoglobin modes which indicated RBCs in arterioles were oxygenated, while those in the capillaries of venules were deoxygenated.³²⁸ Their next paper expanded on this work to involve glucose measurements, as direct spectral evidence of its presence was indicated by a characteristic peak at 1125 cm^{-1} . Using the concentration of hemoglobin as an internal standard, the impact of complexity (i.e., diversity of both tissues and individuals) was reduced and clearly showed a relationship between Raman intensity and glucose concentration in the mice's blood.³²⁹

Metabolites: One early *in vivo* study of blood metabolites saw researchers from Brazil inject a rat with 1 mL of a concentrated lactic acid aqueous solution (120 mM) and use an optical fiber cable to detect the Raman spectrum of the analyte through the skin of the rat groin.²⁵⁸

It was outlined above (section 2.7.2.7.1) how, in the late 1990s and early 2000s, Feld et al. used Raman to measure detect analytes (such as glucose) in whole blood. In 2005, three years after their last *in vitro* study was reported, the same group reported the first successful study of Raman spectroscopy (830 nm excitation) for quantitative, non-invasive measurement of blood glucose from the forearms of 17 healthy human subjects. In order to measure glucose concentrations in human skin, it was necessary to sample the innermost skin layer; the penetration depth of 830 nm excitation light was shown to be sufficient for this as the Raman spectra collected from the forearms were dominated by collagen (the major component of dermis). The underlying subcutaneous fat was also sampled, as the second largest contribution to the data was shown to be from triglyceride.³³⁰ Feld et al. found that their attempts to translate Raman spectroscopy to clinical settings were impeded by the lack of robust in calibration models and the complexity of the

blood/tissue spectra. It became clear that in order to tackle these problems and extract useful information, multivariate analyses of the data were needed. Furthermore, in addition to the generic problems associated with multivariate data analyses (system drift, covariations between constituents, overfitting, etc.) blood applications were limited by variations in sample turbidity. In 2009, they presented turbidity-corrected Raman spectroscopy (TCRS), a technique that required alternate acquisition of diffuse reflectance and Raman spectra and corrected for intensity and shape distortions.³³¹

In 2011, in what were now posthumous publications for the group-leader, a revised version of TCRS was reported which incorporated residue error plot-based wavelength selection and nonlinear support vector regression (SVR). In these experiments, wavelength selection was used to eliminate un-informative regions of the spectrum (and thus reduce the collection time of Raman acquisition), and the SVR was used to model the curved effects such as those created by tissue turbidity and temperature fluctuations.³³² The following month, it was reported that an adapted instrumental set-up had been used to collect Raman spectra (830 nm excitation) had been collected from the hands (thenar skin fold) of 18 human volunteers in transmission mode. The subjects ingested a glucose-rich beverage to induce changes in blood glucose levels and the spectral quantitation was shown to compare well with glucose levels measured using conventional finger-stick glucometers.³³³

2.7.2.8 Conclusions and Future Directions

This literature review has described the utility of Raman spectroscopy for the evaluation of blood components and whole blood. It was shown that the earliest work in the field was associated with the structural characteristics of hemoglobin (e.g., its degree of oxygenation and

the oxidation state of its iron atoms) and that this work laid the groundwork for RBC studies over the following decades. These RBC studies would show the potential of Raman for real-time monitoring of oxygenation and deoxygenation, for elucidating the effects of storage on transfusable RBCs, and for the detection of disease (e.g., sickle-cell disease, methHb, etc.).

The earliest Raman work on WBCs characterized cell composition of various cell subtypes (major components identified were carotenoids, enzymes, lipids, and nucleic acids) and explored the intracellular distribution of substances within the nucleus and cytoplasm. The most effective procedures seemed to have involved laser trapping and multivariate analyses; such reports demonstrated “Raman-based cell classifiers” that were capable of sorting WBCs from one another, and more importantly, from deleterious cells such as tumor and cancer cells.

The chemical composition of plasma (and serum) has received considerable attention from the Raman community due to its inherent utility as a barometer of the body’s health. The earliest results showed the ability to detect relevant metabolites (glucose, cholesterol, triglyceride, urea, total protein, albumin, lactic acid, etc.) and more recent work has focused on resolving relevant biomarkers (nucleic acid and carotenoid intensity changes in cancer patients) using multivariate models.

Raman investigations of whole blood is not as advanced as some of the blood component work because the spectrum is dominated by hemoglobin. There has been some interesting work, however, in the forensic field where Raman has shown promise for discriminating blood between different species and also from other bodily fluids. The other main direction of whole-blood Raman work has been *in vivo* analysis, especially efforts to develop a transcutaneous glucose monitor.

Taken together, the literature demonstrates how a trail of research that began in the 1970s with basic research using highly specialized instrumentation has travelled all the way to the present

day where real-time *in vivo* Raman monitoring of RBC oxygenation/deoxygenation, glucose detection, and disease diagnosis are on the cusp of being realized.

2.7.2.8.1 Limitations in Blood Raman Research

The main limitations for Raman analysis of RBCs/whole-blood and Raman analysis of purified plasma/serum are related to dominating signal from specific components (hemoglobin in the former, macro proteins in the latter) which overwhelm and overlap the signal from the components of interest.

Generic Raman problems, i.e., those associated with fluorescence and the inherent weakness of the Raman effect, also limit application; selection of a suitably long excitation wavelength can alleviate the former but with the drawback of aggravating the latter (the intensity of Raman scatter being inversely proportional to the fourth power of the excitation wavelength). In many situations the weak signal cannot be amplified by increasing the laser power because of the fragile nature of the biochemical cells (i.e., the constant risk of photodegradation or thermal damage) and many of the papers in this review focused on using specialized variants of Raman to circumvent these problems (e.g., using RRS to enhance the signal from specific components).

2.7.2.8.2 Statistical Power Derived from Experiments

Numerous diseases, such as diabetes, malaria, sickle-cell anemia, and even particular types of cancers, induce concomitant changes in the chemical composition of blood. Clinical diagnosis of these diseases can involve time-consuming, expensive and/or invasive analyses that could be replaced with Raman spectroscopy if the technology was suitably developed and the analysis methodology became reliable. In order to bridge the gap between the spectroscopic research

community and clinicians, a new approach and a greater weight of evidence will be needed. For example, in the blood transfusion community there has long been a hypothesis that RBCs that are stored for weeks have deleterious effects on a patient post-transfusion (described in section 1.3.3); in 2015, the New England Journal of Medicine published the results of the ‘Age of Blood Evaluation (ABLE) trial’, a multi-center, randomized, blinded trial, in which critically-ill adults were assigned to receive RBCs that had either been stored for less than 8 days, or standard-issue RBCs (the oldest compatible units available in the blood bank). The study took place at 64 centres throughout Canada, the UK, France, the Netherlands and Belgium and n , the number of patients tracked, was 1,211 (the primary outcome measured was 90-day mortality). The conclusion of the study was that, surprisingly, the storage age of the blood had no effect and the transfusion of fresh red cells, as compared with standard-issue red cells, did not decrease the 90-day mortality among critically-ill adults.⁷⁹

No Raman study reviewed in this chapter carries a weight of evidence that is comparable to the ABLE trial (n in a typical Raman study might be <100) and for spectroscopic techniques to begin to appeal to the readers of the New England Journal of Medicine and make the jump from the lab to the hospital or clinic, this discrepancy will have to be addressed.

2.7.2.8.3 Direction of the Field

Raman spectroscopy, when combined with multivariate analysis, can enable rapid distinction between sub-types of WBCs, and distinction in both healthy and diseased states. The final objective for many Raman studies of blood and blood components is to achieve a method for such a rapid and inexpensive analysis, but with the additional expectation that it can be performed non-invasively. Current glucose-monitoring techniques used by diabetics, for example, require the

extraction of a drop of blood, normally obtained via finger prick; a non-invasive Raman analysis is being actively pursued by a number of research laboratories.

The most feasible instrumental approach to measuring analytes through barriers such as plastic and skin, while reducing signal interference, is the technique of SORS. The difficulty in attaining a sufficient Raman signal detectable above the typical fluorescent background requires a balance between laser power to boost intensity and safety to human skin. Some of these difficulties are more significant among individuals when variables such as skin thickness are introduced, adding error to predictions and concentration estimates deduced from a Raman measurement. The difficulty with the use of SORS for the application of a non-invasive human measurement is twofold: its inability to provide selectivity for a particular analyte, especially not when the analytes of blood are so unique, and its sensitivity, to distinguish a particular analyte.

As translation from laboratory to real-world settings continues, these limitations are being addressed with Raman strategies that are known to offer specific enhancements. As SERS requires direct contact with a metal surface, ‘non-invasive’ SERS would require the implantation of a carefully designed chip. SESORS (the combination of SERS and SORS) may therefore offer a unique contribution to the field of Raman spectroscopy of blood in years to come.

In Chapter 5, a proof-of-principle SORS study shows potential for measuring oxygenation of stored RBCs through the plastic storage bag.

Chapter 3: Interrogating Ageing Effects and Quality in Banked Red Blood Cells³

3.1 Introduction

Human red blood cells (RBCs) are responsible for the delivery of oxygen to tissues and clearing a portion of carbon dioxide from tissues. The unique biconcave disc shape of healthy cells enables them to function in this capacity, as the high surface area-to-volume ratio of the membrane facilitates flexibility and reversible elastic deformation.³³⁴ This feature is important for cell movement through small capillary vessels and permits efficient transport of oxygen and carbon dioxide throughout the body. Changes to the membrane properties or surface area of RBCs can reduce cell deformability and potentially disrupt or impair circulation.

It is known that certain pathological conditions can cause significant alterations to the biconcave shape of healthy RBCs. In patients with anemia, a peripheral smear permits assessment of RBC abundance, shape, size, and color. Abnormalities of RBC shape and other RBC features provide key information in distinguishing conditions that share similar symptoms.³³⁵ For example, a blood smear is useful in the diagnosis of sickle cell disease, particularly if there is an urgent need for identification and if the results of traditional chemical techniques are not available.³³⁶ When used properly, monitoring RBC morphology allows clinicians to recommend appropriate follow-up procedures and to choose the best methods capable of providing a definitive diagnosis.

³ A version of this chapter is to be submitted:

Atkins, C.G.; Chen, D.; Schulze, H.G.; Devine, D.V.; Blades, M.W.; Turner, R.F.B. Raman Spectroscopy as a Tool for Interrogating Ageing Effects and Quality in Banked Red Blood Cells. **2016** (to be submitted).

The storage of RBCs by blood banking agencies has been shown to produce a multitude of biochemical and physiological degradation-related changes that are all categorized under the broad heading of 'storage lesion'. During storage, glycolysis begins to slow down, ATP becomes depleted, lactate accumulates, pH decreases, and free-radical species are generated, among other changes. Oxidative stress is now widely accepted as a major cause of storage lesion formation in long stored RBCs under blood bank conditions.⁶³ These negative effects combine to also influence distinct changes in both deformability^{337–340} and cell morphology (observed via characteristic shape changes of the cell^{341–345}). The appearance of distinct morphologies has been previously associated with decreasing ATP levels,^{342,346–348} and work by Usry et al.³⁴⁹ monitored the RBC shape changes by scanning electron microscopy (SEM) on blood samples stored for three to six weeks.

The utility of classifying cells based on their morphology resulted in the creation of a 'morphological index' (MI), a score-based system able to provide qualitative insight into cell quality. This MI represents structural alterations (i.e., membrane deformability) and chemical damage (i.e., loss of functionality) and thereby reflects the overall oxygen carrying capacity of the cells. Membrane deterioration would significantly alter oxygen exchange across the membrane. For example, microvesiculation (a blebbing process associated with RBC storage) would promote loss of membrane surface and reduce the cell surface area-to-volume ratio³⁵⁰, thereby affecting mass transport processes. Chemical damage might also affect the oxygen uptake or retention capacity of RBCs. The main function of the most abundant RBC membrane protein (Band 3) is modulation of gas transport, and lesions targeting this protein lead to the progressive loss of metabolic modulation.³⁵⁰ The membrane seems especially vulnerable to chemical damage from ROS,²⁷ an inherent danger due to the oxygen transport role of RBCs.

Though controversy exists about the clinical impact of the age of stored blood,⁶⁶ it is generally believed to be important to have a means to assess the apparent quality of stored blood prior to transfusion. The MI is a good visual metric that provides a qualitative illustration of cell breakdown, but current practice dictates that morphological information can only be obtained when the sterility of a stored unit is breached and a sample is directly extracted. Hence, it would be beneficial for clinicians to receive similar information without the necessity of sampling. Indeed, there is a need to develop rapid and robust measures and metrics to assess human RBC storage quality before releasing units from the blood bank.³⁵¹

Existing literature suggests that oxygen saturation of stored blood⁸² changes in a similar fashion as irreversible RBC morphological changes³⁵² over a 42 day storage period, consistent with the vulnerability of membrane components and structural proteins to oxidative damage.³⁵³ Thus, the oxygenation state (OS) of hemoglobin might serve as a potential surrogate of the MI. If a reliable relationship exists between OS and MI, and the OS of stored RBCs could easily be assessed objectively and without sampling, it would pave the way for determining the quality of individual units of stored blood in a clinical setting.

The technique of Raman spectroscopy, which has potential for non-invasive *in situ* measurements, could offer an instrumental approach for assessing OS. Virtually any change that takes place in the composition or structure of a chemical system is, in principle, reflected in the molecular vibrational modes of the system. Spectroscopic techniques that probe molecular vibrations are thus inherently information rich, and the benefits of using vibrations as a label-free, non-destructive method for measuring biomolecules have been well established.^{354–356} In particular, Raman spectroscopy has previously shown promise for identifying features associated with the oxygenation of hemoglobin in RBCs^{135,141,188}, both extra- and intracellular.

In the work presented in this chapter, the potential utility of oxygenation information obtained from Raman spectra was investigated as an objective non-invasive optical surrogate for traditional MI scores. Raman data was obtained from both dry-fixed smears and liquid samples; the results show a close relationship in ageing patterns between OS and MI, and thus provide proof-of-principle that blood quality could be assessed spectroscopically.

3.2 Experimental

3.2.1 Blood Collection and Sampling

Twenty-nine healthy volunteer adults (aged between 26 and 71 years; 16 females and 13 males) each donated a whole blood unit ($450 \text{ mL} \pm 10\%$) at the Canadian Blood Service (CBS) NetCAD facility in Vancouver, Canada. RBC concentrates were isolated from the blood, subjected to in-line leucoreduction filtering, and suspended in 110 mL of SAG-M additive solution (saline with 1.25 mM adenine, 43.4 mM glucose and 28.8 mM mannitol). The concentrates were stored in standard PVC storage bags at $4 \pm 2^\circ\text{C}$ in accordance with CBS' standard operation procedures. Beginning shortly after donation, 1 mL aliquots were extracted on a weekly basis from the storage bag by a trained technician (units were brought to room temperature, mixed via gentle massaging, and extracted via the site-coupler in a Biological Safety Cabinet). This process occurred three to four times throughout the forty-two day FDA stipulated shelf-life of the stored blood. The samples were extracted in one laboratory and analyzed in another with an approximate transit time of ten minutes between extraction and analysis.

3.2.1.1 Dry-Fixed Smear Analysis

A single droplet of stored RBCs was deposited with a Pasteur pipette onto the edge of an opaque gold-coated glass microscope slide, rapidly smeared across the length of the slide using a spreader slide held at a $\sim 45^\circ$ angle, and dry-fixed under a stream of compressed air for a minute. Except for the dry-fixing, this is similar to the procedure conventionally used to facilitate microscopic observations of sampled RBCs, including for morphology assessment (Figure 3-1). The slide was secured in the stage of the microscope platform and Raman data was acquired from a dense part of the smear (Figure 3-4) using the Raman microspectrometer described below in section 3.2.2.

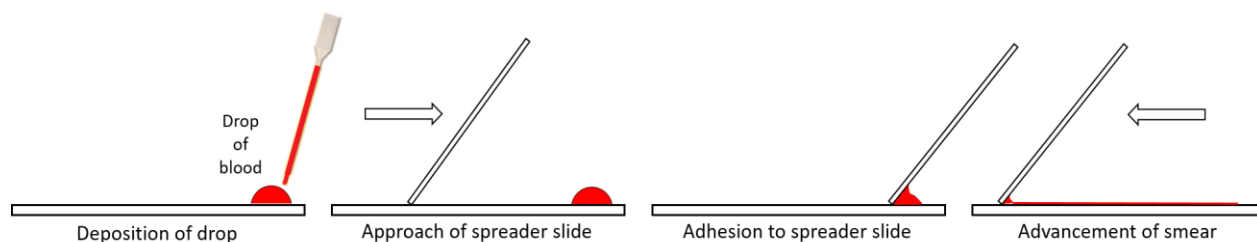


Figure 3-1: Experimental method of dry-fixed smear. A drop of stored RBCs was deposited onto a gold-coated slide and smeared across that slide using a spreader slide. The cells were then dry-fixed under a stream of air.

3.2.1.2 Bulk RBC Analysis

With a view toward the long-term goal of adapting Raman spectroscopy as a tool for non-invasive analysis of stored RBCs, performing preliminary measurements on a representative liquid sample of the bulk environment would provide insight on relevant spectral features, especially those that might correlate with the MI. In this analysis, $\sim 200\ \mu\text{L}$ of the stored RBC sample were

deposited into a glass microscope well-slide using a Pasteur pipette and then isolated from atmosphere with a glass coverslip (Figure 3-2). The slide was secured in the stage of the microscope platform and the laser excitation was focused beyond the surface of the coverslip and into the liquid cells. A downfall of this methodology was that the $1300\text{-}1450\text{ cm}^{-1}$ spectral region suffered from fluorescence originating from the glass coverslip which masked any cellular information contained within that spectral region (it is excluded from Figure 3-6). The full spectral region could be observed by substituting the glass coverslip with a more chemically-inert alternative (e.g., CaF_2), but the inclusion of this region was not deemed necessary for the current investigation because hemoglobin oxygenation bands of interest also exist at lower wavenumbers.

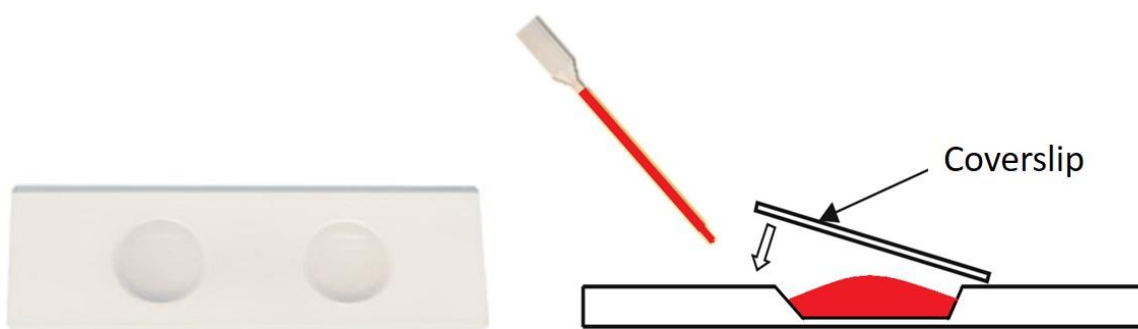


Figure 3-2: Experimental method for the bulk RBC analysis. A glass microscope double-welled-slide is shown on the left and a cross-section of a single-welled-slide is shown on the right. $\sim 200\text{ }\mu\text{L}$ of a stored RBC sample is added into the well which is then isolated from atmosphere using a coverslip slide.

3.2.1.3 Morphological Index

An adapted protocol developed in-house at the Centre for Blood Research (Vancouver, BC, Canada) was implemented for obtaining morphology scores from seven of the twenty-nine donors. 10 μL of freshly-sampled RBCs were added to 80 μL of a 2% glutaraldehyde solution. A smear of these fixed cells was created on a glass microscope slide which was then enclosed with a coverslip. The RBCs were viewed under 100 \times magnification with an oil-immersion objective lens and a total of 100 cells were counted (in duplicate) using the previously developed morphology score index shown in Table 3-1.³⁴⁹ Samples from the studied donors were split, where one half was used for morphology scoring and the other for spectral analysis of the liquid RBC samples. The half earmarked for scoring was blinded (i.e., an arbitrary label was assigned) by the author such that the technician would not be aware of the storage age for a given sample of RBCs.

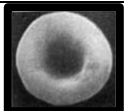
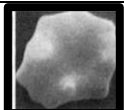
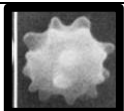
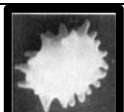
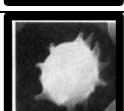
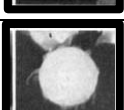
	1. Smooth Disc	1.0
	2. Crenated Disc	0.8
	3. Crenated Discoid	0.6
	4. Crenated Spheroid	0.4
	5. Crenated Sphere	0.2
	6. Smooth Sphere	0.0

Table 3-1: Gold-standard morphology scoring system. Images and scoring protocol were adopted from Reference 349 and reprinted with permission from John Wiley & Sons, Inc.

3.2.2 Data Collection

Raman spectra of the smears and liquid RBC measurements were collected using a commercial Renishaw *inVia* Raman microscope (Gloucestershire, UK) equipped with a 785 nm excitation laser. The light was focused through a 20× objective lens (Leica Microsystems, Wetzlar, Germany) and the resulting spot size was a 3 μm \times 30 μm rectangle. In the smear experiments, laser power on the sample was <5mW and seven to ten spectra (100 seconds accumulation time for each) were collected and averaged. For the liquid RBC sample measurements, the power on the sample was larger (10–20 mW) and ten to fifteen spectra (60 seconds accumulation time) were collected from the centre of each well-pool and averaged. This measurement technique, for both

the smear and liquid analysis, involved data collection from the *same* sample area multiple times, instead of collecting from a *different* sample spot with each accumulation, as multiple spots would require movement of the translation stage and re-focusing of the excitation beam thereby creating larger deviations. Prior to data collection each day, the Raman instrument was calibrated using the phonon band of silicon (520 cm^{-1}) as a reference.

The dry-fixation was intended to capture a “snapshot” of the condition and environment of the stored cells at specific time points of storage. The liquid samples, however, were indirectly (i.e., while under a coverslip) exposed to ambient atmosphere for a longer period of time (up to a few hours) immediately prior to and during the measurements, and a concern was that the oxygenation states could have been effected. To minimize this concern, the spectroscopy of the liquid RBC samples was always performed as soon as possible after receiving samples extracted from the bag. Accumulations were also done with a larger laser power than used for the dry-fixed samples to compensate for reductions in Raman scattering caused by dilution of cells and turbidity of the media. Beneficially, the liquid media was also able to distribute potential heating effects from the laser and limit the extent of damage due to photo degradation. Figure 3-3 demonstrates the effect of continual laser and (indirect) air exposure on the cells from a particular unit and storage time point. The averages for the first 15 accumulations and the second 15 accumulations appear to be consistent for both the deoxyHb and oxyHb bands in the $1200\text{-}1230\text{ cm}^{-1}$ region. It is not until the third set of 15 accumulations that substantial variation occurs to these regions, as the deoxyHb band is almost entirely diminished. This gives confidence that the described protocol for collecting 10 to 15 accumulations per sample accurately measures the condition of the cells.

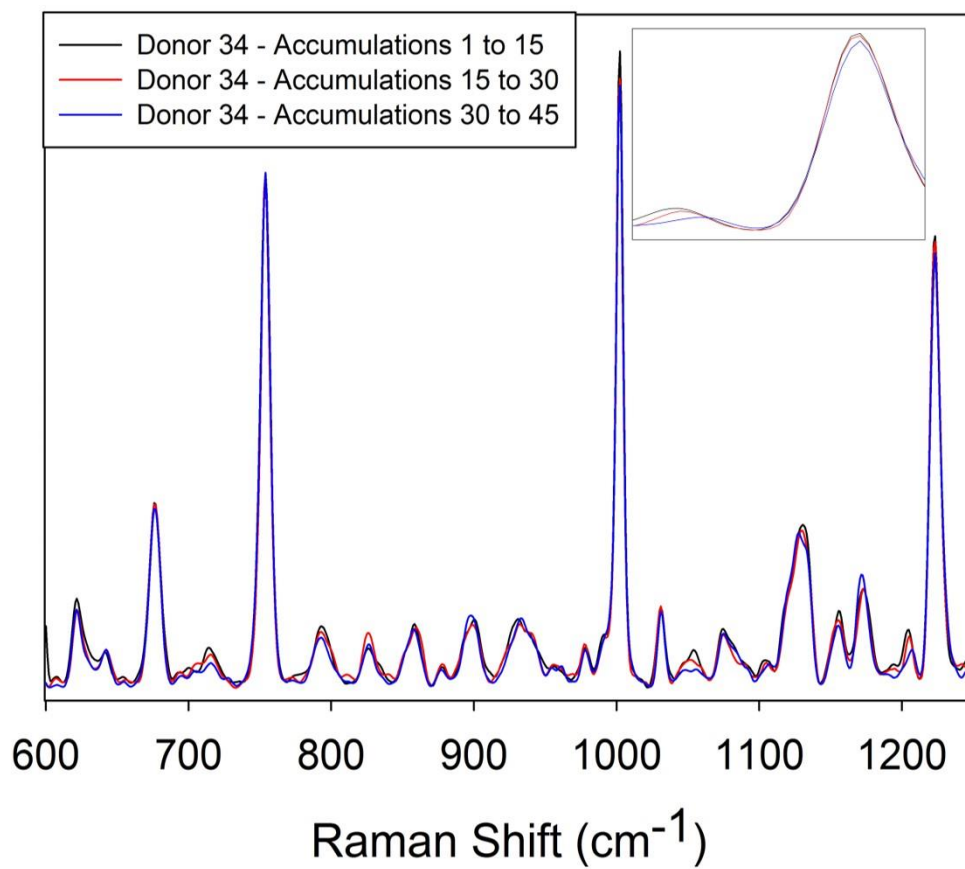


Figure 3-3: Shown are three averaged spectra collected from the liquid RBCs of Donor 34 over an extended period of accumulation time. The same sample region is analyzed for all 45 accumulations. The inset is a magnified view of the 1200-1230 cm^{-1} region.

Reference spectra of human hemoglobin (normal human hemoglobin variant HbA, Sigma Aldrich, St Louis, Missouri, USA) were collected for comparison.

3.2.3 Data Processing

For a set of data collected following a given calibration, a background measurement would be obtained using the same parameters and sample scans. In the case of the gold-coated slide background, a spot without any cellular material was analyzed. For the well-microscope slide,

a well was filled with water, covered, and analyzed. All Raman spectra were baseline corrected³⁵⁷ and smoothed³⁵⁸ with automated algorithms coded in-house with MATLAB R2009a (The MathWorks, Natick, Massachusetts, USA). Stored RBC spectra were then normalized to the intensity of the 753 cm⁻¹ pyrrole breathing band, a mode believed to be present for all possible inter-conversions of hemoglobin and one that remains consistent throughout storage.

The trends extracted from spectral ratios and morphology scores were normalized for comparison to the same 0-1 scale using Equation (3.1):

$$Z_i = \frac{x_i - \min(x)}{\max(x) - \min(x)} \quad (3.1)$$

where $\mathbf{x} = (x_1, \dots, x_n)$ and represents the ratios/scores, while z_i is the i^{th} normalized datum.

3.3 Results and Discussion

3.3.1 Raman Spectrum of Dry-Fixed Smears

The physical and biochemical characteristics of RBCs are known to change over time spent in storage, and these changes are expected to correlate with the functionality of the cells. Blood smears have historically been used to distinguish between morphological shapes (e.g., smooth biconcave disc, crenated spheroid, smooth sphere, sickle-cell, etc.) that may indicate disease or diminished cell quality. Such smears are considered to be representative of the characteristics of the bulk sample. Similarly, a dry-fixed smear approach was selected in this study as it could provide Raman information pertaining to the quality of the entire unit by measuring a small representative population of fixed-cells. The results that follow highlight the potential for

combining the measurable information from a Raman analysis with the more traditional morphology-based identification process.

Figure 3-4A is a representative bright-field light microscopy image of a dry-fixed smear of stored RBCs on a gold-coated microscope slide. The approximate center of the smear was chosen for analysis as it allowed measurement of a high-density population of cells that could reflect the biochemical nature of the unit. It also provided an adequate signal-to-noise ratio such that, in contrast to the edge of the smear (shown in the inset of Figure 3-4A), the measurement could be performed in a time frame where degradation from air exposure would be negligible. Figure 3-4B shows typical Raman spectra collected from the “dense” region of the smear for five different donors, and also shows a spectrum of pure hemoglobin for comparison.

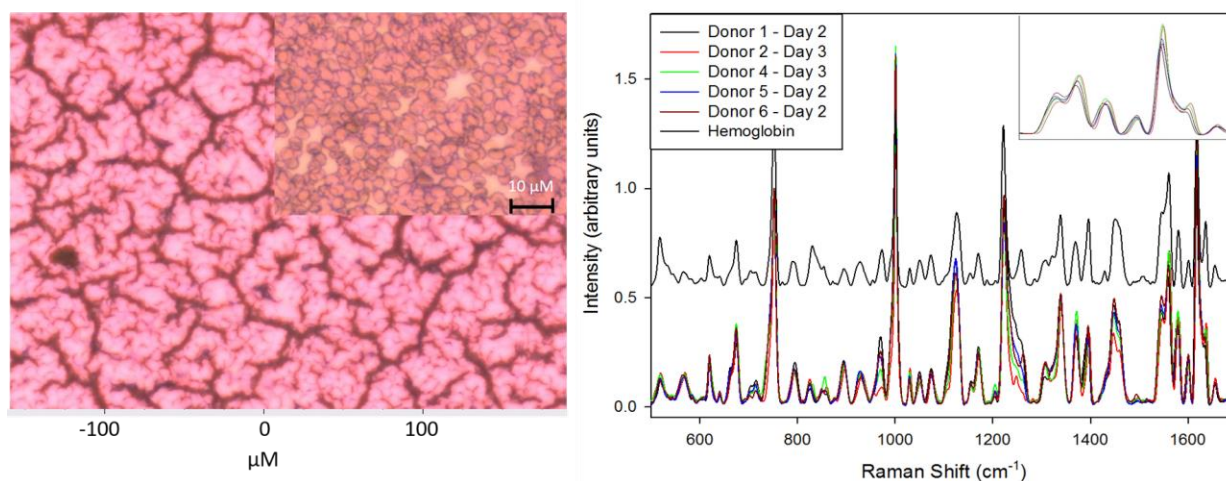


Figure 3-4: (A) A bright-field microscope image showing clusters of RBCs that have aggregated together during the fixation process. The inset depicts the edge of the smear at a single-cell level. (B) The average (10 accumulations, 100 second accumulation each) Raman spectrum of (powdered) hemoglobin is shown vertically offset while the average Raman spectra of dry-fixed smears for 5 different donors are also shown. The inset depicts the variation for the bands found in the 1520-1680 cm⁻¹ region for the donors.

It is clear from the data presented in Figure 3-4B that the Raman spectrum of a dry-fixed smear is completely dominated by features associated with hemoglobin. Also evident from this plot is the comparison of different smears at approximately the same point in storage. While the majority of bands are similar, it is apparent there are donor-dependent differences attributable to specific differences in the structure of hemoglobin with the major variations in regions previously characterized to its oxygenation. The Raman signatures of oxyHb and deoxyHb have several bands that can be used to distinguish among them; for example, distinct Raman spectroscopic markers of oxygenation occur at 1222 cm⁻¹ and 1208 cm⁻¹ and are C-H methine bending vibrations

corresponding to oxyHb and deoxyHb, respectively. Bands at 1545 cm^{-1} , 1561 cm^{-1} , 1619 cm^{-1} , and 1639 cm^{-1} have also been assigned to hemoglobin modes that are dependent on whether the molecule was oxygenated or deoxygenated (inset of Figure 3-4B). For all five donors, the intensity of these oxygenation bands were quite variable between the donors.

As evidenced from the image presented in Figure 3-4A, the bulk regions of the smear that were spectroscopically sampled contained clumped cells of unknown depth, restricting control over the amount of aggregation. The shoulder at 1249 cm^{-1} , a mode assigned to hemoglobin stacking and aggregation¹⁴⁰, demonstrates difficulty in controlling the extent of aggregation and sampling from a region that is similar.

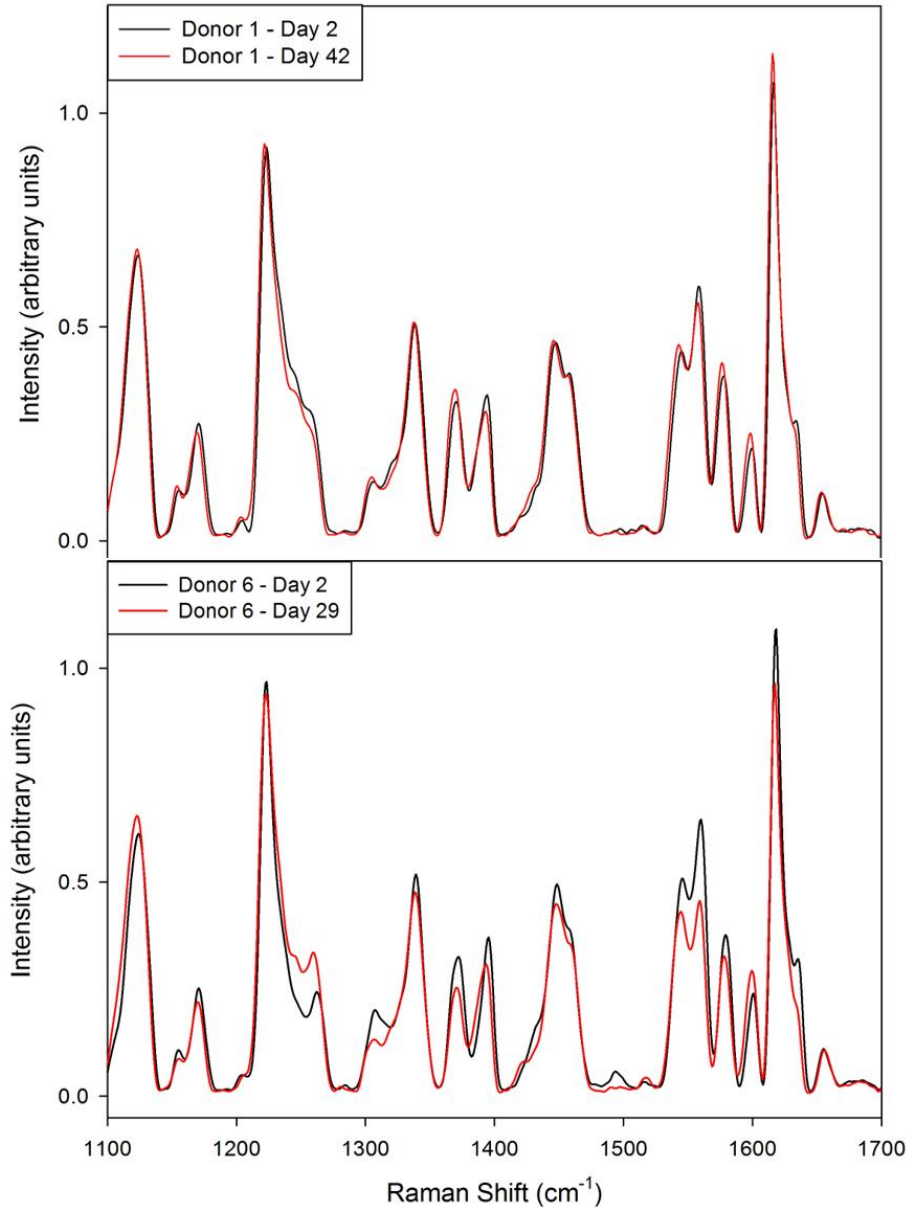


Figure 3-5: The progression of storage for RBC samples from two donors, Donor 1 (top) and Donor 6 (bottom), using the smear technique.

The effect of storage time on the Raman features measured in smears from two particular donors is illustrated in Figure 3-5. The spectra presented for Donor 1 originate from smears obtained after two days and forty-two days of storage, while the spectra for Donor 6 originate from

smears representing two days and twenty-nine days of storage. These donors exemplify the potential outcomes of this approach for making inferences about the condition of the cells. It is clear from inspection of Donor 1 that spectral differences between the two time-points are minimal, an interpretation that suggests RBCs remained largely unchanged despite significant time spent in storage. This is in contrast to the spectra presented for Donor 6 where, after just twenty-nine days of storage, differences appear in regions identified earlier as markers for hemoglobin oxygenation. While the ultimate utility of the smear approach would involve connecting Raman features related to storage with obvious morphologies, a concern is that the cellular components may be altered during the fixation process, thereby resulting in the possible loss or aberration of vibrational information about the true condition of the RBCs. To investigate this concern, liquid samples were also measured.

3.3.2 Raman Spectrum of Liquid Samples

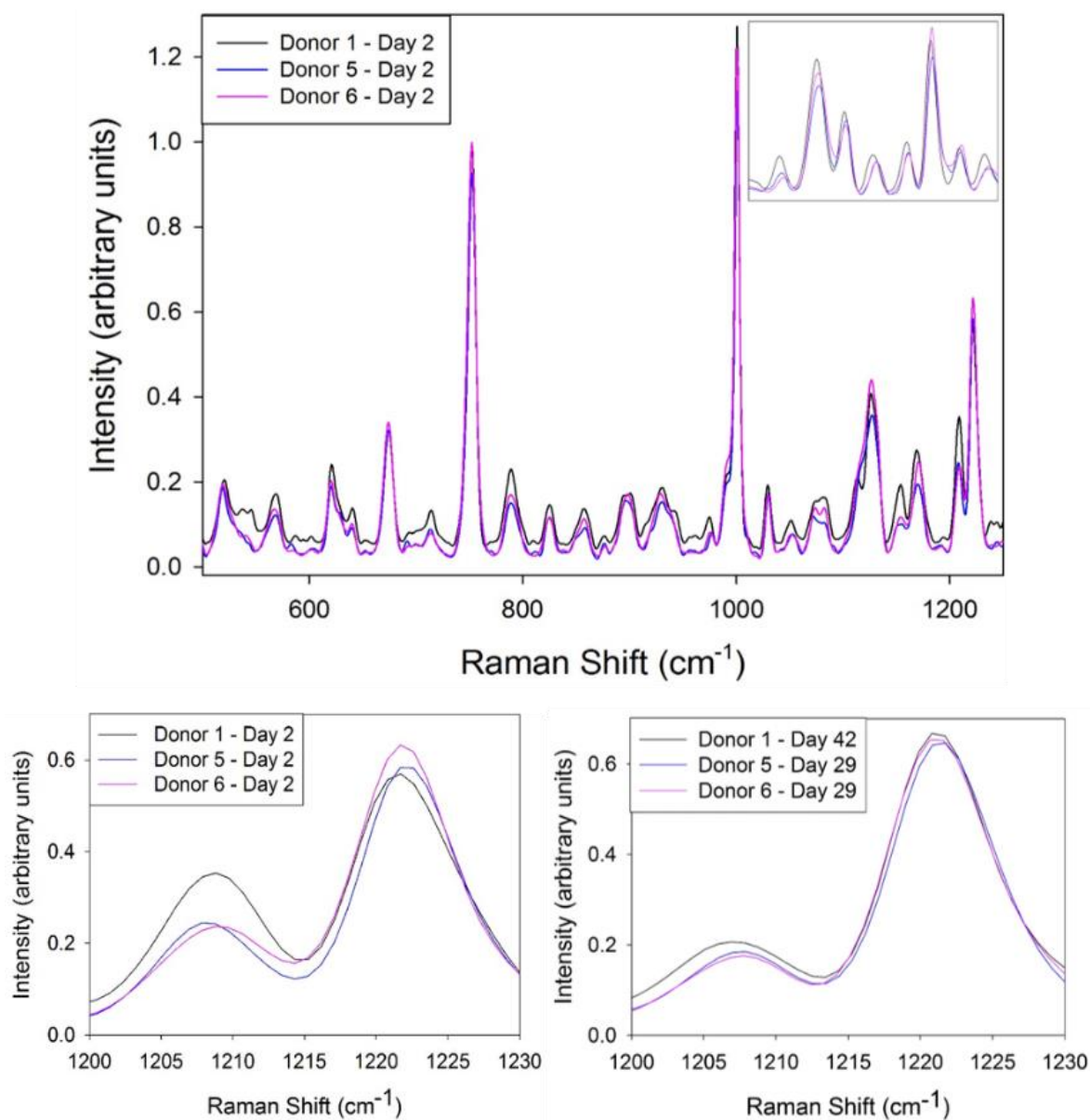


Figure 3-6: (A) Spectra obtained from stored liquid RBCs (2 days of storage) for three different donors are presented. The inset is a magnification of the 1500-1660 cm^{-1} region. The excitation beam was focused through the coverslip and into the turbid media. (B) The effect of storage length is shown for these three donors by inspection of the oxygenation marker band region of 1200-1230 cm^{-1} .

Results of the first experiments on the liquid samples are shown in Figure 3-6A. Similar to results presented in Figure 3-4 for the smears, the spectra have complex features (attributable mainly to hemoglobin), again with measurable donor-dependent differences. These changes tend to occur in regions associated with the oxygenation marker bands (i.e., 1200-1230 cm^{-1} as seen in Figure 3-4B, and 1500-1660 cm^{-1} as seen in Figure 3-4B inset). The advantage of analyzing the stored cells as a liquid is that the RBCs are still ‘suspended’ in their additive solution matrix, better reflecting their true chemical environment in the storage bag. Figure 3-6B shows evidence of a general trend for the oxygenation bands at 1208 cm^{-1} and 1222 cm^{-1} . It would appear that over the considered period of storage (forty-two days in the case of Donor 1, and twenty-nine days for Donors 5 and 6) the deoxygenated band *decreases* while the oxygenated band *increases*. This observation is not unexpected, as researchers in the field of transfusion medicine have long understood that hemoglobin becomes oxygenated during its lifetime in storage, due in large part to the semi-permeable nature of the storage bag and the metabolic pathways that are disrupted.⁸² For example, 2,3-DPG, an effector molecule that binds to hemoglobin and shifts the Hb-O₂ saturation curve to lower values of PO₂ (triggering the release of oxygen to tissues deprived of oxygen), is completely released from stored RBCs by twenty-one days of storage. Without intracellular 2,3-DPG, oxygenated hemoglobin is favored. To reduce the influence of oxygen on stored RBCs, investigators have also examined anaerobic storage, but found that oxidative stress markers still accumulate under these conditions.⁶³

Investigating this experimental trend further, the data set was expanded to 27 different donors and it became apparent that the observed tendency of hemoglobin oxygenation to increase for stored RBCs over their storage lifetime is not consistent for all donors. A representation of the oxygenation trend is shown in Figure 3-7 and presented as a ratio (1208 cm^{-1} /1222 cm^{-1}) of the

deoxyHb/oxyHb bands in the 1200 cm^{-1} to 1230 cm^{-1} spectral region. While the data from earlier storage time points (ten days or less) are more dispersed, because they have more high-ratio points, than the more clustered data at later points of storage (forty to fifty days), the apparent lack of an overall trend suggests that cells from each donor behave uniquely. The inset of Figure 3-7 shows the oxygenation trend for two specific donors, Donor 40 and Donor 42, to portray the extremes of what were observed exist for oxygenation trends as determined with Raman for this cohort of donors. In the case of Donor 40, the deoxyHb (1208 cm^{-1}) band exists in an appreciable quantity until at least twenty days of storage. The spectral data obtained from Donor 42, on the other hand, suggests the sample was almost completely oxygenated from the first measured time-point of eight days and remained this way over the course of fifty days of storage.

This discrepancy may point to specific characteristics within each donor that might be difficult or impossible to account for (e.g., smoker vs non-smoker, dietary habits, physical fitness, metabolism, etc.). Such donor-to-donor variations observed through the 1208 cm^{-1} /1222 cm^{-1} ratio of spectral bands may originate from morphological characteristics of the cell. The reversibility of morphologic alterations is dependent on membrane–cytoskeletal interactions and changes inversely proportional to storage duration.^{59,350} If the membrane of the cell has undergone alterations due to oxidative damage²⁷ along with the increased oxygenation state (but reduced ability to repair oxidative damage) of the cells' hemoglobin content, it would suggest that oxygenation may have contributed to the morphological changes. Such processes are likely to affect all donors to some extent. Indeed, as will be explained further below, the greater dispersion of points earlier in storage might reflect an oxidative damage deterioration process that can be modeled with a power curve and that applies to all donors. The uniqueness of trends for individual

donors might reflect different individual variations for this process that become manifested as different fit-parameters for the function.

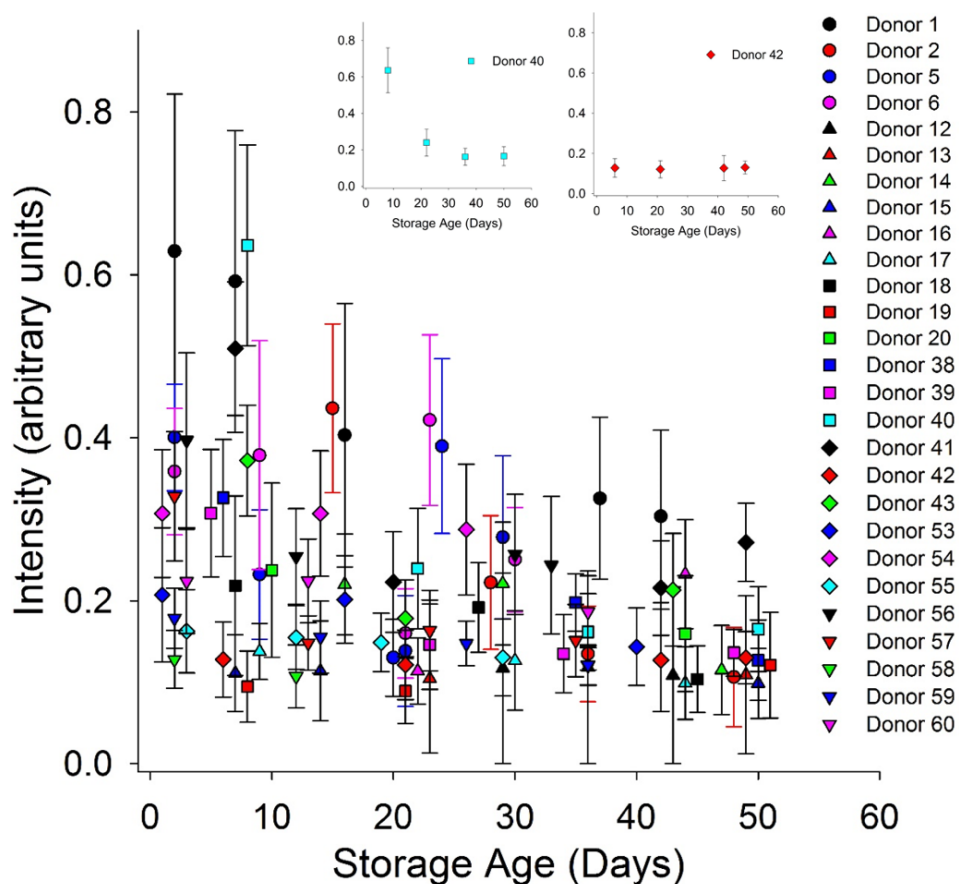


Figure 3-7: The ratio of marker bands ($1208\text{ cm}^{-1}/1222\text{ cm}^{-1}$) associated with hemoglobin oxygenation states as determined from the stored liquid RBC analysis. The inset highlights the trends for Donors 40 and 42.

3.3.3 Stored RBC Quality

To compare the Raman measurements reflecting OS with the MI, the standard metric used in transfusion medicine to gain qualitative insight into cell processes and cell quality, 100 smeared

cells were manually counted by an experienced technician and each was assigned a value based on its morphology; the higher the score for the representative sample, the higher quality the cells from that particular unit. The scoring system was outlined in Table 3-1. While recognizing cell features and correctly classifying them into their respective category is a subjective process, the process was done blind (as described in section 3.2.1.3), in duplicate, and scores were consistently comparable (within $\leq \pm 5\%$ difference). Samples from seven of the donors plotted in Figure 3-7 were subjected to this scoring, and these scores are presented in Figure 3-8.

It is apparent from inspection of these scores that each particular unit behaves uniquely from a morphological perspective. The raw data presented in Figure 3-8 are fitted with similar power curves to demonstrate this correlation (as will be seen later, however, linear fits may be more appropriate in some cases after normalization). Donor 56, after three days of storage, produced a morphology score of 96, implying that the vast majority of cells were still smooth biconcave discs (i.e., completely healthy RBCs). This is in contrast to Donor 39, where the morphology score was recorded as 81 after two days of storage. Furthermore, there are also variations in the rates of change of the morphology scores as a function of time. Even though Donor 56 had the highest morphology score after three days of storage, it does not have the highest score after thirty days of storage. This suggests that, if the same morphological cell degradation pathways are involved, they are uniquely expressed for each unit.

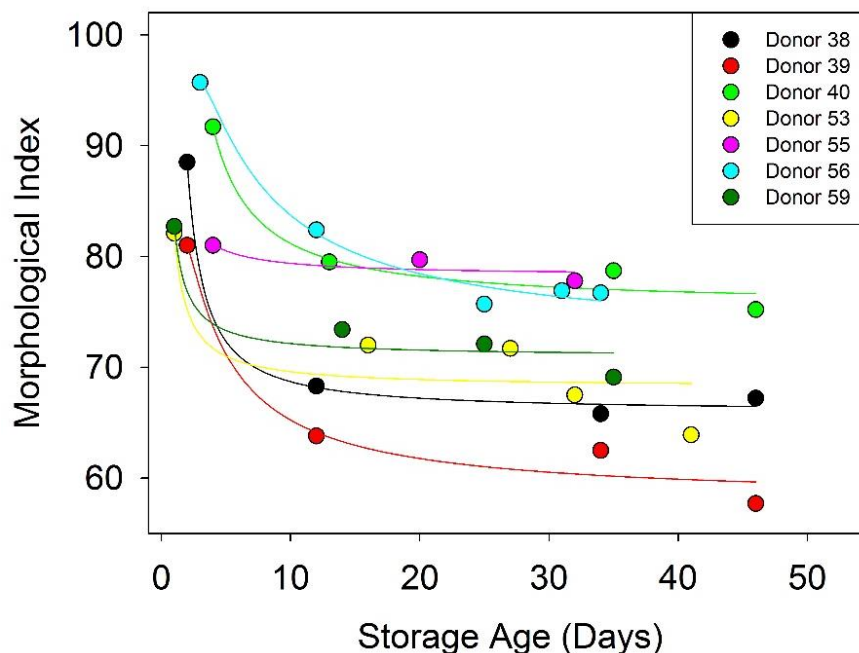


Figure 3-8: The absolute morphology index results for seven donors. Counts were done in duplicate and these scores were within $<\pm 5\%$. The regression lines were obtained using power-curve fits.

3.3.4 Raman Spectra and Stored RBC Quality

Like the aggregate trend observed in Figure 3-7, the initial points in Figure 3-8 had higher scores than later points, pointing to a possible relationship between the trends exhibited by the morphological features of the cell and the oxygenation state of the cells throughout the storage period. To investigate this relationship, the trends that have been presented above in Figure 3-7 and in Figure 3-8 were normalized to the same scale using Equation (3.1). This treatment revealed that the data for some donors appeared to change in a non-linear manner while those for other donors appeared to have linear relationships. If the processes that affect morphological changes and hemoglobin oxygenation are closely related, it is reasonable to expect that they will change

over time in a similar manner for each donor individually. A cross-correlation plot of the data set is shown in Figure 3-9, and the linearity of the clustering confirms the existence of a relationship between the MI and OS.

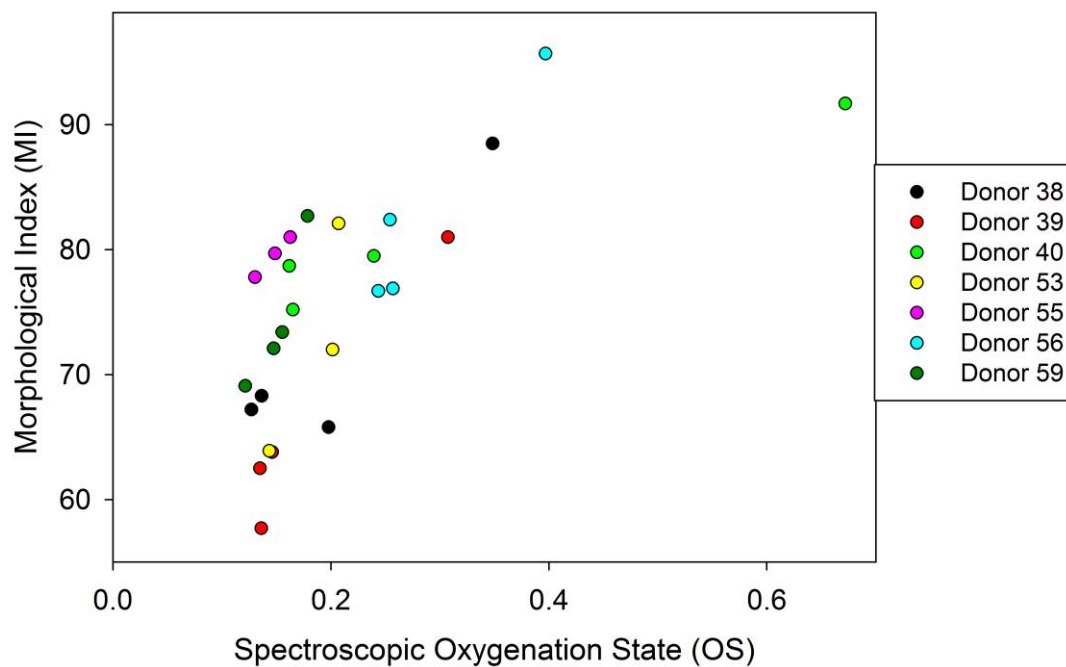


Figure 3-9: A cross-correlation plot of the morphological index (MI) and the oxygenation state (OS). Data was included only if time-points were comparable (± 1 day).

The implications of similar trends between MI and OS would provide evidence that Raman spectroscopy can be used to provide a metric related to the quality of stored RBCs. However, due to the small sample size considered here, further data manipulations are needed in order to temporally align the data from the two independent assessments, and these are described below.

One difficulty with comparing the normalized data was that the starting and ending time points of the morphology scores and the oxygenation ratios often differed by a day or two. This

was a result of scheduling conflicts, as the availability to perform the Raman measurements did not always coincide with the day the blood units arrived to the Centre for Blood Research after processing, which is when morphology samples were typically extracted and analyzed. For example, the MI data for Donor 39 covered the period from days 2 to 46 of storage, but the oxygenation data covered a different period from days 5 to 49. This discrepancy needed to be accounted for to effect a meaningful comparison of the similarities between MI and OS data.

Curve fitting was used to provide quantitative insight into the relationship between the MI and the spectroscopic ratio reflecting hemoglobin OS. The raw measurements were first fitted with a function that provided the best regression, either linear or non-linear, and the fit was then used to obtain extrapolated values at time points that corresponded to the extreme values of the time period covered by all the measurements for a particular donor. After the initial fit, the measurements (including extrapolated points), were then scaled according to Equation (3.1). This was then followed by further fitting of the extended data set with both power and linear relationships and an evaluation of the best fit correspondences between MI and OS data for each donor. Data from Donor 39 illustrate these analyses in Figure 3-10 and the results are demonstrated in Figure 3-11 for all seven donors.

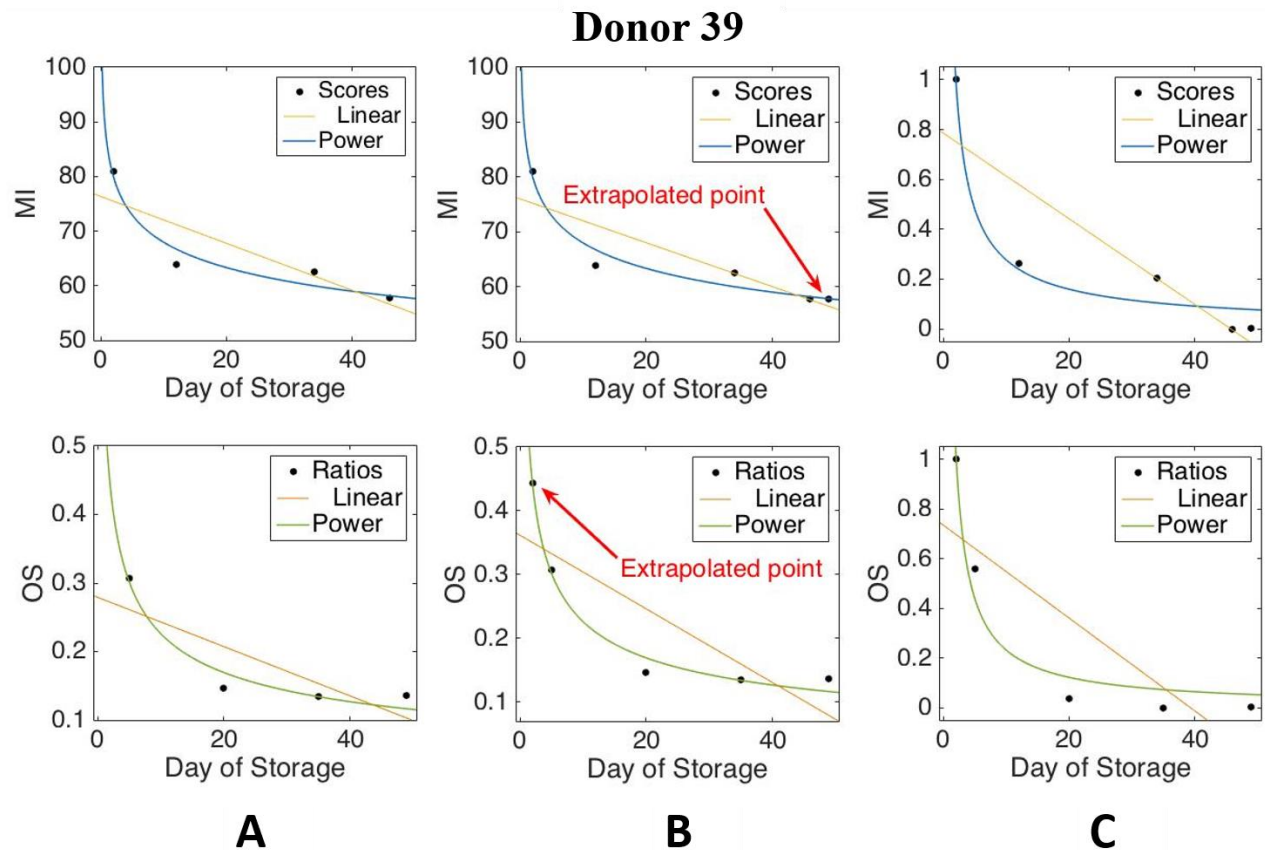


Figure 3-10: Complete data set obtained for Donor 39. The top row depicts plots related to MI scores while the bottom row presents the OS ratios. Column A represents plots of the raw data, Column B represents the fitting process used to match the storage range, and Column C is the final data. Power fit and linear fit curves are shown in each case.

To equate the sampling ranges for the MI and the oxygenation data for Donor 39, the one-term power law fits for these two measurements were used to augment the MI data with an estimate for day 49 and the OS data with an estimate for day 2. Thus both MI and OS measurements, when including these estimates, would cover days 2 to 49. The R^2 for the power law fits of MI and OS

data as measured were 0.9491 and 0.9266, respectively. After extrapolating and applying Equation (3.1), the fits of rescaled data that included extrapolated values produced R^2 values of 0.9666 and 0.9752, respectively.

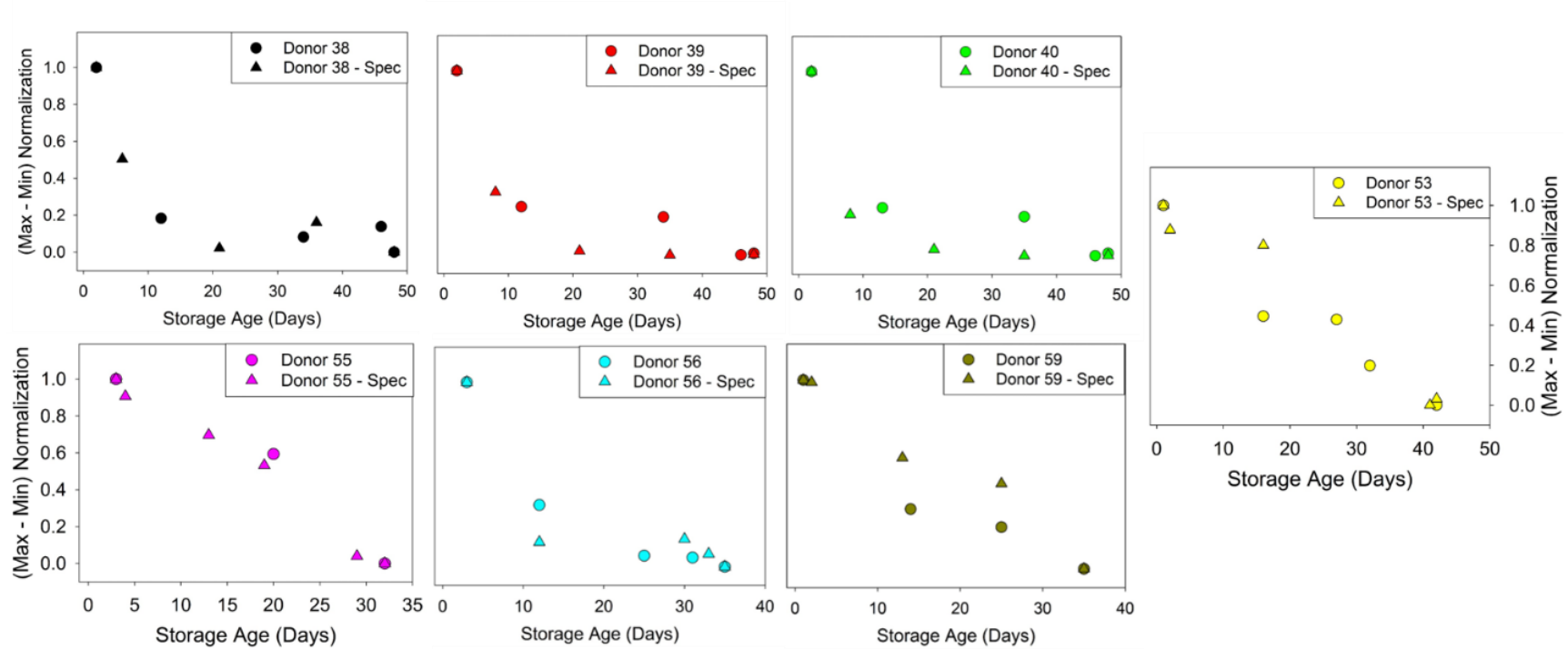


Figure 3-11: Morphology scores and spectral ratios are normalized and compared. Circle data points are the morphology scores and triangles represent the normalized spectral ratios for all donors.

In contrast to the power law fits, linear fits were worse with R^2 of 0.7205 and 0.6569, respectively. Thus, neither the MI nor the OS data set for this donor could be better fit with a straight line. Although both sets could credibly be fit with power equations, fitting the same power equation to both sets would lend support to the notion that the OS data could be used as a surrogate for MI data and hence be indicative of stored blood quality. After processing, the Donor 39 MI set had parameter values (95% confidence intervals in brackets) of 1.746 (0.9184, 2.574) and -0.7993 (-1.2580, -0.3409), and these intervals included the parameter values of the OS set of 1.9630 and -0.9272. It is reasonable, then, to suggest that for Donor 39 the OS data set closely tracked the MI data set.

Donor 55, in contrast to Donor 39, produced MI data that were better fit with a linear function ($R^2 = 0.9476$) than a power fit ($R^2 = 0.8174$). Likewise, OS data from Donor 55 were better fit with a linear fit ($R^2 = 0.9601$) than a power fit ($R^2 = 0.7652$). For the normalized data sets that included the extrapolates to cover the same range, power fits for the MI data ($R^2 = 0.7413$) and the OS data ($R^2 = 0.6726$) were poorer than linear fits for the MI data ($R^2 = 0.9476$) and the OS data ($R^2 = 0.9747$). As before, the normalized and extended data sets' best fit parameters were similar and their CIs included the parameter values of the other set. The fitting results for all 7 donors are presented in Table 3-2.

Donor	Best fit type	R ² - MI	R ² - OS	MI best fit parameters and 95% CIs		OS best fit parameters and 95% CIs		Mutuality of MI / OS best fit parameters
38	Power	0.9852	0.9514	a = 1.866	(1.212, 2.52)	a = 1.809	(0.7442, 2.874)	both
				b = -0.9017	(-1.281, -0.5224)	b = -0.826	(-1.374, -0.278)	
39	Power	0.9666	0.9752	a = 1.744	(0.9295, 2.558)	a = 2.024	(0.9999, 3.048)	both
				b = -0.7973	(-1.247, -0.3473)	b = -1.002	(-1.556, -0.4485)	
40	Power	0.9639	0.9956	a = 1.719	(0.9047, 2.533)	a = 2.293	(1.675, 2.91)	one
				b = -0.7765	(-1.224, -0.3284)	b = -1.193	(-1.523, -0.863)	
53	Linear	0.9391	0.961	p1 = -0.02311	(-0.03393, -0.0123)	p1 = -0.02362	(-0.03235, -0.01488)	both
				p2 = 0.9598	(0.6627, 1.257)	p2 = 1.024	(0.7859, 1.262)	
55	Linear	0.9406	0.9821	p1 = -0.03332	(-0.1397, 0.07311)	p1 = -0.03449	(-0.04095, -0.02802)	both
				p2 = 1.153	(-1.206, 3.512)	p2 = 1.104	(0.9741, 1.234)	
56	Power	0.972	0.9806	a = 3.208	(0.9131, 5.503)	a = 3.992	(0.7395, 7.244)	both
				b = -1.053	(-1.604, -0.5016)	b = -1.262	(-1.944, -0.5807)	
59	Linear	0.8931	0.9661	p1 = -0.02789	(-0.05725, 0.001463)	p1 = -0.02775	(-0.0373, -0.0182)	both
				p2 = 0.9072	(0.2431, 1.571)	p2 = 1.027	(0.8353, 1.219)	

Table 3-2: Best fits and corresponding fit parameters for each donor. Power fit curves were of the form $f(x) = a \cdot x^b$, while linear fits were of the form $f(x) = p1 \cdot x + p2$.

In 7 out of 7 cases, when the MI data is best fit with a power curve, the OS data are too, and when the OS data are not best fit with power curve, the MI data are not either. Furthermore, for both parameters in 6 out of 7 cases, the best fit parameter values of one fit are within the 95% CIs of the best fit parameter values for the other data set and vice versa. Thus, not only do they share the same type of temporal trend, but it could be argued that the same curve (i.e. curve with given parameter values) fits both normalized data sets.

When evaluating these results statistically and testing for the hypothesis that the same type of function that best fits the MI data is also the one that best fits the OS data, the smallest value for which the cumulative binomial distribution is equal to or greater than 0.95 is 6. Therefore, the results are significantly different from random variations. This is also true for the stricter requirement of similar types of functions with similar parameters.

Though it is possible to test whether each pair of data sets come from the same distribution, this does not provide insight into the nature of the changes as a function of time. The latter is of interest because different decay rates have a bearing on the ‘storability’ and ‘usability’ of blood with its concomitant implications for blood banking administration and clinical practice. In this regard, the following three points are worth noting. First, there is substantial donor variation in decay rates and blood quality throughout the storage period. It would be valuable to link them with readily-identifiable donor characteristics such as gender, age, body mass index, and so on, if possible. Second, some measurement data are better fit with linear curves and some with power curves. It is unclear why different processes would be at work for different donors. Though different processes are a possibility, it seems more likely that similar decay mechanisms apply to all donors, but that the rates of decay vary substantially^{351,359} and that the linear fits are the result of power functions that approach linearity over the portion of the storage period where

measurements were taken. Third, because power functions decay fast initially, one could argue, *a priori* and given these results, that ‘fresh’ blood is better than ‘old’ blood. However, clinical trials have thus far not shown a significant difference in clinical outcomes between fresh and old blood’,^{79,81,360,361} perhaps because the temporal definition of fresh blood in these studies is not standardized.

Also worth noting is the lack of biophysical significance associated with power law fits. Though an exponential decay might seem to be of greater biophysical significance, the law of mass action that describes chemical reaction kinetics reliably in dilute and homogeneous media is inadequate to describe reaction progress in intracellular environments. In such environments, reaction progress is affected by low dimensionality, volume-exclusion from macromolecular crowding and inhomogeneity, ionic interactions, and covalent interactions. As a result, rate constants can be time dependent and reaction kinetic parameters can be fractal.^{362–365} Furthermore, multiple exponential decay functions can mimic a power law function *in vivo*.³⁶⁶ It is not unreasonable to expect the kinetics of membrane oxidative damage to be complex and to deviate substantially from kinetics that might be applicable to homogeneous, three-dimensional environments. Therefore, if the oxygenation status of Hb is associated with membrane oxidative damage and RBC morphological changes are due to membrane oxidative damage, the OS and MI time-dependent changes might not reflect standard rate laws.

These results also raise a number of interesting questions. What determines the initial OS of RBCs (i.e., immediately following processing as units of RBC concentrate)? Is this affected by the actual processing? The processing of blood (i.e., the isolation of individual cellular components from donated whole blood) could introduce artifacts that a recent study has suggested could be a main factor in the onset of storage lesion.^{367,368} Perhaps it is also important to ask if OS is affected

by the hematocrit of the donor. Should a particular unit have more RBCs per unit volume than another unit, would the measure of its oxygenation be representative as the same sample volume would have more RBCs? Realistically, the hematocrit of units can vary from 40-60%, so some variation in oxygenation could be attributed to this. In addition, it's possible to wonder if the transit time of receiving a sample in one laboratory and performing the analysis in another laboratory could disturb the OS. However, because the transit time was always the same and aliquots were analyzed immediately after the sample was obtained, any effect would be minimized.

Venous blood, normally used for donation, is about 94 % oxygenated. Why then, do the spectroscopic results show that the blood from numerous donors seem to be only partly oxygenated? Poor oxygenation is also consistent with literature data⁸² showing average Hb oxygen saturation to be about 35% at the onset of storage. Furthermore, the main purpose of RBC transfusion is to improve tissue oxygenation.³⁶⁹ Would the transfusion of inadequately oxygenated blood not present a risk at the moment of transfusion (albeit later, once in circulation, transfused RBC might become adequately oxygenated)? Should blood not be separated, stored, and used based on OS because this could reflect initial blood quality and affect storability? If so, Raman spectroscopy might be a valuable technique to assess the OS of stored blood.

3.4 Conclusions

This work demonstrates the utility of Raman spectroscopy for the investigation of stored RBC ageing effects and RBC quality in dry-fixed blood smears and in liquid blood. Specifically, it was possible to monitor spectral features associated with hemoglobin oxygenation as they changed over the storage period. These features changed in a manner that closely tracked RBC morphological changes over the same period. Because morphological changes are indicative of

blood quality, it implies that blood quality could be inferred from Raman measurements of hemoglobin oxygenation.

Though the MI sample size was small, these results have a number of important implications and justify more extensive investigations. These results also offer some insights relevant to blood banking and clinical use. First, RBCs seem to deteriorate, on average, faster in the earlier period of storage. This implies that fresh blood should generally be better quality than older blood as mentioned above, notwithstanding some recent clinical studies. Second, some donors' blood stores better than others. It would be valuable to identify newly collected units that would be expected to store well, based on an objective measurement, so that other units could be used first to minimize collection and storage expenses and reduce clinical and patient concerns. Third, due to substantial variations in the quality of individual units, assessing the quality of blood at hospital sites, immediately before use, might facilitate better patient outcomes.

Because near-infrared Raman spectroscopy can be performed through the wall of intervening barriers and without damaging RBCs, Raman measurements can be performed on blood-bags to evaluate the quality of RBCs without compromising their integrity. Indeed, Raman spectroscopy offers unique attributes to assist in effective blood banking and clinical use.

Chapter 4: Raman Spectroscopy as a Novel Tool for Monitoring Biochemical Changes and Inter-Donor Variability in Stored Red Blood Cell Units⁴

4.1 Introduction

Current regulatory regimes permit storage of RBCs in specially formulated additive solutions for up to six weeks (at 4°C). Throughout the storage period the RBCs remain metabolically active and convert glucose (from the additive solution) into lactate, via the glycolytic pathway.^{13,350,370–372} The lactate is transported out of the cells and its concentration in the bag increases over time; a recent nuclear magnetic resonance (NMR) spectroscopy study of RBCs collected from eight healthy male donors (aged between 25 and 50 years) showed that, on average, lactate concentration increases seven-fold (~5 mM to ~35 mM) over a six-week storage period.^{63,82,370,373–375}

When RBCs are transfused, the concomitant lactate is cleared from the circulatory system by the liver and kidneys but it can be poorly tolerated by sick infants if given in large quantities.^{374,376–379} Current pediatric transfusion practices are based mainly on considerations of a patient's blood markers (e.g., on hemoglobin concentration and hematocrit) and it is recommended that i) certain at-risk patients only be given fresh units (<5 day storage), ii) that the total number of units transfused be limited, and iii) that older cells be washed if they are the only

⁴ A version of this chapter has been published:

Atkins, C. G.; Buckley, K.; Chen, D.; Schulze, H. G.; Devine, D.V.; Blades, M. W.; Turner, R. F. B. Raman Spectroscopy as a Novel Tool for Monitoring Biochemical Changes and Inter-Donor Variability in Stored Red Blood Cell units. *Analyst* **2016**, *141*, 3319-3327.

units available. These precautionary steps are recommended for disparate reasons but they all have a beneficial side-effect of reducing the risk of hyperlactataemia.^{380–391} Current transfusion practices thus reduce the risk of harm from lactate, but it would still be useful to the transfusion-medicine community to fully understand metabolite accumulation in RBC bags because it could offer an indirect way of assessing stored blood quality.^{80,392}

Raman Spectroscopy is an analytical technique that produces specific chemical information from inelastically scattered light. It is a well-established tool for the accurate monitoring of biochemical analytes and recent studies have used it to investigate aqueous solutions containing lactate, glucose, urea, and other similar metabolites.^{247,329,393–397} As described in section 2.6, the Raman method does not require sample preparation or labelling; it is non-destructive, non-contact, and capable of being used remotely. Several reports have demonstrated the utility of RS in disease diagnosis, and hand-held probe designs are currently being devised that will enable clinicians to identify diseased tissues via biochemical abnormalities.^{398–401} The technique has also been applied as a scientific tool for probing RBCs; work by Wood et al. has shown that specific spectral features are associated with the oxygenation and deoxygenation of hemoglobin¹³³ and that certain spectral features are indicative of heme aggregation and denaturation.¹⁴⁰ They and other groups have used optical tweezing techniques to trap live RBCs and to obtain Raman spectra of the cells under various conditions.^{162,168,169,197,221,402} These works were described in greater detail within Chapter 2. Most recently, stored RBCs were measured non-invasively using a confocal-based SORS approach, and this work will be described further in Chapter 5.⁴⁰³

It is well-known that biochemical changes occur gradually in the first 14 days of RBC storage^{350,404} but accelerate notably at later stages.^{370,405} Published data suggest that concentrations of specific metabolites in individual units can stray far from the average trend-line^{87,350,370,374,405,406}

and that the integrity of RBCs as a function of storage-time has a wide inter-donor variability.^{370,405,406} This chapter will describe the first Raman study to identify spectral features associated with these phenomena and it aims to shed light on the current practice of using storage-time as a proxy measure of RBC degeneration.

4.2 Experimental

4.2.1 Blood Collection

Thirty healthy volunteer adults (aged between 21 and 70 years; 12 females and 18 males) each donated a whole blood unit ($450 \text{ mL} \pm 10\%$) at the Canadian Blood Service (CBS) NetCAD facility in Vancouver, Canada. RBC concentrates were isolated from the blood, subjected to in-line leucoreduction filtering, and suspended in 110 mL of SAG-M additive solution (saline with 1.25 mM adenine, 43.4 mM glucose and 28.8 mM mannitol). The concentrates were stored in standard PVC storage bags at $4 \pm 2^\circ\text{C}$ in accordance with CBS' standard operation procedures.

4.2.2 Supernatant Preparation

Raman spectra of isolated RBCs are dominated by features associated with hemoglobin^{133,140} and thus it is difficult to investigate spectral features associated with metabolism in stored RBC units. Furthermore, in order to maintain standard conditions in the bag over a 42-day storage period it is necessary to minimize losses of volume from the unit. In order to overcome both problems, a preliminary sampling protocol was developed to isolate the supernatant and analyze it separately from the cells. Approximately once a week, a sample of RBC concentrate ($\sim 1 \text{ mL}$) was aseptically removed via the site-coupler (Macropharma, Pasig City, Philippines) of each stored bag using a syringe and was transferred into a microcentrifuge tube. Intact RBCs were

separated from the additive solution by centrifugation at 3,000 RPM for 10 minutes. A small aliquot of the resulting supernatant (20 μ L) was extracted with a Pasteur pipette and deposited on a gold-coated mirror (Thor Labs, Newton, New Jersey, USA) for Raman analysis. The drop was left to dry at room temperature (for a minimum of 20 minutes) after which Raman data were collected. The time for each data point measurement, from sampling to completed experimental analysis, was approximately two hours.

4.2.3 Data Collection

Raman spectra of the dried-drops of supernatant were collected using a commercial Renishaw *inVia* microscope (Gloucestershire, UK) equipped with a 785 nm excitation laser. The light was focused through a 20 \times objective lens (Leica Microsystems, Wetzlar, Germany) and the resulting spot size was a rectangle, 3 μ m \times 30 μ m. The power on the sample was approximately 10 – 20 mW and the instrument was calibrated using the 520 cm^{-1} line of a silicon wafer. Seven to ten spectra (100 seconds accumulation time) were collected from the centre of each dried-drop and averaged to enhance the signal-to-noise ratio. Reference spectra of human hemoglobin (normal human hemoglobin variant A₀, Sigma Aldrich, St. Louis, Missouri, USA) and sodium lactate (Sigma Aldrich, St. Louis, Missouri, USA) were collected for comparison.

In order to validate the Raman analysis, the actual concentration of lactate was quantified in two of the stored RBC units. The lactate was measured using a commercial YSI Lactate Analyzer (Ohio, USA), a biosensor that uses an immobilized L-lactate oxidase enzyme to oxidize lactate into hydrogen peroxide. The electrochemical detection of the hydrogen peroxide produces a current proportional to the amount of lactate originally present. Calibration standards run through the instrument before and after every measurement of RBC supernatant.

4.2.4 Data Processing and Analysis

All Raman spectra were background subtracted, baseline corrected, and smoothed with automated algorithms coded in-house with MATLAB R2009a (The MathWorks, Natick, Massachusetts, USA).^{358,407,408} The spectra were then normalized to the 883 cm⁻¹ mannitol band and compared (mannitol acts as a free-radical scavenger and its concentration over 42 days has been shown to be almost constant).³⁷⁵

Principal component analysis (PCA) was performed in order to understand the variance in the spectral data. PCA decomposes the total variance of the spectral data set into mutually orthogonal, size-ranked sub-variances, each of which resembles a spectral pattern and represents a decreasing contribution towards the total variance within the data set. In this study, the PCA analysis included the entire data set and five PCs were used for the decomposition. A second multivariate technique, band target entropy minimization (BTEM), was used to recombine the PCA spectral patterns (which are known as eigenvectors) into meaningful spectra. The BTEM algorithm combines the eigenvectors in various ways until it finds a local minimum for the Shannon entropy (i.e., it finds the simplest combination of eigenvectors that fits inside a set of user-determined constraints). The software for these multivariate analyses was also written in-house with MATLAB. Statistics were performed using MATLAB.^{409–411}

4.3 Results and Discussion

4.3.1 Raman Spectrum of Stored RBC Supernatant

Donated RBCs are known to undergo physiological, morphological and biochemical changes during their time spent in storage. In order to test the ability of Raman spectroscopy to elucidate metabolic changes in RBCs, it was important to reduce the spectral contribution from

hemoglobin, a metalloprotein that comprises over a third of the total content in a RBC and is a strong Raman scatterer. Thus, before Raman measurements were made, supernatants from thirty different units of donated RBCs were isolated and dried as a drop on a gold mirror.^{412–414} Figure 4-1A is a representative microscope image of a dried-drop of RBC supernatant on a gold mirror, and Figure 4-1B shows a typical Raman spectrum collected from the center of the drop (from one individual, Donor 9). Figure 4-1B also shows other relevant spectra, those of hemoglobin and the SAG-M additive solution.

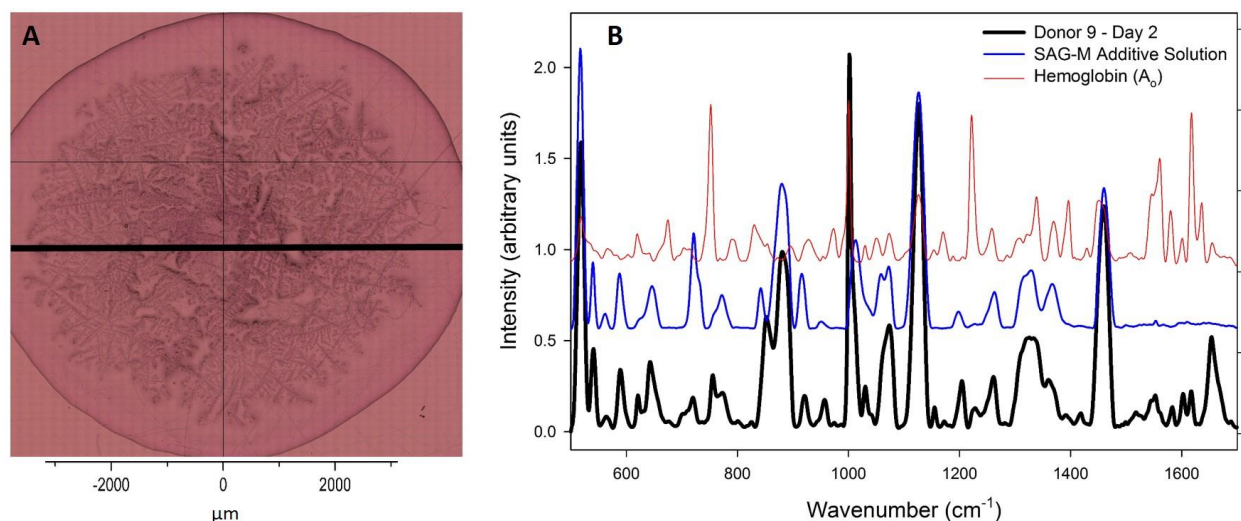


Figure 4-1: (A) A bright-field image showing the uneven topography of a typical drop of supernatant. (B) The average (10 spectra, 100 second accumulation each) Raman spectrum of RBC supernatant after two days of storage (in black), a Raman spectrum of pure SAG-M solution (in blue), and a Raman spectrum of (powdered) hemoglobin (in red); both supernatant and hemoglobin spectra show contributions from the internal porphyrin ring and from the amide modes (753 cm^{-1} , $1500\text{-}1600 \text{ cm}^{-1}$).

The Raman spectrum of the dried supernatant is relatively complex (i.e., it has many Raman bands) and is still heavily influenced by the spectrum of hemoglobin (for example, in the 1500 – 1600 cm^{-1} region both spectra show bands associated with the internal porphyrin ring of the heme structure, as well as amine stretching modes characteristic of the globular section of the protein). Hemoglobin accumulation in the supernatant generally represents a measure of cell-breakdown, and we see from Figure 4-1 that it is present in the additive solution after only two days of storage. This discovery was somewhat surprising, and suggested that hemoglobin was released into the additive solution through an equilibration process or that some of the cells had already undergone hemolysis. Realistically, collection and preparation processes, such as mixing with anticoagulant or additive solutions, variation in centrifugation speeds, and shear stress through tubing and ports, can contribute to red cell hemolysis. We have no corresponding hemolysis data for this experiment but the results imply that Raman could hold promise as a tool for measuring hemolysis-progression over storage time. Interestingly, the intensities and structure of the hemoglobin bands in the supernatant spectrum do not completely match its pure form. This suggests the conformation and composition of the hemoglobin becomes altered after it is externalized.

Features other than those associated with hemoglobin can also be discerned in the supernatant spectrum; some of the observed bands originate from cell fragments (e.g., microvesicles, proteins, lipids, etc.)⁴¹⁵ and others are linked with the biochemical components of the additive solution (the more prominent bands are labelled and assigned in Table 4-1).

It is worth noting that supernatant data presented in this study has been normalized to the mannitol band at 883 cm^{-1} , a component of the additive solution whose concentration has been shown to stay relatively constant throughout the period of storage.

Raman Shift (cm⁻¹)	Mode Assignment	Biochemical Component
520	S-S disulfide stretch	Hb*; protein
536	w (CO₂)⁴¹⁶	Lactate
565	v(Fe-O₂)	Hb
622	C-C twisting of Tyr, Phe	Hb; protein
677	δ(pyrrole deformation)	Hb
724	-	Adenine
753	v(pyrrole breathing)	Hb
853	C-C aliphatic stretch	Lactate
880	CH₂ rocking⁴¹⁷	Mannitol
926		Hb
1000	Phe	Proteins
1031	δ(=C_bH₂)₄	Hb
1040	C-CH₃ vibration	Lactate
1071	δ(=C_bH₂)₄	Hb
1081	C-O vibration	Lactate
1124	CH₃ rocking / C-O vibration	Lactate
1127	v(C_β-methyl)	Hb
1338	v(pyrrole half-ring)_{sym}	Hb
1448	δ(CH₂/CH₃)	Proteins, phospholipids
1526	v(pyrrole breathing)	Hb
1547 & 1566	v(C_βC_β)	Hb
1582 & 1639	v (C_αC_m)_{asym}	Hb
1604	v (C=C)	Hb
1620	v (C=C)	Hb
1653	Amide I modes	Hb; protein

Table 4-1: Prominent bands and their respective vibrational modes.

A potential artifact of the drop deposition sampling protocol was that the drying could create a so-called “coffee-ring”, whereby a capillary effect from solvent evaporation distributes analyte across the dried-drop in a non-random way.^{412,418–421} In order to test whether these effects were relevant to RBC supernatant, we collected 92 spectra across the diameter of a dried-drop (shown as a bold horizontal line shown on Figure 4-1A).

Figure 4-2 shows the variation in intensity across the width of the drop for two spectral features, one which is associated with hemoglobin (753 cm^{-1} , see Table 4-1) and the other which is a metabolic by-product of the cells (853 cm^{-1} , see Table 4-1). The “coffee-ring” chromatographic effect is not substantial for these components (the series averages are almost flat), though it may appear more significant for the hemoglobin than the metabolic by-product (standard deviations of 0.31 and 0.25, respectively). To further minimize the already small chromatographic phenomenon, all the RBC data in this study was collected from as close to centre of the drop as possible.

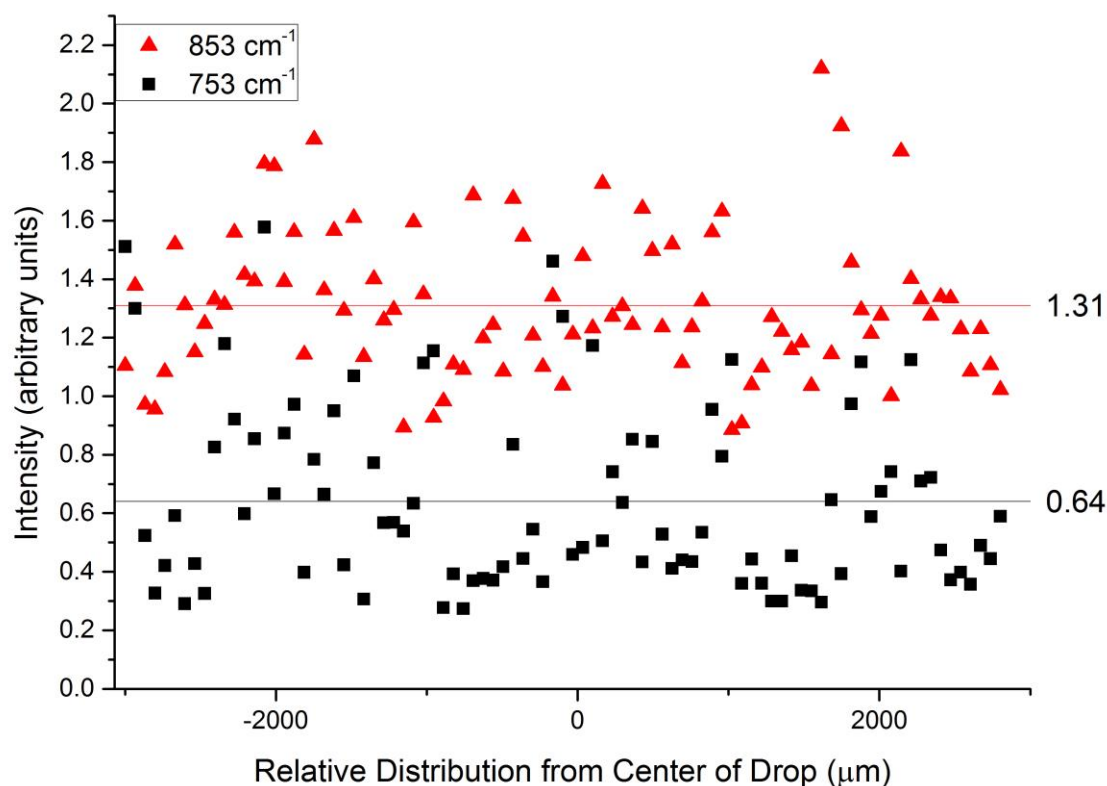


Figure 4-2: Distribution of two distinct spectral features across the width of a dried-drop supernatant sample after two days of storage. The x-axis approximately corresponds to Figure 4-1A; the drop looks inhomogeneous but the *chemical composition* across the drop is uniform for the chemicals of interest.

4.3.2 Variation with Storage Time

Figure 4-3A shows Raman spectra from a representative donor (Donor 26) on days 2, 20 and 42 of storage. It is clear that many of the Raman bands are increasing as a function of storage time, e.g., 530 cm^{-1} , 753 cm^{-1} , 853 cm^{-1} , 926 cm^{-1} , 1031 cm^{-1} , 1127 cm^{-1} , 1338 cm^{-1} , 1448 cm^{-1} , 1620 cm^{-1} . The band at 853 cm^{-1} is clearly undergoing the most significant relative intensity change. Chemometric analyses were used to isolate Raman bands that varied in intensity along

with the 853 cm^{-1} band and the resultant spectral pattern became the target of a literature search (the result is shown in the side-panels of Figure 4-3). Figure 4-3B shows the spectral pattern of the first PCA eigenvector, Figure 4-3C is a BTEM decomposition (targeting the 853 cm^{-1} band)⁴⁰⁹, and a spectrum of sodium lactate is shown in Figure 4-3D. After ascertaining that the major spectral variation with time was due to an accumulation of lactate in the supernatant, its build-up over the course of the 42 day storage-period was investigated.

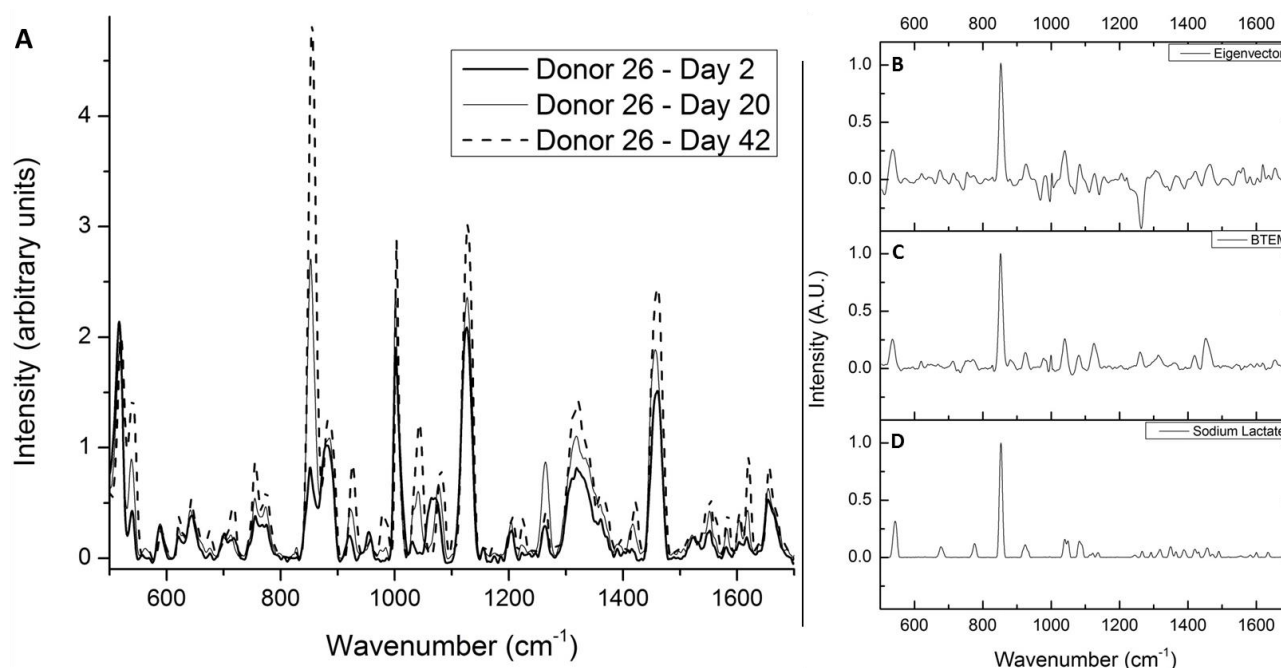


Figure 4-3: (A) The development of the supernatant spectrum over the course of a 42 day storage-period. The dominant spectral change is the increase in band-intensity at 853 cm^{-1} . (B) and (C) show PCA and BTEM analyses of the whole data set (all donors, all time-points) that isolate other spectral changes that are associated with the 853 cm^{-1} band. (D) is a Raman spectrum of pure sodium lactate.

Figure 4-4A shows the progression of lactate for two donors over the course of a complete storage period (as would be expected from published observations, its relative concentration increases). Each circle represents the average spectral intensities of the 853 cm^{-1} band (from seven to ten acquisitions) performed on the sample on a particular day. The spread of a donor's data at each time-point illustrates the reproducibility of the measurement^{63,82}, while the spread of points between two donors illustrates inter-donor variability.

At present, storage duration is used as the proxy measure of biochemical change in an RBC unit. This practice relies on the assumption that storage-related effects occur uniformly in every bag. Figure 4-4B, however, shows that the metabolism of stored RBCs can vary considerably between different donors (measurements beyond the 42 day storage limit are included to assess trend behaviour). For example, the rate of lactate production for Donor 8 (green circles, 49 year old female) is relatively slow when compared to that of Donor 9 (red circles, 55 year old male); after approximately 21 days of storage, the lactate content in RBC concentrate from Donor 8 has approximately doubled, while that of the Donor 9 has more than quadrupled. This suggests that the rates of cellular metabolism are different for these donors and that the use of storage duration as a proxy measure of RBC biochemical changes may not be adequate. Though extensive work has been done describing the biochemical effects of storage on RBCs, the size of variation among units of similar storage age has not been thoroughly investigated and is not fully understood. It is also unclear what clinical significance the lactate variation has for patients.

After the analysis of lactate, it was investigated if similar trend information could be obtained for hemoglobin. It was found that, unlike lactate, the hemoglobin bands did not have consistent trends related to storage time. Therefore, the lack of clear trends was hypothesized to be related to the formation of microvesicles, small structures of cell membrane that bleb off from

cells as they age in storage. These vesicles are known to contain hemoglobin and their distribution across dried drops of supernatant may not be uniform.⁴¹⁵

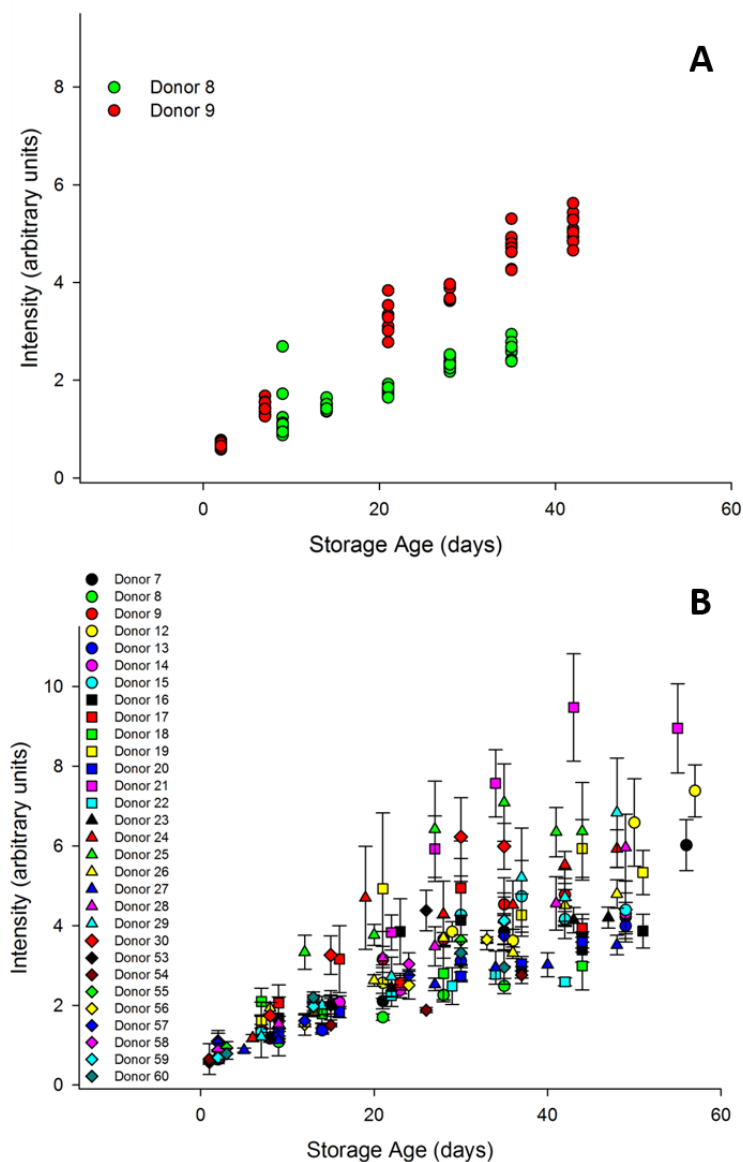


Figure 4-4: (A) The change in relative intensity of the 853 cm⁻¹ (lactate) band with storage age for two (randomly chosen) donors (donor 9 and donor 18) is shown for all supernatant sample points. (B) The average value of the lactate band at each time-point is shown for all 30 donors (bars are \pm std. dev.).

The (first) PCA eigenvector shown in Figure 4-3B was obtained by decomposing the whole data set (i.e., every spectrum) at the same time. Once this decomposition was performed one could look at the contribution that this eigenvector made to each spectrum (the size of this contribution is called a ‘loading’ and, in this data, can be regarded as a measure of lactate content). Figure 4-5 shows the average loading and the variation (std. dev.) that is obtained when all the data are analyzed together. As expected (from a consideration of Figure 4-3B), the contribution from the lactate bands increases, on average, with storage-time; interestingly, the data suggest that the variability between individuals also increases with storage-time and that there is an increase in variability after day 21.

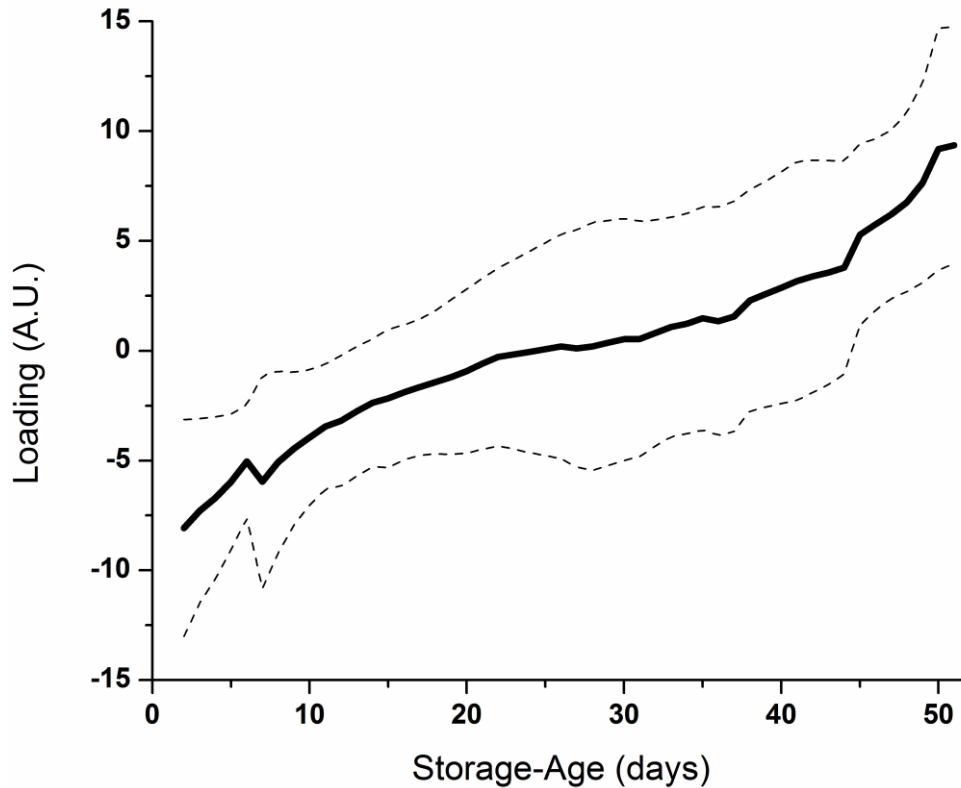


Figure 4-5: Every supernatant spectrum has a contribution (or ‘loading’) from the first PCA eigenvector shown in Figure 4-3B, the average contribution increases with storage age, and the variability between donors (the std. dev.) increases from (approximately) day 21.

The degree of inter-donor variability is such that even ‘fresh’ blood (i.e., defined as ≤ 8 days in this work, but the definition varies in different studies)^{374,376–379} can have sizable variability; for example, Figure 4-6 shows that in supernatant from Donor 26 the relative concentration of lactate increases approximately 150% (from 0.78 ± 0.05 units to 1.93 ± 0.14 units) between day 2 and day 8, but the supernatant from Donor 27 doesn’t even increase 50% (i.e., it changes from approximately 0.75 units to 1.12 ± 0.04 units) over a 9 day storage period. These differences mean

that units from some donors can contain as much lactate after 8 days as units from other donors do after >20 days.

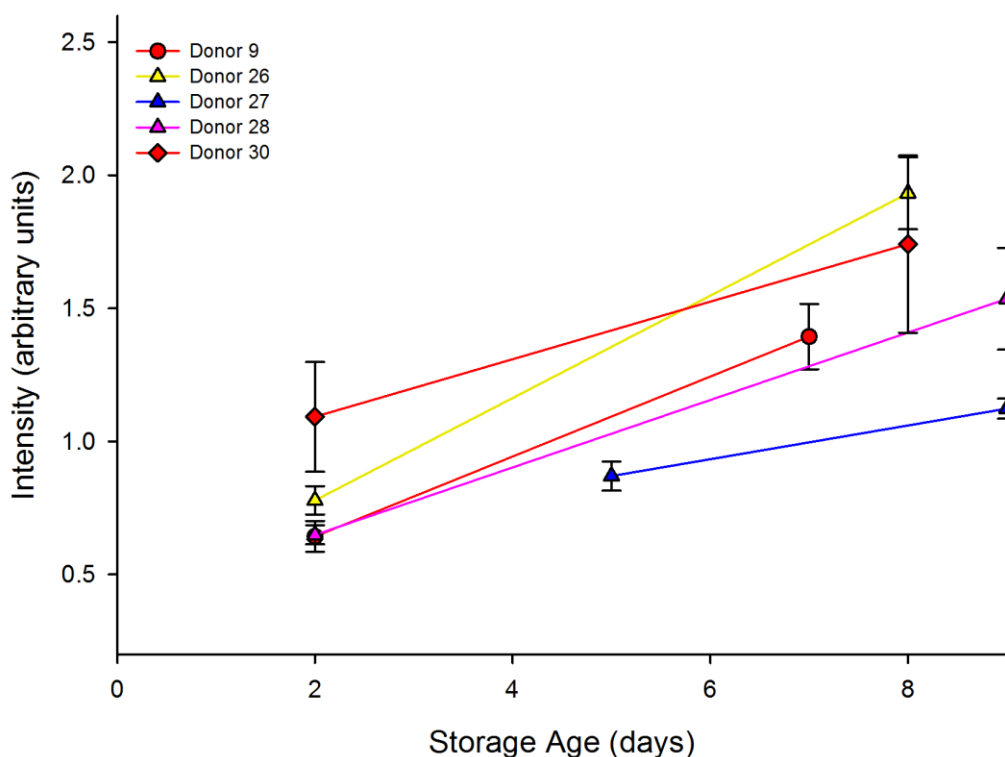


Figure 4-6: The current practice is to use 'fresh' blood (≤ 8 days) for very ill infants. The Raman supernatant data shows that lactate content can vary by a factor of approximately two after 8 days (each data point is measurement of a single individual at a single time-point).

4.3.3 Quantification of Lactate

Raman spectral intensities are linearly correlated with analyte concentrations but they do not provide an absolute measurement of quantity. Obtaining concentrations from a Raman measurement requires intensities to be related to analyte standards on a calibration plot. In order to understand the relationship between intensity and concentration for stored RBC supernatant, a

commercial YSI biosensor instrument was used to quantify the lactate in two of the stored units. Extracted samples were split and half was utilized for spectroscopy whilst half was used for lactate quantification. Figure 4-7 shows the results for the two methods, and while there are no deviation bars included on the YSI measurements due to lack of sample volume for replicate measurements, the comparison appears to be quite robust. The lactate concentration was estimated to be ~7 mM at two days of storage and ~27 mM at thirty-five days of storage. Noting that this final time point is a week earlier than from quantitative lactate numbers reported by an NMR study³⁷⁵, the values compare well with time points included in this NMR report (~8 mM after two days of storage and ~35 mM after forty-two days of storage). It would be possible to further explore the relationship between intensity and concentration, but for the purpose of this chapter, the qualitative relationship in Figure 4-7 is clear enough to provide confidence that the presented trends are directly reflective of lactate concentration.

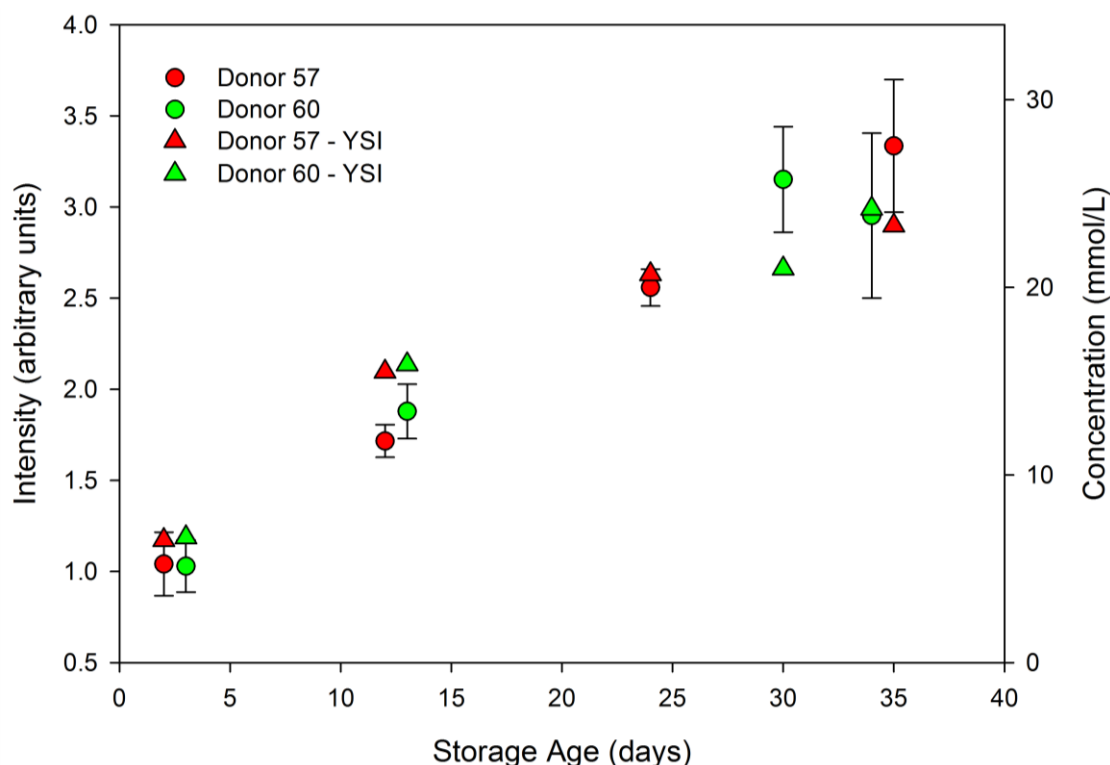


Figure 4-7: The comparison of Raman spectral intensity for the 853 cm^{-1} lactate band with traditional quantification of lactate concentration as determined by a YSI analyzer.

4.3.4 Interpretations of Donor Characteristics and Variability

It has been proposed that the variable metabolic rate of stored RBCs could be affected by certain characteristics of a blood-donor (e.g., age, gender),^{422,423} and with this in mind the data was divided by gender and the groups reanalyzed separately. Figure 4-8 shows that, on average, the units from female donors had less lactate (2.812) than those from male (3.694) donors (ANOVA, $F = 8.49$; $df = 1$; $p = 0.004$, $s = 1.792$). The slopes of the linear fits (and their 95% prediction bounds) in Figure 4-8 suggest that the accumulation of lactate is slower in units from female donors. The slope for males (0.101; 95% CI: 0.085 – 0.118) fell marginally outside the 95% confidence bounds of the slope for females (0.085; 95% CI: 0.071 – 0.098).

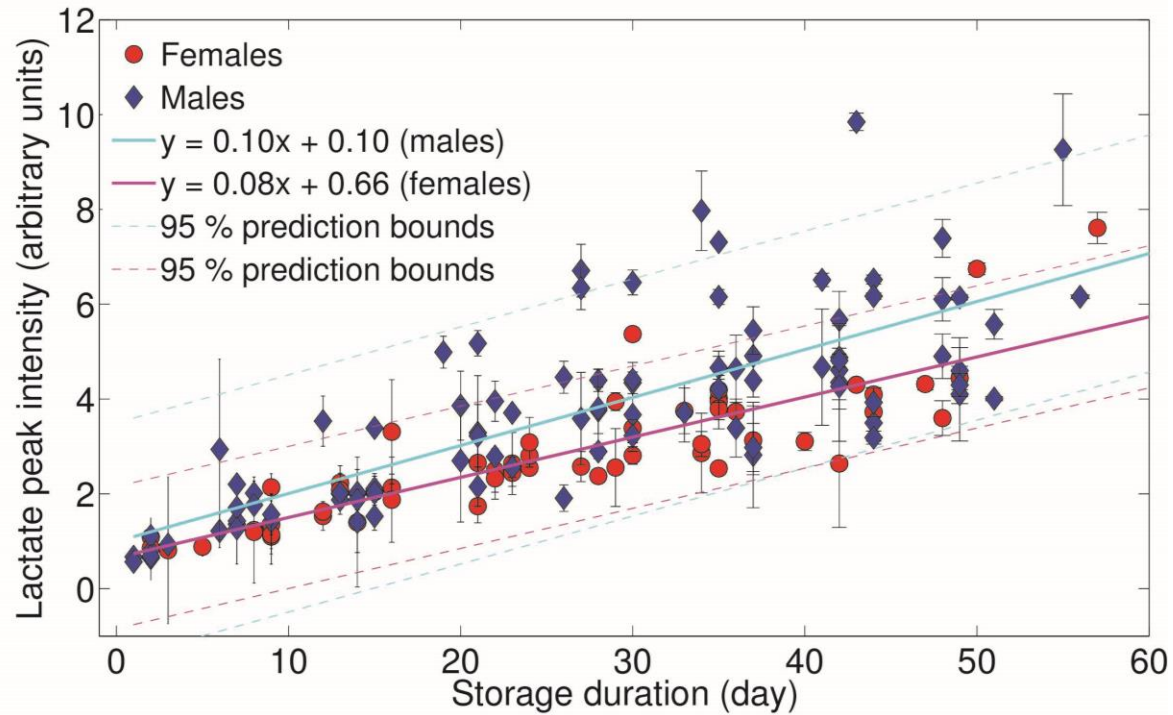


Figure 4-8: Intensity changes of the 853 cm^{-1} lactate band for females (reds) and males (blue) reveal gender-related differences in lactate dynamics during storage. Separate gender-based linear fits show that lactate levels in blood from female donors increase more slowly than in blood from male donors.

To explore the effect of donor-age on stored RBC concentrates, the data was divided by age (at a 45-year-old threshold) and the groups reanalyzed (Figure 4-9). The cohort was not large enough to make single-sex, age-separated groups of any great size (of 30 donors there were 10 donors who were under 45 years old (5 males and 5 females) and 20 donors who were 45 years or older (13 males and 7 females)) and there was no observation of statistically significant differences. However, lactate accumulated more slowly in units from younger females with a regression slope (0.079, CI: 0.070 – 0.088) that had 95% confidence bounds that did not overlap

the slopes of the other groups (0.092, 0.088 and 0.101 for younger males, older females and older males, respectively).

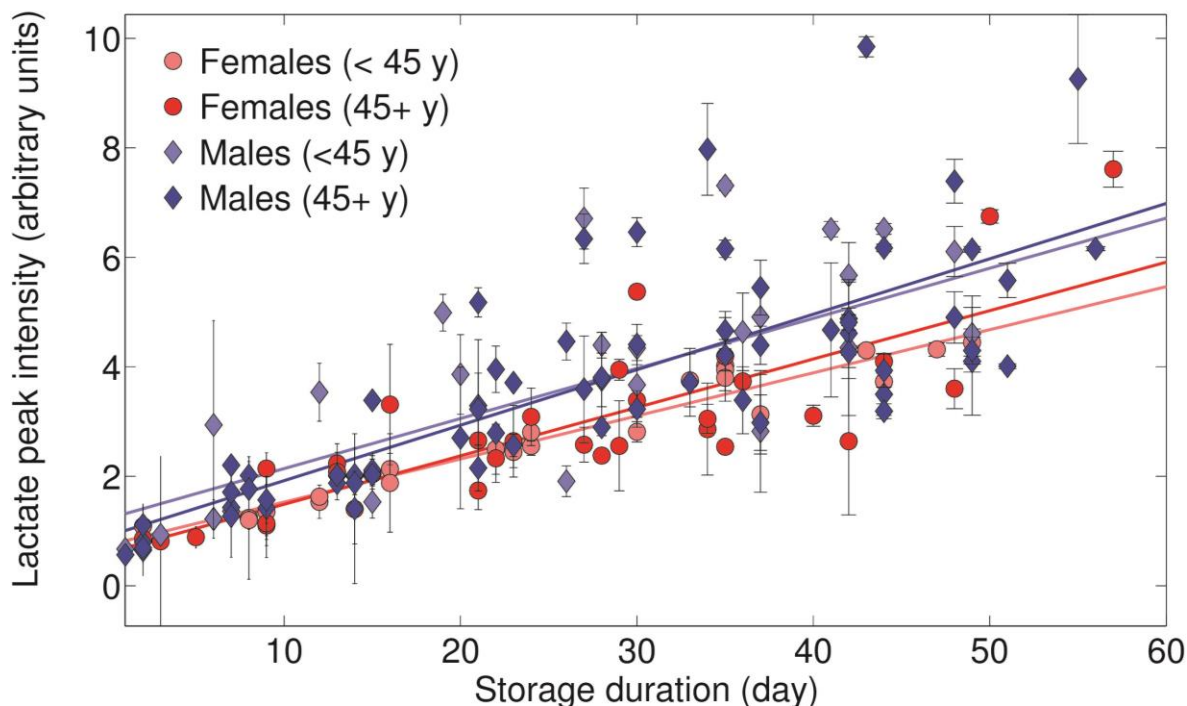


Figure 4-9: Intensity changes of the 853 cm^{-1} lactate band for younger females (light red), older females (red), younger males (light blue), and older males (blue). Linear fits suggest both age- and gender-related differences. The slowest lactate increases in stored RBCs occur for younger females.

The age/gender contribution to the phenomenon that was illustrated in Figure 4-5, i.e., the increase in lactate-variation observed after ~21 days, was also investigated. Three *F*-tests for differing variances were performed and three statistically significant results were found (significant at the Bonferroni-corrected $\alpha = 0.0167$ level): first, the variations increased at the 21-day cut-off for older male donors ($F = 0.377$; df. 40, 26; $p = 0.01$), second, those increases were

much larger than those for younger female donors ($F = 5.14$; df. 40, 13; $p = 0.003$), and third, the variations in older female donors were larger than those in younger female donors ($F = 3.87$; df. 19, 13; $p = 0.0161$). At this point, there is no explanation as to *why* the inter-donor variability increases at 21 days of storage. One possible hypothesis is that the shift in cell metabolism (towards the oxidative phase of the pentose phosphate pathway) that is known to occur in the second week of storage is variable for different donors. It has previously been proposed that during the first two weeks of storage the RBC metabolism works to sustain RBC energy production, but from day 14 onwards it produces metabolites that are known to initiate anti-oxidant responses. If this is the mechanism responsible for the variation, then the data would suggest that cells from different donors have variable resistance to the oxidative stresses that are encountered during storage.^{352,374}

Ultimately, the cohort of donors in the present chapter was not large enough to draw solid conclusions about donor characteristics. For example, evidence was presented above that the increase in inter-donor variation observed after 21 days of storage was largely due to changes occurring in units from older male donors, and it will take another specially designed study to test any biological hypotheses satisfactorily. In these studies, it will be necessary to have more information about the donors; in this case, there was access to age, gender, and the awareness that each donor was healthy enough to donate, but nothing further about their lifestyle (for example, whether donors were smokers or not).

4.3.5 Future Directions

The current regulatory management of RBC inventory is based solely on storage age and inter-donor variability is not considered. The same is true of transfusion medicine, where suitable units are differentiated from unsuitable units by consideration of their ‘freshness’ (storage age).^{87,66}

The data presented above suggest that there are relationships between donor-gender/donor-age and stored-RBC metabolism, and they suggest that Raman spectroscopy could be used to investigate these relationships in larger (properly controlled) studies. The ability to measure the biochemical constitution of an RBC unit rather than rely on the proxy measure of storage age could have implications for the management of blood supplies and for the design of randomized clinical trials that aim to determine if RBC quality has any effect on patient outcome, especially if the data could be collected non-invasively from intact blood-bags.

The data generated in this study, like those typically generated in investigations of stored RBCs, were obtained by taking aliquots of blood and analyzing them in the laboratory. In addition to being slow and often complex, the sampling requirements for these analyses prevent the unit from ever being used for transfusion. They are thus of little use to a clinician who wants to assess if an aspect of the unit content is within an acceptable range before transfusing the unit into a high-risk patient.^{384–386}

Spatially offset Raman spectroscopy (SORS) has been developed for collecting spectra through plastic containers^{424–426} and as will be shown in Chapter 5, SORS can be used to acquire information from RBCs stored in intact plastic storage bags.⁴⁰³ As expected, the Raman data from the RBCs are dominated by spectral features associated with hemoglobin and it is likely that the features would obscure the biochemical information described in the present chapter. It is believed, however, that a SORS instrument would be capable of performing a through-bag measurement of the cell-free supernatant which exists once the RBCs have settled to the bottom of the bag. This analysis could aid a more accurate determination of useful shelf-life – as a function of metabolite concentrations – and would provide blood service organizations with another means for quality

control and inventory management. It could also equip clinicians with additional information on the “metabolically active substrates and electrolytes” contained in stored RBC units.^{374,403,427,428}

4.4 Conclusions

The goal of this study was to use the non-destructive analytical technique, Raman Spectroscopy, to investigate biochemical changes that occur in units of RBCs as the cells age. The most prominent spectral change was the large variation in the intensity of Raman bands associated with lactate. The data revealed detail of the magnitude of inter-donor variability and variability associated with gender and age (though larger controlled studies will be needed to draw stronger conclusions). The findings point the way to the development of a Raman instrument for probing intact RBC units in blood banks and hospitals; such a tool could also be useful for investigating which biochemical pathways dominate in units of RBCs from different donors and for correlating these effects with patient outcomes.

Chapter 5: Non-Invasive Spectroscopy of Transfusable Red Blood Cells Stored Inside Sealed Plastic Blood-Bags⁵

5.1 Introduction

Modern medicine relies on safe, secure, and cost-effective supplies of transfusable RBCs. Blood banking agencies obtain whole blood from volunteer donors, separate the RBCs by differential centrifugation, suspend them in specially formulated additive solutions such as SAG-M, and store them in PVC blood-bags at 4°C until they are needed for transfusion.

Despite extensive efforts to maintain RBC viability and function, RBCs degenerate and disintegrate whilst being stored.^{37,379,405,429–432} Degraded cells have lower post-transfusion survival rates and thus regulatory authorities limit the amount of time they can be stored; most agencies specify that unused units be disposed of after five to six weeks (e.g., the storage period in SAG-M is limited to 42 days. At this point, ~40% of RBCs show irreversible morphological changes and ~0.5% of RBCs have lysed).^{37,379,405,429–432}

The causes and effects of stored-RBC degeneration (the so-called storage lesion) are complex, but the biochemistry that occurs inside blood-bags has been subject to much study.^{37,82,352,370,373–375,379,405,429–433} For example, it is well known that RBCs continue to metabolize and convert glucose (from the additive solution) into lactate via the glycolytic pathway, and it is known that as the concentration of lactate increases (from ~5 mM to ~35 mM) over a six-week

⁵ A version of this chapter has been published:

Buckley, K.; Atkins, C.G.; Chen, D.; Schulze, H. G.; Devine, D. V.; Blades, M. W.; Turner, R. F. B. Non-Invasive Spectroscopy of Transfusable Red Blood Cells Stored Inside Sealed Plastic Blood-Bags. *Analyst* **2016**, *141*, 1678-1685.

storage period, the pH drops from ~7.0 to ~6.5.^{82,374,375,379,433} Concomitant with these metabolic effects are various degenerations of cellular membranes and changes in the concentration of various cellular metabolites. For example, the intracellular concentration of 2,3-DPG, a metabolic intermediate which affects the oxygen-carrying capacity of hemoglobin, decreases with storage-time.^{352,370,373} At present, the absence of a metric to quantify storage lesion, and concerns over violating the integrity of closed sterile systems, mean there are no procedures in place for the analytical testing of individual units of red cell concentrate (RCC).

SORS is a variant of Raman spectroscopy that allows the retrieval of chemical information through over-lying surfaces and turbid media.^{434,435} The technique involves the acquisition of Raman spectra from locations on the sample-surface that are laterally separated from the laser illumination zone. Photon diffusion causes spectra collected with larger spatial-offsets to have greater relative-contributions from larger depths within the sample, i.e., photons that find their way to the surface from greater depths are more likely to be found at greater (lateral) distances from the illumination point.⁴³⁴ The development of SORS has unlocked a host of new applications ranging from aviation security and pharmaceutical analysis, to the non-invasive detection of disease (e.g., cancer).^{411,424–426,436}

Recently, a form of “micro-SORS” that can interrogate samples through ~1 μm -thick diffusely-scattering layers has been reported. The technique, which has applications in biology, quality control, and material sciences, involves the introduction of a SORS offset along the plane of the incident beam,^{437–439} or the introduction of a lateral-offset across the plane of the surface.^{440,441} In the past, the lateral-offset has been achieved by spatially resolving images on the CCD detector⁴⁴⁰ or by delivering the laser beam via a different path (i.e., completely bypassing the microscope optics).⁴⁴¹

The current chapter will describe the application of a different form of micro-SORS to probe RCC through standard ($\sim 400\ \mu\text{m}$ -thick) blood-bags. In this formulation, the lateral-offset was introduced across the plane of the sample-surface using the standard beam-steering optics of the Raman microscope. This simple work-around did not require any optical or optomechanical engineering yet it revealed rich chemical information about the oxygenation state of the stored cells.

Until now, scientific investigations of the RCC storage lesion have relied on analytical techniques that destroy the sample and/or breach the sterility of the bag. The demonstration that RCCs can be interrogated non-destructively and non-invasively through standard storage bags points the way to a tool for investigating RBC degeneration/disintegration *in situ*, and potentially a Raman-based instrument for quality control in a blood bank or hospital setting.

5.2 Experimental

5.2.1 Blood Collection

Fifteen healthy adults (6 females and 9 males) aged between 20 and 68 years (Mean = 50 years, std. dev. = 15 years) each voluntarily donated a whole blood unit ($450\ \text{mL} \pm 10\%$) at the Canadian Blood Service NetCAD facility in Vancouver, Canada. The RBCs were isolated from the blood, suspended in 110 mL of SAG-M additive solution (saline with 1.25 mM adenine, 43.4 mM glucose and 28.8 mM mannitol), subjected to an in-line leucoreduction filtering and put into standard PVC storage bags. The units of prepared RCC (Figure 5-1) were then stored under standard blood banking conditions at $4 \pm 2^\circ\text{C}$. The protocols used for the donation and preparation the isolation of the RBCs have previously been described.³⁵



Figure 5-1: A standard bag of transfusable RBCs in a PVC blood-bag (the white panel obscures barcodes and identification-labels).

5.2.2 Data Collection and Processing

5.2.2.1 Collection of SORS Data

The intact units of RCC were probed with a commercial Raman microscope (Renishaw *inVia* Raman microscope, Gloucestershire, England) that was equipped with a 785 nm excitation laser (laser power at the sample 105 - 110 mW), a 50 μm confocal aperture, and a 5 \times microscope lens (Leica, Wetzlar, Germany). The Renishaw WiRE™ software allowed visualization of the laser spot on a video image of the sample and the laser spot appeared as a rectangular profile ($\sim 40\text{ }\mu\text{m}$ wide and $\sim 300\text{ }\mu\text{m}$ long) on the surface of the blood-bag (see Figure 5-2, position A). The software gives the user the option of moving the laser spot across the focal plane with ‘beam-steer’ alignment mirrors. The mirrors are accessible in order to allow the operator to move the laser illumination spot to the center of the lens focal point and thereby maximize the Raman signal. In this SORS experiment, however, the mirrors were used for the opposite purpose and the laser illumination line was moved away from the illumination point, through a SORS offset of 200 μm to position B in Figure 5-2 (200 μm was the largest offset that could be introduced without warping the illumination line with the edge of the lens). To collect the spectra, each blood-bag was taken, in turn, directly from the refrigerator and placed on the microscope stage. A zero-offset spectrum (Figure 5-2, position A) was first collected for 180 seconds (18 accumulations x 10 second acquisition time) and then a SORS spectrum (Figure 5-2, position B) was collected for 180 seconds (18 accumulations x 10 second acquisition time). After spectral data had been collected from a bag it was returned to the refrigerator; previous research has shown that exposure to uncontrolled temperatures for 60 min or less does not affect RBC quality.^{442,443}

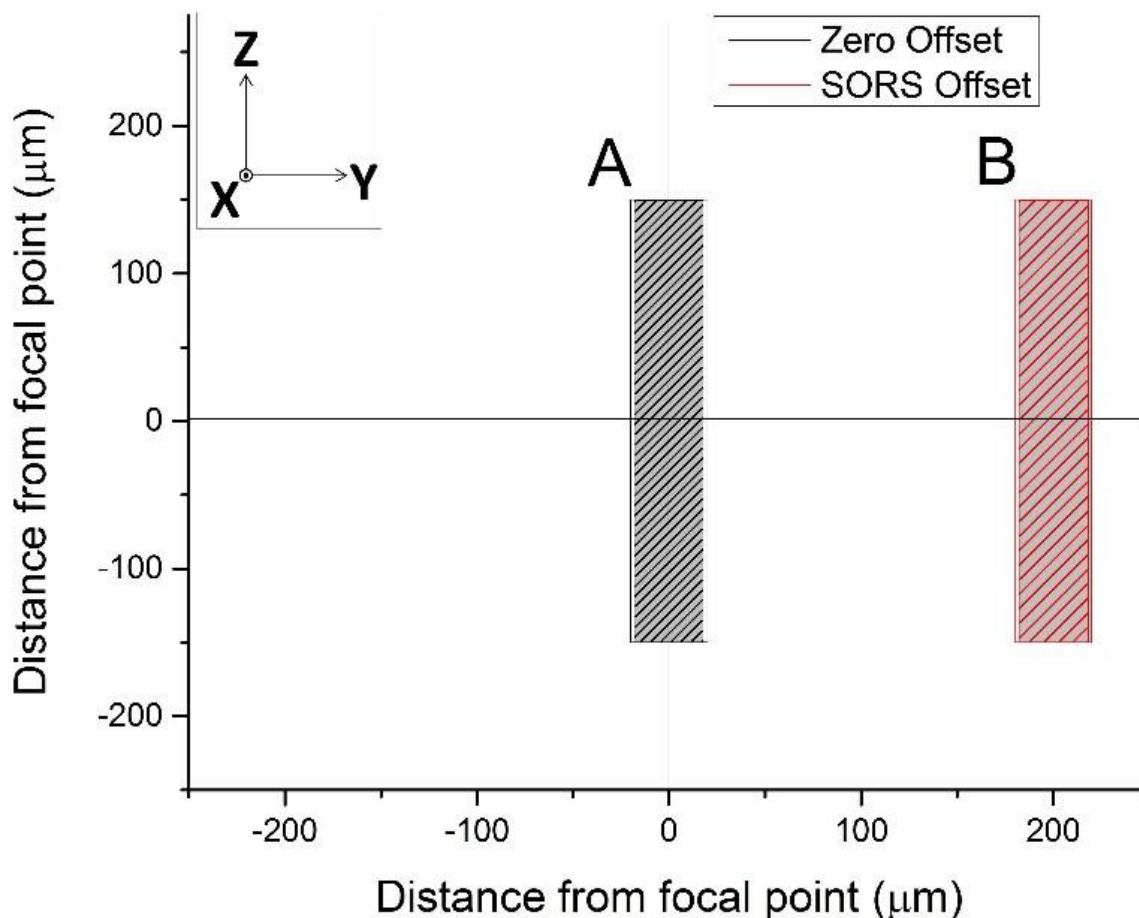


Figure 5-2: Position A is the set-up for collecting a conventional Raman spectrum with the laser line centered on the microscope's focal point (the cross-hairs). In order to collect a SORS spectrum, the laser illumination line was moved 200 μm away from the focal point using the beam-steer alignment mirrors (Position B).

5.2.2.2 Collection of Supporting Data

The comparison spectrum shown in Figure 5-4 was collected by removing an aliquot of RCC aseptically from a blood-bag and pipetting it onto a gold mirror (Thor Labs, Newton, New Jersey, USA). The laser was directed onto the top of the liquid and a Raman spectrum collected in the conventional manner. For ease of interpretation, the spectra in Figure 5-4 were normalized to

make the hemoglobin features above 1500 cm^{-1} have comparable intensity. The spectra in Figure 5-5 were collected with longer accumulation times (an equivalent of 6 minutes) in order to improve the signal-to-noise ratio. The fluorescence backgrounds were removed by fitting a polynomial baseline to each spectrum and subtracting it from the raw data (MATLAB, MathWorks, Natick, USA).⁴⁴⁴

5.3 Results

A SORS experiment to probe the contents of a standard ($400\text{ }\mu\text{m}$ thick) blood-bag is shown in Figure 5-3. A zero-offset measurement (labelled A in both panels) produces a spectrum dominated by the PVC blood-bag whereas a $200\text{ }\mu\text{m}$ offset measurement (labelled B in both panels) produces a very different spectrum. The spectra are plotted as raw unprocessed data.

The $200\text{ }\mu\text{m}$ offset SORS spectrum shown in panel B of Figure 5-3 is plotted again in Figure 5-4, along with a spectrum of RCC that has been removed from a blood-bag, placed on a gold mirror and probed using conventional (i.e., zero-offset) Raman spectroscopy. It is clear that the two spectra share many of the same Raman bands and that both are dominated by spectral features associated with hemoglobin (e.g., bands at 752 cm^{-1} , 1224 cm^{-1} , 1547 cm^{-1} , 1582 cm^{-1} , 1606 cm^{-1} , 1617 cm^{-1} , and 1636 cm^{-1} ; see Table 5-1 for assignments).^{133,445}

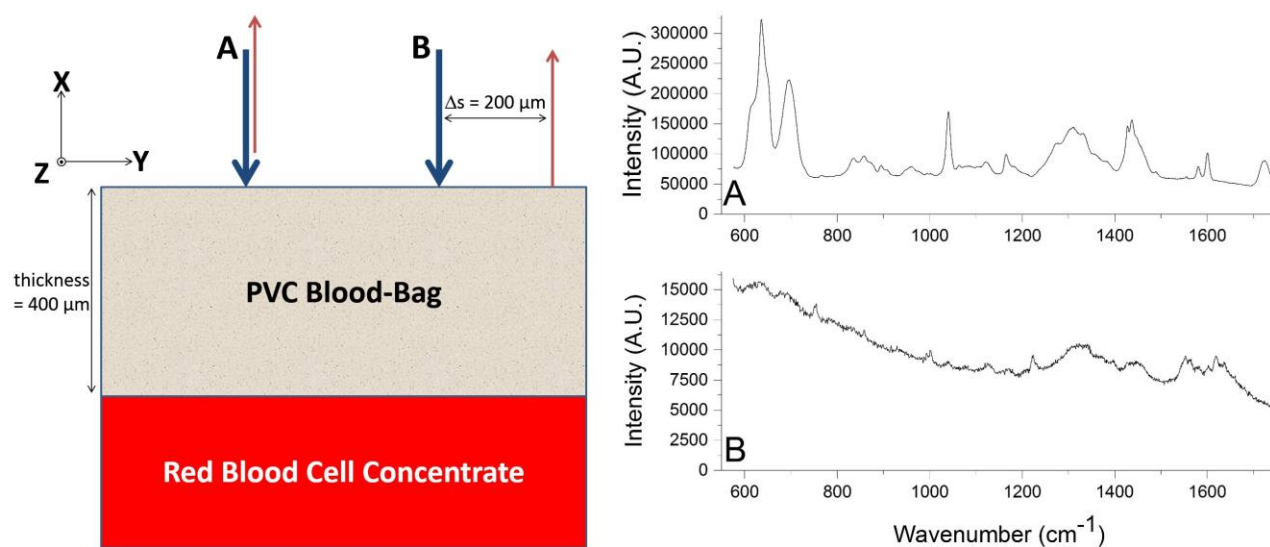


Figure 5-3: The schematic diagram of a blood-bag on the left shows two different experimental geometries: conventional Raman spectroscopy, in which the backscattered light is from the laser illumination point (geometry A) and SORS, in which the collection point is laterally offset from the laser illumination point by $200\ \mu\text{m}$ (geometry B). The plots on the right show the corresponding spectral data.

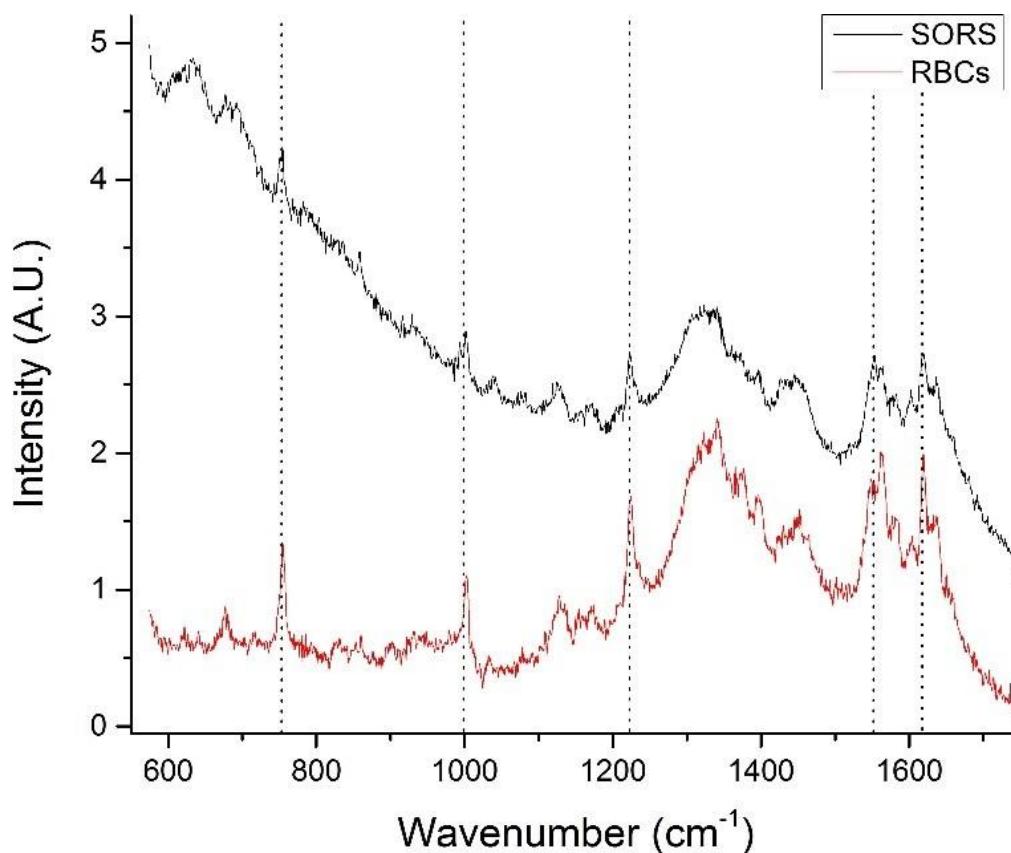


Figure 5-4: The SORS spectrum of the blood-bag contents (from Figure 5-3; top trace) plotted with a conventional Raman spectrum of RCC (i.e., the contents of a blood-bag; bottom trace). Both spectra exhibit many of the same Raman bands, in particular those associated with hemoglobin.

Raman Shift (cm⁻¹)	Mode Assignment	Biochemical Component
622	C-C twisting of Tyr, Phe	Hb; protein
635 & 695	C-Cl stretching	PVC bag
677	δ(Pyrrole deformation)	Hb
753	ν(Pyrrole breathing)	Hb
853	C-C aliphatic stretch	Lactate
880	CH₂ rocking	Mannitol
1000	Phe	Proteins
1031	δ(=C_bH₂)₄	Hb
1040	Ester of phthalic acid	Plasticizer additive (PVC)
1040	C-CH₃ vibration	Lactate
1071	δ(=C_bH₂)₄	Hb
1081	C-O vibration	Lactate
1124	CH₃ rocking/C-O vibration	Lactate
1127	ν(C_b-methyl)	Hb
1212	δ(C_mH)	Hb
1226	δ(C_mH)	Hb
1448	δ(CH₂/CH₃)	Proteins, phospholipids
1427 & 1437	CH₂ scissors vibration	PVC
1526	Pyrrole stretching	Hb
1547 & 1566	C_βC_β stretching	Hb
1580 & 1600	Ester of phthalic acid	Plasticizer additive (PVC)
1482 & 1639	Asymmetric C_αC_m stretching	Hb
1604	C=C stretching	Hb
1653	Amide I modes	Hb; protein
1723	Carbonyl stretching	PVC

Table 5-1: A list of the more prominent Raman bands in the SORS spectra.

Figure 5-5A shows SORS spectra that were collected from two units chosen at random and scanned on the same day (in this figure the fluorescence background has been removed for ease of comparison); the main features of the SORS spectra show that similar biochemical information has been retrieved from each unit and there is no substantial increase in the relative intensity of bands at 662 cm^{-1} , 972 cm^{-1} , 1248 cm^{-1} , 1365 cm^{-1} , or 1396 cm^{-1} , which would indicate that the cells are undergoing photo-damage.¹⁴⁰ Figure 5-5B shows the 1200 to 1650 cm^{-1} region of Figure 5-5A on an expanded scale. In this plot, slight differences between the spectra can be seen; these subtle features have previously been reported in Raman studies of RBC oxygenation and deoxygenation cycles and are well characterized.^{135,140} They indicate that the hemoglobin in cells from Donor 15 are fully oxygenated inside the bag and the hemoglobin in cells from Donor 1 are partially deoxygenated inside the bag. The only other plausible explanation for these spectral features is the presence of metHb, which can be ruled out because there is no increase in intensity of the Raman bands at 1516 cm^{-1} and 1610 cm^{-1} .^{135,140}

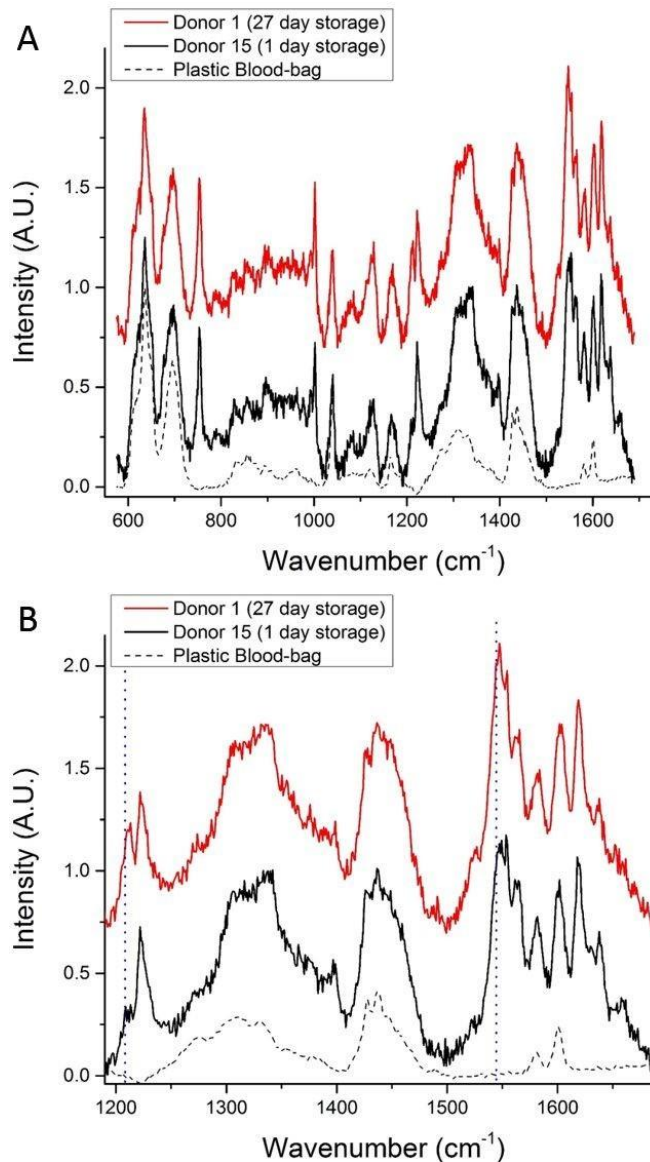


Figure 5-5: A) A comparison between a SORS spectrum of 27 day old RBCs and a SORS spectrum of 1 day old RBCs (from a different donor). B) Emphasis on spectral features related to oxygenation in the 1200-1650 cm⁻¹ region, the increase in intensity of the bands at ~1212 cm⁻¹ and ~1547 cm⁻¹ (dotted lines) reveal that the 1 day old RBCs are oxygenated and the 27 day old RBCs are partially deoxygenated. The Raman features associated with molecular bonds that do not change confirmation or position with oxygenation, are unchanged.

The oxygenation state of hemoglobin in stored RBCs is an important topic in the transfusion-research community and the diffusion of oxygen through the (gas-permeable) PVC storage bags has been a subject of study.⁸² This work has shown that hemoglobin is affected in complex ways by cold storage (for example, the drop in pH increases the oxygen-pressure needed to saturate hemoglobin, but the loss of cellular 2,3-DPG decreases it).⁴⁴⁶ Despite the complexity of the system there is consensus that ~99% of the hemoglobin in an RBC unit is oxygen-saturated by the end of a six-week storage period.⁸²

The expected trend towards increased oxygenation with storage time is inconsistent with the results in Figure 5-5 where the cells in the 1-day-old bag from Donor 15 are more oxygenated than the cells in the 27-day-old bag from Donor 1. In order to further investigate this apparent anomaly, the relationship between hemoglobin oxygenation and storage age was analyzed for all fifteen bags. No simple correlation between oxygenation and time was found when all the data were analyzed together (Figure 5-6, $R^2 = 0.02$), but there were some weak trends found in specific bags. For example, the oxygenation of the hemoglobin in RBCs from Donor 1 (Figure 5-7, top panel) decreased as storage time progressed ($R^2 = 0.38$) whereas a slight trend towards increased oxygenation with time was more typical of the whole data set and more consistent with expected trends.

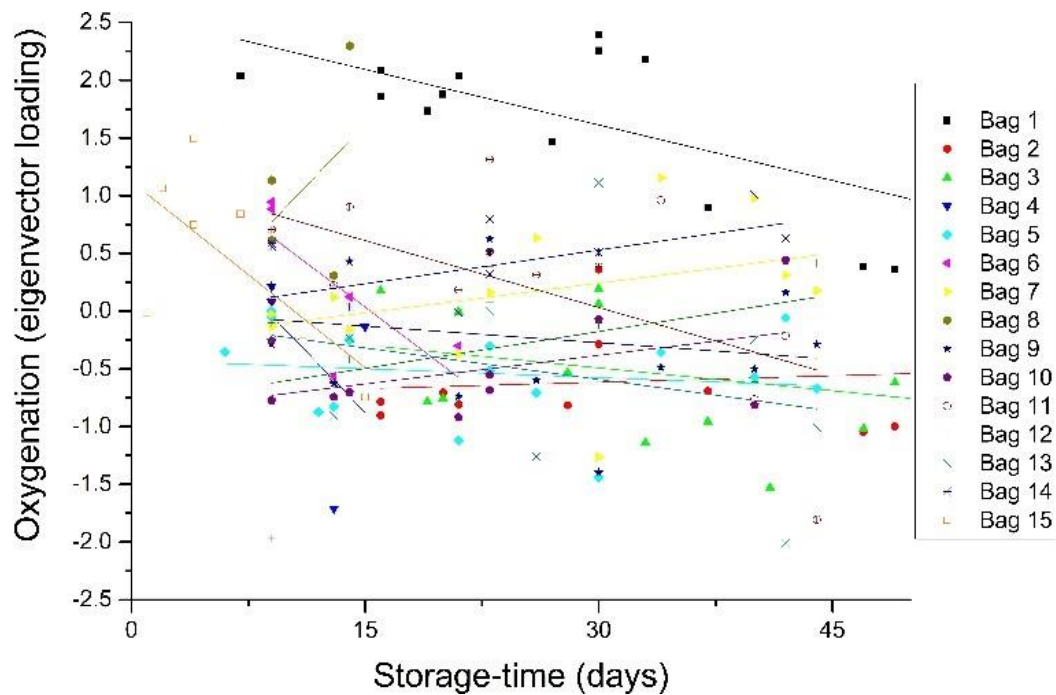


Figure 5-6: The data from each bag were decomposed with multivariate (Principal Component) analysis. The primary difference between the spectra (the first eigenvector) was associated with oxygenation/deoxygenation, as shown in the bottom panel in Figure 5-7. The degree to which each spectrum is dominated by this eigenvector is plotted here. The large scatter and absence of any simple relationship is discussed below.

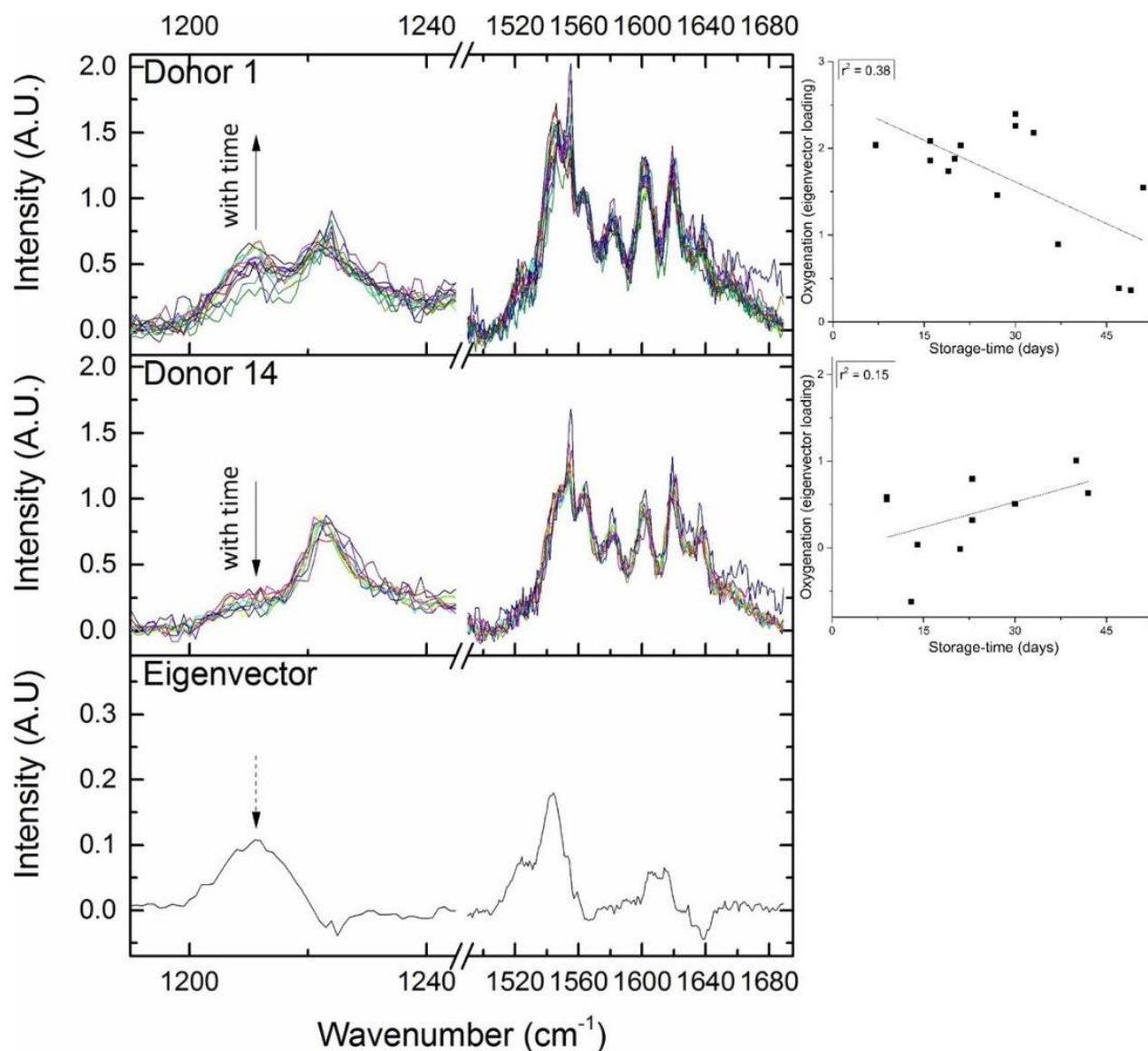


Figure 5-7: Certain regions of the RBC spectrum are seen to vary with oxygenation (see Figure 5-5). The eigenvector which correlates with oxygenation-changes is plotted in the bottom panel. The top panel shows Donor 1, an example of an RBC unit where oxygenation decreases with storage age (spectra are on the left and the trend from Figure 5-6 is on the right). The middle panel shows Donor 14, an example of an RBC unit where oxygenation increases with storage age (again, spectra are on the left and the trend from Figure 5-6 is on the right).

The aim of the present study was to assess whether or not SORS could be used to probe RCC non-invasively inside PVC bags. It was not designed to test a specific clinical or biological hypothesis and did not have the statistical power to draw conclusions about the characteristics of particular donors (e.g., spectral features related to age, gender, etc.). Nevertheless, the observation is interesting and will be investigated in further studies (see below).

5.4 Discussion

Donated RBCs are not routinely subjected to analytical testing before they are transfused because current techniques for evaluating cell-biochemistry are relatively slow, and they require that the sterility of the unit be breached so aliquots can be taken. The present study shows that SORS can be used to retrieve pertinent biochemical information from RBCs that are being stored in standard PVC blood-bags. The non-invasive probing of stored RBCs creates new opportunities to investigate the oxygenation-levels of the stored cells and, in the longer term, potentially offers a powerful methodology for elucidating the relationship between storage lesion and patient outcome.

5.4.1.1 Oxygenation State of Hemoglobin

Hemoglobin accounts for 97% of the dry weight of RBCs⁴⁴⁷ and >90% of hemoglobin is oxygenated at the time of donation. As mentioned above, there is plentiful oxygen available to the RBC hemoglobin during storage as atmospheric oxygen can diffuse through the gas permeable PVC bags and it is thought that by the end of the storage period ~99% of the hemoglobin are oxygen-saturated.⁸²

The SORS technique, as deployed in this study, only interrogates RBCs that are close to the inner surface of PVC bag (i.e., within $\sim 100\ \mu\text{m}$ of the inner surface). No rigorous protocol was deployed to shake the bag before the SORS spectra were collected and thus it is probable that the data are weighted towards cells that had spent more time interacting with atmospheric oxygen (and in regions of the bag that had a lower concentration of RBCs per unit supernatant due to settling). Nevertheless, the SORS spectra presented confirm that in some blood-bags measurable amounts of deoxygenated hemoglobin are present after six weeks of storage. The design of the study, to test SORS as an analytical technique rather than to test a specific clinical/biological hypothesis, means that it is not possible to draw any deeper findings from the data. The results do suggest two interesting courses for future work: it would be useful to repeat the study in a situation where each bag was agitated gently before scanning, and also to repeat the study in a situation where each bag was disturbed as little as possible so as to intentionally look at oxygenation in cells that spend more time near the PVC membrane. The large scatter in Figure 5-6 shows that, in all probability, the present study looked at some combination of the two.

5.4.1.2 Relationship Between Storage Lesion and Patient Outcome

Multi-center, randomized, blinded trials have shown that for critically ill adults in general, there are no significant clinical consequences for receiving transfused RBCs that are reaching the end of their shelf-life.⁷⁹ More specific randomized controlled trials involving certain vulnerable groups of patients also suggest that outcomes are unaffected by the storage age of the RBCs. For example, RBC storage age does not have deleterious effects on premature, very low-birth-weight infants⁴⁴⁸ or on adult patients that are undergoing cardiac surgical procedures.⁴⁴⁹ However, the evidence that there is no link between storage age and patient outcome in some cohorts, does not

prove that there is no link between those variables in all cohorts and randomized controlled trials of children⁴⁵⁰ and adults⁴⁴⁹ are on-going.

For ethical and practical reasons, the clinical trials that have been reported so far have compared outcomes of patients who have received blood that is ‘fresh’ (defined as being $< 7^{79,448}$ or $< 10^{449}$ days old) with outcomes of patients who have received ‘standard’ blood of variable age (for example 22.0 ± 8.4 days old in one study⁷⁹ and 14.6 ± 8.3^{448} days old in another), therefore, in addition to the unanswered questions surrounding particularly vulnerable patient-groups, there are still questions to be answered about the biochemical changes that occur at the extremes of the storage-period, i.e., the earliest and latest days of storage.

Chapter 4 described attempts at using conventional Raman spectroscopy of supernatant (aliquots) to investigate the related problem of lactate build-up in the RBC additive solution during storage. It was shown that blood-bags can exhibit measurable variability in lactate concentration and that some units of RCC carry a significantly larger load of metabolites than others.^{415,451} Although most transfusion recipients have the ability to compensate for lactate (and the concomitant pH change) by metabolic and respiratory mechanisms, massive transfusions may overwhelm some patients and lead to transfusion-induced acid-base abnormalities.^{75,350,370,451} Future work will focus on methodological and/or data-analysis techniques that will enable the use of analytical techniques described in the current chapter to interrogate supernatant *in situ* so that bags containing irregular excesses of lactate can be identified. It is envisaged that SORS will be used to probe the thin layer of additive solution that forms in stored bags when the RBCs settle to the bottom, a natural sorting analogous to the centrifugation in the metabolic load study.

5.5 Conclusions

SORS has been used to retrieve biochemical information from RBCs that have been packaged for transfusion in PVC bags. Most analytical techniques that have been used to analyze RBCs previously require a breach of sterility and an invasive sampling of aliquots from the bag, actions which renders the contents unusable for transfusion. The ability to probe the cells that are inside standard blood-bags (i.e., the plastic containers that are used in blood banks and hospitals) will open new avenues of research in the study the red cell storage lesion and could form the basis of a clinical tool for probing of individual blood-bags before they are transfused into higher-risk patients.

Chapter 6: Conclusions and Future Work

The research presented in this thesis demonstrated that each unit of donated blood has a unique, albeit changing, Raman fingerprint throughout storage. These unique features originated primarily from differing lactate concentrations and hemoglobin oxygenation levels. Though the exact clinical relevance of these fingerprints needs to be assessed, they appear to pertain to metabolic load and RBC quality. Recent developments bode well for monitoring these fingerprints non-invasively with an instrumental apparatus, potentially enabling a clinician to make better informed decisions regarding the suitability of a given unit of stored RBCs prior to transfusion. Furthermore, the utility of such a technique would extend to the management of the blood supply, and could significantly facilitate the task of blood banking.

This chapter presents a summary of important findings from each of the research chapters along with a brief discussion of future implications and research directions.

6.1 Raman Spectroscopy as a Tool for Interrogating Ageing Effects and Quality in Banked Red Blood Cells

The ability of Raman spectroscopy to measure age-related chemical changes to RBCs during blood bank storage was evaluated on dry-fixed RBC smears and liquid RBC samples. These spectra were dominated by hemoglobin Raman features. For dry-fixed smears, distinct donor-dependent spectral differences were observed in regions associated with hemoglobin oxygenation. However, because dry-fixing affected the oxygenation of hemoglobin and created protein aggregation, the results were deemed unreliable. Liquid RBC samples, considered more robust,

also revealed donor-dependent differences in hemoglobin oxygenation as inferred from the ratio of bands in the 1200-1230 cm^{-1} region.

Hemoglobin oxygenation was hypothesized to be related to red cell morphology, a measure of cell quality. Simultaneous analyses of the oxygenation status and cell morphology of a particular unit revealed that RBC hemoglobin oxygenation trends closely mirrored RBC morphological changes over the same period. These trends showed that the RBCs generally deteriorated faster in the earlier period of storage and that some blood stored better than others.

The discovery that blood quality could be inferred from Raman measurements through analysis of hemoglobin oxygenation is the first of its kind. It highlights the potential benefits of using through-bag Raman measurements to assess the quality of stored units, without compromising their integrity, for clinicians and blood banking agencies alike.

6.2 Raman Spectroscopy as a Novel Tool for Monitoring Biochemical Changes and Inter-Donor Variability in Stored Red Blood Cell Units

Hemoglobin is both a strong Raman scatterer and a major RBC constituent, and rendering spectral information from other chemical species within the cells is challenging. Because RBCs, containing the great majority of hemoglobin, settle gradually over time, a supernatant emerges that is relatively enriched in additive solution components (adenine, glucose, mannitol) and RBC breakdown products. The supernatant fingerprint easily revealed the presence of features that were not associated with hemoglobin or the additive solution. The most significant relative intensity change identified was for the 853 cm^{-1} band of lactate, a major metabolic breakdown-product. Changes in Raman spectral intensities were confirmed with a commercial YSI biosensor. The clear

relationship between the methods provided confidence that the spectral trends for the 853 cm^{-1} lactate band were reflective of lactate concentration.

Analyses of storage-related trends of this band revealed up to three-fold differences in the 'fresh' blood (i.e., defined as ≤ 8 days) from different donors. Furthermore, the inter-donor variability of this band increased after day 21. Differences between donors also clustered by certain readily obtainable characteristics such as age and gender. Statistical analyses of storage-related trends demonstrated that, on average, units from female donors had significantly less lactate than those from male donors, and that the accumulation of lactate was slower in units from female donors. Additionally, when the data was further divided by age (at a 45-year-old threshold), it appeared that lactate accumulated slowest in units from younger females, as the 95% confidence bounds did not overlap with the slopes of the other groups.

Ultimately, though they need to be replicated with a larger cohort of donors, the findings reported in this chapter have important implications for the improved design of randomized clinical trials and for improving blood collection, blood bank administration, and clinical use. Thus, gender and age differences should be taken into account when designing clinical trials to improve the likelihood of observing meaningful outcomes. Finally, due to substantial inter-donor variations, the RBC quality of each individual bag needs to be determined before use. The discovery that lactate, a metabolic waste product of RBCs, could be measured in the supernatant of stored RBC units with Raman spectroscopy has revealed the potential of Raman spectroscopy to realize these benefits.

6.3 Non-Invasive Spectroscopy of Transfusable Red Blood Cells Stored Inside Sealed Plastic Blood-Bags

Modern investigations of the RBC storage lesion have relied on analytical techniques that destroy the sample and/or breach the sterility of the bag. However, the non-destructive capabilities of Raman spectroscopy can be implemented non-invasively with the use of Spatially offset Raman spectroscopy (SORS) to permit the retrieval of chemical information through over-lying surfaces and turbid media. With SORS, Raman spectra are acquired from locations on a sample-surface that are laterally separated from the laser illumination zone; spectra collected with larger spatial-offsets have greater relative contributions from larger depths within the sample. With micro-SORS, the SORS technique is implemented on a Raman microscope by making minor optical adjustments to achieve an appreciable offset of the excitation laser. This permits the interrogation of RBCs through their plastic storage-barrier.

The zero-offset spectrum of RBCs stored within a plastic blood-bag (i.e., a conventional Raman experiment) probed the surface of the storage bag and produced a Raman spectrum that was dominated by chemical features associated with the PVC, its major constituent. Using micro-SORS with a 200 μm offset of the excitation laser allowed the collection of photons scattered from within the bag. Comparing the RBC fingerprint of SORS spectra to Raman spectra obtained from liquid samples showed that the SORS spectra exhibited many of the same Raman bands. Furthermore, these spectra could be used to analyze RBC storage-related changes.

Micro-SORS investigations of features associated with oxygenation for fifteen different RBC units demonstrated a weak trend towards increased oxygenation with time, consistent with expectations. In addition, inter-donor variability was again evident with RBCs from one particular donor *decreasing* as storage time progressed. Though interesting, the findings need to be

substantiated in more focused studies as the only objective with this work was to demonstrate that the RBCs could be interrogated inside the bag without compromising them. Replication would need to address factors related to oxygen diffusion into the bag, the depth inside the bag from which scattering is collected, the separation of bag contents due to settling of RBCs, and the effects of handling on these factors. Regardless, the principle of using SORS to investigate the contents of storage bags was clearly demonstrated in this chapter. Thus, not only can hemoglobin oxygenation status, and by inference, RBC quality, be interrogated *in situ*, but there is also potential to similarly measure the supernatant to attain its complementary information.

6.4 Outcomes and Future Work

6.4.1 Improvement to Clinical Trials

Much effort and substantial funds have been spent on randomized and controlled studies to obtain definitive evidence of a relationship between deleterious effects to a transfusion patient and the storage age of the RBC units. The most recent results of these multiple-year studies have suggested that storage age may have no relationship to negative outcome, although the presence of storage lesion clearly creates a product that is not optimal for transfusion. The work presented in this thesis has demonstrated that each unit of stored RBCs has unique characteristics, whether these pertain to metabolic products, such as lactate, or internal cell markers, such as hemoglobin oxygenation. This highlights that storage age is, by itself, an inappropriate metric to use in clinical trials. To obtain valid data about the effects of RBC storage lesion on recipients, randomized clinical trials must use an appropriate metric that reflects the degree of storage lesion. It has been shown here that Raman spectroscopy has the capabilities to contribute to the measurements required for formulating such a metric.

6.4.2 Improvement to Transfusion

The decision to transfuse RBCs should always be based on a thorough assessment of medical indications that transfusion is necessary to save life or prevent serious illness. The motivation to characterize aspects of the RBC storage lesion using Raman spectroscopy is based on enabling future studies of how such degradation processes could affect a patient following a transfusion. As mentioned, the potential of Raman spectroscopy to non-invasively inspect RBC units without breaching the sterility of a bag or causing damage to the cells makes it an ideal technique for providing detailed chemical information to a clinician, or a blood bank. These professionals would then be better informed as to the status of a unit prior to transfusion and would be able to serve particular patient groups more effectively dependent on perceived needs.

6.4.3 Future Work

Throughout the course of this thesis, a number of interesting questions have been raised which can be addressed in the near future.

6.4.3.1 Smears of Stored RBCs

The dense part of the smear was investigated in Chapter 3 to model the bulk conditions of the RBCs within a unit. However, can the smear be used to also obtain specific Raman images of the various cell morphologies (as presented in Figure 1-9)? Could these images provide chemical information related to the breakdown of the cell and give insight into the different metabolic conditions in each? The inner leaflet of the RBC membrane is exposed during times of distress; could these phospholipids be measured?

6.4.3.2 Characterization of Supernatant

Separating the RBCs from the additive solution via centrifugation demonstrated that biochemical information, such as the presence of lactate, was measured in Chapter 4 using Raman spectroscopy. What other biochemical features could be measured if sampling effects were eliminated and the measurement was performed non-invasively using a SORS strategy? One of the current methods for evaluating the quality of a red cell unit is measuring the extent of hemolysis. As mentioned earlier, technologists working in blood banks qualitatively identify badly storing RBC units by sight (as units that undergo hemolysis have a distinct reddish supernatant). The quantitative method for the determination of hemolysis is not standardized across different quality labs, but involves a measurement (often with spectrophotometry) to determine the free hemoglobin released into the supernatant relative to the total hemoglobin contained in the unit. Could a non-invasive measurement of extra-cellular hemoglobin or the detection of released microvesicles provide insight into the hemolysis of the stored RBCs? Acquiring such information would allow additional insight into the metabolic pathways of stored red cells and further serve to empower the decision-making of a clinician.

6.4.3.3 Instrument Development

In Chapter 5, the application of micro-SORS confirmed that RBCs could be assessed through their plastic storage bag. The utility of a Raman microscope platform, however, is not ideal if the technique is to be feasible for clinicians in a hospital or a blood bank. A more convenient adaptation would be required that can rapidly measure both the RBC portion of the unit and the supernatant (visible after the stored cells have settled). Parameters such as hemoglobin

oxygenation, lactate accumulation, and other biochemical features could be easily obtained with a low-barrier to proficient instrument operation.

6.4.3.4 Assessment of Other Blood Products

When whole blood is donated, it is separated into its individual component parts (RBCs, WBCs/platelets, plasma) as depicted in Figure 1-8. Although this thesis only described the utility of Raman spectroscopy for assessing stored RBCs, platelets also have value to modern healthcare for therapies such as prevention of bleeding. They are enriched from the recovered buffy-coat layer and stored upwards of 5 days at room temperature under constant agitation. The literature review presented in section 2.7 revealed that Raman investigations of platelet chemistry are sparse. It would therefore be useful to apply some of the techniques outlined in this thesis to assess features related to the biochemistry associated with stored platelets.

6.5 Summary of Findings and Overall Impact

The results presented in this work demonstrated the first application of Raman spectroscopy for assessing physiological, morphological, and biochemical aspects of transfusable RBCs. The technique has potential in the field of transfusion medicine, as it has non-destructive capabilities that can be implemented non-invasively. In this thesis, Raman spectroscopy was used to investigate changes to hemoglobin oxygenation and lactate concentration in stored RBCs by studying blood smears, bulk liquid, cell-free supernatant solutions, and measuring spectra directly through a plastic over-barrier.

The main conclusions of this thesis are:

- A correlation was found between the oxygenation state of hemoglobin (as determined from a spectral ratio of bands) and the morphology of stored RBCs (as determined with an index scoring protocol). The trends of both metrics changed rapidly in the early stages of storage, and could be modeled using power-functions. It was evident that both trends were also unique for different donors.
- Using Raman spectroscopy, the main waste product of stored RBCs, lactate, could be measured in RBC supernatant due to less interference from hemoglobin. The accumulation of this biochemical was quite distinct between different donors and also differed by other donor characteristics such as gender and age.
- A variant of Raman spectroscopy, known as SORS, is capable of retrieving chemical information through over-lying surfaces. It was demonstrated that micro-SORS could be used to identify and measure RBCs through their plastic over-barrier, the first such non-invasive measurement of stored RBCs. The potential exists to optimize this experimental procedure such that both supernatant and RBCs can be interrogated non-invasively to provide a clinician or blood bank with concrete chemical information pertaining to the quality of a particular stored unit.

Overall, these conclusions confirm that Raman spectroscopy is a capable tool for the assessment of stored RBCs.

References

- (1) Greenwalt, T. J. A Short History of Transfusion Medicine. *Transfusion* **1997**, 37, 550–563.
- (2) Naumann, D. Vibrational Spectroscopy in Microbiology and Medical Diagnostics. In *Biomedical Vibrational Spectroscopy*; John Wiley & Sons, Inc., 2007; pp. 1–8.
- (3) Bain, B. J. The Blood Film and Count. In *Beginner's Guide to Blood Cells*; Blackwell Publishing Ltd, 2004; pp. 1–28.
- (4) Bessis, M.; Weed, R. I. *Living Blood Cells and Their Ultrastructure*; Springer-Verlag, 1973.
- (5) Hillman, R. S.; Finch, C. A. *Red Cell Manual 7th Edition*; F.A. Davis Co., 1996.
- (6) Mohandas, N.; Evans, E. Mechanical Properties of the Red Cell Membrane in Relation to Molecular Structure and Genetic Defects. *Annu. Rev. Biophys. Biomol. Struct.* **1994**, 23, 787–818.
- (7) Cooper, G. M.; Hausman, R. E. *The Cell: A Molecular Approach 2nd Edition*; Sinauer Associates Inc., 2000.
- (8) Tse, W. T.; Lux, S. E. Red Blood Cell Membrane Disorders. *Br. J. Haematol.* **1999**, 104, 2–13.
- (9) Mohandas, N.; Gallagher, P. G. Red Cell Membrane: Past, Present, and Future. *Blood* **2008**, 112, 3939–3948.
- (10) Toumey, C. Compare and Contrast as Microscopes Get Up Close and Personal. *Nat. Nanotechnol.* **2011**, 6, 191–193.
- (11) Johnson, R. M. Membrane Stress Increases Cation Permeability in Red Cells. *Biophys. J.* **1994**, 67, 1876–1881.

- (12) Yoshida, T.; Shevkoplyas, S. S. Anaerobic Storage of Red Blood Cells. *Blood Transfus.* **2010**, *8*, 220–236.
- (13) Castagnola, M.; Messana, I.; Sanna, M. T.; Giardina, B. Oxygen-Linked Modulation of Erythrocyte Metabolism: State of the Art. *Blood Transfus.* **2010**, *8*, s53–s58.
- (14) Chu, H.; Breite, A.; Ciruolo, P.; Franco, R. S.; Low, P. S. Characterization of the Deoxyhemoglobin Binding Site on Human Erythrocyte Band 3: Implications for O₂ Regulation of Erythrocyte Properties. *Blood* **2008**, *111*, 932–938.
- (15) Campanella, M. E.; Chu, H.; Low, P. S. Assembly and Regulation of a Glycolytic Enzyme Complex on the Human Erythrocyte Membrane. *Proc. Natl. Acad. Sci.* **2005**, *102*, 2402–2407.
- (16) De Rosa, M. C.; Alinovi, C. C.; Galtieri, A.; Russo, A.; Giardina, B. Allosteric Properties of Hemoglobin and the Plasma Membrane of the Erythrocyte: New Insights in Gas Transport and Metabolic Modulation. *IUBMB Life* **2008**, *60*, 87–93.
- (17) Messana, I.; Orlando, M.; Cassiano, L.; Pennacchietti, L.; Zuppi, C.; Castagnola, M.; Giardina, B. Human Erythrocyte Metabolism Is Modulated by the O₂-Linked Transition of Hemoglobin. *FEBS Lett.* **1996**, *390*, 25–28.
- (18) Schrader, M. C.; Eskey, C. J.; Simplaceanu, V.; Ho, C. A Carbon-13 Nuclear Magnetic Resonance Investigation of the Metabolic Fluxes Associated with Glucose Metabolism in Human Erythrocytes. *Biochim. Biophys. Acta* **1993**, *1182*, 162–178.
- (19) Sembulingam, K. *Essentials of Medical Physiology 4th Edition*; Juta Legal and Academic Publishers, 2008.
- (20) Bain, B. J.; Wild, B. J.; Stephens, A. D.; Phelan, L. A. Globin Genes and Haemoglobin. In *Variant Haemoglobins*; Wiley-Blackwell, 2010; pp. 1–8.

- (21) Bettati, S.; Mozzarelli, A. Hemoglobin Reactivity and Regulation. In *Chemistry and Biochemistry of Oxygen Therapeutics*; John Wiley & Sons, Ltd., 2011; pp. 9–22.
- (22) Pittman, R. N. *Regulation of Tissue Oxygenation*; Morgan & Claypool Life Sciences, 2011.
- (23) Weight, L. M.; Byrne, M. J.; Jacobs, P. Hemolytic Effects of Exercise. *Clin. Sci.* **1991**, *81*, 147–152.
- (24) Smith, J. A. Exercise, Training and Red-Blood-Cell Turnover. *Sport. Med.* **1995**, *19*, 9–31.
- (25) Nakayama, Y.; Kinoshita, A.; Tomita, M. Dynamic Simulation of Red Blood Cell Metabolism and Its Application to the Analysis of a Pathological Condition. *Theor. Biol. Med. Model.* **2005**, *2*, 1–11.
- (26) Pratt, D. A.; Tallman, K. A.; Porter, N. A. Free Radical Oxidation of Polyunsaturated Lipids: New Mechanistic Insights and the Development of Peroxyl Radical Clocks. *Acc. Chem. Res.* **2011**, *44*, 458–467.
- (27) Nagababu, E.; Mohanty, J. G.; Bhamidipaty, S.; Ostera, G. R.; Rifkind, J. M. Role of the Membrane in the Formation of Heme Degradation Products in Red Blood Cells. *Life Sci.* **2010**, *86*, 133–138.
- (28) Hess, J. R. Red Cell Changes During Storage. *Transfus. Apher. Sci.* **2010**, *43*, 51–59.
- (29) Marden, M. C.; Griffon, N.; Poyart, C. Oxygen Delivery and Autoxidation of Hemoglobin. *Transfus. Clin. Biol.* **1995**, *2*, 473–480.
- (30) Shikama, K.; Matsuoka, A.; Sugawara, Y. The Molecular Mechanism of Autoxidation for Myoglobin and Hemoglobin. *Seibutsu Butsuri* **2001**, *41*, 74–79.
- (31) Landsteiner, K. Ueber Agglutinationserscheinungen Normalen Menschlichen Blutes. Reprint from: *Wien Klin Wochenschr* (1901) 14/46 : 1132-1134. *Wien. Klin. Wochenschr.* **2001**, *113*, 768–769.

- (32) Robertson, O. H. Transfusion with Preserved Red Blood Cells. *Br. Med. J.* **1918**, *1*, 691–695.
- (33) Wood, C. S. A Short History of Blood Transfusion. *Transfusion* **1967**, *7*, 299–303.
- (34) Pavenski, K.; Saidenberg, E.; Lavoie, M.; Tokessy, M.; Branch, D. R.; Services, B. Red Blood Cell Storage Lesions and Related Transfusion Issues: A Canadian Blood Services Research and Development Symposium. *Transfus. Med. Rev.* **2011**, *26*, 68–84.
- (35) Devine, D. V.; Howe, D. Processing of Whole Blood into Cellular Components and Plasma. *ISBT Sci. Ser.* **2010**, *5*, 78–82.
- (36) D'Alessandro, A.; Liunbruno, G.; Grazzini, G.; Zolla, L. Red Blood Cell Storage: The Story so Far. *Blood Transfus.* **2010**, *8*, 82–88.
- (37) Hess, J. R. An Update on Solutions for Red Cell Storage. *Vox Sang.* **2006**, *91*, 13–19.
- (38) McAteer, M. J.; Dumont, L. J.; Cancelas, J.; Rugg, N.; Vassallo, R.; Whitley, P.; Graminske, S.; Friedman, K. Multi-Institutional Randomized Control Study of Haemolysis in Stored Red Cell Units Prepared Manually or by an Automated System. *Vox Sang.* **2010**, *99*, 34–43.
- (39) Fontaine, M. J.; Chung, Y. T.; Erhun, F.; Goodnough, L. T. Age of Blood as a Limitation for Transfusion: Potential Impact on Blood Inventory and Availability. *Transfusion* **2010**, *50*, 2233–2239.
- (40) Genoe, K.; Cioffi, J. M.; Givisiez, F. N.; Rogerson, M.; Howe, D.; Delage, G.; Sarappa, C.; Charbonneau, Y.; Fu, Y.; Ali, A.; *et al.* Inventory Management. *Vox Sang.* **2010**, *98*, e295–e363.

- (41) van de Watering, L.; Lorinser, J.; Versteegh, M.; Westendord, R.; Brand, A. Effects of Storage Time of Red Blood Cell Transfusions on the Prognosis of Coronary Artery Bypass Graft Patients. *Transfusion* **2006**, *46*, 1712–1718.
- (42) Tinmouth, A.; Fergusson, D.; Yee, I. C.; Hebert, P. C. Clinical Consequences of Red Cell Storage in the Critically Ill. *Transfusion* **2006**, *46*, 2014–2027.
- (43) Zimrin, A. B.; Hess, J. R. Current Issues Relating to the Transfusion of Stored Red Blood Cells. *Vox Sang.* **2009**, *96*, 93–103.
- (44) Liunbruno, G. M.; AuBuchon, J. P. Old Blood, New Blood or Better Stored Blood? *Blood Transfus.* **2010**, *8*, 217–219.
- (45) Dumont, L. J.; AuBuchon, J. P. Evaluation of Proposed FDA Criteria for the Evaluation of Radiolabeled Red Cell Recovery Trials. *Transfusion* **2008**, *48*, 1053–1060.
- (46) Kim-Shapiro, D. B.; Lee, J.; Gladwin, M. T. Storage Lesion: Role of Red Blood Cell Breakdown. *Transfusion* **2011**, *51*, 844–851.
- (47) Kriebardis, A. G.; Antonelou, M. H.; Stamoulis, K. E.; Economou-Petersen, E.; Margaritis, L. H.; Papassideri, I. S. Progressive Oxidation of Cytoskeletal Proteins and Accumulation of Denatured Hemoglobin in Stored Red Cells. *J. Cell. Mol. Med.* **2007**, *11*, 148–155.
- (48) Lion, N.; Crettaz, D.; Rubin, O.; Tissot, J. D. Stored Red Blood Cells: A Changing Universe Waiting for Its Map(s). *J. Proteomics* **2010**, *73*, 374–385.
- (49) Kriebardis, A. G.; Antonelou, M. H.; Stamoulis, K. E.; Economou-Petersen, E.; Margaritis, L. H.; Papassideri, I. S. RBC-Derived Vesicles during Storage: Ultrastructure, Protein Composition, Oxidation, and Signaling Components. *Transfusion* **2008**, *48*, 1943–1953.
- (50) Boas, F. E.; Forman, L.; Beutler, E. Phosphatidylserine Exposure and Red Cell Viability in Red Cell Aging and in Hemolytic Anemia. *Proc. Natl. Acad. Sci.* **1998**, *95*, 3077–3081.

- (51) Sparrow, R. L.; Veale, M. F.; Healey, G.; Payne, K. A. Red Blood Cell (RBC) Age at Collection and Storage Influences RBC Membrane-Associated Carbohydrates and Lectin Binding. *Transfusion* **2007**, *47*, 966–968.
- (52) Dumaswala, U. J.; Zhuo, L.; Mahajan, S.; Nair, P. N.; Shertzer, H. G.; Dibello, P.; Jacobsen, D. W. Glutathione Protects Chemokine-Scavenging and Antioxidative Defense Functions in Human RBCs. *Am. J. Physiol. Cell Physiol.* **2001**, *280*, C867–C873.
- (53) Heaton, W. A.; Holme, S.; Smith, K.; Brecher, M. E.; Pineda, A.; AuBuchon, J. P.; Nelson, E. Effects of 3-5 log₁₀ Pre-Storage Leucocyte Depletion on Red Cell Storage and Metabolism. *Br. J. Haematol.* **1994**, *87*, 363–368.
- (54) Riedner, C.; Heim, M. U.; Mempel, W.; Wilmanns, W. Possibility to Improve Preservation of Whole Blood by Leukocyte-Depletion before Storage. *Vox Sang.* **1990**, *59*, 78–82.
- (55) Tuvia, S.; Levin, S.; Bitler, A.; Korenstein, R. Mechanical Fluctuations of the Membrane Skeleton Are Dependent on F-Actin ATPase in Human Erythrocytes. *J. Cell Biol.* **1998**, *141*, 1551–1561.
- (56) Park, Y.; Best, C. A.; Auth, T.; Gov, N. S.; Safran, S. A.; Popescu, G.; Suresh, S.; Feld, M. S. Metabolic Remodeling of the Human Red Blood Cell Membrane. *Proc. Natl. Acad. Sci.* **2010**, *107*, 1289–1294.
- (57) Lutz, H. U.; Liu, S. C.; Palek, J. Release of Spectrin-Free Vesicles from Human Erythrocytes during ATP Depletion. I. Characterization of Spectrin-Free Vesicles. *J. Cell Biol.* **1977**, *73*, 548–560.
- (58) Salzer, U.; Hinterdorfer, P.; Hunger, U.; Borken, C.; Prohaska, R. Ca(++)-Dependent Vesicle Release from Erythrocytes Involves Stomatin-Specific Lipid Rafts, Synexin (Annexin VII), and Sorcin. *Blood* **2002**, *99*, 2569–2577.

- (59) Sens, P.; Gov, N. Force Balance and Membrane Shedding at the Red-Blood-Cell Surface. *Phys. Rev. Lett.* **2007**, *98*, 1–4.
- (60) Werre, J. M.; Willekens, F. L.; Bosch, F. H.; de Haans, L. D.; van der Vegt, S. G.; van den Bos, A. G.; Bosman, G. J. The Red Cell Revisited--Matters of Life and Death. *Cell. Mol. Biol.* **2004**, *50*, 139–145.
- (61) Sutura, S. P.; Gardner, R. A.; Boylan, C. W.; Carroll, G. L.; Chang, K. C.; Marvel, J. S.; Kilo, C.; Gonen, B.; Williamson, J. R. Age-Related Changes in Deformability of Human Erythrocytes. *Blood* **1985**, *65*, 275–282.
- (62) Liu, F.; Mizukami, H.; Sarnaik, S.; Ostafin, A. Calcium-Dependent Human Erythrocyte Cytoskeleton Stability Analysis through Atomic Force Microscopy. *J. Struct. Biol.* **2005**, *150*, 200–210.
- (63) D'Alessandro, A.; Gevi, F.; Zolla, L. Red Blood Cell Metabolism under Prolonged Anaerobic Storage. *Mol. Biosyst.* **2013**, *9*, 1196–1209.
- (64) Bessis, M. *Blood Smears Reinterpreted*; Springer Berlin Heidelberg, 1977.
- (65) Klein, H. G. Red-Cell Transfusion in Clinical Practice. In *Chemistry and Biochemistry of Oxygen Therapeutics*; John Wiley & Sons, Ltd, 2011; pp. 213–220.
- (66) Flegel, W. A.; Natanson, C.; Klein, H. G. Does Prolonged Storage of Red Blood Cells Cause Harm? *Br. J. Haematol.* **2014**, *165*, 3–16.
- (67) Triulzi, D. J.; Yazer, M. H. Clinical Studies of the Effect of Blood Storage on Patient Outcomes. *Transfus. Apher. Sci.* **2010**, *43*, 95–106.
- (68) Steiner, M. E.; Stowell, C. Does Red Blood Cell Storage Affect Clinical Outcome? When in Doubt, Do the Experiment. *Transfusion* **2009**, *49*, 1286–1290.

- (69) Isbister, J. P.; Shander, A.; Spahn, D. R.; Erhard, J.; Farmer, S. L.; Hofmann, A. Adverse Blood Transfusion Outcomes: Establishing Causation. *Transfus. Med. Rev.* **2011**, *25*, 89–101.
- (70) Istaphanous, G. K.; Wheeler, D. S.; Lisco, S. J.; Shander, A. Red Blood Cell Transfusion in Critically Ill Children: A Narrative Review. *Pediatr. Crit. Care Med.* **2011**, *12*, 174–183.
- (71) Koch, C. G.; Li, L.; Sessler, D. I.; Figueroa, P.; Hoeltge, G. A.; Mihaljevic, T.; Blackstone, E. H. Duration of Red-Cell Storage and Complications after Cardiac Surgery. *N. Engl. J. Med.* **2008**, *358*, 1229–1239.
- (72) Yap, C. H.; Lau, L.; Krishnaswamy, M.; Gaskell, M.; Yui, M. Age of Transfused Red Cells and Early Outcomes after Cardiac Surgery. *Ann. Thorac. Surg.* **2008**, *86*, 554–559.
- (73) Leal-Noval, S. R.; Munoz-Gomez, M.; Arellano-Orden, V.; Marin-Caballos, A.; Amaya-Villar, R.; Marin, A.; Puppo-Moreno, A.; Ferrandiz-Millon, C.; Flores-Cordero, J. M.; Murillo-Cabezas, F. Impact of Age of Transfused Blood on Cerebral Oxygenation in Male Patients with Severe Traumatic Brain Injury. *Crit. Care Med.* **2008**, *36*, 1290–1296.
- (74) Edna, T. H.; Bjerkeset, T. Association between Transfusion of Stored Blood and Infective Bacterial Complications after Resection for Colorectal Cancer. *Eur. J. Surg.* **1998**, *164*, 449–456.
- (75) Chen, D.; Serrano, K.; Devine, D. V. Introducing the Red Cell Storage Lesion. *ISBT Sci. Ser.* **2016**, *11*, 26–33.
- (76) van de Watering, L. Red Cell Storage and Prognosis. *Vox Sang.* **2011**, *100*, 36–45.
- (77) van de Watering, L. Pitfalls in the Current Published Observational Literature on the Effects of Red Blood Cell Storage. *Transfusion* **2011**, *51*, 1847–1854.

- (78) Spinella, P. C.; Doctor, A.; Blumberg, N.; Holcomb, J. B. Does the Storage Duration of Blood Products Affect Outcomes in Critically Ill Patients? *Transfusion* **2011**, *51*, 1644–1650.
- (79) Lacroix, J.; Hébert, P. C.; Fergusson, D. A.; Tinmouth, A.; Cook, D. J.; Marshall, J. C.; Clayton, L.; McIntyre, L.; Callum, J.; Turgeon, A. F.; *et al.* Age of Transfused Blood in Critically Ill Adults. *N. Engl. J. Med.* **2015**, *372*, 1410–1418.
- (80) Fergusson, D. A.; Hébert, P.; Hogan, D. L.; LeBel, L.; Rouvinez-Bouali, N.; Smyth, J. A.; Sankaran, K.; Tinmouth, A.; Blajchman, M. A.; Kovacs, L.; *et al.* Effect of Fresh Red Blood Cell Transfusions on Clinical Outcomes in Premature, Very Low-Birth-Weight Infants: The ARIPI Randomized Trial. *J. Am. Med. Assoc.* **2012**, *308*, 1443–1451.
- (81) Steiner, M. E.; Ness, P. M.; Assmann, S. F.; Triulzi, D. J.; Sloan, S. R.; Delaney, M.; Granger, S.; Bennett-Guerrero, E.; Blajchman, M. A.; Scavo, V.; *et al.* Effects of Red-Cell Storage Duration on Patients Undergoing Cardiac Surgery. *N. Engl. J. Med.* **2015**, *372*, 1419–1429.
- (82) Bennett-Guerrero, E.; Veldman, T. H.; Doctor, A.; Telen, M. J.; Ortel, T. L.; Reid, T. S.; Mulherin, M. A.; Zhu, H. M.; Buck, R. D.; Califf, R. M.; *et al.* Evolution of Adverse Changes in Stored RBCs. *Proc. Natl. Acad. Sci.* **2007**, *104*, 17063–17068.
- (83) Hess, J. R. Measures of Stored Red Blood Cell Quality. *Vox Sang.* **2014**, *107*, 1–9.
- (84) Alter, H. J.; Klein, H. G. The Hazards of Blood Transfusion in Historical Perspective. *Blood* **2008**, *112*, 2617–2626.
- (85) Shander, A.; Hofmann, A.; Ozawa, S.; Theusinger, O. M.; Gombotz, H.; Spahn, D. R. Activity-Based Costs of Blood Transfusions in Surgical Patients at Four Hospitals. *Transfusion* **2010**, *50*, 753–765.

- (86) Hess, J. R.; Grazzini, G. Transfusion: Political, Administrative and Logistic Issues. In *Chemistry and Biochemistry of Oxygen Therapeutics*; John Wiley & Sons, Ltd, 2011; pp. 193–204.
- (87) Tarasev, M.; Alfano, K.; Chakraborty, S.; Light, L.; Doeden, K.; Gorlin, J. B. Similar Donors-Similar Blood? *Transfusion* **2014**, *54*, 933–941.
- (88) Smith, E.; Dent, G. The Theory of Raman Spectroscopy. In *Modern Raman Spectroscopy – A Practical Approach*; John Wiley & Sons, Ltd, 2004; pp. 71–92.
- (89) Raman, C. V.; Krishnan, K. S. A New Type of Secondary Radiation. *Nature* **1928**, *121*, 501–502.
- (90) Raman, C. V. A New Radiation. *Indian J. Phys* **1928**, *2*, 387–398.
- (91) Grasselli, J. G.; Bulkin, B. J. *Analytical Raman Spectroscopy*; John Wiley & Sons, Ltd: New York, NY, USA, 1991.
- (92) McCreery, R. L. Introduction and Scope. In *Raman Spectroscopy for Chemical Analysis*; John Wiley & Sons, Inc., 2000; pp. 1–14.
- (93) Vandenabeele, P. Theoretical Aspects. In *Practical Raman Spectroscopy – An Introduction*; John Wiley & Sons, Ltd, 2013; pp. 1–38.
- (94) Long, D. A. *The Raman Effect: A Unified Treatment of the Theory of Raman Scattering by Molecules*; John Wiley & Sons, Ltd: West Sussex, England, 2002.
- (95) Tu, A. T. *Raman Spectroscopy in Biology: Principles and Applications*; John Wiley & Sons, Ltd., 1982.
- (96) Lewis, I. R.; Edwards, H. *Handbook of Raman Spectroscopy: From the Research Laboratory to the Process Line*; CRC Press, 2001.

- (97) Vandenabeele, P. Raman Instrumentation. In *Practical Raman Spectroscopy – An Introduction*; John Wiley & Sons, Ltd, 2013; pp. 61–100.
- (98) Vandenabeele, P. Interferences and Side-Effects. In *Practical Raman Spectroscopy – An Introduction*; John Wiley & Sons, Ltd, 2013; pp. 39–45.
- (99) Missov, E.; Calzolari, C.; Pau, B. Circulating Cardiac Troponin I in Severe Congestive Heart Failure. *Circulation* **1997**, *96*, 2953–2958.
- (100) Petry, R.; Schmitt, M.; Popp, J. Raman Spectroscopy - A Prospective Tool in the Life Sciences. *ChemPhysChem* **2003**, *4*, 14–30.
- (101) Efremov, E. V.; Ariese, F.; Gooijer, C. Achievements in Resonance Raman Spectroscopy. Review of a Technique with a Distinct Analytical Chemistry Potential. *Anal. Chim. Acta* **2008**, *606*, 119–134.
- (102) Fleischmann, M.; Hendra, P. J.; McQuillan, A. J. Raman Spectra of Pyridine Adsorbed at a Silver Electrode. *Chem. Phys. Lett.* **1974**, *26*, 163–166.
- (103) Jeanmaire, D. L.; Van Duyne, R. P. Surface Raman Spectroelectrochemistry: Part I. Heterocyclic, Aromatic, and Aliphatic Amines Adsorbed on the Anodized Silver Electrode. *J. Electroanal. Chem. Interfacial Electrochem.* **1977**, *84*, 1–20.
- (104) Schlücker, S. Surface-Enhanced Raman Spectroscopy: Concepts and Chemical Applications. *Angew. Chemie - Int. Ed.* **2014**, *53*, 4756–4795.
- (105) Langelüddecke, L.; Singh, P.; Deckert, V. Exploring the Nanoscale: Fifteen Years of Tip-Enhanced Raman Spectroscopy. *Appl. Spectrosc.* **2015**, *69*, 1357–1371.
- (106) Stone, N.; Kerssens, M.; Lloyd, G. R.; Faulds, K.; Graham, D.; Matousek, P. Surface Enhanced Spatially Offset Raman Spectroscopic (SESORS) Imaging – the next Dimension. *Chem. Sci.* **2011**, *2*, 776–780.

- (107) Parker, F. S. Biochemical Applications of Infrared and Raman Spectroscopy. *Appl. Spectrosc.* **1975**, 29, 129–148.
- (108) Strekas, T. C.; Spiro, T. G. Hemoglobin: Resonance Raman Spectra. *Biochim. Biophys. Acta - Protein Struct.* **1972**, 263, 830–833.
- (109) Brunner, H.; Sussner, H.; Mayer, A. Resonance Raman Scattering on the Haem Group of Oxy- and Deoxyhaemoglobin. *J. Mol. Biol.* **1972**, 70, 153–156.
- (110) Spiro, T. G.; Strekas, T. C. Resonance Raman Spectra of Hemoglobin and Cytochrome c: Inverse Polarization and Vibronic Scattering. *Proc. Natl. Acad. Sci.* **1972**, 69, 2622–2626.
- (111) Brunner, H.; Sussner, H. Resonance Raman Scattering on Haemoglobin. *Biochim. Biophys. Acta* **1973**, 310, 20–31.
- (112) Brunner, H. Identification of the Iron-Ligand Vibration of Oxyhemoglobin. *Naturwissenschaften* **1974**, 61, 129.
- (113) Yamamoto, T.; Palmer, G.; Gill, D.; Salmeen, I. T.; Rimai, L. The Valence and Spin State of Iron in Oxyhemoglobin as Inferred from Resonance Raman Spectroscopy. *J. Biol. Chem.* **1973**, 248, 5211–5213.
- (114) Spiro, T. G.; Strekas, T. C. Resonance Raman Spectra of Heme Proteins. Effects of Oxidation and Spin State. *J. Am. Chem. Soc.* **1974**, 96, 338–345.
- (115) Woodruff, W. H.; Spiro, T. G. A Circulating Sample Cell for Temperature Control in Resonance Raman Spectroscopy. *Appl. Spectrosc.* **1974**, 28, 74–75.
- (116) Walters, M. A.; Spiro, T. G.; Suslick, K. S.; Collman, J. P. Resonance Raman Spectra of (Dioxygen)(porphyrinato)(hindered imidazole)iron(II) Complexes: Implications for Hemoglobin Cooperativity. *J. Am. Chem. Soc.* **1980**, 6857–6858.

- (117) Walters, M. A.; Spiro, T. G. Resonance Raman Spectroscopic Studies of Axial Ligation in Oxyhemoglobin, Oxymyoglobin, and Nitrosylmyoglobin. *Biochemistry* **1982**, *21*, 6989–6995.
- (118) Tsubaki, M.; Nagai, K.; Kitagawa, T. Resonance Raman Spectra of Myoglobins Reconstituted with Spirographis and Isospirographis Hemes and Iron 2,4-Diformylprotoporphyrin IX. Effect of Formyl Substitution at the Heme Periphery. *Biochemistry* **1980**, *19*, 379–385.
- (119) Nagai, K.; Kitagawa, T.; Morimoto, H. Quaternary Structures and Low Frequency Molecular Vibrations of Haems of Deoxy and Oxyhaemoglobin Studied by Resonance Raman Scattering. *J. Mol. Biol.* **1980**, *136*, 271–289.
- (120) Freier, S. M.; Duff, L. L.; Shriver, D. F.; Klotz, I. M. Resonance Raman Spectroscopy of Iron-Oxygen Vibrations in Hemerythrin. *Arch. Biochem. Biophys.* **1980**, *205*, 449–463.
- (121) Irwin, M. J.; Atkinson, G. H. Low-Frequency Resonance Raman Spectroscopy of the Deoxyhaemoglobin Transient of Photolysed Carboxyhaemoglobin. *Nature* **1981**, *293*, 317–318.
- (122) Armstrong, R. S.; Irwin, M. J.; Wright, P. E. Soret-Excited Resonance Raman Spectrum of (Carbon Monoxy)leghemoglobin: Assignment of Fe-CO Stretch. *J. Am. Chem. Soc.* **1982**, *104*, 626–627.
- (123) Spiro, T. G.; Turner, J. Structure and Dynamics in the Photolysis of CO- and O₂-Hemoglobin, Monitored by Time-Resolved Resonance Raman Spectroscopy. In *Time-Resolved Vibrational Spectroscopy*; Atkinson, G. H., Ed.; Academic Press, Inc.: New York, New York, USA, 1983; pp. 297–306.

- (124) Smulevich, G.; Spiro, T. G. Surface Enhanced Raman Spectroscopic Evidence That Adsorption on Silver Particles Can Denature Heme Proteins. *J. Phys. Chem.* **1985**, *89*, 5168–5173.
- (125) de Groot, J.; Hester, R. E. Surface-Enhanced Resonance Raman Spectroscopy of Oxyhemoglobin Adsorbed onto Colloidal Silver. *J. Phys. Chem.* **1987**, *91*, 1693–1696.
- (126) de Groot, J.; Hester, R. E.; Kaminaka, S.; Kitagawa, T. Functional Activity of Hemoglobins Adsorbed on Colloidal Silver: A Surface-Enhanced Resonance Raman Spectroscopy Study. *J. Phys. Chem.* **1988**, *92*, 2044–2048.
- (127) Su, C.; Park, Y. D.; Liu, G. Y.; Spiro, T. G. Hemoglobin Quaternary Structure Change Monitored Directly by Transient UV Resonance Raman Spectroscopy. *J. Am. Chem. Soc.* **1989**, *111*, 3457–3459.
- (128) Ozaki, Y.; Mizuno, A.; Sato, H.; Kawauchi, K.; Muraishi, S. Biomedical Application of Near-Infrared Fourier Transform Raman Spectroscopy. Part I: The 1064-Nm Excited Raman Spectra of Blood and Met Hemoglobin. *Appl. Spectrosc.* **1992**, *46*, 533–536.
- (129) Wang, D. J.; Spiro, T. G. Structure Changes in Hemoglobin upon Deletion of C-Terminal Residues, Monitored by Resonance Raman Spectroscopy. *Biochemistry* **1998**, *37*, 9940–9951.
- (130) Jin, Y.; Nagai, M.; Nagai, Y.; Nagatomo, S.; Kitagawa, T. Heme Structures of Five Variants of Hemoglobin M Probed by Resonance Raman Spectroscopy. *Biochemistry* **2004**, *43*, 8517–8527.
- (131) Rinia, H. A.; Bonn, M.; Vartiainen, E. M.; Schaffer, C. B.; Müller, M. Spectroscopic Analysis of the Oxygenation State of Hemoglobin Using Coherent Anti-Stokes Raman Scattering. *J. Biomed. Opt.* **2006**, *11*, 50502.

- (132) Xu, H. X.; Bjerneld, E. J.; Käll, M.; Börjesson, L. Spectroscopy of Single Hemoglobin Molecules by Surface Enhanced Raman Scattering. *Phys. Rev. Lett.* **1999**, *83*, 4357–4360.
- (133) Wood, B. R.; Tait, B.; McNaughton, D. Micro-Raman Characterisation of the R to T State Transition of Haemoglobin within a Single Living Erythrocyte. *Biochim. Biophys. Acta-Molecular Cell Res.* **2001**, *1539*, 58–70.
- (134) Wood, B. R.; McNaughton, D. Resonant Raman Studies on Functional Erythrocytes. In *New Developments in Sickle Cell Disease Research*; O'Malley, P. D., Ed.; Nova Publishers, 2006; pp. 63–119.
- (135) Wood, B. R.; Caspers, P.; Puppels, G. J.; Pandiancherri, S.; McNaughton, D. Resonance Raman Spectroscopy of Red Blood Cells Using near-Infrared Laser Excitation. *Anal. Bioanal. Chem.* **2007**, *387*, 1691–1703.
- (136) Wood, B. R.; McNaughton, D. Micro-Raman Characterization of High- and Low-Spin Heme Moieties within Single Living Erythrocytes. *Biopolymers* **2002**, *67*, 259–262.
- (137) Ramser, K.; Bjerneld, E. J.; Fant, C.; Käll, M. Raman Imaging and Spectroscopy of Single Functional Erythrocytes: A Feasibility Study. *Proc. SPIE - Biomed. Vib. Spectrosc. II* **2002**, *4614*, 20–27.
- (138) Ramser, K.; Bjerneld, E. J.; Fant, C.; Käll, M. Importance of Substrate and Photo-Induced Effects in Raman Spectroscopy of Single Functional Erythrocytes. *J. Biomed. Opt.* **2003**, *8*, 173–178.
- (139) Wood, B. R.; Hammer, L.; McNaughton, D. Resonance Raman Spectroscopy Provides Evidence of Heme Ordering within the Functional Erythrocyte. *Vib. Spectrosc.* **2005**, *38*, 71–78.

- (140) Wood, B. R.; Hammer, L.; Davis, L.; McNaughton, D. Raman Microspectroscopy and Imaging Provides Insights into Heme Aggregation and Denaturation within Human Erythrocytes. *J. Biomed. Opt.* **2005**, *10*, 014005–014013.
- (141) Asghari-Khiavi, M.; Mechler, A.; Bambery, K. R.; McNaughton, D.; Wood, B. R. A Resonance Raman Spectroscopic Investigation into the Effects of Fixation and Dehydration on Heme Environment of Hemoglobin. *J. Raman Spectrosc.* **2009**, *40*, 1668–1674.
- (142) Asghari-Khiavi, M.; Wood, B. R.; Mechler, A.; Bambery, K. R.; Buckingham, D. W.; Cooke, B. M.; McNaughton, D. Correlation of Atomic Force Microscopy and Raman Micro-Spectroscopy to Study the Effects of Ex Vivo Treatment Procedures on Human Red Blood Cells. *Analyst* **2010**, *135*, 525–530.
- (143) Wood, B. R.; Asghari-Khiavi, M.; Bailo, E.; McNaughton, D.; Deckert, V. Detection of Nano-Oxidation Sites on the Surface of Hemoglobin Crystals Using Tip-Enhanced Raman Scattering. *Nano Lett.* **2012**, *12*, 1555–1560.
- (144) Wood, B. R.; McNaughton, D. Raman Excitation Wavelength Investigation of Single Red Blood Cells in Vivo. *J. Raman Spectrosc.* **2002**, *33*, 517–523.
- (145) Brazhe, N. A.; Abdali, S.; Brazhe, A. R.; Luneva, O. G.; Bryzgalova, N. Y.; Parshina, E. Y.; Sosnovtseva, O. V; Maksimov, G. V. New Insight into Erythrocyte through In Vivo Surface-Enhanced Raman Spectroscopy. *Biophys. J.* **2009**, *97*, 3206–3214.
- (146) Premasiri, W. R.; Lee, J. C.; Ziegler, L. D. Surface-Enhanced Raman Scattering of Whole Human Blood, Blood Plasma, and Red Blood Cells: Cellular Processes and Bioanalytical Sensing. *J. Phys. Chem. B* **2012**, *116*, 9376–9386.

- (147) Drescher, D.; Büchner, T.; McNaughton, D.; Kneipp, J. SERS Reveals the Specific Interaction of Silver and Gold Nanoparticles with Hemoglobin and Red Blood Cell Components. *Phys. Chem. Chem. Phys.* **2013**, *15*, 5364–5373.
- (148) Marzec, K. M.; Perez-Guaita, D.; de Veij, M.; McNaughton, D.; Baranska, M.; Dixon, M. W. A.; Tilley, L.; Wood, B. R. Red Blood Cells Polarize Green Laser Light Revealing Hemoglobin's Enhanced Non-Fundamental Raman Modes. *ChemPhysChem* **2014**, *15*, 3963–3968.
- (149) Marzec, K. M.; Rygula, A.; Wood, B. R.; Chlopicki, S.; Baranska, M. High-Resolution Raman Imaging Reveals Spatial Location of Heme Oxidation Sites in Single Red Blood Cells of Dried Smears. *J. Raman Spectrosc.* **2015**, *46*, 76–83.
- (150) Xie, C. G.; Dinno, M. A.; Li, Y. Q. Near-Infrared Raman Spectroscopy of Single Optically Trapped Biological Cells. *Opt. Lett.* **2002**, *27*, 249–251.
- (151) Xie, C.; Li, Y. Q. Confocal Micro-Raman Spectroscopy of Single Biological Cells Using Optical Trapping and Shifted Excitation Difference Techniques. *J. Appl. Phys.* **2003**, *93*, 2982–2986.
- (152) Ramser, K.; Logg, K.; Goksör, M.; Enger, J.; Käll, M.; Hanstorp, D. Resonance Raman Spectroscopy of Optically Trapped Functional Erythrocytes. *J. Biomed. Opt.* **2004**, *9*, 593–600.
- (153) Cojoc, D.; Ferrari, E.; Garbin, V.; Di Fabrizio, E. Multiple Optical Tweezers for Micro Raman Spectroscopy. *Proc. SPIE - Opt. Trapp. Opt. Micromanipulation II* **2005**, *5930*, 64–74.

- (154) Dasgupta, R.; Ahlawat, S.; Verma, R. S.; Uppal, A.; Gupta, P. K. Hemoglobin Degradation in Human Erythrocytes with Long-Duration near-Infrared Laser Exposure in Raman Optical Tweezers. *J. Biomed. Opt.* **2010**, *15*, 55009–55011.
- (155) Ahlawat, S.; Chowdhury, A.; Kumar, N.; Uppal, A.; Verma, R. S.; Gupta, P. K. Polarized Raman Spectroscopic Investigations on Hemoglobin Ordering in Red Blood Cells. *J. Biomed. Opt.* **2014**, *19*, 87002.
- (156) Rao, S.; Bálint, S.; Cossins, B.; Guallar, V.; Petrov, D. Raman Study of Mechanically Induced Oxygenation State Transition of Red Blood Cells Using Optical Tweezers. *Biophys. J.* **2009**, *96*, 209–216.
- (157) Rao, S.; Bálint, Š.; del Carmen Frias, L.; Petrov, D. Polarization Raman Study of Protein Ordering by Controllable RBC Deformation. *J. Raman Spectrosc.* **2009**, *40*, 1257–1261.
- (158) Rusciano, G. Experimental Analysis of Hb Oxy-Deoxy Transition in Single Optically Stretched Red Blood Cells. *Phys. Medica* **2010**, *26*, 233–239.
- (159) Ramser, K.; Enger, J.; Goksor, M.; Hanstorp, D.; Logg, K.; Kall, M.; Goksör, M.; Hanstorp, D.; Logg, K.; Käll, M. A Microfluidic System Enabling Raman Measurements of the Oxygenation Cycle in Single Optically Trapped Red Blood Cells. *Lab Chip* **2005**, *5*, 431–436.
- (160) Ahlawat, S.; Kumar, N.; Dasgupta, R.; Verma, R. S.; Uppal, A.; Gupta, P. K.; Ahlawat, S.; Kumar, N.; Dasgupta, R.; Verma, R. S.; *et al.* Raman Spectroscopic Investigations on Optical Trap Induced Deoxygenation of Red Blood Cells. *Appl. Phys. Lett.* **2013**, *103*, 183704.

- (161) Ahlawat, S.; Kumar, N.; Uppal, A.; Kumar Gupta, P. Visible Raman Excitation Laser Induced Power and Exposure Dependent Effects in Red Blood Cells. *J. Biophotonics* **2016**, doi: 10.1002/jbio.201500325.
- (162) Deng, J. L.; Wei, Q.; Zhang, M. H.; Wang, Y. Z.; Li, Y. Q. Study of the Effect of Alcohol on Single Human Red Blood Cells Using near-Infrared Laser Tweezers Raman Spectroscopy. *J. Raman Spectrosc.* **2005**, *36*, 257–261.
- (163) Yue, L.; Wang, G.; Fang, L.; Yao, H.; Yuan, Z.; Mo, H. Study of Raman spectroscopy of Optically Trapped Human Red Blood Cell Affected by Direct Current. *Sheng Wu Yi Xue Gong Cheng Xue Za Zhi* **2007**, *24*, 404–408.
- (164) Zachariah, E.; Bankapur, A.; Santhosh, C.; Valiathan, M.; Mathur, D. Probing Oxidative Stress in Single Erythrocytes with Raman Tweezers. *J. Photochem. Photobiol. B* **2010**, *100*, 113–116.
- (165) Wu, Y.; Huang, Y.-X.; Kang, L.-L.; Wu, Z.-J.; Luo, M. Effect of pH on Molecular Constitution and Distribution of Hemoglobin in Living Erythrocyte. *Biopolymers* **2010**, *93*, 348–354.
- (166) Ramser, K.; Wenseleers, W.; Dewilde, S.; Van Doorslaer, S.; Moens, L. The Combination of Resonance Raman Spectroscopy, Optical Tweezers and Microfluidic Systems Applied to the Study of Various Heme-Containing Single Cells. *Spectroscopy* **2008**, *22*, 287–295.
- (167) Liu, R.; Zheng, L.; Matthews, D. L.; Satake, N.; Chan, J. W. Power Dependent Oxygenation State Transition of Red Blood Cells in a Single Beam Optical Trap. *Appl. Phys. Lett.* **2011**, *99*, 43702.

- (168) Chan, J. W.; Liu, R.; Matthews, D. L. Application of Laser Tweezers Raman Spectroscopy Techniques to the Monitoring of Single Cell Response to Stimuli. *Proc. SPIE - Biophotonics Photonic Solut. Better Heal. Care III* **2012**, 8427, 84270M.
- (169) Liu, R.; Mao, Z.; Matthews, D. L.; Li, C.-S.; Chan, J. W.; Satake, N. Novel Single-Cell Functional Analysis of Red Blood Cells Using Laser Tweezers Raman Spectroscopy: Application for Sick Cell Disease. *Exp. Hematol.* **2013**, 41, 656–661.e1.
- (170) Bulkin, B. J. Raman Spectroscopic Study of Human Erythrocyte Membranes. *Biochim. Biophys. Acta - Biomembr.* **1972**, 274, 649–651.
- (171) Lippert, J. L.; Gorczyca, L. E.; Meiklejohn, G. A Laser Raman Spectroscopic Investigation of Phospholipid and Protein Configurations in Hemoglobin-Free Erythrocyte Ghosts. *Biochim. Biophys. Acta* **1975**, 382, 51–57.
- (172) Wallach, D. F. H.; Verma, S. P. Raman and Resonance-Raman Scattering by Erythrocyte Ghosts. *Biochim. Biophys. Acta - Biomembr.* **1975**, 382, 542–551.
- (173) Verma, S. P.; Hoelzl Wallach, D. F. Carotenoids as Raman-Active Probes of Erythrocyte Membrane Structure. *Biochim. Biophys. Acta - Biomembr.* **1975**, 401, 168–176.
- (174) Mikkelsen, R. B.; Verma, S. P.; Wallach, D. F. H. Effect of Transmembrane Ion Gradients on Raman Spectra of Sealed, Hemoglobin-Free Erythrocyte Membrane Vesicles. *Proc. Natl. Acad. Sci.* **1978**, 75, 5478–5482.
- (175) Verma, S. P.; Wallach, D. F. H. Multiple Thermotropic State Transitions in Erythrocyte Membranes - A Laser Study of the CH-Stretching and Acoustical Regions. *Biochim. Biophys. Acta* **1976**, 436, 307–318.

- (176) Verma, S. P.; Wallach, D. F. Erythrocyte Membranes Undergo Cooperative, pH-Sensitive State Transitions in the Physiological Temperature Range: Evidence from Raman Spectroscopy. *Proc. Natl. Acad. Sci.* **1976**, *73*, 3558–3561.
- (177) Milanovich, F. P.; Shore, B.; Harney, R. C.; Tu, A. T. Raman Spectroscopic Analysis of Dutch Belt Rabbit Erythrocyte Ghosts. *Chem. Phys. Lipids* **1976**, *17*, 79–84.
- (178) Goheen, S. C.; Gilman, T. H.; Kauffman, J. W.; Garvin, J. E. The Effect on Raman Spectra of Extraction of Peripheral Proteins from Human Erythrocyte Membranes. *Biochem. Biophys. Res. Commun.* **1977**, *79*, 805–814.
- (179) Goheen, S. C. Study of Intact and Modified Erythrocyte Membranes with Laser Raman Spectroscopy. *J. Raman Spectrosc.* **1993**, *24*, 599–602.
- (180) Goheen, S. C.; Kauffman, J. W. Compositional Dependence of Spectral Features in the Raman Spectra of Erythrocyte Membranes. *J. Raman Spectrosc.* **1993**, *24*, 275–279.
- (181) Li, N.; Li, S. X.; Guo, Z. Y.; Zhuang, Z. F.; Li, R.; Xiong, K.; Chen, S. J.; Liu, S. H. Micro-Raman Spectroscopy Study of the Effect of Mid-Ultraviolet Radiation on Erythrocyte Membrane. *J. Photochem. Photobiol. B.* **2012**, *112*, 37–42.
- (182) Kang, L. L.; Huang, Y. X.; Liu, W. J.; Zheng, X. J.; Wu, Z. J.; Luo, M. Confocal Raman Microscopy on Single Living Young and Old Erythrocytes. *Biopolymers* **2008**, *89*, 951–959.
- (183) Huang, Y. X.; Wu, Z. J.; Mehrishi, J.; Huang, B. T.; Chen, X. Y.; Zheng, X. J.; Liu, W. J.; Luo, M. Human Red Blood Cell Aging: Correlative Changes in Surface Charge and Cell Properties. *J. Cell. Mol. Med.* **2011**, *15*, 2634–2642.

- (184) Weselucha-Birczyńska, A.; Kozicki, M.; Czepiel, J.; Łabanowska, M.; Nowak, P.; Kowalczyk, G.; Kurdziel, M.; Birczyńska, M.; Biesiada, G. G.; Mach, T.; *et al.* Human Erythrocytes Analyzed by Generalized 2D Raman Correlation Spectroscopy. *J. Mol. Struct.* **2014**, *1069*, 305–312.
- (185) Breimard, C.; Girerd, J. J.; Kowalewski, P.; Merlin, J. C.; Moreaut, S. Spectroscopic Investigations of Malaria Pigment. *Appl. Spectrosc.* **1993**, *47*, 1837–1842.
- (186) Ong, C. W.; Shen, Z. X.; Ang, K. K. H.; Kara, U. A. K.; Tang, S. H. Resonance Raman Microspectroscopy of Normal Erythrocytes and Plasmodium Berghei -Infected Erythrocytes. *Appl. Spectrosc.* **1999**, *53*, 1097–1101.
- (187) Ong, C. W.; Shen, Z. X.; Ang, K. K. H.; Kara, U. A. K.; Tang, S. H. Raman Microspectroscopy of Normal Erythrocytes and Plasmodium Berghei-Infected Erythrocytes. *Appl. Spectrosc.* **2002**, *56*, 1126–1131.
- (188) Wood, B. R.; McNaughton, D. Raman Excitation Wavelength Investigation of Single Red Blood Cells in Vivo. *J. Raman Spectrosc.* **2002**, *33*, 517–523.
- (189) Wood, B. R.; Langford, S. J.; Cooke, B. M.; Glenister, F. K.; Lim, J.; McNaughton, D. Raman Imaging of Hemozoin within the Food Vacuole of Plasmodium Falciparum Trophozoites. *FEBS Lett.* **2003**, *554*, 247–252.
- (190) Wood, B. R.; Langford, S. J.; Cooke, B. M.; Lim, J.; Glenister, F. K.; Duriska, M.; Unthank, J. K.; McNaughton, D. Resonance Raman Spectroscopy Reveals New Insight into the Electronic Structure of Beta-Hematin and Malaria Pigment. *J. Am. Chem. Soc.* **2004**, *126*, 9233–9239.

- (191) Puskar, L.; Tuckermann, R.; Frosch, T.; Popp, J.; Ly, V.; McNaughton, D.; Wood, B. R. Raman Acoustic Levitation Spectroscopy of Red Blood Cells and Plasmodium Falciparum Trophozoites. *Lab Chip* **2007**, *7*, 1125–1131.
- (192) Ge, R.; Winter, C.; Rösch, P.; Schmitt, M.; Petry, R.; Kiefer, W.; Lankers, M.; Popp, J. Identification of Biotic and Abiotic Particles by Using a Combination of Optical Tweezers and In Situ Raman Spectroscopy. *ChemPhysChem* **2004**, *5*, 1159–1170.
- (193) Frosch, T.; Koncarevic, S.; Becker, K.; Popp, J. Morphology-Sensitive Raman Modes of the Malaria Pigment Hemozoin. *Analyst* **2009**, *134*, 1126–1132.
- (194) Brückner, M.; Becker, K.; Popp, J.; Frosch, T. Fiber Array Based Hyperspectral Raman Imaging for Chemical Selective Analysis of Malaria-Infected Red Blood Cells. *Anal. Chim. Acta* **2015**, *894*, 76–84.
- (195) Wood, B. R.; Hermelink, A.; Lasch, P.; Bambery, K. R.; Webster, G. T.; Khiavi, M. A.; Cooke, B. M.; Deed, S.; Naumann, D.; McNaughton, D. Resonance Raman Microscopy in Combination with Partial Dark-Field Microscopy Lights up a New Path in Malaria Diagnostics. *Analyst* **2009**, *134*, 1119–1125.
- (196) Bonifacio, A.; Finaurini, S.; Krafft, C.; Parapini, S.; Taramelli, D.; Sergo, V. Spatial Distribution of Heme Species in Erythrocytes Infected with Plasmodium Falciparum by Use of Resonance Raman Imaging and Multivariate Analysis. *Anal. Bioanal. Chem.* **2008**, *392*, 1277–1282.
- (197) Dasgupta, R.; Verma, R. S.; Ahlawat, S.; Uppal, A.; Gupta, P. K.; Raktim, D.; Ravi Shanker, V.; Sunita, A.; Abha, U.; Pradeep Kumar, G. Studies on Erythrocytes in Malaria Infected Blood Sample with Raman Optical Tweezers. *J. Biomed. Opt.* **2011**, *16*, 77009.

- (198) Webster, G. T.; Tilley, L.; Deed, S.; McNaughton, D.; Wood, B. R. Resonance Raman Spectroscopy Can Detect Structural Changes in Haemozoin (Malaria Pigment) Following Incubation with Chloroquine in Infected Erythrocytes. *FEBS Lett.* **2008**, *582*, 1087–1092.
- (199) Wood, B. R.; Bailo, E.; Khiavi, M. A.; Tilley, L.; Deed, S.; Deckert-Gaudig, T.; Mcnaughton, D.; Deckert, V.; Chemie, P. Tip-Enhanced Raman Scattering (TERS) from Hemozoin Crystals within a Sectioned Erythrocyte. *Nano Lett.* **2011**, *11*, 1868–1873.
- (200) Hobro, A. J.; Konishi, A.; Coban, C.; Smith, N. I. Raman Spectroscopic Analysis of Malaria Disease Progression via Blood and Plasma Samples. *Analyst* **2013**, *138*, 3927–3933.
- (201) Chen, K.; Yuen, C.; Aniweh, Y.; Preiser, P.; Liu, Q. Towards Ultrasensitive Malaria Diagnosis Using Surface Enhanced Raman Spectroscopy. *Sci. Rep.* **2016**, *6*, 1–9.
- (202) De Luca, A. C.; Rusciano, G.; Ciancia, R.; Martinelli, V.; Pesce, G.; Rotoli, B.; Selvaggi, L.; Sasso, A. Spectroscopical and Mechanical Characterization of Normal and Thalassemic Red Blood Cells by Raman Tweezers. *Opt. Express* **2008**, *16*, 7943–7957.
- (203) Filho, A. C. B.; Silveira, L.; Yanai, A. L. S.; Fernandes, A. B. Raman Spectroscopy for a Rapid Diagnosis of Sick Cell Disease in Human Blood Samples: A Preliminary Study. *Lasers Med. Sci.* **2014**, *30*, 247–253.
- (204) Hoey, S.; Brown, D. H.; McConnell, A. A.; Smith, W. E.; Marabani, M.; Sturrock, R. D. Resonance Raman Spectroscopy of Hemoglobin in Intact Cells: A Probe of Oxygen Uptake by Erythrocytes in Rheumatoid Arthritis. *J. Inorg. Biochem.* **1988**, *34*, 189–199.
- (205) Rodnenkov, O. V.; Luneva, O. G.; Ulyanova, N. A.; Maksimov, G. V.; Rubin, A. B.; Orlov, S. N.; Chazov, E. I. Erythrocyte Membrane Fluidity and Haemoglobin Haemoporphyrin Conformation: Features Revealed in Patients with Heart Failure. *Pathophysiology* **2005**, *11*, 209–213.

- (206) Kiran, M.; Itoh, T.; Yoshida, K.; Kawashima, N.; Biju, V.; Ishikawa, M. Selective Detection of HbA1c Using Surface Enhanced Resonance Raman Spectroscopy. *Anal. Chem.* **2010**, *82*, 1342–1348.
- (207) Lin, J.; Lin, J.; Huang, Z.; Lu, P.; Wang, J.; Wang, X.; Chen, R. Raman Spectroscopy of Human Hemoglobin for Diabetes Detection. *J. Innov. Opt. Health Sci.* **2014**, *7*, 1350051.
- (208) Lin, J.; Zeng, Y.; Lin, J.; Wang, J.; Li, L.; Huang, Z.; Li, B.; Zeng, H.; Chen, R. Erythrocyte Membrane Analysis for Type II Diabetes Detection Using Raman Spectroscopy in High-Wavenumber Region. *Appl. Phys. Lett.* **2014**, *104*, 104102.
- (209) Kumar, S.; Kumar, V.; Jain, D. C. Laser Raman Spectroscopic Studies on Hemeproteins in Epileptic Children. *Open J. Appl. Sci.* **2013**, *3*, 123–135.
- (210) Zhu, M. F.; Ye, X. P.; Huang, Y. Y.; Guo, Z. Y.; Zhuang, Z. F.; Liu, S. H. Detection of Methemoglobin in Whole Blood Based on Confocal Micro-Raman Spectroscopy and Multivariate Statistical Techniques. *Scanning* **2014**, *36*, 471–478.
- (211) Lu, M.; Zhao, L.; Wang, Y.; You, G.; Kan, X.; Zhang, Y.; Zhang, N.; Wang, B.; Guo, Y.-J.; Zhou, H. Measurement of the Methemoglobin Concentration Using Raman Spectroscopy. *Artif. Cells. Nanomed. Biotechnol.* **2014**, *42*, 63–69.
- (212) Puppels, G. J.; Demul, F. F. M.; Otto, C.; Greve, J.; Robertnicoud, M.; Arndtjovin, D. J.; Jovin, T. M. Studying Single Living Cells and Chromosomes by Confocal Raman Microspectroscopy. *Nature* **1990**, *347*, 301–303.
- (213) Puppels, G. J.; Garritsen, H. S.; Segers-Nolten, G. M.; de Mul, F. F.; Greve, J. Raman Microspectroscopic Approach to the Study of Human Granulocytes. *Biophys. J.* **1991**, *60*, 1046–1056.

- (214) Puppels, G. J.; Garritsen, H. S. A.; Kummer, J. A.; Greve, J. Carotenoids Located in Human Lymphocyte Subpopulations and Natural Killer Cells by Raman Microspectroscopy. *Cytometry* **1993**, *14*, 251–256.
- (215) Hurst, J. K.; Loehr, T. M.; Curnutte, J. T.; Rosen, H. Resonance Raman and Electron Paramagnetic Resonance Structural Investigations of Neutrophil Cytochrome b558. *J. Biol. Chem.* **1991**, *266*, 1627–1634.
- (216) Ramanauskaite, R. B.; Segers-Nolten, I. G. M. J.; DeGrauw, K. J.; Sijtsma, N. M.; VanderMaas, L.; Greve, J.; Otto, C.; Figdor, C. G. Carotenoid Levels in Human Lymphocytes, Measured by Raman Microspectroscopy. *Pure Appl. Chem.* **1997**, *69*, 2131–2134.
- (217) Sijtsma, N. M.; Otto, C.; Segers-Nolten, G. M.; Verhoeven, A. J.; Greve, J. Resonance Raman Microspectroscopy of Myeloperoxidase and Cytochrome b558 in Human Neutrophilic Granulocytes. *Biophys. J.* **1998**, *74*, 3250–3255.
- (218) Otto, C.; Sijtsma, N. M.; Greve, J. Confocal Raman Microspectroscopy of the Activation of Single Neutrophilic Granulocytes. *Eur. Biophys. J.* **1998**, *27*, 582–589.
- (219) Sijtsma, N. M.; Tibbe, A. G.; Segers-Nolten, I. G.; Verhoeven, A. J.; Weening, R. S.; Greve, J.; Otto, C. Intracellular Reactions in Single Human Granulocytes upon Phorbol Myristate Acetate Activation Using Confocal Raman Microspectroscopy. *Biophys. J.* **2000**, *78*, 2606–2613.
- (220) van Manen, H. J.; Uzunbajakava, N.; van Bruggen, R.; Roos, D.; Otto, C. Resonance Raman Imaging of the NADPH Oxidase Subunit Cytochrome b558 in Single Neutrophilic Granulocytes. *J. Am. Chem. Soc.* **2003**, *125*, 12112–12113.

- (221) Bankapur, A.; Zachariah, E.; Chidangil, S.; Valiathan, M.; Mathur, D. Raman Tweezers Spectroscopy of Live, Single Red and White Blood Cells. *PLoS One* **2010**, *5*, e10427.
- (222) Harz, M.; Kiehntopf, M.; Stockel, S.; Rosch, P.; Deufel, T.; Popp, J.; Stöckel, S.; Rösch, P.; Deufel, T.; Popp, J. Analysis of Single Blood Cells for CSF Diagnostics via a Combination of Fluorescence Staining and Micro-Raman Spectroscopy. *Analyst* **2008**, *133*, 1416–1423.
- (223) Ramoji, A.; Neugebauer, U.; Bocklitz, T.; Foerster, M.; Kiehntopf, M.; Bauer, M.; Popp, J. Toward a Spectroscopic Hemogram: Raman Spectroscopic Differentiation of the Two Most Abundant Leukocytes from Peripheral Blood. *Anal. Chem.* **2012**, *84*, 5335–5342.
- (224) Pully, V. V.; Lenferink, A. T. M.; Otto, C. Time-Lapse Raman Imaging of Single Live Lymphocytes. *J. Raman Spectrosc.* **2011**, *42*, 167–173.
- (225) Schmidt-Ullrich, R.; Verma, S. P.; Wallach, D. F. H. Anomalous Side Chain Amidation in Plasma Membrane Proteins of Simian Virus 40-Transformed Lymphocytes Indicated by Isoelectric Focussing and Laser Raman Spectroscopy. *Biochem. Biophys. Res. Commun.* **1975**, *67*, 1062–1069.
- (226) Neugebauer, U.; Clement, J. H.; Bocklitz, T.; Krafft, C.; Popp, J. Identification and Differentiation of Single Cells from Peripheral Blood by Raman Spectroscopic Imaging. *J. Biophotonics* **2010**, *3*, 579–587.
- (227) Neugebauer, U.; Bocklitz, T.; Clement, J. H.; Krafft, C.; Popp, J. Towards Detection and Identification of Circulating Tumour Cells Using Raman Spectroscopy. *Analyst* **2010**, *135*, 3178–3182.
- (228) Dochow, S.; Krafft, C.; Neugebauer, U.; Bocklitz, T.; Henkel, T.; Mayer, G.; Albert, J.; Popp, J. Tumour Cell Identification by Means of Raman Spectroscopy in Combination with Optical Traps and Microfluidic Environments. *Lab Chip* **2011**, *11*, 1484–1490.

- (229) Wang, X.; Qian, X.; Beitler, J. J.; Chen, Z. G.; Khuri, F. R.; Lewis, M. M.; Shin, H. J.; Nie, S.; Shin, D. M. Detection of Circulating Tumor Cells in Human Peripheral Blood Using Surface-Enhanced Raman Scattering Nanoparticles. *Cancer Res.* **2011**, *71*, 1526–1532.
- (230) Chan, J. W.; Taylor, D. S.; Zwerdling, T.; Lane, S. M.; Ihara, K.; Huser, T. Micro-Raman Spectroscopy Detects Individual Neoplastic and Normal Hematopoietic Cells. *Biophys. J.* **2006**, *90*, 648–656.
- (231) Chan, J. W.; Taylor, D. S.; Lane, S. M.; Zwerdling, T.; Tuscano, J.; Huser, T. Nondestructive Identification of Individual Leukemia Cells by Laser Trapping Raman Spectroscopy. *Anal. Chem.* **2008**, *80*, 2180–2187.
- (232) Moritz, T. J.; Taylor, D. S.; Krol, D. M.; Fritch, J.; Chan, J. W. Detection of Doxorubicin-Induced Apoptosis of Leukemic T-Lymphocytes by Laser Tweezers Raman Spectroscopy. *Biomed. Opt. Express* **2010**, *1*, 1138–1147.
- (233) Schie, I. W.; Alber, L.; Gryshuk, A. L.; Chan, J. W. Investigating Drug Induced Changes in Single, Living Lymphocytes Based on Raman Micro-Spectroscopy. *Analyst* **2014**, *139*, 2726–2733.
- (234) Aslanian, D.; Vainer, H.; Bolard, J.; Guesdon, J.-P.; Balkanski, M. Resonance Raman Spectrometric Study of Human Blood Platelets. *FEBS Lett.* **1979**, *101*, 39–42.
- (235) Aslanian, D.; Vainer, H.; Guesdon, J. P. Thermotropic State Transition in Isolated Platelet Membranes Studied by Raman Spectroscopy. *Eur. J. Biochem.* **1983**, *131*, 555–558.
- (236) Okpalugo, T. I.; Ogwu, A. A.; Maguire, P. D.; McLaughlin, J. A. Platelet Adhesion on Silicon Modified Hydrogenated Amorphous Carbon Films. *Biomaterials* **2004**, *25*, 239–245.

- (237) Wang, G.-W.; Yao, H.-L.; He, B.-J.; Peng, L.-X.; Li, Y.-Q. Raman Micro-Spectroscopy of Single Blood Platelets. *Guang Pu Xue Yu Guang Pu Fen Xi* **2007**, *27*, 1347–1350.
- (238) Chen, P.; Tian, Q.; Baek, S. J.; Shang, X. L.; Park, A.; Liu, Z. C.; Yao, X. Q.; Wang, J. Z.; Wang, X. H.; Cheng, Y.; *et al.* Laser Raman Detection of Platelet as a Non-Invasive Approach for Early and Differential Diagnosis of Alzheimer's Disease. *Laser Phys. Lett.* **2011**, *8*, 547–552.
- (239) Park, A.; Baek, S. J.; Shen, A.; Hu, J. Detection of Alzheimer's Disease by Raman Spectra of Rat's Platelet with a Simple Feature Selection. *Chemom. Intell. Lab. Syst.* **2013**, *121*, 52–56.
- (240) Wang, L. J.; Du, X. Q.; Du, Z. W.; Yang, Y. Y.; Chen, P.; Tian, Q.; Shang, X. L.; Liu, Z. C.; Yao, X. Q.; Wang, J. Z.; *et al.* Raman Spectroscopy Detection of Platelet for Alzheimer's Disease with Predictive Probabilities. *Laser Phys.* **2014**, *24*, 85702.
- (241) Hu, Y. L.; Du, Z. W.; Yang, Y. J.; Chen, P.; Tian, Q.; Shang, X. L.; Liu, Z. C.; Yao, X. Q.; Wang, J. Z.; Wang, X. H.; *et al.* Laser Raman Detection of Platelets for Early and Differential Diagnosis of Alzheimer's Disease Based on an Adaptive Gaussian Process Classification Algorithm. *Laser Phys.* **2013**, *23*, 45603.
- (242) Larsson, K.; Hellgren, L. A Study of the Combined Raman and Fluorescence Scattering from Human Blood Plasma. *Experientia* **1974**, *30*, 481–483.
- (243) Rein, A. J.; Saperstein, D.; Pines, S. H.; Radlick, P. C. Blood Plasma Investigations by Resonance Raman Spectroscopy : Detection of Carotenoid Pigments. *Experientia* **1976**, *32*, 1352–1354.

- (244) Verma, S. P.; Wallach, D. F. H.; Philippot, J. R.; Zanca, M.; Bonnet, B. Abnormal Raman Scattering by Plasma of Patients With Cancer. *J. Natl. Cancer Inst.* **1987**, 78, 587–589.
- (245) Dou, X.; Yamaguchi, Y.; Yamamoto, H.; Uenoyama, H.; Ozaki, Y. Biological Applications of Anti-Stokes Raman Spectroscopy: Quantitative Analysis of Glucose in Plasma and Serum by a Highly Sensitive Multichannel Raman Spectrometer. *Appl. Spectrosc.* **1996**, 50, 1301–1306.
- (246) Qu, J. Y.; Wilson, B. C.; Suria, D. Concentration Measurements of Multiple Analytes in Human Sera by near-Infrared Laser Raman Spectroscopy. *Appl. Opt.* **1999**, 38, 5491–5498.
- (247) Berger, A. J.; Koo, T.-W. W.; Itzkan, I.; Horowitz, G.; Feld, M. S. Multicomponent Blood Analysis by near-Infrared Raman Spectroscopy. *Appl. Opt.* **1999**, 38, 2916–2926.
- (248) Rohleder, D.; Kiefer, W.; Petrich, W. Quantitative Analysis of Serum and Serum Ultrafiltrate by Means of Raman Spectroscopy. *Analyst* **2004**, 129, 906–911.
- (249) Rohleder, D.; Kocherscheidt, G.; Gerber, K.; Kiefer, W.; Köhler, W.; Möcks, J.; Petrich, W. Comparison of Mid-Infrared and Raman Spectroscopy in the Quantitative Analysis of Serum. *J. Biomed. Opt.* **2005**, 10, 31108.
- (250) Qi, D.; Berger, A. J. Chemical Concentration Measurement in Blood Serum and Urine Samples Using Liquid-Core Optical Fiber Raman Spectroscopy. *Appl. Opt.* **2007**, 46, 1726–1734.
- (251) Poon, K. W. C.; Lyng, F. M.; Knief, P.; Howe, O.; Meade, A. D.; Curtin, J. F.; Byrne, H. J.; Vaughan, J. Quantitative Reagent-Free Detection of Fibrinogen Levels in Human Blood Plasma Using Raman Spectroscopy. *Analyst* **2012**, 137, 1807–1814.

- (252) Lyandres, O.; Shah, N. C.; Yonzon, C. R.; Walsh, J. T.; Glucksberg, M. R.; Van Duyne, R. P. Real-Time Glucose Sensing by Surface-Enhanced Raman Spectroscopy in Bovine Plasma Facilitated by a Mixed Decanethiol/Mercaptohexanol Partition Layer. **2005**, *77*, 6134–6139.
- (253) Zhang, X.; Shah, N. C.; Van Duyne, R. P. Sensitive and Selective Chem/bio Sensing Based on Surface-Enhanced Raman Spectroscopy (SERS). *Vib. Spectrosc.* **2006**, *42*, 2–8.
- (254) Lyandres, O.; Yuen, J. M.; Shah, N. C.; Van Duyne, R. P.; Walsh, J. T.; Glucksberg, M. R. Progress toward an in Vivo Surface-Enhanced Raman Spectroscopy Glucose Sensor. *Diabetes Technol. Ther.* **2008**, *10*, 257–265.
- (255) Ma, K.; Yuen, J. M.; Shah, N. C.; Walsh, J. T.; Glucksberg, M. R.; Van Duyne, R. P. In Vivo, Transcutaneous Glucose Sensing Using Surface-Enhanced Spatially Offset Raman Spectroscopy: Multiple Rats, Improved Hypoglycemic Accuracy, Low Incident Power, and Continuous Monitoring for Greater than 17 Days. *Anal. Chem.* **2011**, *83*, 9146–9152.
- (256) Stosch, R.; Henrion, A.; Schiel, D.; Güttler, B. Surface-Enhanced Raman Scattering Based Approach for Quantitative Determination of Creatinine in Human Serum. *Anal. Chem.* **2005**, *77*, 7386–7392.
- (257) Stokes, R. J.; McBride, E.; Wilson, C. G.; Girkin, J. M.; Smith, W. E.; Graham, D. Surface-Enhanced Raman Scattering Spectroscopy as a Sensitive and Selective Technique for the Detection of Folic Acid in Water and Human Serum. *Appl. Spectrosc.* **2008**, *62*, 371–376.
- (258) Pilotto, S.; Pacheco, M. T.; Silveira, L.; Villaverde, A. B.; Zângaro, R. A. Analysis of near-Infrared Raman Spectroscopy as a New Technique for a Transcutaneous Non-Invasive Diagnosis of Blood Components. *Lasers Med. Sci.* **2001**, *16*, 2–9.

- (259) Hsu, P.-H.; Chiang, H. K. Surface-Enhanced Raman Spectroscopy for Quantitative Measurement of Lactic Acid at Physiological Concentration in Human Serum. *J. Raman Spectrosc.* **2010**, *41*, 1610–1614.
- (260) Bergholt, M. S.; Hassing, S. Quantification of C-Reactive Protein in Human Blood Plasma Using near-Infrared Raman Spectroscopy. *Analyst* **2009**, *134*, 2123–2127.
- (261) Bonifacio, A.; Dalla Marta, S.; Spizzo, R.; Cervo, S.; Steffan, A.; Colombatti, A.; Sergo, V. Surface-Enhanced Raman Spectroscopy of Blood Plasma and Serum Using Ag and Au Nanoparticles: A Systematic Study. *Anal. Bioanal. Chem.* **2014**, *406*, 2355–2365.
- (262) Pichardo-Molina, J. L.; Frausto-Reyes, C.; Barbosa-García, O.; Huerta-Franco, R.; González-Trujillo, J. L.; Ramírez-Alvarado, C. A.; Gutiérrez-Juárez, G.; Medina-Gutiérrez, C. Raman Spectroscopy and Multivariate Analysis of Serum Samples from Breast Cancer Patients. *Lasers Med. Sci.* **2007**, *22*, 229–236.
- (263) Martínez Espinosa, J. C.; González Solís, J. L.; Frausto Reyes, C.; Miranda Beltrán, M. L.; Soria Fregoso, C.; Medina Valtierra, J. Detection of Leukemia with Blood Samples Using Raman Spectroscopy and Multivariate Analysis. *AIP Conf. Proc.* **2009**, *99*, 99–104.
- (264) Harris, A. T.; Lungari, A.; Needham, C. J.; Smith, S. L.; Lones, M. A.; Fisher, S. E.; Yang, X. B.; Cooper, N.; Kirkham, J.; Smith, D. A.; *et al.* Potential for Raman Spectroscopy to Provide Cancer Screening Using a Peripheral Blood Sample. *Head Neck Oncol.* **2009**, *1*, 1–8.
- (265) González-Solís, J. L.; Rodríguez-López, J.; Martínez-Espinosa, J. C.; Frausto-Reyes, C.; Jave-Suárez, L. F.; Aguilar-Lemarroy, A. C.; Vargas-Rodríguez, H.; Martínez-Cano, E.; Longo, L. Detection of Cervical Cancer Analyzing Blood Samples with Raman Spectroscopy and Multivariate Analysis. *AIP Conf. Proc.* **2010**, *91*, 91–95.

- (266) Sahu, A.; Sawant, S.; Mamgain, H.; Krishna, C. M. Raman Spectroscopy of Serum: An Exploratory Study for Detection of Oral Cancers. *Analyst* **2013**, *138*, 4161–4174.
- (267) Sahu, A. K.; Dhoot, S.; Singh, A.; Nandakumar, N.; Talathi-Desai, S.; Garud, M.; Pagare, S.; Srivastava, S.; Nair, S.; Chaturvedi, P.; *et al.* Oral Cancer Screening: Serum Raman Spectroscopic Approach. *J. Biomed. Opt.* **2015**, *20*, 115006.
- (268) Sahu, A.; Nandakumar, N.; Sawant, S.; Krishna, C. M. Recurrence Prediction in Oral Cancers: A Serum Raman Spectroscopy Study. *Analyst* **2015**, *140*, 2294–2301.
- (269) Li, P.; Chen, C.; Deng, X.; Mao, H.; Jin, S. Drop Coating Deposition Raman Spectroscopy of Blood Plasma for the Detection of Colorectal Cancer. *J. Biomed. Opt.* **2015**, *20*, 37004.
- (270) Feng, S.; Chen, R.; Lin, J.; Pan, J.; Chen, G.; Li, Y.; Cheng, M.; Huang, Z.; Chen, J.; Zeng, H.; *et al.* Nasopharyngeal Cancer Detection Based on Blood Plasma Surface-Enhanced Raman Spectroscopy and Multivariate Analysis. *Biosens. Bioelectron.* **2010**, *25*, 2414–2419.
- (271) Lin, D.; Pan, J.; Huang, H.; Chen, G.; Qiu, S.; Shi, H.; Chen, W.; Yu, Y.; Feng, S.; Chen, R. Label-Free Blood Plasma Test Based on Surface-Enhanced Raman Scattering for Tumor Stages Detection in Nasopharyngeal Cancer. *Sci. Rep.* **2014**, *4*, 1–8.
- (272) Feng, S.; Pan, J.; Wu, Y.; Lin, D.; Chen, Y.; Xi, G.; Lin, J.; Chen, R. Study on Gastric Cancer Blood Plasma Based on Surface-Enhanced Raman Spectroscopy Combined with Multivariate Analysis. *Sci. China Life Sci.* **2011**, *54*, 828–834.
- (273) Lin, J.; Chen, R.; Feng, S.; Pan, J.; Li, Y.; Chen, G.; Cheng, M.; Huang, Z.; Yu, Y.; Zeng, H. A Novel Blood Plasma Analysis Technique Combining Membrane Electrophoresis with Silver Nanoparticle-Based SERS Spectroscopy for Potential Applications in Noninvasive Cancer Detection. *Nanomedicine* **2011**, *7*, 655–663.

- (274) Feng, S.; Chen, R.; Lin, J.; Pan, J.; Wu, Y.; Li, Y.; Chen, J.; Zeng, H. Gastric Cancer Detection Based on Blood Plasma Surface-Enhanced Raman Spectroscopy Excited by Polarized Laser Light. *Biosens. Bioelectron.* **2011**, *26*, 3167–3174.
- (275) Lin, D.; Feng, S.; Pan, J.; Chen, Y.; Lin, J.; Chen, G.; Xie, S.; Zeng, H.; Chen, R. Colorectal Cancer Detection by Gold Nanoparticle Based Surface-Enhanced Raman Spectroscopy of Blood Serum and Statistical Analysis. *Opt. Express* **2011**, *19*, 13565–13577.
- (276) Feng, S.; Wang, W.; Tai, I. T.; Chen, G.; Chen, R.; Zeng, H. Label-Free Surface-Enhanced Raman Spectroscopy for Detection of Colorectal Cancer and Precursor Lesions Using Blood Plasma. *Biomed. Opt. Express* **2015**, *6*, 3494–3502.
- (277) Feng, S.; Lin, D.; Lin, J.; Li, B.; Huang, Z.; Chen, G.; Zhang, W.; Wang, L.; Pan, J.; Chen, R.; *et al.* Blood Plasma Surface-Enhanced Raman Spectroscopy for Non-Invasive Optical Detection of Cervical Cancer. *Analyst* **2013**, *138*, 3967–3974.
- (278) Yan, B.; Li, B.; Wen, Z.; Luo, X.; Xue, L.; Li, L. Label-Free Blood Serum Detection by Using Surface-Enhanced Raman Spectroscopy and Support Vector Machine for the Preoperative Diagnosis of Parotid Gland Tumors. *BMC Cancer* **2015**, *15*, 1–9.
- (279) Harz, M.; Claus, R. A.; Bockmeyer, C. L.; Baum, M.; Rösch, P.; Kentouche, K.; Deigner, H.-P.; Popp, J. UV-Resonance Raman Spectroscopic Study of Human Plasma of Healthy Donors and Patients with Thrombotic Microangiopathy. *Biopolymers* **2006**, *82*, 317–324.
- (280) Neugebauer, U.; Trenkmann, S.; Bocklitz, T.; Schmerler, D.; Kiehntopf, M.; Popp, J. Fast Differentiation of SIRS and Sepsis from Blood Plasma of ICU Patients Using Raman Spectroscopy. *J. Biophotonics* **2014**, *7*, 232–240.

- (281) Rehman, A.; Anwar, S.; Firdous, S.; Ahmed, M.; Rasheed, R.; Nawaz, M.; Rashid, R.; Mahmood, A. Dengue Blood Analysis by Raman Spectroscopy. *Laser Phys.* **2012**, *22*, 1085–1089.
- (282) Saleem, M.; Bilal, M.; Anwar, S.; Rehman, A.; Ahmed, M. Optical Diagnosis of Dengue Virus Infection in Human Blood Serum Using Raman Spectroscopy. *Laser Phys. Lett.* **2013**, *10*, 35602.
- (283) Khan, S.; Ullah, R.; Saleem, M.; Bilal, M.; Rashid, R.; Khan, I.; Mahmood, A.; Nawaz, M. Raman Spectroscopic Analysis of Dengue Virus Infection in Human Blood Sera. *Opt. - Int. J. Light Electron Opt.* **2016**, *127*, 2086–2088.
- (284) Bilal, M.; Saleem, M.; Amanat, S. T.; Shakoor, H. A.; Rashid, R.; Mahmood, A.; Ahmed, M. Optical Diagnosis of Malaria Infection in Human Plasma Using Raman Spectroscopy. *J. Biomed. Opt.* **2015**, *20*, 17002.
- (285) Vlasova, I. M.; Buravtsov, D. E.; Dolmatova, E. V.; Koshelev, V. B.; Saletsky, A. M. Research of Protective Action of Ischemic Preconditioning on Components of Blood Serum at a Brain Ischemia by Raman Spectroscopy Method. *Laser Phys. Lett.* **2006**, *3*, 401–405.
- (286) Vlasova, I. M.; Saletsky, A. M. Investigation of Neuroprotective Action of Drug “Semax” at Ischemic Insult by Raman Spectroscopy Method by Estimation of Damage of Low Density Lipoprotein of Rat Blood. *Laser Phys.* **2009**, *19*, 2219–2223.
- (287) Saade, J.; Tadeu, M.; Pacheco, T.; Rodrigues, M. R. Identification of Hepatitis C in Human Blood Serum by near-Infrared Raman Spectroscopy. *Spectroscopy* **2008**, *22*, 387–395.

- (288) Delfino, I.; Camerlingo, C.; Zenone, F.; Perna, G.; Capozzi, V.; Cirillo, N.; Gaeta, G. M.; De Mol, E.; Lepore, M. Oral Pathology Follow-up by Means of Micro-Raman Spectroscopy on Tissue and Blood Serum Samples: An Application of Wavelet and Multivariate Data Analysis. *Proc. SPIE - Lasers Dent. XV* **2009**, 7162, 71620L.
- (289) Basar, G.; Parlatan, U.; Seninak, S.; Gunel, T.; Benian, A.; Kalelioglu, I. Investigation of Preeclampsia Using Raman Spectroscopy. *Spectrosc. Int. J.* **2012**, 27, 239–252.
- (290) Sahu, A.; Dalal, K.; Naglot, S.; Aggarwal, P.; Krishna, C. M. Serum Based Diagnosis of Asthma Using Raman Spectroscopy: An Early Phase Pilot Study. *PLoS One* **2013**, 8, e78921.
- (291) Carmona, P.; Molina, M.; Calero, M.; Bermejo-Pareja, F.; Martínez-Martín, P.; Toledano, A. Discrimination Analysis of Blood Plasma Associated with Alzheimer's Disease Using Vibrational Spectroscopy. *J. Alzheimers. Dis.* **2013**, 34, 911–920.
- (292) Ryzhikova, E.; Kazakov, O.; Halamkova, L.; Celmins, D.; Malone, P.; Molho, E.; Zimmerman, E. A.; Lednev, I. K. Raman Spectroscopy of Blood Serum for Alzheimer's Disease Diagnostics: Specificity Relative to Other Types of Dementia. *J. Biophotonics* **2015**, 8, 584–596.
- (293) Schrader, B.; Dippel, B.; Fendel, S.; Keller, S.; Löchte, T.; Riedl, M.; Schulte, R.; Tatsch, E. NIR FT Raman Spectroscopy-a New Tool in Medical Diagnostics. *J. Mol. Struct.* **1997**, 408, 23–31.
- (294) Sato, H.; Chiba, H.; Tashiro, H.; Ozaki, Y. Excitation Wavelength-Dependent Changes in Raman Spectra of Whole Blood and Hemoglobin: Comparison of the Spectra with 514.5-, 720-, and 1064-Nm Excitation. *J. Biomed. Opt.* **2001**, 6, 366–370.

- (295) Lemler, P.; Premasiri, W. R.; DelMonaco, A.; Ziegler, L. D. NIR Raman Spectra of Whole Human Blood: Effects of Laser-Induced and in Vitro Hemoglobin Denaturation. *Anal. Bioanal. Chem.* **2014**, *406*, 193–200.
- (296) Berger, A. J.; Itzkan, I.; Feld, M. S. Feasibility of Measuring Blood Glucose Concentration by near-Infrared Raman Spectroscopy. *Spectrochim. Acta. A. Mol. Biomol. Spectrosc.* **1997**, *53*, 287–292.
- (297) Enejder, A. M. K.; Koo, T.-W.; Oh, J.; Hunter, M.; Sasic, S.; Feld, M. S.; Horowitz, G. L. Blood Analysis by Raman Spectroscopy. *Opt. Lett.* **2002**, *27*, 2004.
- (298) Dogariu, A.; Goltsov, A.; Scully, M. O. Real-Time Monitoring of Blood Using Coherent Anti-Stokes Raman Spectroscopy. *J. Biomed. Opt.* **2008**, *13*, 54004.
- (299) Casella, M.; Lucotti, A.; Tommasini, M.; Bedoni, M.; Forvi, E.; Gramatica, F.; Zerbi, G. Raman and SERS Recognition of β -Carotene and Haemoglobin Fingerprints in Human Whole Blood. *Spectrochim. Acta. A. Mol. Biomol. Spectrosc.* **2011**, *79*, 915–919.
- (300) De Wael, K.; Lepot, L.; Gason, F.; Gilbert, B. In Search of Blood—Detection of Minute Particles Using Spectroscopic Methods. *Forensic Sci. Int.* **2008**, *180*, 37–42.
- (301) Virkler, K.; Lednev, I. K. Raman Spectroscopy Offers Great Potential for the Nondestructive Confirmatory Identification of Body Fluids. *Forensic Sci. Int.* **2008**, *181*, e1-5.
- (302) Virkler, K.; Lednev, I. K. Blood Species Identification for Forensic Purposes Using Raman Spectroscopy Combined with Advanced Statistical Analysis. *Anal. Chem.* **2009**, *81*, 7773–7777.
- (303) McLaughlin, G.; Doty, K. C.; Lednev, I. K. Discrimination of Human and Animal Blood Traces via Raman Spectroscopy. *Forensic Sci. Int.* **2014**, *238*, 91–95.

- (304) Virkler, K.; Lednev, I. K. Raman Spectroscopic Signature of Blood and Its Potential Application to Forensic Body Fluid Identification. *Anal. Bioanal. Chem.* **2010**, *396*, 525–534.
- (305) McLaughlin, G.; Lednev, I. K. A Modified Raman Multidimensional Spectroscopic Signature of Blood to Account for the Effect of Laser Power. *Forensic Sci. Int.* **2014**, *240*, 88–94.
- (306) Sikirzhytski, V.; Sikirzhytskaya, A.; Lednev, I. K. Multidimensional Raman Spectroscopic Signatures as a Tool for Forensic Identification of Body Fluid Traces: A Review. *Appl. Spectrosc.* **2011**, *65*, 1223–1232.
- (307) Sikirzhytski, V.; Sikirzhytskaya, A.; Lednev, I. K. Advanced Statistical Analysis of Raman Spectroscopic Data for the Identification of Body Fluid Traces: Semen and Blood Mixtures. *Forensic Sci. Int.* **2012**, *222*, 259–265.
- (308) Sikirzhytskaya, A.; Sikirzhytski, V.; Lednev, I. K. Raman Spectroscopy Coupled with Advanced Statistics for Differentiating Menstrual and Peripheral Blood. *J. Biophotonics* **2012**, *9*, 1–9.
- (309) Mistek, E.; Halámková, L.; Doty, K. C.; Muro, C. K.; Lednev, I. K. Race Differentiation by Raman Spectroscopy of a Bloodstain for Forensic Purposes. *Anal. Chem.* **2016**, *88*, 7453–7456.
- (310) Boyd, S.; Bertino, M. F.; Seashols, S. J. Raman Spectroscopy of Blood Samples for Forensic Applications. *Forensic Sci. Int.* **2011**, *208*, 124–128.
- (311) McLaughlin, G.; Sikirzhytski, V.; Lednev, I. K. Circumventing Substrate Interference in the Raman Spectroscopic Identification of Blood Stains. *Forensic Sci. Int.* **2013**, *231*, 157–166.

- (312) Sikirzhyskaya, A.; Sikirzhyski, V.; McLaughlin, G.; Lednev, I. K. Forensic Identification of Blood in the Presence of Contaminations Using Raman Microspectroscopy Coupled with Advanced Statistics: Effect of Sand, Dust, and Soil. *J. Forensic Sci.* **2013**, *58*, 1141–1148.
- (313) Boyd, S.; Bertino, M. F.; Ye, D.; White, L. S.; Seashols, S. J. Highly Sensitive Detection of Blood by Surface Enhanced Raman Scattering. *J. Forensic Sci.* **2013**, *58*, 753–756.
- (314) Janko, M.; Stark, R. W.; Zink, A. Preservation of 5300 Year Old Red Blood Cells in the Iceman. *J. R. Soc. Interface* **2012**, *9*, 2581–2590.
- (315) Sulk, R.; Chan, C.; Guicheteau, J.; Gomez, C.; Heyns, J. B. B.; Corcoran, R.; Carron, K. Surface-Enhanced Raman Assays (SERA): Measurement of Bilirubin and Salicylate. *J. Raman Spectrosc.* **1999**, *30*, 853–859.
- (316) Carmona, P.; Monleón, E.; Monzón, M.; Badiola, J. J.; Monreal, J. Raman Analysis of Prion Protein in Blood Cell Membranes from Naturally Affected Scrapie Sheep. *Chem. Biol.* **2004**, *11*, 759–764.
- (317) Liu, T.-Y.; Tsai, K.-T.; Wang, H.-H.; Chen, Y.; Chen, Y.-H.; Chao, Y.-C.; Chang, H.-H.; Lin, C.-H.; Wang, J.-K.; Wang, Y.-L. Functionalized Arrays of Raman-Enhancing Nanoparticles for Capture and Culture-Free Analysis of Bacteria in Human Blood. *Nat. Commun.* **2011**, *2*, 538.
- (318) Cheng, I.-F.; Chang, H.-C.; Chen, T.-Y.; Hu, C.; Yang, F.-L. Rapid Identification of Pathogen in Human Blood by Electrokinetic Concentration and Surface-Enhanced Raman Spectroscopy. *Sci. Rep.* **2013**, *3*, 1–8.

- (319) Chaiken, J.; Finney, W. F.; Peterson, C. M.; Peterson, K. P.; Knudson, P. E.; Weinstock, R. S.; Lein, P. Noninvasive in-Vivo Tissue-Modulated near-Infrared Vibrational Spectroscopic Study of Mobile and Static Tissues: Blood Chemistry. *Proc. SPIE - Biomed. Spectrosc. Vib. Spectrosc. Other Nov. Tech.* **2000**, 3918, 135–143.
- (320) Chaiken, J.; Finney, W. F.; Knudson, P. E.; Peterson, K. P.; Peterson, C. M.; Yang, X.; Weinstock, R. S. Noninvasive Blood Analysis by Tissue Modulated NIR Raman Spectroscopy. *Proc. SPIE - Vis. Temporal Spat. Data Civ. Def. Appl.* **2001**, 4368, 134–145.
- (321) Chaiken, J.; Finney, W. F.; Yang, X. K.; Knudson, P. E.; Peterson, K. P.; Peterson, C. M.; Weinstock, R. S.; Hagrman, D. Progress in the Noninvasive, in-Vivo, Tissue Modulated Raman Spectroscopy of Human Blood. *Proc. SPIE - Biomed. Diagnostic, Guid. Surg. Syst. III* **2001**, 2, 216–227.
- (322) Chaiken, J.; Finney, W. F.; Knudson, P. E.; Peterson, K. P.; Peterson, C. M.; Yang, X.; Weinstock, R. S. Noninvasive , in-Vivo, Tissue Modulated Raman Spectroscopy of Human Blood : Microcirculation and Viscosity Effects. *Proc. SPIE - Biomed. Diagnostic, Guid. Surg. Syst. III* **2001**, 4254, 106–118.
- (323) Chaiken, J.; Finney, W.; Knudson, P. E.; Weinstock, R. S.; Khan, M.; Bussjager, R. J.; Hagrman, D.; Hagrman, P.; Zhao, Y.; Peterson, C. M.; *et al.* Effect of Hemoglobin Concentration Variation on the Accuracy and Precision of Glucose Analysis Using Tissue Modulated, Noninvasive, in Vivo Raman Spectroscopy of Human Blood: A Small Clinical Study. *J. Biomed. Opt.* **2005**, 10, 31111.
- (324) Torres Filho, I. P.; Turner, J.; Pittman, R. N.; Somera, L. G.; Ward, K. R. Hemoglobin Oxygen Saturation Measurements Using Resonance Raman Intravital Microscopy. *Am. J. Physiol. Heart Circ. Physiol.* **2005**, 289, H488-95.

- (325) Torres Filho, I. P.; Turner, J.; Pittman, R. N.; Proffitt, E.; Ward, K. R. Measurement of Hemoglobin Oxygen Saturation Using Raman Microspectroscopy and 532-Nm Excitation. *J. Appl. Physiol.* **2008**, *104*, 1809–1817.
- (326) Ward, K. R.; Torres Filho, I.; Barbee, R. W.; Torres, L.; Tiba, M. H.; Reynolds, P. S.; Pittman, R. N.; Ivatury, R. R.; Turner, J. Resonance Raman Spectroscopy: A New Technology for Tissue Oxygenation Monitoring. *Crit. Care Med.* **2006**, *34*, 792–799.
- (327) Ward, K. R.; Barbee, R. W.; Reynolds, P. S.; Torres Filho, I. P.; Tiba, M. H.; Torres, L.; Pittman, R. N.; Turner, J. Oxygenation Monitoring of Tissue Vasculature by Resonance Raman Spectroscopy. *Anal. Chem.* **2007**, *79*, 1514–1518.
- (328) Shao, J.; Yao, H.; Meng, L.; Li, Y.; Lin, M.; Li, X.; Liu, J.; Liang, J. Raman Spectroscopy of Circulating Single Red Blood Cells in Microvessels in Vivo. *Vib. Spectrosc.* **2012**, *63*, 367–370.
- (329) Shao, J.; Lin, M.; Li, Y.; Li, X.; Liu, J.; Liang, J.; Yao, H. In Vivo Blood Glucose Quantification Using Raman Spectroscopy. *PLoS One* **2012**, *7*, e48127.
- (330) Enejder, A.; Scecina, T.; Oh, J.; Hunter, M.; Shih, W.; Sasic, S.; Horowitz, G.; Feld, M. Raman Spectroscopy for Noninvasive Glucose Measurements. *J. Biomed. Opt.* **2005**, *10*, 31114.
- (331) Barman, I.; Singh, G. P.; Dasari, R. R.; Feld, M. S. Turbidity-Corrected Raman Spectroscopy for Blood Analyte Detection. *Anal. Chem.* **2009**, *81*, 4233–4240.
- (332) Dingari, N. C.; Barman, I.; Kang, J. W.; Kong, C.-R.; Dasari, R. R.; Feld, M. S. Wavelength Selection-Based Nonlinear Calibration for Transcutaneous Blood Glucose Sensing Using Raman Spectroscopy. *J. Biomed. Opt.* **2011**, *16*, 87009.

- (333) Kong, C.-R. R.; Barman, I.; Dingari, N. C.; Kang, J. W.; Galindo, L.; Dasari, R. R.; Feld, M. S. A Novel Non-Imaging Optics Based Raman Spectroscopy Device for Transdermal Blood Analyte Measurement. *AIP Adv.* **2011**, *1*, 32175.
- (334) Diez-Silva, M.; Dao, M.; Han, J.; Lim, C.-T.; Suresh, S. Shape and Biomechanical Characteristics of Human Red Blood Cells in Health and Disease. *MRS Bull.* **2010**, *35*, 382–388.
- (335) Ford, J. Red Blood Cell Morphology. *Int. J. Lab. Hematol.* **2013**, *35*, 351–357.
- (336) Bain, B. J. Diagnosis from the Blood Smear. *N. Engl. J. Med.* **2005**, *353*, 498–507.
- (337) Frank, S. M.; Abazyan, B.; Ono, M.; Hogue, C. W.; Cohen, D. B.; Berkowitz, D. E.; Ness, P. M.; Barodka, V. M. Decreased Erythrocyte Deformability after Transfusion and the Effects of Erythrocyte Storage Duration. *Anesth. Analg.* **2013**, *116*, 975–981.
- (338) Card, R. T.; Mohandas, N.; Perkins, H. A.; Shohet, S. B. Deformability of Stored Red Blood Cells. Relationship to Degree of Packing. *Transfusion* **1982**, *22*, 96–101.
- (339) La Celle, P. L. Alteration of Deformability of the Erythrocyte Membrane in Stored Blood. *Transfusion* **1969**, *9*, 238–245.
- (340) Weed, R. I.; LaCelle, P. L.; Merrill, E. W. Metabolic Dependence of Red Cell Deformability. *J. Clin. Invest.* **1969**, *48*, 795–809.
- (341) Furchgott, R. F.; Ponder, E. Disk-Sphere Transformation in Mammalian Red Cells. *J. Exp. Biol.* **1940**, *XVII*, 117–127.
- (342) Longster, G. H.; Buckley, T.; Sikorski, J.; Tovey, L. A. D. Scanning Electron Microscope Studies of Red Cell Morphology. *Vox Sang.* **1972**, *22*, 161–170.
- (343) Nakao, M.; Nakao, T.; Yamazoe, S.; Yoshikawa, H. Adenosine Triphosphate and Shape of Erythrocytes. *J. Biochem.* **1961**, *49*, 487–492.

- (344) Rapoport, S. Dimensional, Osmotic, and Chemical Changes of Erythrocytes in Stored Blood Blood Preserved in Sodium Citrate, Neutral, and Acid Citrate-Glucose (ACD) Mixtures. *J. Clin. Invest.* **1947**, 26, 591–615.
- (345) Bessis, M. *Red Cell Shape: Physiology, Pathology, Ultrastructure*; Springer Berlin Heidelberg: Berlin, Heidelberg, 1973.
- (346) Haradin, A. R.; Weed, R. I.; Reed, C. F. Changes in Physical Properties of Stored Erythrocytes Relationship to Survival in Vivo. *Transfusion* **1969**, 9, 229–237.
- (347) Nakao, M.; Nakao, T.; Tatibana, M.; Yoshikawa, H.; Abe, T. Effect of Inosine and Adenine on Adenosine Triphosphate Regeneration and Shape Transformation in Long-Stored Erythrocytes. *Biochim. Biophys. Acta* **1959**, 32, 564–565.
- (348) Laczko, J.; Feo, C. J.; Phillips, W. Discocyte-Echinocyte Reversibility in Blood Stored in CPD over a Period of 56 Days. *Transfusion* **1979**, 19, 379–388.
- (349) Usry, R. T.; Moore, G. L.; Manalo, F. W. Morphology of Stored, Rejuvenated Human Erythrocytes. *Vox Sang.* **1975**, 28, 176–183.
- (350) D'Alessandro, A.; Kriebardis, A. G.; Rinalducci, S.; Antonelou, M. H.; Hansen, K. C.; Papassideri, I. S.; Zolla, L. An Update on Red Blood Cell Storage Lesions, as Gleaned through Biochemistry and Omics Technologies. *Transfusion* **2015**, 55, 205–219.
- (351) Zimring, J. C.; Spitalnik, S. L. On the Appropriate Use and Interpretation of Animal Models in Transfusion Medicine Research. *Transfusion* **2013**, 53, 2334–2339.
- (352) Blasi, B.; D'Alessandro, A.; Ramundo, N.; Zolla, L. Red Blood Cell Storage and Cell Morphology. *Transfus. Med.* **2012**, 22, 90–96.

- (353) Zimring, J. C.; Smith, N.; Stowell, S. R.; Johnsen, J. M.; Bell, L. N.; Francis, R. O.; Hod, E. A.; Hendrickson, J. E.; Roback, J. D.; Spitalnik, S. L. Strain-Specific Red Blood Cell Storage, Metabolism, and Eicosanoid Generation in a Mouse Model. *Transfusion* **2014**, *54*, 137–148.
- (354) Hamada, K.; Fujita, K.; Smith, N. I.; Kobayashi, M.; Inouye, Y.; Kawata, S. Raman Microscopy for Dynamic Molecular Imaging of Living Cells. *J. Biomed. Opt.* **2008**, *13*, 4.
- (355) Krafft, C.; Dietzek, B.; Popp, J. Raman and CARS Microspectroscopy of Cells and Tissues. *Analyst* **2009**, *134*, 1046–1057.
- (356) Volkmer, A. Vibrational Imaging and Microspectroscopies Based on Coherent Anti-Stokes Raman Scattering Microscopy. *J. Phys. D-Applied Phys.* **2005**, *38*, R59–R81.
- (357) Schulze, H. G.; Foist, R. B.; Okuda, K.; Ivanov, A.; Turner, R. F. B. A Small-Window Moving Average-Based Fully Automated Baseline Estimation Method for Raman Spectra. *Appl. Spectrosc.* **2012**, *66*, 757–764.
- (358) Schulze, H. G.; Foist, R. B.; Ivanov, A.; Turner, R. F. B. Fully Automated High-Performance Signal-to-Noise Ratio Enhancement Based on an Iterative Three-Point Zero-Order Savitzky-Golay Filter. *Appl. Spectrosc.* **2008**, *62*, 1160–1166.
- (359) Dern, R. J.; Gwinn, R. P.; Wiorkows, J. Studies on Preservation of Human Blood. I. Variability in Erythrocyte Storage Characteristics Among Healthy Donors. *J. Lab. Clin. Med.* **1966**, *67*, 955.
- (360) Brunskill, S.; Wilkinson, K.; Doree, C.; Trivella, S.; Stanworth, M. Transfusion of Fresher versus Older Red Blood Cells for All Conditions. *Cochrane Database Syst Rev.* **2015**, *12*, 1–90.

- (361) Alexander, P. E.; Barty, R.; Fei, Y.; Vandvik, P. O.; Pai, M.; Siemieniuk, R. A. C.; Heddle, N. M.; Blumberg, N.; McLeod, S. L.; Liu, J.; *et al.* Transfusion of Fresher versus Older Red Blood Cells in Hospitalized Patients: A Systematic Review and Meta-Analysis. *Blood* **2015**, *127*, 4–6.
- (362) Bajzer, Z.; Huzak, M.; Neff, K. L.; Prendergast, F. G. Mathematical Analysis of Models for Reaction Kinetics in Intracellular Environments. *Math. Biosci.* **2008**, *215*, 35–47.
- (363) Grima, R.; Schnell, S. How Reaction Kinetics with Time-Dependent Rate Coefficients Differs from Generalized Mass Action. *ChemPhysChem* **2006**, *7*, 1422–1424.
- (364) Grima, R.; Schnell, S. A Systematic Investigation of the Rate Laws Valid in Intracellular Environments. *Biophys. Chem.* **2006**, *124*, 1–10.
- (365) Schnell, S.; Turner, T. E. Reaction Kinetics in Intracellular Environments with Macromolecular Crowding: Simulations and Rate Laws. *Prog. Biophys. Mol. Biol.* **2004**, *85*, 235–260.
- (366) Chu-Shore, J.; Westover, M. B.; Bianchi, M. T. Power Law versus Exponential State Transition Dynamics: Application to Sleep-Wake Architecture. *PLoS One* **2010**, *5*, e14204.
- (367) Hansen, A. L.; Kurach, J. D. R.; Turner, T. R.; Jenkins, C.; Busch, M. P.; Norris, P. J.; Dugger, J.; Tomasulo, P. A.; Devine, D. V.; Acker, J. P. The Effect of Processing Method on the in Vitro Characteristics of Red Blood Cell Products. *Vox Sang.* **2015**, *108*, 350–358.
- (368) Bakkour, S.; Acker, J. P.; Chafets, D. M.; Inglis, H. C.; Norris, P. J.; Lee, T. H.; Busch, M. P. Manufacturing Method Affects Mitochondrial DNA Release and Extracellular Vesicle Composition in Stored Red Blood Cells. *Vox Sang.* **2016**, *111*, 22–32.
- (369) Klein, H. G.; Spahn, D. R.; Carson, J. L. Red Blood Cell Transfusion in Clinical Practice. *Lancet* **2007**, *370*, 415–426.

- (370) Flatt, J. F.; Bawazir, W. M.; Bruce, L. J. The Involvement of Cation Leaks in the Storage Lesion of Red Blood Cells. *Front. Physiol.* **2014**, *5*, 1–12.
- (371) Kinoshita, A.; Tsukada, K.; Soga, T.; Hishiki, T.; Ueno, Y.; Nakayama, Y.; Tomita, M.; Suematsu, M. Roles of Hemoglobin Allostery in Hypoxia-Induced Metabolic Alterations in Erythrocytes: Simulation and Its Verification by Metabolome Analysis. *J. Biol. Chem.* **2007**, *282*, 10731–10741.
- (372) Toffalefti, J. G. Blood Lactate: Biochemistry, Laboratory Methods, and Clinical Interpretation. *Crit. Rev. Clin. Lab. Sci.* **1991**, *28*, 253–268.
- (373) D'Alessandro, A.; D'Amici, G. M.; Vaglio, S.; Zolla, L. Time-Course Investigation of SAGM-Stored Leukocyte-Filtered Red Blood Cell Concentrates: From Metabolism to Proteomics. *Haematologica* **2012**, *97*, 107–115.
- (374) Ratcliffe, J. M.; Elliott, M. J.; Wyse, R. K.; Hunter, S.; Alberti, K. G. The Metabolic Load of Stored Blood. Implications for Major Transfusions in Infants. *Arch. Dis. Child.* **1986**, *61*, 1208–1214.
- (375) Pertinhez, T. A.; Casali, E.; Lindner, L.; Spisni, A.; Baricchi, R.; Berni, P. Biochemical Assessment of Red Blood Cells during Storage by (1)H Nuclear Magnetic Resonance Spectroscopy. Identification of a Biomarker of Their Level of Protection against Oxidative Stress. *Blood Transfus.* **2014**, *12*, 1–9.
- (376) Wang, S.; Palanzo, D.; Ündar, A. Current Ultrafiltration Techniques Before, during and after Pediatric Cardiopulmonary Bypass Procedures. *Perfusion* **2012**, *27*, 438–446.
- (377) Osthaus, W. A.; Sievers, J.; Breymann, T.; Suempelmann, R. Bicarbonate Buffered Ultrafiltration Leads to a Physiologic Priming Solution in Pediatric Cardiac Surgery. *Interact. Cardiovasc. Thorac. Surg.* **2008**, *7*, 969–972.

- (378) Morley, S. L. Red Blood Cell Transfusions in Acute Paediatrics. *Arch. Dis. Child. Educ. Pract. Ed.* **2009**, *94*, 65–73.
- (379) Harmening, D. M. *Modern Blood Banking and Transfusion Practices 4th Edition*; F. A. Davis Company: Philadelphia, USA, 1999.
- (380) Lacroix, J.; Hébert, P. C.; Hutchison, J. S.; Hume, H. A.; Tucci, M.; Ducruet, T.; Gauvin, F.; Collet, J.-P.; Toledano, B. J.; Robillard, P.; *et al.* Transfusion Strategies for Patients in Pediatric Intensive Care Units. *N. Engl. J. Med.* **2007**, *356*, 1609–1619.
- (381) Kirpalani, H.; Whyte, R. K.; Andersen, C.; Asztalos, E. V.; Heddle, N.; Blajchman, M. A.; Peliowski, A.; Rios, A.; LaCorte, M.; Connelly, R.; *et al.* The Premature Infants in Need of Transfusion (Pint) Study: A Randomized, Controlled Trial of a Restrictive (LOW) versus Liberal (HIGH) Transfusion Threshold for Extremely Low Birth Weight Infants. *J. Pediatr.* **2006**, *149*, 301–307.
- (382) Gibson, B. E. S.; Todd, A.; Roberts, I.; Pamphilon, D.; Rodeck, C.; Bolton-Maggs, P.; Burbin, G.; Duguid, J.; Boulton, F.; Cohen, H.; *et al.* Transfusion Guidelines for Neonates and Older Children. *Br. J. Haematol.* **2004**, *124*, 433–453.
- (383) Whyte, R. K.; Jefferies, A. L. Red Blood Cell Transfusion in Newborn Infants. *Paediatr. Child Health* **2014**, *19*, 213–222.
- (384) Dos Santos, A. M. N.; Guinsburg, R.; de Almeida, M. F. B.; Procianoy, R. S.; Leone, C. R.; Marba, S. T. M.; de Souza Rugolo, L. M. S.; Fiori, H. H.; de Andrade Lopes, J. M.; Martinez, F. E. Red Blood Cell Transfusions Are Independently Associated with Intra-Hospital Mortality in Very Low Birth Weight Preterm Infants. *J. Pediatr.* **2011**, *159*, 371–376.e3.

- (385) Shander, A.; Gross, I.; Hill, S.; Javidroozi, M.; Sledge, S. A New Perspective on Best Transfusion Practices. *Blood Transfus.* **2013**, *11*, 193–202.
- (386) Venkatesh, V.; Khan, R.; Curley, A.; New, H.; Stanworth, S. How We Decide When a Neonate Needs a Transfusion. *Br. J. Haematol.* **2013**, *160*, 421–433.
- (387) Bakker, J.; Nijsten, M. W.; Jansen, T. C. Clinical Use of Lactate Monitoring in Critically Ill Patients. *Ann. Intensive Care* **2013**, *3*, 12.
- (388) Luban, N. L.; Strauss, R. G.; Hume, H. A. Commentary on the Safety of Red Cells Preserved in Extended-Storage Media for Neonatal Transfusions. *Transfusion* **1991**, *31*, 229–235.
- (389) Diab, Y. A.; Wong, E. C. C.; Luban, N. L. C. Massive Transfusion in Children and Neonates. *Br. J. Haematol.* **2013**, *161*, 15–26.
- (390) Lee, A. C.; Reduque, L. L.; Luban, N. L. C.; Ness, P. M.; Anton, B.; Heitmiller, E. S. Transfusion-Associated Hyperkalemic Cardiac Arrest in Pediatric Patients Receiving Massive Transfusion. *Transfusion* **2014**, *54*, 244–254.
- (391) Martin, R. J.; Fanaroff, A. A.; Walsh, M. C. *Neonatal-Perinatal Medicine: Diseases of the Fetus and Infant 9th Edition*; Mosby: St. Louis, MO, USA, 2010.
- (392) Keidan, I.; Amir, G.; Mandel, M.; Mishali, D. The Metabolic Effects of Fresh versus Old Stored Blood in the Priming of Cardiopulmonary Bypass Solution for Pediatric Patients. *J. Thorac. Cardiovasc. Surg.* **2004**, *127*, 949–952.
- (393) Wang, S. Y.; Hasty, C. E.; Watson, P. A.; Wicksted, J. P.; Stith, R. D.; March, W. F. Analysis of Metabolites in Aqueous Solutions by Using Laser Raman Spectroscopy. *Appl. Opt.* **1993**, *32*, 925–929.

- (394) Berger, A. J.; Wang, Y.; Feld, M. S. Rapid, Noninvasive Concentration Measurements of Aqueous Biological Analytes by near-Infrared Raman Spectroscopy. *Appl. Opt.* **1996**, *35*, 209–212.
- (395) Cassanas, G.; Morssli, M.; Fabrègue, E.; Bardet, L. Vibrational Spectra of Lactic Acid and Lactates. *J. Raman Spectrosc.* **1991**, *22*, 409–413.
- (396) Abu-Absi, N. R.; Kenty, B. M.; Cuellar, M. E.; Borys, M. C.; Sakhamuri, S.; Strachan, D. J.; Hausladen, M. C.; Li, Z. J. Real Time Monitoring of Multiple Parameters in Mammalian Cell Culture Bioreactors Using an In-Line Raman Spectroscopy Probe. *Biotechnol. Bioeng.* **2011**, *108*, 1215–1221.
- (397) Iversen, J.; Berg, R.; Ahring, B. Quantitative Monitoring of Yeast Fermentation Using Raman Spectroscopy. *Anal. Bioanal. Chem.* **2014**, *406*, 4911–4919.
- (398) Sharma, M.; Marple, E.; Reichenberg, J.; Tunnell, J. W. Design and Characterization of a Novel Multimodal Fiber-Optic Probe and Spectroscopy System for Skin Cancer Applications. *Rev. Sci. Instrum.* **2014**, *85*, 83101.
- (399) Jermyn, M.; Mok, K.; Mercier, J.; Desroches, J.; Pichette, J.; Saint-Arnaud, K.; Bernstein, L.; Guiot, M.-C.; Petrecca, K.; Leblond, F. Intraoperative Brain Cancer Detection with Raman Spectroscopy in Humans. **2015**, *7*, 1–10.
- (400) Matousek, P.; Stone, N. Prospects for the Diagnosis of Breast Cancer by Noninvasive Probing of Calcifications Using Transmission Raman Spectroscopy. *J. Biomed. Opt.* **2011**, *12*, 24008.

- (401) Kozicki, M.; Creek, D. J.; Sexton, A.; Morahan, B. J.; Weselucha-Birczyńska, A.; Wood, B. R. An Attenuated Total Reflection (ATR) and Raman Spectroscopic Investigation into the Effects of Chloroquine on Plasmodium Falciparum-Infected Red Blood Cells. *Analyst* **2015**, *140*, 2236–2246.
- (402) de Oliveira, M. A. S.; Smith, Z. J.; Knorr, F.; de Araujo, R. E.; Wachsmann-Hogiu, S. Long Term Raman Spectral Study of Power-Dependent Photodamage in Red Blood Cells. *Appl. Phys. Lett.* **2014**, *104*, 103702–103705.
- (403) Buckley, K.; Atkins, C. G.; Chen, D.; Schulze, H. G.; Devine, D. V.; Blades, M. B.; Turner, R. F. B. Non-Invasive Spectroscopy of Transfusable Red Blood Cells Stored Inside Sealed Plastic Blood-Bags. *Analyst* **2016**, *141*, 1678–1685.
- (404) Karon, B. S.; van Buskirk, C. M.; Jaben, E. A.; Hoyer, J. D.; Thomas, D. D. Temporal Sequence of Major Biochemical Events during Blood Bank Storage of Packed Red Blood Cells. *Blood Transfus.* **2012**, *10*, 453–461.
- (405) Hess, J. R. Scientific Problems in the Regulation of Red Blood Cell Products. *Transfusion* **2012**, *52*, 1827–1835.
- (406) Dinkla, S.; Peppelman, M.; Van Der Raadt, J.; Atsma, F.; Novotný, V. M. J.; Van Kraaij, M. G.; Joosten, I.; Bosman, G. J. Phosphatidylserine Exposure on Stored Red Blood Cells as a Parameter for Donor-Dependent Variation in Product Quality. *Blood Transfus.* **2014**, *12*, 204–209.
- (407) Schulze, G.; Jirasek, A.; Yu, M. M. L.; Lim, A.; Turner, R. F. B.; Blades, M. W. Investigation of Selected Baseline Removal Techniques as Candidates for Automated Implementation. *Appl. Spectrosc.* **2005**, *59*, 545–574.

- (408) Schulze, H. G.; Foist, R. B.; Okuda, K.; Ivanov, A.; Turner, R. F. B. A Model-Free, Fully Automated Baseline-Removal Method for Raman Spectra. *Appl. Spectrosc.* **2011**, *65*, 75–84.
- (409) Chew, W.; Widjaja, E.; Garland, M. Band-Target Entropy Minimization (BTEM): An Advanced Method for Recovering Unknown Pure Component Spectra. Application to the FTIR Spectra of Unstable Organometallic Mixtures. *Organometallics* **2002**, *21*, 1982–1990.
- (410) Widjaja, E.; Li, C.; Chew, W.; Garland, M. Band-Target Entropy Minimization. A Robust Algorithm for Pure Component Spectral Recovery. Application to Complex Randomized Mixtures of Six Components. *Anal. Chem.* **2003**, *75*, 4499–4507.
- (411) Buckley, K.; Kerns, J. G.; Parker, A. W.; Goodship, A. E.; Matousek, P. Decomposition of in Vivo Spatially Offset Raman Spectroscopy Data Using Multivariate Analysis Techniques. *J. Raman Spectrosc.* **2014**, *45*, 188–192.
- (412) Zhang, D.; Xie, Y.; Mrozek, M. F.; Ortiz, C.; Davisson, V. J.; Ben-Amotz, D. Raman Detection of Proteomic Analytes. *Anal. Chem.* **2003**, *75*, 5703–5709.
- (413) Dingari, N. C.; Horowitz, G. L.; Kang, J. W.; Dasari, R. R.; Barman, I. Raman Spectroscopy Provides a Powerful Diagnostic Tool for Accurate Determination of Albumin Glycation. *PLoS One* **2012**, *7*, e32406.
- (414) Barman, I.; Dingari, N. C.; Kang, J. W.; Horowitz, G. L.; Dasari, R. R.; Feld, M. S. Raman Spectroscopy-Based Sensitive and Specific Detection of Glycated Hemoglobin. *Anal. Chem.* **2012**, *84*, 2474–2482.

- (415) Atkins, C. G.; Buckley, K.; Chen, D.; Schulze, H. G.; Devine, D. V.; Blades, M. W.; Turner, R. F. B. Raman Spectroscopy of Stored Red Blood Cells: Evaluating Clinically-Relevant Biochemical Markers in Donated Blood. *Proc. SPIE - Clin. Biomed. Spectrosc. Imaging IV* **2015**, 9537, 95370X.
- (416) Pecul, M.; Rizzo, A.; Leszczynski, J. Vibrational Raman and Raman Optical Activity Spectra of D-Lactic Acid, D-Lactate, and D-Glyceraldehyde: Ab Initio Calculations. *J. Phys. Chem. A* **2002**, 106, 11008–11016.
- (417) Pratap, B.; Gautam, S.; Srivastava, M.; Prasad, R. L.; Yadav, R. A. Quantum Chemical Density Functional Theory Studies on the Molecular Structure and Vibrational Spectra of Mannitol. *Spectrochim. Acta. A. Mol. Biomol. Spectrosc.* **2014**, 129, 241–254.
- (418) Deegan, R. D.; Bakajin, O.; Dupont, T. F.; Huber, G.; Nagel, S. R.; Witten, T. A. Capillary Flow as the Cause of Ring Stains from Dried Liquid Drops. *Nature* **1997**, 389, 827–829.
- (419) Esmonde-White, K. A.; Esmonde-White, F. W. L.; Morris, M. D.; Roessler, B. J. Characterization of Biofluids Prepared by Sessile Drop Formation. *Analyst* **2014**, 139, 2734–2741.
- (420) Filik, J.; Stone, N. Drop Coating Deposition Raman Spectroscopy of Protein Mixtures. *Analyst* **2007**, 132, 544–550.
- (421) Zhang, D.; Mrozek, M. F.; Xie, Y.; Ben-Amotz, D. Chemical Segregation and Reduction of Raman Background Interference Using Drop Coating Deposition. *Appl. Spectrosc.* **2004**, 58, 929–933.
- (422) Kaniyas, T.; Gladwin, M. T. Nitric Oxide, Hemolysis, and the Red Blood Cell Storage Lesion: Interactions between Transfusion, Donor, and Recipient. *Transfusion* **2012**, 52, 1388–1392.

- (423) Daly, A.; Raval, J. S.; Waters, J. H.; Yazer, M. H.; Kameneva, M. V. Effect of Blood Bank Storage on the Rheological Properties of Male and Female Donor Red Blood Cells. *Clin. Hemorheol. Microcirc.* **2014**, *56*, 337–345.
- (424) Buckley, K.; Matousek, P. Recent Advances in the Application of Transmission Raman Spectroscopy to Pharmaceutical Analysis. *J. Pharm. Biomed. Anal.* **2011**, *55*, 645–652.
- (425) Hopkins, R. J.; Pelfrey, S. H.; Shand, N. C. Short-Wave Infrared Excited Spatially Offset Raman Spectroscopy (SORS) for through-Barrier Detection. *Analyst* **2012**, *137*, 4408–4410.
- (426) Matousek, P.; Stone, N. Recent Advances in the Development of Raman Spectroscopy for Deep Non-Invasive Medical Diagnosis. *J. Biophotonics* **2013**, *6*, 7–19.
- (427) Noordally, O.; Vincent, J.-L. Evaluation of a New, Rapid Lactate Analyzer in Critical Care. *Intensive Care Med.* **1999**, *25*, 508–513.
- (428) Goodwin, M. L.; Harris, J. E.; Hernández, A.; Gladden, L. B. Blood Lactate Measurements and Analysis during Exercise: A Guide for Clinicians. *J. Diabetes Sci. Technol.* **2007**, *1*, 558–569.
- (429) Moore, G. L. Additive Solutions for Better Blood Preservation. *CRC Crit. Rev. Clin. Lab. Sci.* **1987**, *25*, 211–229.
- (430) Orlina, A. R.; Josephson, A. M.; McDonald, B.; Sobucki, J. Comparative Viability of Blood Stored in ACD and CPD. *Transfusion* **1969**, *9*, 62–69.
- (431) Dumont, L. J.; AuBuchon, J. P. Evaluation of Proposed FDA Criteria for the Evaluation of Radiolabeled Red Cell Recovery Trials. *Transfusion* **2008**, *48*, 1053–1060.
- (432) Moroff, G.; Sohmer, P. R.; Button, L. N. Proposed Standardization of Methods for Determining the 24-Hour Survival of Stored Red Cells. *Transfusion* **1984**, *24*, 109–114.

- (433) Schroeder, T. H.; Hansen, M. Effects of Fresh versus Old Stored Blood in the Priming Solution on Whole Blood Lactate Levels during Paediatric Cardiac Surgery. *Perfusion* **2005**, *20*, 17–19.
- (434) Matousek, P.; Clark, I. P.; Draper, E. R. C.; Morris, M. D.; Goodship, A. E.; Everall, N.; Towrie, M.; Finney, W. F.; Parker, A. W. Subsurface Probing in Diffusely Scattering Media Using Spatially Offset Raman Spectroscopy. *Appl. Spe* **2005**, *59*, 393–400.
- (435) Matousek, P.; Morris, M. D.; Everall, N.; Clark, I. P.; Towrie, M.; Draper, E.; Goodship, A.; Parker, A. W. Numerical Simulations of Subsurface Probing in Diffusely Scattering Media Using Spatially Offset Raman Spectroscopy. *Appl. Spectrosc.* **2005**, *59*, 1485–1492.
- (436) Buckley, K.; Matousek, P. Non-Invasive Analysis of Turbid Samples Using Deep Raman Spectroscopy. *Analyst* **2011**, *136*, 3039–3050.
- (437) Conti, C.; Colombo, C.; Realini, M.; Zerbi, G.; Matousek, P. Subsurface Raman Analysis of Thin Painted Layers. *Appl. Spectrosc.* **2014**, *68*, 686–691.
- (438) Conti, C.; Colombo, C.; Realini, M.; Matousek, P. Subsurface Analysis of Painted Sculptures and Plasters Using Micrometre-Scale Spatially Offset Raman Spectroscopy (Micro-SORS). *J. Raman Spectrosc.* **2015**, *46*, 476–482.
- (439) Conti, C.; Realini, M.; Colombo, C.; Sowoidnich, K.; Afseth, N. K.; Bertasa, M.; Botteon, A.; Matousek, P. Noninvasive Analysis of Thin Turbid Layers Using Microscale Spatially Offset Raman Spectroscopy. *Anal. Chem.* **2015**, *87*, 5810–5815.
- (440) Di, Z.; Hokr, B. H.; Cai, H.; Wang, K.; Yakovlev, V. V.; Sokolov, A. V.; Scully, M. O. Spatially Offset Raman Microspectroscopy of Highly Scattering Tissue: Theory and Experiment. *J. Mod. Opt.* **2014**, *340*, 1–5.

- (441) Conti, C.; Realini, M.; Colombo, C.; Matousek, P. Comparison of Key Modalities of Micro-Scale Spatially Offset Raman Spectroscopy. *Analyst* **2015**, 8127–8133.
- (442) Ramirez-Arcos, S.; Perkins, H.; Kou, Y.; Mastronardi, C.; Kumaran, D.; Taha, M.; Yi, Q.-L.; McLaughlin, N.; Kahwash, E.; Lin, Y.; *et al.* Bacterial Growth in Red Blood Cell Units Exposed to Uncontrolled Temperatures: Challenging the 30-Minute Rule. *Vox Sang.* **2013**, 105, 100–107.
- (443) Ramirez-Arcos, S.; Mastronardi, C.; Perkins, H.; Kou, Y.; Turner, T.; Mastronardi, E.; Hansen, A.; Yi, Q. L.; McLaughlin, N.; Kahwash, E.; *et al.* Evaluating the 4-Hour and 30-Minute Rules: Effects of Room Temperature Exposure on Red Blood Cell Quality and Bacterial Growth. *Transfusion* **2013**, 53, 851–859.
- (444) Lieber, C. A.; Mahadevan-Jansen, A. Automated Method for Subtraction of Fluorescence from Biological Raman Spectra. *Appl. Spectrosc.* **2003**, 57, 1363–1367.
- (445) Hu, S. Z.; Smith, K. M.; Spiro, T. G. Assignment of Protoheme Resonance Raman Spectrum by Heme Labeling in Myoglobin. *J. Am. Chem. Soc.* **1996**, 118, 12638–12646.
- (446) Jin, X. X.; Yazer, M. H.; Chalmers, J. J.; Zborowski, M. Quantification of Changes in Oxygen Release from Red Blood Cells as a Function of Age Based on Magnetic Susceptibility Measurements. *Analyst* **2011**, 136, 2996–3003.
- (447) Weed, R. I.; Reed, C. F.; Berg, G. Is Hemoglobin an Essential Structural Component of Human Erythrocyte Membranes? *J. Clin. Invest.* **1963**, 42, 581–588.
- (448) Fergusson, D. A.; Hébert, P.; Hogan, D. L.; LeBel, L.; Rouvinez-Bouali, N.; Smyth, J. A.; Sankaran, K.; Tinmouth, A.; Blajchman, M. A.; Kovacs, L.; *et al.* Effect of Fresh Red Blood Cell Transfusions on Clinical Outcomes in Premature, Very Low-Birth-Weight Infants: The ARIPI Randomized Trial. *J. Am. Med. Assoc.* **2012**, 308, 1443–1451.

- (449) Steiner, M. E.; Triulzi, D. J.; Assmann, S. F.; Sloan, S. R.; Delaney, M.; Blajchman, M. A.; Granger, S.; D'Andrea, P. A.; Pulkrabek, S.; Stowell, C. P. Randomized Trial Results: Red Cell Storage Age Is Not Associated with a Significant Difference in Multiple-Organ Dysfunction Score or Mortality in Transfused Cardiac Surgery Patients. In *Abstract Presentations from the AABB Annual Meeting Philadelphia, PA, October 25-28;* 2014; p. 15A.
- (450) Spinella, P.; Tucci, M. Age of Blood in Children in Pediatric Intensive Care Units (ABC-PICU) <https://clinicaltrials.gov/ct2/show/NCT01977547>.
- (451) Doctor, A.; Spinella, P. Effect of Processing and Storage on Red Blood Cell Function in Vivo. *Semin. Perinatol.* **2012**, *36*, 248–259.